

**Silyl Chalcogenolates:  
Synthesis, Reactivity  
and Transition Metal Complexes**

Dissertation  
zur Erlangung des Doktorgrades  
der Naturwissenschaften

vorgelegt beim Fachbereich Chemische und Pharmazeutische Wissenschaften  
der Johann Wolfgang Goethe-Universität  
in Frankfurt am Main

von  
Theresa Irene Kückmann  
aus Stevens Point, WI, USA

Frankfurt am Main, 2006

Vom Fachbereich Chemische und Pharmazeutische Wissenschaften der  
Johann Wolfgang Goethe-Universität als Dissertation angenommen.

Dekan: Prof. Dr. H. Schwalbe

Gutachter: (1) Prof. Dr. M. Wagner, (2) Prof. Dr. M. Holthausen

Only by dealing with the difficulty does the creativity come forth.

Brian Swimme and Thomas Berry

The Universe Story

My special thanks go to:

Prof. Wagner for his help and support, for his encouragement to work independently, for the scientific freedom, and for the many helpful conversations.

Dr. Hans-Wolfram Lerner for sharing his expertise in silicon chemistry, for his many ideas, for his open door and the fruitful discussions.

Dr. Michael Bolte for his crystallographic efforts, especially with all the crystals that weren't.

Prof. Holthausen for serving as second referee.

Everyone in the NMR department, especially Herrn R. Olbrich and Herrn Dr. J. G. Zimmermann, for all of their help.

Frau I. Prieß and Frau H. Brill for the mass spectrometry, Frau M. Christof for the elemental analyses, and all of the glass blowers, especially Herrn M. Röder.

The Wagner research group, past and present, for the friendly atmosphere and the support, especially Franz Dornhaus for the productive collaboration, and Thorsten Morawitz and Kerstin Kunz not least for their help with crystals when Michael wasn't there, and to Kai Ruth for not blowing us all to pieces.

To my family, especially my parents, for their love, support, and open ear, even from far away.

And to Marc, for learning that silicon also has four arms (but sometimes six), and for Faith, Hope, and Love.

# Table of Contents

<b>Zusammenfassung</b> .....	<b>1</b>
<b>1 Introduction and Objectives</b> .....	<b>9</b>
<b>2 Results and Discussion</b> .....	<b>15</b>
2.1 Sodium silyl chalcogenolates - synthesis, characterization and reactivity...	15
2.1.1 Sodium silanides.....	15
2.1.1.1 Sterically overloaded silanides <i>t</i> Bu <sub>3</sub> SiNa and <i>t</i> Bu <sub>2</sub> PhSiNa.....	15
2.1.1.2 Smaller sodium silanides <i>t</i> Bu <sub>2</sub> MeSiNa and Ph <sub>2</sub> MeSiNa.....	16
2.1.2 Sodium silyl chalcogenolates.....	20
2.1.2.1 Sodium siloxides.....	20
2.1.2.2 Higher silyl chalcogenolates <i>t</i> Bu <sub>2</sub> RSiENa (R = <i>t</i> Bu, Ph; E = S, Se, Te).....	30
2.1.3 Disilyl dichalcogenides.....	36
2.1.4 Oligochalcogen compounds.....	41
2.2 Transition metal complexes of silanides and silyl chalcogenolates.....	46
2.2.1 Complexes of the type [CpFe(CO) <sub>2</sub> L].....	46
2.2.1.1 CpFe(CO) <sub>2</sub> SiPh <sub>2</sub> Me: comparison to CpFe(CO) <sub>2</sub> PPh <sub>2</sub> BH <sub>3</sub> and [CpFe(CO) <sub>2</sub> PPh <sub>2</sub> Me]I.....	46
2.2.1.2 Reactions of [CpFe(CO) <sub>2</sub> ] <sup>+</sup> with silyl chalcogenolates.....	51
2.2.2 Other transition metal complexes.....	55
2.2.2.1 Synthesis via salt metathesis.....	55
2.2.2.2 Synthesis via oxidative addition.....	66
<b>3 Conclusion</b> .....	<b>70</b>
<b>4 Experimental</b> .....	<b>76</b>
4.1 General considerations.....	76
4.2 Syntheses associated with 2.1.1 <i>Sodium silanides</i> .....	76
4.3 Syntheses associated with 2.1.2 <i>Sodium silyl chalcogenolates</i> .....	78
4.4 Syntheses associated with 2.1.3 <i>Disilyl dichalcogenides</i> .....	83
4.5 Syntheses associated with 2.1.4 <i>Oligochalcogen compounds</i> .....	85
4.6 Syntheses associated with 2.2.1 <i>Complexes of the type [CpFe(CO)<sub>2</sub>L]</i> .....	86
4.7 Syntheses associated with 2.2.2 <i>Other transition metal complexes</i> .....	89
4.8 X-ray structure determination.....	92
<b>5 Literature</b> .....	<b>93</b>

<b>6 Appendix</b> .....	<b>102</b>
6.1 Crystallographic data.....	102
6.2 Abbreviations.....	134
6.3 Curriculum Vitae.....	136
6.4 Eidesstattliche Erklärung.....	137

## Zusammenfassung

Chalcogenderivate werden häufig als Liganden in der Übergangsmetallchemie eingesetzt und ermöglichen eine Vielfalt unterschiedlicher Koordinationsmodi. Chalcogenolate  $RE^-$  ( $E = O, S, Se, Te$ ) koordinieren im Allgemeinen terminal aber häufig auch verbrückend. Auch die Chalcogenide  $E^{2-}$  und  $E_2^{2-}$  sind interessante Liganden, die unter anderem in biologischen Systemen vorkommen (z. B. in unterschiedlichen Eisen-Schwefel-Clustern; Abb. 1).

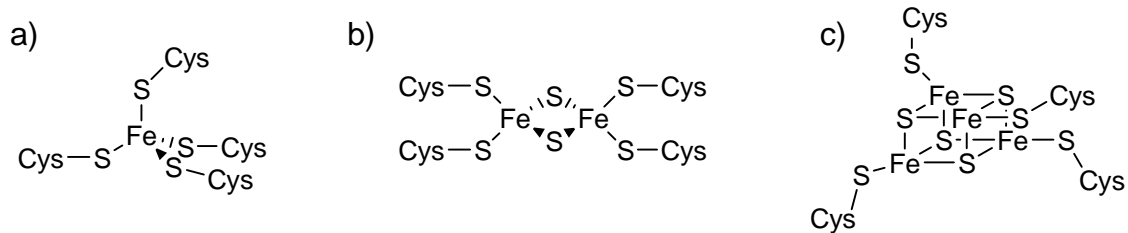


Abb. 1. Koordination in Eisen-Schwefel-Proteinen a) Rubredoxin b)  $Fe_2S_2$  Ferredoxine c)  $Fe_4S_4$  Ferredoxine<sup>[1]</sup>

Neben Alkyl- und Arylchalcogenolaten vermögen auch Silylchalcogenolate Übergangsmetallkomplexe zu stabilisieren.<sup>[2-10]</sup> Metallchalcogenolate  $L_nM-ESiR_3$  mit kleinen organischen Resten R können als Vorgängerkomplexe für größere Metallchalcogenidcluster eingesetzt werden. Diese Cluster lassen sich durch die Spaltung der E-Si Bindung erzeugen.<sup>[2, 4]</sup> Des weiteren führen größere Silylreste am Chalcogenatom zur kinetischen Stabilisierung reaktiver Systeme.<sup>[7, 9]</sup>

Das Silanolat  $Ph_2MeSiONa$  (**6**), im Rahmen dieser Arbeit dargestellt durch Reaktion von Natrium mit  $Ph_2MeSiOH$  in Benzol, bildet eine Reihe von Addukten mit interessanten Strukturen (vgl. Abb. 2). Aus Benzol kristallisiert  $Ph_2MeSiONa$  als donorfreies Hexamer (**6**)<sub>6</sub>, das eine Doppelheterocubanstruktur aufweist. Diese Struktur enthält vier dreifach von Sauerstoff koordinierte Natriumatome, die ihre Koordinationssphäre durch Kontakte zu *ipso*- und *ortho*-Kohlenstoffatomen benachbarter Phenylringe absättigen. Der Zusatz von überschüssigem Donorlösungsmittel (THF) bricht die hexamere Struktur auf. Aus dieser Lösung scheidet sich tetrameres Silanolat (**6**)<sub>4</sub>(THF)<sub>4</sub> ab, das eine Heterocubanstruktur aufweist. In dieser Verbindung wird jedes Natriumatom von einem THF-Molekül gebunden. Das Entfernen des überschüssigen Lösungsmittels und Umkristallisation aus einem nichtkoordinierenden Lösungsmittel liefert Kristalle aus hexamerem Silanolat (**6**)<sub>6</sub>(THF)<sub>2</sub>. Dessen Struktur enthält entsprechend zwei von Sauerstoff nur dreifach koordinierte Natriumatome, die sich durch Kontakte zu Kohlenstoffatomen absättigen. Analoge Addukte

des Hexamers und des Tetramers wurden auch mit dem dimeren Eisencarbonylkomplex  $[\text{CpFe}(\text{CO})_2]_2$  erhalten.

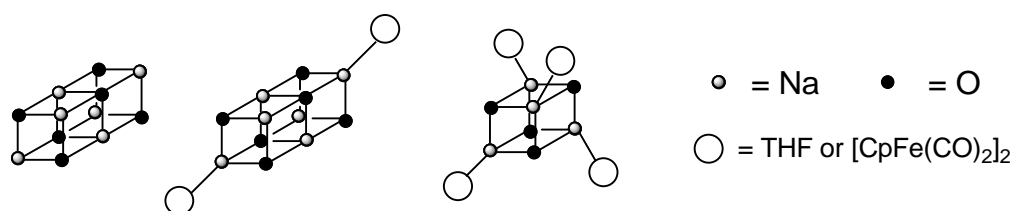


Abb. 2. Schematische des Silanolats  $\text{Ph}_2\text{MeSiONa}$  (**6**) und seiner Addukte

Im Rahmen der vorliegenden Arbeit wurden darüber hinaus die Chalcogenderivate der sterisch extrem anspruchsvollen Silylreste  $t\text{Bu}_2\text{PhSi}$ - und  $t\text{Bu}_3\text{Si}$ - untersucht. Die anionischen Silylspezies  $t\text{Bu}_2\text{PhSiNa}$  und  $t\text{Bu}_3\text{SiNa}$  sind dazu in der Lage, elementare Chalcogene (S, Se und Te) abzubauen. Durch diese Reaktionen entstehen die Silylchalcogenolate  $t\text{Bu}_2\text{PhSiENa}$  (**7 – 9**) und  $t\text{Bu}_3\text{SiENa}$  (**10 – 12**; E = S, Se, Te; Abb. 3).

Die Silylchalcogenolate **7 – 12** kristallisieren entweder als Tetramere mit  $\text{Na}_4\text{E}_4$  Heterocubankern oder als Dimere mit zentralen  $\text{Na}_2\text{E}_2$  viergliedrigen Ringen. Die Natriumatome der Tetramere sind von je einem THF-Molekül und drei Chalcogenolaten gebunden; bei den Dimeren werden die Natriumatome von je zwei Molekülen THF und zwei Chalcogenolatliganden koordiniert.

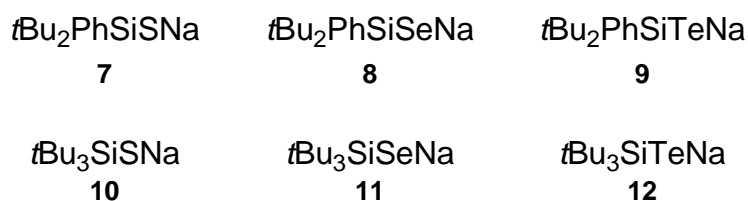


Abb. 3. Im Rahmen dieser Arbeit dargestellte Natrium Silylchalcogenolate

Die Silylchalcogenolate **7 – 12** können leicht derivatisiert werden. Durch Protolyse bilden sich die entsprechenden Chalcogenole  $t\text{Bu}_2\text{RSiEH}$  (R =  $t\text{Bu}$ , Ph; E = S, Se, Te; **14 – 19**), die sich durch die charakteristischen Hochfeldverschiebungen der -EH Protonen in ihren  $^1\text{H}$  NMR Spektren leicht identifizieren lassen (in  $\text{C}_6\text{D}_6$ : TeH ca.  $-7$  ppm; SeH ca.  $-2$  ppm; SH ca.  $-0.5$  ppm). Die Chalcogenole sind in Lösung unter inerter Atmosphäre über Wochen stabil.

An der Luft oxidieren die Chalcogenolate schnell zu den entsprechenden Dichalcogeniden  $t\text{Bu}_2\text{RSiE-ESiR}t\text{Bu}_2$  (R =  $t\text{Bu}$ , Ph; E = S, Se, Te; **20 – 25**). Die farblosen Disulfide  $t\text{Bu}_2\text{RSiS-SSiR}t\text{Bu}_2$  (R = Ph (**20**),  $t\text{Bu}$  (**23**)) können darüber hinaus durch nucleophile Substitution aus den Silaniden  $t\text{Bu}_2\text{RSiNa}$  und  $\text{S}_2\text{Cl}_2$  dargestellt werden. Beide Diselenide  $t\text{Bu}_2\text{RSiSe-$



SeSiR*t*Bu<sub>2</sub> (**21** und **24**) besitzen eine tiefrote Farbe; die Ditelluride *t*Bu<sub>2</sub>RSiTe-TeSiR*t*Bu<sub>2</sub> (**22** und **25**) sind dunkelblau gefärbt.

Die Röntgenstrukturanalyse der Dichalcogenide zeigt eine *s-trans*-Anordnung der Silylreste. Jedes Dichalcogenid weist ein kristallographisches Inversionszentrum in der Mitte der E-E Bindung auf, das einen Torsionswinkel Si-E-E-Si von genau 180° bedingt.

Die oxidative Addition von Dichalcogeniden an Metallzentren in niedrigen Oxidationsstufen eröffnet einen Zugang zu Chalcogenolatkomplexen. Es ist vorstellbar auf diesem Wege nicht nur Chalcogenolatliganden RE<sup>-</sup> einzuführen, sondern auch Chalcogenide E<sup>2-</sup> oder Dichalcogenide E<sub>2</sub><sup>2-</sup>. Um dies umzusetzen benötigt man Moleküle aus denen sich sowohl Chalcogenolat- als auch Chalcogenid- oder Dichalcogenideinheiten erzeugen lassen. Zum Beispiel könnte man mit dem Molekül RS-S-SR zwei Thiolate RS<sup>-</sup> sowie einen Sulfidliganden S<sup>2-</sup> einführen.

Um die Tragfähigkeit dieses Konzeptes zu prüfen wurden in der vorliegenden Arbeit drei Oligochalcogenverbindungen synthetisiert. Das Tetrasulfan *t*Bu<sub>3</sub>SiS-S<sub>2</sub>-SSi*t*Bu<sub>3</sub> (**29**) lässt sich durch nucleophile Substitution aus *t*Bu<sub>3</sub>SiSNa(THF)<sub>2</sub> (**10**(THF)<sub>2</sub>) und S<sub>2</sub>Cl<sub>2</sub> darstellen (Festkörperstruktur Abb. 4). Diese Verbindung weist eine hohe Beständigkeit gegen Luft und Wasser auf. Sowohl in Lösung als auch in fester Form zeigt das Tetrasulfan keine Tendenz, Schwefel zu eliminieren.

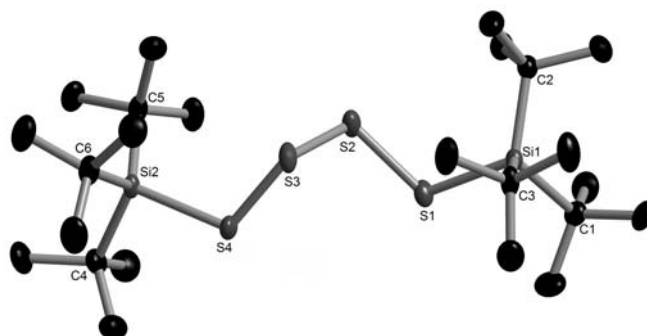


Abb. 4. Festkörperstruktur von *t*Bu<sub>3</sub>Si-S<sub>4</sub>-Si*t*Bu<sub>3</sub> (**29**). Aus Gründen der Übersichtlichkeit sind Protonen nicht dargestellt.

Bei der Reaktion von Se<sub>2</sub>Cl<sub>2</sub> mit *t*Bu<sub>3</sub>SiSNa(THF)<sub>2</sub> (**10**(THF)<sub>2</sub>) gab es zunächst Hinweise auf die Bildung des 1,4-Disilyl-2,3-diselentetrasulfans *t*Bu<sub>3</sub>SiS-Se<sub>2</sub>-SSi*t*Bu<sub>3</sub>, jedoch konnte die Substanz nicht isoliert werden, und es schied sich unter Bildung des Selen(II)dithiolats (*t*Bu<sub>3</sub>SiS)<sub>2</sub>Se (**28**) schnell elementares Selen ab. Die dreigliedrige Kette des Selen(II)dithiolats **28** ist weitaus beständiger als die viergliedrige Kette des Diselentetrasulfans; **28** zersetzt sich allerdings im Laufe der Zeit zu dem Disulfid *t*Bu<sub>3</sub>SiS-SSi*t*Bu<sub>3</sub> (**23**) und Se<sup>0</sup>.

Das homologe, wesentlich stabilere Tellur(II)dithiolat  $(t\text{Bu}_3\text{SiS})_2\text{Te}$  (**27**) lässt sich ebenfalls darstellen, jedoch auf einem anderen Syntheseweg. In einer Gleichgewichtsreaktion von  $(t\text{BuS})_2\text{Te}$  mit  $t\text{Bu}_3\text{SiSH}$  (**17**) entstehen  $(t\text{Bu}_3\text{SiS})_2\text{Te}$  (**27**) und  $t\text{BuSH}$ . Letzteres ist ein niedrig siedendes Alkylthiol, das durch langsames Abdestillieren zusammen mit dem Reaktionsmedium (Toluol) bei Normaldruck entfernt wird. Hiermit konnte das Gleichgewicht zugunsten der Produkte verschoben werden.

Sowohl in der Koordinationschemie, als auch in der Chemie im Allgemeinen, ist es von Interesse, isoelektronische Spezies miteinander zu vergleichen, um mehr über ihre Ähnlichkeiten und Unterschiede zu lernen. Silanide  $\text{R}_3\text{Si}^-$  können als die anionischen Analoga der Phosphane betrachtet werden, in denen ein Phosphoratom formal gegen eine  $\text{Si}^-$ -Einheit ausgetauscht wird. Phosphanylborhydride  $\text{R}_2\text{BH}_3\text{P}^-$  sind ebenfalls isoelektronisch zu Silaniden und Phosphanen.<sup>[11-13]</sup> In diesen Verbindungen ist in einem der organischen, P-gebundenen Reste eines Phosphans ein Kohlenstoffatom durch eine  $\text{B}^-$ -Einheit ersetzt worden, wodurch das Zentralatom (Phosphor) unverändert bleibt, aber eine negative Ladung entsteht. Die gleiche Betrachtungsweise gilt für die Chalcogenderivate, zum Beispiel Phosphanoxid  $\text{R}_3\text{P}=\text{O}$ , Phosphanylborhydridoxid  $\text{R}_2\text{BH}_3\text{P}=\text{O}^-$  und Silanolat  $\text{R}_3\text{SiO}^-$  (Abb. 5).

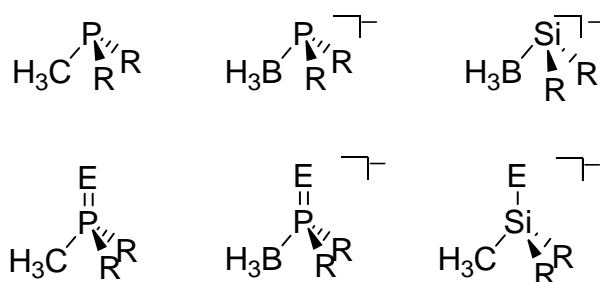


Abb. 5. Isoelektronische Liganden: Phosphane, Phosphanylborhydride, und Silanide sowie ihre Chalcogenderivate

In diesem Sinne wurden die Komplexe  $\text{CpFe}(\text{CO})_2\text{SiPh}_2\text{Me}$  (**31**) und  $\text{CpFe}(\text{CO})_2\text{SSi}t\text{Bu}_3$  (**34**) im Rahmen dieser Arbeit synthetisiert. Die Synthese von  $\text{CpFe}(\text{CO})_2\text{SiPh}_2\text{Me}$  (**31**) gelang durch Reaktion von  $\text{K}[\text{CpFe}(\text{CO})_2]$  mit  $\text{Ph}_2\text{MeSiCl}$ . Dieser Komplex wurde spektroskopisch und kristallographisch untersucht und mit den isosteren, isoelektronischen Komplexen  $\text{CpFe}(\text{CO})_2\text{PPh}_2\text{BH}_3$  und  $[\text{CpFe}(\text{CO})_2\text{PPh}_2\text{Me}]\text{I}$  verglichen. Dieser Vergleich ergab, dass der Silylligand ein stärkerer Donor ist als das Phosphanylborhydrid, das seinerseits ein stärkerer Donor ist als das entsprechende Phosphan.

Der Eisen-Schwefel Komplex  $\text{CpFe}(\text{CO})_2\text{SSi}t\text{Bu}_3$  (**34**) wurde aus  $[\text{CpFe}(\text{CO})_2(\text{THF})]^+$  und  $t\text{Bu}_3\text{SiSNa}(\text{THF})_2$  (**10**(THF)<sub>2</sub>) dargestellt. Eingehende Untersuchungen (NMR, IR, Röntgenstrukturanalyse) und Vergleich mit den analogen Koordinationsverbindungen

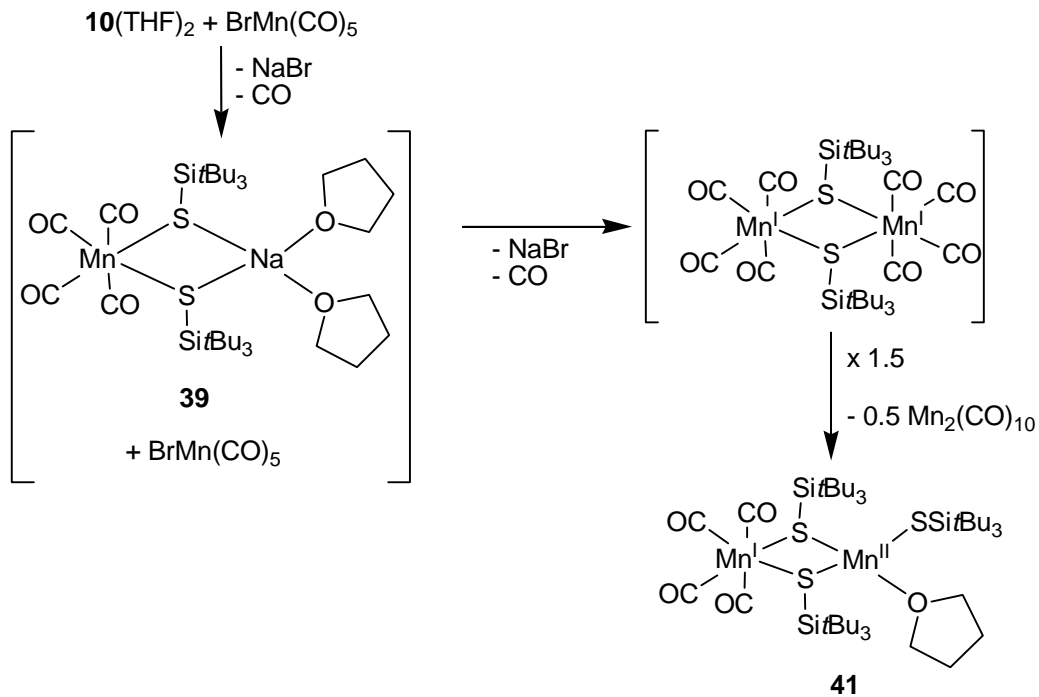
$\text{CpFe}(\text{CO})_2\text{SP}t\text{Bu}_2\text{BH}_3$  und  $[\text{CpFe}(\text{CO})_2\text{SP}t\text{Bu}_3]^+$  führte ebenfalls zu dem Ergebnis, dass der silylhaltige Ligand der stärkste Donor ist, gefolgt von Phosphanylborhydridsulfid und Phosphansulfid. Die Unterschiede im Donorvermögen sind jedoch nur etwa halb so stark ausgeprägt wie bei den nicht chalcogenhaltigen Liganden.

In der Literatur haben Silylchalcogenolatliganden in vielen interessanten Systemen Anwendung gefunden. Sterisch anspruchsvolle Silanolatliganden  $t\text{Bu}_3\text{SiO}^-$  sind dazu in der Lage, Nb- und Ta-Komplexe  $(t\text{Bu}_3\text{SiO})_3\text{ML}$  ( $\text{L} = \text{CH}_2=\text{CHR}$ ) zu stabilisieren, anhand derer die Olefin-zu-Alkyliden-Umlagerung untersucht werden kann.<sup>[9]</sup> Darüber hinaus gibt es Beispiele für die Spaltung der Si-E Bindung in isolierbaren Komplexen  $\text{L}_n\text{M}(\text{ESiR}_3)_m$ , wodurch Chalcogenidliganden  $\text{E}^{2-}$  entstehen.<sup>[2, 4, 5, 14]</sup>

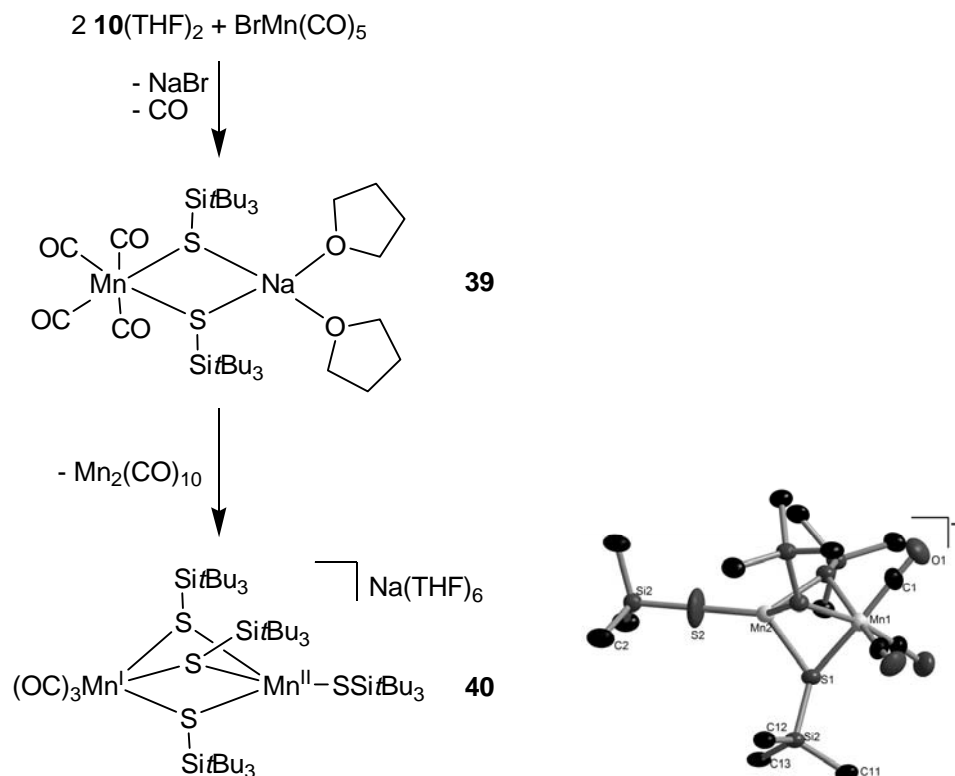
Um die reichhaltige Chemie der Übergangsmetallsilylchalcogenolate weiter auszubauen wurde im Rahmen dieser Arbeit die Komplexchemie der Chalcogenolate **7 – 12** untersucht. Durch Salzmetathese von  $\text{CuCl}$  mit  $t\text{Bu}_2\text{PhSiSNa}(\text{THF})$  (**7(THF)**) konnte der tetramere Komplex  $[\text{Cu}(\text{SSi}t\text{Bu}_2\text{Ph})]_4$  (**37**) dargestellt werden, dessen Festkörperstruktur einen zentralen  $\text{Cu}_4\text{S}_4$  Ring mit kurzen  $\text{Cu}\cdots\text{Cu}$ -Abständen aufweist. Ebenfalls durch Salzmetathese gelang die Synthese des dimeren Zinkkomplexes  $[\text{ZnCl}(\text{SSi}t\text{Bu}_3)(\text{THF})]_2$  (**38**). Sein zentraler viergliedriger  $\text{Zn}_2\text{S}_2$  Ring ist ein Strukturmotiv, das bei homoleptischen Komplexen häufiger beobachtet wird; bei heteroleptischen Komplexen sind solche Motive allerdings selten. Außergewöhnlich ist darüber hinaus, dass die Festkörperstruktur von **38** eine *cis*-ständige Anordnung der THF bzw. Chlorliganden aufweist.

Die Methathesereaktion von Chalcogenolaten und Metallcarbonylhalogeniden eröffnet ebenfalls die Möglichkeit der Darstellung neuer Chalcogenolatkomplexe. Die verbleibenden reaktiven Carbonylliganden ermöglichen weitere chemische Umsetzungen und damit die Darstellung neuartiger Komplexe.

Bei der Umsetzung von  $\text{BrMn}(\text{CO})_5$  mit einem oder zwei Äquivalenten  $t\text{Bu}_3\text{SiSNa}(\text{THF})_2$  (**10(THF)**) entsteht zunächst das 1:2 Produkt  $(\text{CO})_4\text{Mn}(\mu\text{-SSi}t\text{Bu}_3)_2\text{Na}(\text{THF})_2$  (**39**). Wenn ein weiteres Äquivalent  $\text{BrMn}(\text{CO})_5$  vorhanden ist (in der 1:1 Reaktion) oder nachträglich zugegeben wird, entsteht das 1:1 Substitutionsprodukt, welches in den NMR-Spektren ( $^1\text{H}$ ,  $^{13}\text{C}$  und  $^{29}\text{Si}$ ) der Reaktionslösung eindeutig nachgewiesen werden konnte. Diese jedoch instabile Spezies disproportioniert, wobei Kristalle des dinuklearen Mn(I)Mn(II)-Komplexes  $(\text{CO})_4\text{Mn}(\mu\text{-SSi}t\text{Bu}_3)_2\text{Mn}(\text{SSi}t\text{Bu}_3)(\text{THF})$  (**41**) neben  $\text{Mn}_2(\text{CO})_{10}$  gebildet werden (Schema 1). Der 1:2 Komplex  $(\text{CO})_4\text{Mn}(\mu\text{-SSi}t\text{Bu}_3)_2\text{Na}(\text{THF})_2$  (**39**) disproportioniert nach längerem Stehen ebenfalls, und das gebildete komplexe Anion  $[(\text{CO})_3\text{Mn}(\mu\text{-SSi}t\text{Bu}_3)_3\text{Mn}(\text{SSi}t\text{Bu}_3)]^-$  (**40**) kristallisiert aus der Lösung (Schema 2).



Schema 1. Reaktion von  $\text{BrMn}(\text{CO})_5$  mit einem Äquivalent  $t\text{Bu}_3\text{SiSNa}(\text{THF})_2$  (**10**(THF)<sub>2</sub>)



Schema 2. Reaktion von  $\text{BrMn}(\text{CO})_5$  mit zwei Äquivalenten  $t\text{Bu}_3\text{SiSNa}(\text{THF})_2$  (**10**(THF)<sub>2</sub>); links) und Festkörperstruktur des anionischen Dimangankomplexes **40** (rechts). Aus Gründen der Übersichtlichkeit sind nur die quartären Kohlenstoffatome der  $t\text{Bu}_3\text{Si}$ -Gruppen dargestellt.

Die Festkörperstruktur dieses dinuclearen Komplexes weist drei verbrückenden und einen terminalen  $t\text{Bu}_3\text{SiS}^-$ -Liganden auf. Bemerkenswerterweise koordiniert der terminale Thiolatligand in **40** mit einem Mn-S-Si Winkel von  $180^\circ$ . In der Literatur ist postuliert worden, dass linear gebundene Chalcogenolatliganden als Sechselektronendonoren ( $2\sigma e^-$ ,  $4\pi e^-$ ) fungieren und insofern als Cp-Analoga betrachtet werden können.<sup>[7, 15]</sup> Der linear koordinierte Thiolatligand in **40** ist eines der ersten Beispiele für eine solche Koordinationsgeometrie.<sup>[16]</sup>

Durch oxidative Addition lassen sich Übergangsmetall-chalcogenolatkomplexen einfach darstellen.<sup>[17, 18]</sup> Die Anwendung dieser Methode auf die zuvor dargestellten Disilyldichalcogenide wurde im Rahmen dieser Arbeit ebenfalls untersucht. Wenn  $\text{Fe}(\text{CO})_5$  mit den Dichalcogeniden  $t\text{Bu}_3\text{SiE-ESi}t\text{Bu}_3$  (E = S, Se, Te; **22** – **25**) umgesetzt wird, findet eine oxidative Addition statt, und die dimeren Komplexe  $[(\text{CO})_3\text{Fe}(\text{ESi}t\text{Bu}_3)]_2$  **42** – **44** konnten isoliert werden. Die Kristallstrukturanalysen von **42** – **44** ergaben in allen Fällen „Butterfly“-Strukturen in denen die Eisenatome von je drei Carbonylliganden und zwei verbrückenden Chalcogenolatsubstituenten koordiniert sind. Die verzerrt oktaedrischen Koordinationssphären werden jeweils durch eine Eisen-Eisen Bindung vervollständigt. Die Festkörperstruktur des Tellurolatkomplexes **44** ist in Abb. 6 dargestellt.

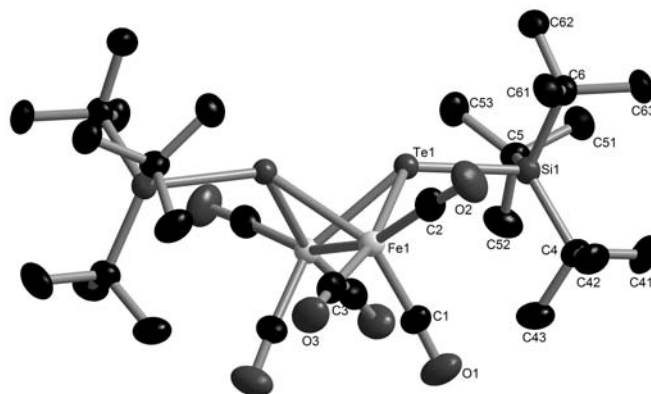


Abb. 6. Festkörperstruktur des Eisentellurolats  $[(\text{CO})_3\text{Fe}(\text{TeSi}t\text{Bu}_3)]_2$  (**44**). Wasserstoffatome sind der Übersichtlichkeit halber nicht dargestellt.

Bei schwacher Bestrahlung mit einer Leuchtstoffröhre reagiert das Ditellurid mit  $\text{Fe}(\text{CO})_5$  innerhalb von 8 h quantitativ. Unter den gleichen Bedingungen dauert die Reaktion des Diselenids mit  $\text{Fe}(\text{CO})_5$  14 d. Der entsprechende Thiolatkomplex **42** bildet sich noch wesentlich langsamer über einen Zeitraum von sechs Monate aus  $t\text{Bu}_3\text{SiS-SSi}t\text{Bu}_3$  und  $\text{Fe}(\text{CO})_5$ . Somit ist der geschwindigkeitsbestimmende Schritt dieser Reaktion wahrscheinlich nicht die Bildung einer reaktiven  $\text{Fe}(\text{CO})_4$ -Spezies, die in allen drei Reaktionen ähnlich schnell ablaufen sollte, sondern vermutlich die Aktivierung der E-E Bindung. Die IR-

spektroskopische Untersuchung der CO-Schwingungen der homologen Komplexe **42 – 44** ergab, dass das Tellurolat der stärkste Donor dieser Serie ist.

In der vorliegenden Arbeit wurde eine Reihe von Silylchalcogenolatderivate dargestellt und vollständig charakterisiert. Ihre Reaktivität und Eignung als Liganden in der Übergangsmetallkomplexchemie wurden untersucht. Sowohl die Salzmetathese als auch oxidative Additionsreaktion erwiesen sich als geeignete Methoden, entsprechende Koordinationsverbindungen darzustellen. Durch die Entwicklung von Oligochalcogenverbindungen mit Silyl-Endkappen eröffnet sich eine neue Möglichkeit, in einem Schritt sowohl Chalcogenolatliganden  $RE^-$  als auch Chalcogenidliganden  $E^{2-}$  in einen Metallkomplex einzuführen.

# 1 Introduction and Objectives

In pursuit of unusual and often unstable compounds, chemists employ a number of strategies in order to increase the stability of elusive structures. To this end, two main variables are electronics and sterics. Increased steric bulk often shields inherently reactive functional groups from attack, thus kinetically stabilizing novel molecules. One textbook example of this approach is the stabilization of the silicon-silicon double bond  $R_2Si=SiR_2$  with bulky substituents (e. g.  $R = \text{mesityl}$ ).<sup>[19]</sup> Substituted aryl groups are a popular choice in the preparation of sterically hindered systems, but much success has also been had with extremely bulky silicon-based systems. In analogy to 2,4,6-tri-*tert*-butylphenyl, which has been dubbed “supermesityl”, the tri-*tert*-butylsilyl group is often referred to as “supersilyl.”<sup>[20]</sup> Other related systems are tris(trimethylsilyl)methyl (“trisyl”) and tris(trimethylsilyl)silyl (“hypersilyl”) (Figure 1.1). Supersilyl is bulkier than hypersilyl, since the steric hindrance of the  $SiMe_3$  groups in hypersilyl is further removed from the central silicon atom than is the case for the  $CMe_3$  groups of supersilyl.

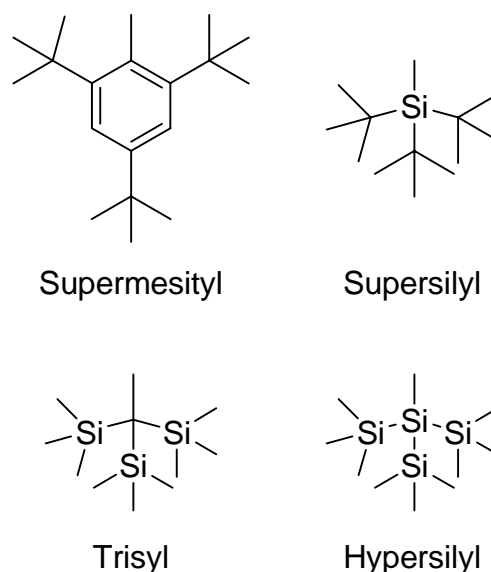
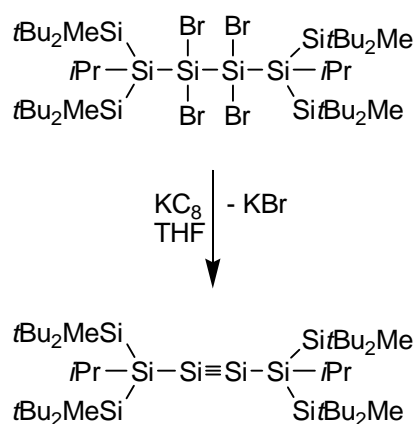


Figure 1.1. Sterically demanding substituents<sup>[21]</sup>

These systems, in particular the supersilyl residue, have been used to stabilize unusual main group element clusters. For example, molecules  $R_2Tl-TlR_2$  with covalent  $Tl-Tl$  bonds are stabilized by hypersilyl and supersilyl residues, as well as by the di-*tert*-butylphenylsilyl moiety ( $R = (Me_3Si)_3Si$ ,<sup>[22]</sup>  $tBu_3Si$ ,<sup>[23]</sup>  $tBu_2PhSi$ <sup>[24]</sup>). From the reaction of  $tBu_3SiNa$  with  $TlCl_3$ , the larger supersilyl-supported thallium clusters  $(tBu_3Si)_4Tl_3Cl$  and  $(tBu_3Si)_6Tl_6Cl_2$  can be

isolated.<sup>[24]</sup> Similarly,  $(t\text{Bu}_3\text{Si})_2\text{Sn}=\text{Sn}=\text{Sn}(\text{Si}t\text{Bu}_3)_2$  can be prepared from the reaction of  $t\text{Bu}_3\text{SiNa}$  and  $\text{Sn}[\text{N}(\text{SiMe}_3)_2]_2$ .<sup>[25]</sup>

When a larger number of the somewhat smaller di-*tert*-butylmethylsilyl residues are used together, quite unusual systems can be stabilized. For example, silyl and germyl radicals of the type  $(t\text{Bu}_2\text{MeSi})_3\text{E}\cdot$  ( $\text{E} = \text{Si}, \text{Ge}$ ) can be isolated.<sup>[26]</sup> These are significant because they are completely lacking of  $\pi$ -bond conjugation, which is often observed in isolable radical systems. In a recent milestone in silicon chemistry, the same  $t\text{Bu}_2\text{MeSi}$ -residue was used in the synthesis of the first stable molecule containing a silicon-silicon triple bond (Scheme 1.1).<sup>[27]</sup>



Scheme 1.1. Synthesis of the first stable silicon-silicon triple bond<sup>[27]</sup>

Furthermore, changes in conformational geometry induced by steric crowding often influence the electronic configuration of a given compound. For example, sterically hindered substituents such as supersilyl and tri-*iso*-propylsilyl have been used to generate silylenes which react from a triplet rather than a singlet state.<sup>[28]</sup>

In transition metal complexes, the electronic nature of the ligands often plays a decisive role in determining the electronic situation at the metal center. Chalcogen-based ligands offer a variety of possible binding modes, with chalcogenide  $\text{E}^{2-}$ , dichalcogenide  $\text{E}_2^{2-}$  and chalcogenolate  $\text{RE}^-$  being common. In addition, chalcogenides and chalcogenolates are often found bridging two or more metal ions but can also act as terminal ligands.

This flexibility is manifested in a number of biological systems, most notably iron-sulfur clusters such as the  $\text{FeCys}_4$  active site in rubredoxin, and the  $\text{Fe}_2\text{S}_2\text{Cys}_4$  and  $\text{Fe}_4\text{S}_4\text{Cys}_4$  sites in ferredoxins (Figure 1.2; Cys = thiolate coordination from cysteinate).<sup>[1]</sup>



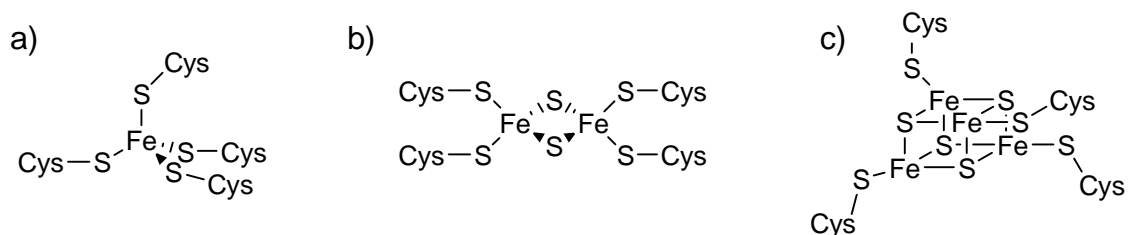
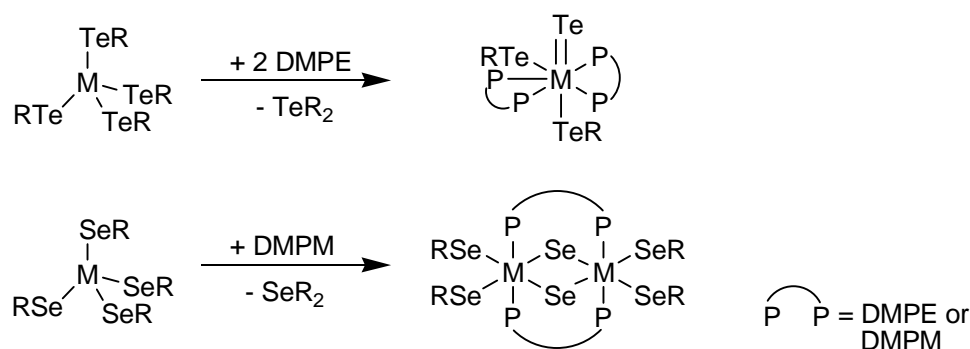


Figure 1.2. Coordination in iron-sulfur proteins a) rubredoxin b)  $\text{Fe}_2\text{S}_2$  ferredoxins c)  $\text{Fe}_4\text{S}_4$  ferredoxins<sup>[1]</sup>

Chalcogen-based systems are also potentially redox active. The oxidative formation and reductive breaking of sulfur-sulfur bonds, for example between cysteine residues or glutathione molecules, is biologically relevant from both a structural and an electrochemical viewpoint.<sup>[1, 29]</sup> This redox activity can also be exploited in the synthesis of transition metal complexes, making oxidative addition of dichalcogenides  $\text{RE-ER}$  to low oxidation state metal centers a viable route to new coordination compounds.<sup>[18, 30, 31]</sup> This concept has even been developed catalytically in the palladium-catalyzed addition of dichalcogenides to alkynes.<sup>[17]</sup> When the advantages of bulky silyl groups and chalcogenolates are combined, intriguing systems can be studied. Wolczanski et al., for example, employed supersiloxide ( $t\text{Bu}_3\text{SiO}^-$ ) as a ligand for olefin complexes ( $t\text{Bu}_3\text{SiO})_3\text{ML}$  ( $\text{M} = \text{Nb}, \text{Ta}$ ;  $\text{L} = \text{CH}_2=\text{CHR}$ ). The kinetic stabilization provided by the bulky siloxide ligands allows for investigation of the olefin-to-alkylidene rearrangement, a process which is relevant to metal-catalyzed olefin metathesis.<sup>[9]</sup>



Scheme 1.2. Synthesis of terminal and bridging chalcogenide ligands from silyl chalcogenolate complexes ( $\text{M} = \text{Zr}, \text{Hf}$ ;  $\text{R} = \text{Si}(\text{SiMe}_3)_3$ )<sup>[5]</sup>

In another example of early transition metal chemistry, homoleptic complexes of zirconium and hafnium hypersilyl tellurolates and selenolates  $\text{M}(\text{ER})_4$  ( $\text{M} = \text{Zr}, \text{Hf}$ ;  $\text{E} = \text{Se}, \text{Te}$ ;  $\text{R} = \text{Si}(\text{SiMe}_3)_3$ ) can be prepared. When these are treated with the chelating phosphines DMPE ( $\text{Me}_2\text{PCH}_2\text{CH}_2\text{PMe}_2$ ) or DMPM ( $\text{Me}_2\text{PCH}_2\text{PMe}_2$ ),  $\text{ER}_2$  is eliminated, leaving complexes with terminal or bridging chalcogenides  $\text{E}^{2-}$  (Scheme 1.2).<sup>[5]</sup>

Silyl chalcogenolates also play a role in catalytic systems. Palladium complexes of siloxides with unsaturated substituents have been shown to be key intermediates in the silicon-based catalytic cross-coupling of alkenes and aryl iodides,<sup>[32]</sup> and compounds of the type  $[(\text{diene})\text{Rh}(\mu\text{-OSiMe}_3)]_2$  have been shown to be active in catalytic hydrosilylation reactions.<sup>[33, 34]</sup>

In macromolecular chemistry, silyl chalcogenolates have also found application. Cyclic structures of the general form  $[(t\text{Bu}_3\text{SiS})\text{MX}]_n$  ( $M = \text{Fe, Co, Ni}$ ;  $X = \text{Cl, Br, I}$ ;  $n = 12, 14$ ) can be prepared by heating solvated monomeric or dimeric precursors under vacuum.<sup>[10]</sup> Disilyl chalcogenides  $\text{E}(\text{SiMe}_3)_2$  ( $E = \text{S, Se}$ ) have been employed in the synthesis of polynuclear metal clusters, driven by the release of  $\text{Me}_3\text{SiX}$  when  $\text{E}(\text{SiMe}_3)_2$  is treated with metal halides  $\text{MX}_n$ .<sup>[35, 36]</sup> This general principle, when applied in a step-wise fashion, can be used in the generation of heterobimetallic complexes.<sup>[2]</sup> For example, if  $(\text{DPPE})\text{NiCl}_2$  ( $\text{DPPE} = \text{Ph}_2\text{PCH}_2\text{CH}_2\text{PPh}_2$ ) is treated with  $\text{Me}_3\text{SiSLi}$ ,  $(\text{DPPE})\text{Ni}(\text{SSiMe}_3)_2$  is formed. When this nickel silyl thiolate complex is reacted with  $\text{CpTiCl}_3$ ,  $\text{Me}_3\text{SiCl}$  is eliminated, yielding the heterobimetallic compound  $\text{CpClTi}(\mu\text{-S})_2\text{Ni}(\text{DPPE})$ .<sup>[14]</sup> This reaction, however, is sensitive to steric congestion at the silicon center. When the *tert*-butyl derivative  $(\text{DPPE})\text{Ni}(\text{SSi}t\text{BuMe}_2)_2$  is treated with  $\text{CpTiCl}_3$ , an intractable mixture of products results.

In general, a fair amount of work has been published concerning the reactivity of silyl chalcogenolates with relatively small silyl residues such as  $\text{SiMe}_3$  or  $\text{SiPh}_3$ .<sup>[3, 4, 14, 37]</sup> Thorough investigation of chalcogenolates with sterically overloaded silyl residues has concentrated mainly on the lighter siloxides and, to a lesser extent, thiolates.<sup>[7, 9, 10]</sup> A large portion of the research associated with silyl selenolates and tellurolates was carried out using the hypersilyl residue, which is prone to degradation via  $\text{SiMe}_3$  transfer<sup>[5, 6, 38, 39]</sup>

One primary goal of the work presented here is the synthesis and characterization of extremely sterically hindered silyl thiolates, selenolates, and tellurolates, in particular those with large hydrocarbon residues, which decrease the risk of substituent migration. To be able to compare not only the different chalcogen species with each other, but to also investigate the role of small differences in steric bulk, the silyl residues  $t\text{Bu}_2\text{PhSi}$  and  $t\text{Bu}_3\text{Si}$  were chosen, leading to the six sodium chalcogenolates  $t\text{Bu}_2\text{PhSiSNa}$ ,  $t\text{Bu}_2\text{PhSiSeNa}$ ,  $t\text{Bu}_2\text{PhSiTeNa}$ ,  $t\text{Bu}_3\text{SiSNa}$ ,  $t\text{Bu}_3\text{SiSeNa}$  and  $t\text{Bu}_3\text{SiTeNa}$ .

Due to the strong bridging tendency of heavier chalcogenolates, it is expected that metal-chalcogenolate clusters can be stabilized with these compounds. To this end, the complexation chemistry of the silyl chalcogenolates with transition metal compounds is a primary field of investigation. Furthermore, selective introduction of chalcogenolate ligands

should be explored with the goal of synthesizing metal complexes and clusters coordinated by different chalcogenolates (e. g. thiolate and selenolate) or chalcogen-donor ligands in different coordination environments (e. g. thiolate and selenide). For example, this goal could be achieved through the oxidative addition of compounds of the type RE-E'-ER to transition metal centers in low oxidation states. In this way, two chalcogenolates RE<sup>-</sup> and one chalcogenide E'<sup>2-</sup> could be introduced simultaneously.

Despite the bridging tendency of chalcogenolate ligands, the steric hindrance of the selected systems should help to control the nuclearity of metal complexes.<sup>[6]</sup> In addition, silyl residues are very soluble in organic solvents and should contribute to the overall solubility of silyl chalcogenolate complexes. This should enable the solution-phase characterization of resulting complexes and clusters, even those of significant size.

Furthermore, chalcogenolates can donate a varying number of electrons when bound to a transition metal center.<sup>[7]</sup> As pure  $\sigma$ -donors, they donate two electrons to a coordinated metal site. The free *p*-orbital lone pairs, however, can both potentially donate in a  $\pi$ -fashion. This corresponds to four or six-electron donation (Figure 1.3). The necessary prerequisite for six-electron donation is linear M-E-Si coordination. This coordination geometry can only be effectively induced by sterically hindered residues. These, by their very nature, have a large coordination cone angle (for *t*Bu<sub>3</sub>SiO<sup>-</sup> ca. 120°), making them comparable to Cp (cone angle ca. 130°) both in their electron donation (6 e<sup>-</sup>) and in their steric demands.<sup>[15]</sup> This sort of coordination and electron donation has rarely been observed for silyl chalcogenolates.<sup>[7, 16]</sup> The sterically hindered residues *t*Bu<sub>3</sub>Si and *t*Bu<sub>2</sub>PhSi should make linear coordination and thus six-electron donation more likely.

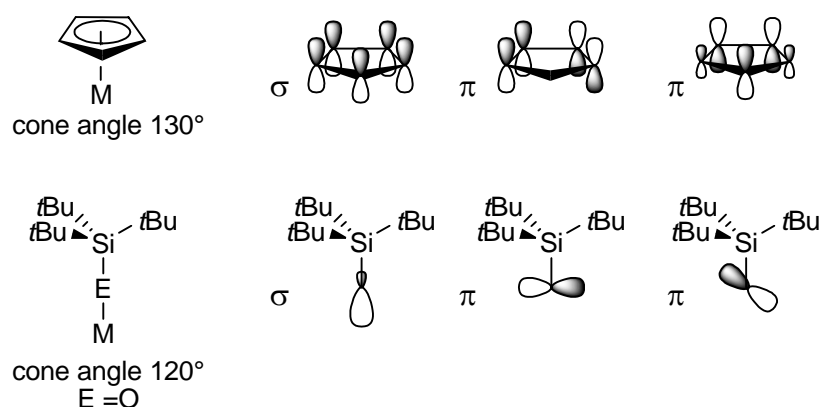


Figure 1.3. Isolobal analogy between Cp and silyl chalcogenolates<sup>[7]</sup>

Silyl chalcogenolates are thus, in a sense, isolobal to the cyclopentadienyl ligand. Two more directly related classes of ligands are silyl residues and phosphines, both of which have been

used extensively in coordination chemistry.<sup>[40, 41]</sup> Phosphines are ubiquitous ligands in homogeneous catalysis, and silyl ligands can be thought of as their anionic analogs, where the phosphorus atom has been replaced with a silicon atom, resulting in a negatively charged moiety without changing the periphery of the molecule. More recently, the chemistry of phosphanyl borohydrides has been developed.<sup>[11, 12, 42-46]</sup> In these phosphine derivatives, a methyl group has been replaced with a BH<sub>3</sub> moiety, introducing a negative charge without changing the steric demand of the ligand. They can be considered intermediate species in this isoelectronic comparison. Phosphines and phosphanyl borohydrides can also be easily oxidized or chalcogenated, and the chalcogen derivatives R<sub>3</sub>P=E, R<sub>2</sub>BH<sub>3</sub>P=E<sup>-</sup> and R<sub>3</sub>Si-E<sup>-</sup> are also isoelectronic (Figure 1.4).

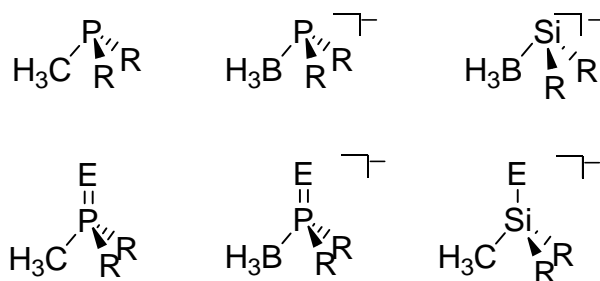


Figure 1.4. Isoelectronic species phosphines, phosphanyl borohydrides, and silanides with their chalcogen derivatives.

Just as the investigation of the Cp/silyl chalcogenolate analogy is of interest, it is instructive to compare the properties of these two series of isoelectronic, isosteric ligands. To this end, a systematic comparison of the reactivity and transition metal complexes of silanides, phosphanyl borohydrides, and phosphines as well as of silyl oxides and phosphanyl borohydride oxides and silyl thiolates, phosphanyl borohydride sulfides and phosphine sulfides was carried out in cooperation with Franz Dornhaus.<sup>[13]</sup>

## 2 Results and Discussion

### 2.1 Sodium silyl chalcogenolates - synthesis, characterization and reactivity

The first main goal of the research presented here was the synthesis of sodium silyl chalcogenolates  $t\text{Bu}_2\text{RSiENa}$  ( $E = \text{S, Se, Te}$ ;  $R = \text{Ph, } t\text{Bu}$ ). To this end, sodium silanides were explored as potential silicon-containing precursors.

#### 2.1.1 Sodium silanides

Due to its low electronegativity, silicon is most often found in compounds where it is bound to electronegative elements such as halides or oxygen. The widely occurring silicate minerals are a good example of this behavior. On the other hand, it is also possible to synthesize silicon-containing compounds in which the silicon atom bears a formal negative charge, such as when it is bound to alkali metals.

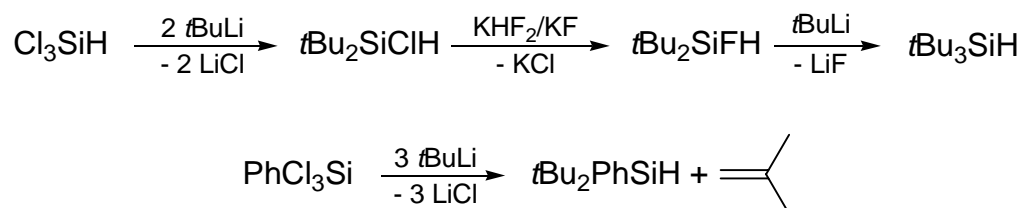
Silyl anions are interesting for a number of reasons. Since they have an “umpolung” at the silicon atom, they can be used to prepare new compounds, which would be inaccessible using only reagents where the silicon atom bears a partial positive charge. This is especially true when the silanide anion is supported by bulky substituents such as *tert*-butyl or trimethylsilyl. These species, both electronically through their strong  $\sigma$ -donation and kinetically because of their large size, stabilize low coordination numbers and unusual oxidation states,<sup>[21, 47-49]</sup> including the main group element clusters  $(t\text{Bu}_3\text{Si})_6\text{Tl}_6\text{Cl}_2$ <sup>[50]</sup> and  $(t\text{Bu}_3\text{Si})_2\text{Sn}=\text{Sn}=\text{Sn}(t\text{Bu}_3\text{Si})_2$ <sup>[25]</sup> and the thallium(II) species  $[(\text{Me}_3\text{Si})_3\text{Si}]_4\text{Tl}_2$ .<sup>[51]</sup>

In a more academic sense, silanides are also interesting because they are the isoelectronic analogues of phosphines ( $\text{R}_3\text{P}$ ) and phosphanyl borohydrides ( $\text{R}_2\text{BH}_3\text{P}^-$ ). A comparison of isoelectronic, isosteric compounds lends insight into the underlying similarities and differences between formally related species.

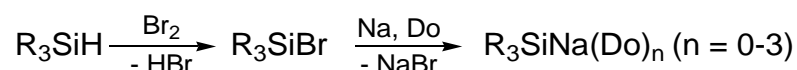
##### 2.1.1.1 Sterically overloaded silanides $t\text{Bu}_3\text{SiNa}$ and $t\text{Bu}_2\text{PhSiNa}$

The sodium silanides  $t\text{Bu}_3\text{SiNa}$  and  $t\text{Bu}_2\text{PhSiNa}$  have been reported in the literature and are well characterized. In both cases, the starting point for silanide synthesis is the silane  $\text{R}_3\text{SiH}$ , which can be prepared from *tert*-butyllithium and the appropriate silyl halide. For  $t\text{Bu}_3\text{SiH}$  (“supersilane”), only two *tert*-butyl groups can be introduced in the reaction of silicochloroform ( $\text{SiCl}_3\text{H}$ ) with *tert*-butyllithium; introduction of the third *tert*-butyl group is

successful only after treatment of intermediate  $t\text{Bu}_2\text{SiClH}$  with  $\text{KHF}_2/\text{KF}$  to give the corresponding silyl fluoride (Scheme 2.1.1).<sup>[52-54]</sup> Alternatively, this compound can also be prepared directly from  $\text{SiF}_4$ .<sup>[55, 56]</sup> Phenyl derivative  $t\text{Bu}_2\text{PhSiH}$  can be prepared by treating  $\text{PhSiCl}_3$  with three equivalents of *tert*-butyllithium.<sup>[57]</sup> Two equivalents substitute quickly after addition of the lithium reagent, at which point the mixture is heated in boiling heptane, thus initiating decomposition of the third equivalent of *tert*-butyllithium to isobutene and  $\text{LiH}$ , which in turn reacts with  $t\text{Bu}_2\text{PhSiCl}$  to give the desired product,  $t\text{Bu}_2\text{PhSiH}$  (Scheme 2.1.1).

Scheme 2.1.1. Synthesis of  $t\text{Bu}_3\text{SiH}$  and  $t\text{Bu}_2\text{PhSiH}$ 

These silanes  $t\text{Bu}_2\text{RSiH}$  ( $\text{R} = t\text{Bu}, \text{Ph}$ ) are then treated with  $\text{Br}_2$  to give the silyl bromides and finally reduced with elemental sodium to produce the desired sodium silanides (Scheme 2.1.2). The reduction with sodium can take place either in heptane, giving donor-free silanides, or in a variety of donor solvents (e.g. benzene, THF, or dibutylether).<sup>[47, 57, 58]</sup> This methodology is not limited to sodium, but can also be carried out with other alkali metals.



Scheme 2.1.2. Synthesis of sodium silanides

In the solid state, regardless of whether the structure is donor-free or supported by Lewis base, contact ion pairs are formed. Compounds  $t\text{Bu}_2\text{PhSiM}$  show additional  $\text{Ph-M}$  cation- $\pi$  interactions,<sup>[58]</sup> while agostic interactions between protons from the methyl group of one *tert*-butyl group and the metal center can be observed for a number of solid state structures of  $t\text{Bu}_3\text{SiM}$ , both with and without additional donors.<sup>[47]</sup>

### 2.1.1.2 Smaller sodium silanides $t\text{Bu}_2\text{MeSiNa}$ and $\text{Ph}_2\text{MeSiNa}$

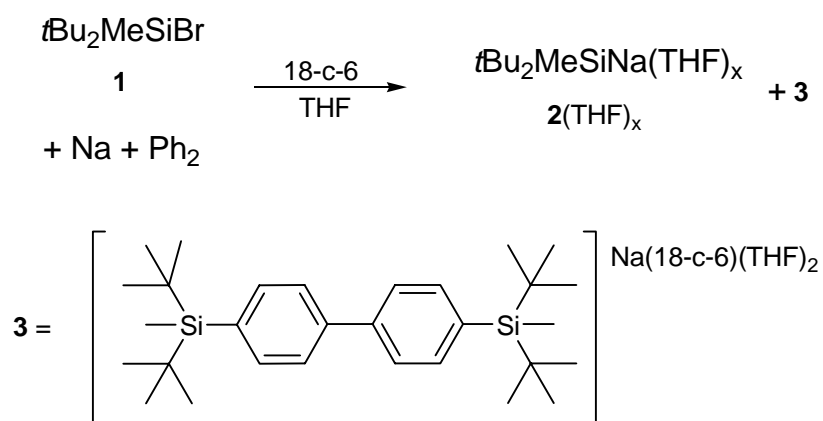
Independent of the interesting results in the literature using sterically overloaded silanides, which promise a rich chemistry resulting from these species, one goal of this project was to be able to compare isoelectronic, isosteric silanides, phosphanyl borohydrides, and phosphines, and their derivatives. For comparison to  $t\text{Bu}_3\text{SiNa}$  and  $t\text{Bu}_2\text{PhSiNa}$ , the compounds

$t\text{Bu}_2(\text{BMe}_3)\text{PM}$  and  $t\text{Bu}(\text{BMe}_3)\text{PhPM}$  would be required. However, synthesis of phosphanyl borohydride analogs with a  $\text{BMe}_3$  moiety failed due to the poor stability of the phosphine-borane adducts  $\text{HPR}_2\cdot\text{BMe}_3$ , which consequently could not be deprotonated to give the desired alkali metal species.<sup>[13]</sup> The most readily accessible phosphanyl borohydrides are  $\text{Ph}_2\text{BH}_3\text{PK}$  and  $t\text{Bu}_2\text{BH}_3\text{PK}$ .<sup>[11, 12]</sup> Both analogous sodium silanides  $\text{Ph}_2\text{MeSiNa}$ <sup>[59]</sup> and  $t\text{Bu}_2\text{MeSiNa}$ <sup>[26]</sup> are known in the literature, although the former has been characterized only via boiling point determination of the corresponding silane after hydrolysis. The di-*tert*-butyl species, on the other hand, is well documented.

After synthesis of  $t\text{Bu}_2\text{MeSiH}$  from  $\text{Cl}_2\text{MeSiH}$  and *tert*-butyllithium,<sup>[60]</sup> the bromosilane  $t\text{Bu}_2\text{MeSiBr}$  (**1**) is prepared using the same method employed in the synthesis of the bulkier species  $t\text{Bu}_2\text{PhSiBr}$  and  $t\text{Bu}_3\text{SiBr}$  (cf. experimental section 4.2.1 for synthetic details). However, reduction with sodium in boiling heptane to give the donor-free compound as described by Sekiguchi results in a significant amount of disilane impurity.<sup>[26]</sup> Indeed, the success of this method appears to depend on the aggregation state of the sodium metal. Melted sodium results in a high yield of silanide and only a small amount of disilane contamination, while solid sodium produces disilane quantitatively via Wurz-coupling of the bromosilane. Since the melting point of sodium and the boiling point of heptane are very close, this preparative method is sensitive to the variation of a number of uncontrollable factors. For these reasons, it seemed prudent to search for a more reliable approach.

The attempted conversion of **1** to  $t\text{Bu}_2\text{MeSiNa}(\text{THF})_x$  (**2**( $\text{THF}$ )<sub>x</sub>) using elemental sodium in boiling THF in analogy to the synthesis of  $t\text{Bu}_3\text{SiNa}$  and  $t\text{Bu}_2\text{PhSiNa}$  also led to disilane as the main product. It is, however, well known that aromatic systems such as naphthalene and biphenyl are effective reduction assistants, which serve to solubilize the active reducing agent. In an effort to avoid unnecessary and unwanted byproducts, biphenyl was employed as a reduction catalyst to prepare **2**( $\text{THF}$ )<sub>x</sub> (4.2.2). When **1** is reduced with sodium metal in THF at room temperature using sub-stoichiometric amounts of biphenyl (0.6 equivalents), **2**( $\text{THF}$ )<sub>x</sub> is formed in good yield with indications of only minor disilane contamination. Excess sodium metal and byproduct salts can be removed by changing the solvent to pentane and filtering. Naturally, biphenyl presents a challenge during isolation of silanide **2**( $\text{THF}$ )<sub>x</sub>. It is, however, fairly volatile and most of it can be removed in vacuo. The NMR chemical shifts (<sup>1</sup>H, <sup>13</sup>C and <sup>29</sup>Si) of **2** produced by this route are in good agreement with the published values. Slight variations can be attributed to the fact that this procedure results in a donor-supported silanide **2**( $\text{THF}$ )<sub>x</sub>, while the literature describes the synthesis of the donor-free compound.

Unfortunately, crystallization attempts using THF as a donor failed to yield X-ray quality crystals of **2**, and crown ether was employed in an attempt to aid crystallization. Addition of an equimolar amount of 18-crown-6 to a concentrated THF solution of **2** followed by standing for several days led to the deposition of dark green, nearly opaque, X-ray quality needles. Solution of the crystal structure revealed that the crystals consisted not of the sodium silanide **2**, but of the silylated biphenyl radical **3**, bis(THF)(18-crown-6)sodium 4,4'-bis(di-*tert*-butylmethylsilyl)biphenylide (**4.2.3**, Scheme 2.1.3). It is not clear whether this compound is the result of increased ion separation due to the crown ether, which causes an activation of the silanide, or if it is formed during the reduction of bromosilane to silanide before the crown ether is added.



Scheme 2.1.3. Reduction of  $t\text{Bu}_2\text{MeSiBr}$  (**1**) with sodium metal

The silylated biphenyl radical **3** crystallizes in the monoclinic space group  $P2_1/c$  (Figure 2.1.1). The solid state structure contains separated ion pairs, with the coordination sphere of the sodium atom occupied by the oxygen donors 18-crown-6 and THF. The Si-C<sub>Ar</sub> (1.875(4) Å), the Si-C<sub>Me</sub> (1.891(4) Å) and the Si-C<sub>tBu</sub> (1.932(5), 1.931(4) Å) distances are in the normal range for Si-C single bonds.

The rings of the biphenyl moiety are strictly coplanar, as dictated by a crystallographic inversion center in the middle of the C1-C1' bond. This is also the case in the solid state structure of the biphenyl radical anion in the ion pair bis(tetraglyme)potassium biphenyl.<sup>[61]</sup> In that system, however, relatively large thermal parameters were observed for the ring carbon atoms, making a disordered arrangement of non-coplanar rings likely. For **3**, this sort of disorder is unlikely, since only small thermal parameters are observed. In the solid state, the related biphenyl radical salts bis(tetraglyme)rubidium biphenyl and bis(triglyme)sodium biphenyl display dihedral angles between the two rings of 9.4° and 7.3°, respectively.<sup>[61, 62]</sup>



In order to compare the structure of **3** to a related neutral species, 4,4'-bis(trimethylsilyl)biphenyl (**4**)<sup>[63-65]</sup> was prepared, and X-ray quality crystals were obtained from saturated CH<sub>3</sub>CN solution (4.2.5). The asymmetric unit in the monoclinic crystals (*C2/c*) of **4** contains 4.5 independent molecules, the last of which is completed via a twofold rotational axis. The Si-C<sub>Ar</sub> bond lengths (1.877(10) Å avg) are similar to the corresponding distance in the radical anion. The Si-C<sub>Me</sub> distances (1.866(10) Å avg) are somewhat shorter than the Si-C<sub>alkyl</sub> distances in the radical anion. This effect is likely due to the reduced steric congestion in the Me<sub>3</sub>Si substituent in **4** compared to the *t*Bu<sub>2</sub>MeSi moiety in **3**. The torsion angle between the rings of the biphenyl unit in **4** varies between 14.6(6)° and 37.5(4)°, with an average of 31.2(6)°.

In biphenyl and its derivatives, the torsion angle between the two rings reflects a balance between electron delocalization, for which a planar arrangement is favorable, and mutual steric hindrance of the *ortho*-protons, ideally resulting in a torsion angle of 90°. Due to the unpaired electron, which is significantly stabilized by delocalization, the planar arrangement is much more favorable for the radical anion. In the neutral species, this effect is less important, resulting in a significant torsion angle.

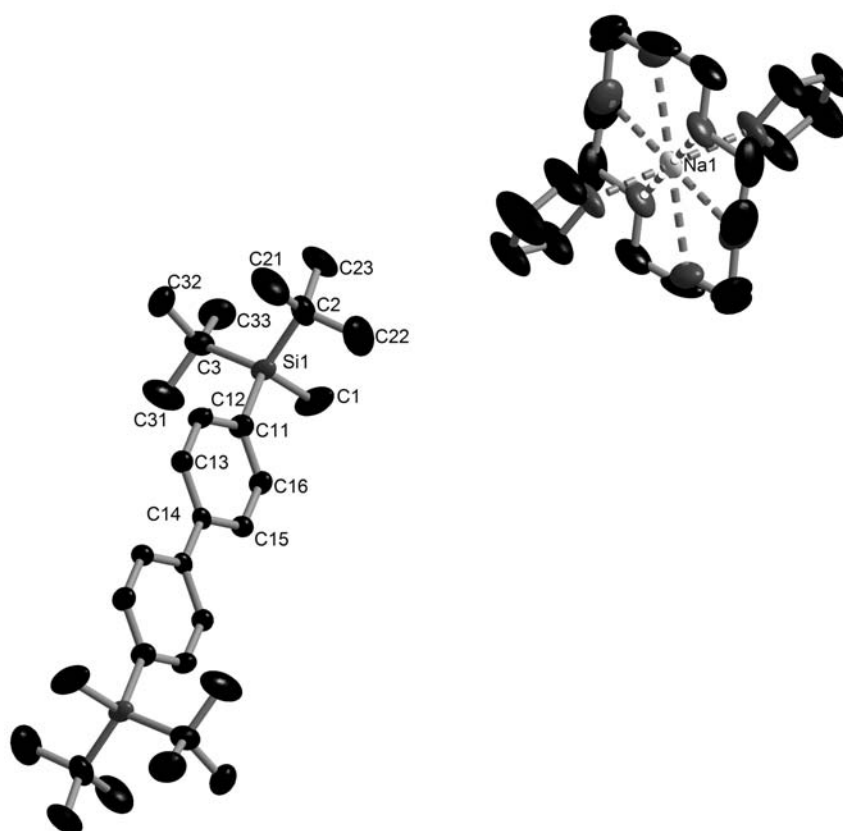


Figure 2.1.1. Molecular structure of **3**. Hydrogen atoms have been omitted for clarity.

In the literature, only one example of a structurally characterized 4,4'-disilylbiphenyl is known, 4,4'-bis(dimethylhydroxysilyl)biphenyl.<sup>[66]</sup> This species forms an extensive hydrogen-bonded network, which is believed to influence the conformational characteristics of the solid state structure. Nevertheless, the ring twist angle in the biphenyl moiety (39°) is comparable to that in the neutral compound **4**, but much larger than in the radical biphenyl derivative **3**. No significant differences in the Si-C bond lengths in comparison to **3** and **4** are observed.

Unfortunately, the crystals of **3** are extremely sensitive to air and moisture, so that after removing a sample for X-ray crystallographic studies, only a colorless residue remained. This residue was characterized via multinucleus NMR spectroscopy, and the results are consistent with the neutral species, 4,4'-bis(di-*tert*-butylmethylsilyl)biphenyl (**4.2.4**). Attempts to prepare this compound via direct organometallic synthesis were unsuccessful. Both the Grignard reaction using 4,4'-biphenyldimagnesium dibromide and **1** and the Wurz-coupling of 4,4'-dibromobiphenyl and **1** with elemental sodium led to nearly quantitative recovery of bromosilane **1**. Changes in the aromatic region of the <sup>1</sup>H and <sup>13</sup>C NMR spectra suggest that the bromobiphenyl has reacted with itself. These reactions, however, were not pursued further. Treatment of 4,4'-dibromobiphenyl with *n*-butyllithium resulted in butylation rather than lithiation, and this route was also deemed unpromising.

Despite the difficulties associated with the preparation of smaller sodium silanides, the straightforward synthesis of sterically hindered species ensures their accessibility and allows the exploration of their utility as starting materials for sodium silyl chalcogenolates.

### 2.1.2 Sodium silyl chalcogenolates

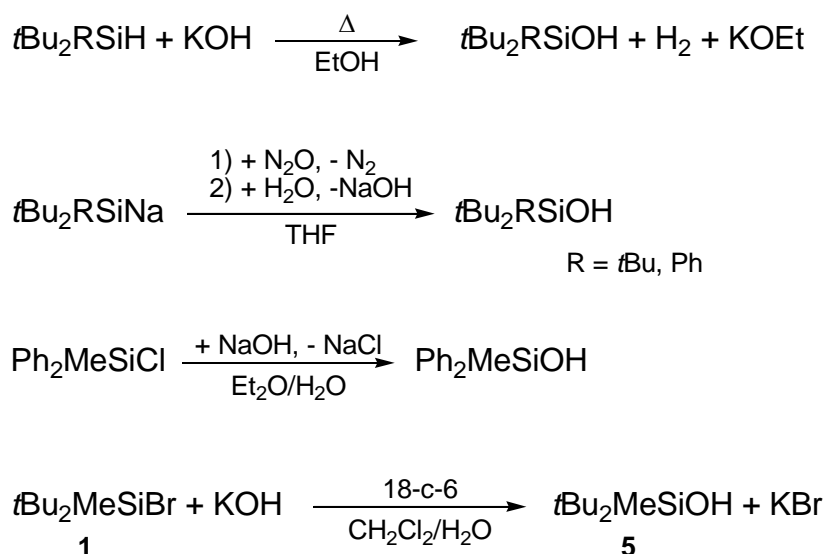
The primary target molecules of the work presented here, sodium silyl chalcogenolates R<sub>3</sub>SiENa (E = O, S, Se, Te), represent convenient precursors to chalcogenolate transition metal complexes. The wide range of electronegativity displayed by the chalcogens mandates a certain diversity in the preparative methods used in the synthesis of silyl chalcogenolates. Due to this variety of potential synthetic methods and the interesting structural properties displayed by chalcogenolates, these compounds merit a closer look.

#### 2.1.2.1 Sodium siloxides

Metal siloxides R<sub>3</sub>SiOM (also referred to as silanolates) have received significant attention in the literature. Transition metal complexes ligated by R<sub>3</sub>SiO<sup>-</sup> have been shown to display intriguing properties, including C-H activation,<sup>[8]</sup> olefin-to-alkylidene rearrangement<sup>[9]</sup> and the catalytic hydrosilylation of alkenes and homocoupling of unsaturated silicon-containing

compounds.<sup>[34]</sup> These transition metal complexes are often prepared via alkali metal siloxides, which in turn can be synthesized by treating silanols with alkali metals.

In the literature, two general methods for the preparation of triorganylsilanols are described. The first involves the oxidation of silanes; the second is based on the hydrolysis of precursor silyl halides or pseudohalides.<sup>[67]</sup> Because the silyl halides of sterically overloaded species such as *t*Bu<sub>3</sub>SiX and *t*Bu<sub>2</sub>PhSiX (X = halide) are comparatively stable to hydrolysis, the oxidation route is the most convenient method to prepare these species, and is generally carried out using KOH in boiling methanol or ethanol (Scheme 2.1.4).<sup>[55, 68]</sup> The sterically somewhat less hindered *t*Bu<sub>2</sub>PhSiOH can also be prepared from *t*Bu<sub>2</sub>PhSiF and NaOH in boiling THF.<sup>[69]</sup> An alternative strategy for the synthesis of these sterically hindered silanols starts from silanides (cf. 2.1.1.1), which are first oxidized with N<sub>2</sub>O to the corresponding siloxides and finally hydrolyzed to silanols.<sup>[70]</sup> The halides of less sterically hindered silanes, on the other hand, are easily converted to silanols. For example, Ph<sub>2</sub>MeSiOH is prepared from Ph<sub>2</sub>MeSiCl and NaOH in an Et<sub>2</sub>O/H<sub>2</sub>O mixture (Scheme 2.1.4).<sup>[71]</sup> For *t*Bu<sub>2</sub>MeSiOH, one literature synthesis uses KOH in neat refluxing *t*Bu<sub>2</sub>MeSiF.<sup>[72]</sup> Since *t*Bu<sub>2</sub>MeSiF is not easily accessible, a new route starting from the silyl bromide was employed.



Scheme 2.1.4. Synthesis of silanols

In a two-phase reaction of *t*Bu<sub>2</sub>MeSiBr (**1**) in CH<sub>2</sub>Cl<sub>2</sub> and KOH in H<sub>2</sub>O using 18-crown-6 as a phase-transfer catalyst, *t*Bu<sub>2</sub>MeSiOH (**5**) is formed in good yield (4.3.1, Scheme 2.1.4). The crude silanol **5** is a colorless oil. Upon standing undisturbed for a period of several weeks, colorless needles form. The crystals belong to the monoclinic space group *P*2<sub>1</sub>/*n*, and the asymmetric unit contains four molecules of **5**, which are hydrogen bonded to a bromide ion

(Figure 2.1.2). Charge neutrality is maintained by an  $\text{H}_3\text{O}^+$  ion. This equivalent of HBr is presumably due to slow ambient hydrolysis of small amounts of residual **1** after organic work up. The asymmetric unit also contains one additional water molecule.

The four crystallographically independent molecules of **5** all have similar structural parameters, which are in the expected range for organosilanols. The hydrogen bond distances between the silanol protons and the bromide ion are between 2.536(2) and 2.594(2) Å. The hydrogen bond O-H-Br angles are nearly linear, at 162.6° to 174.2°. The coordination of the bromide atom is irregular, with H-Br-H angles between 78.85° and 139.91°.

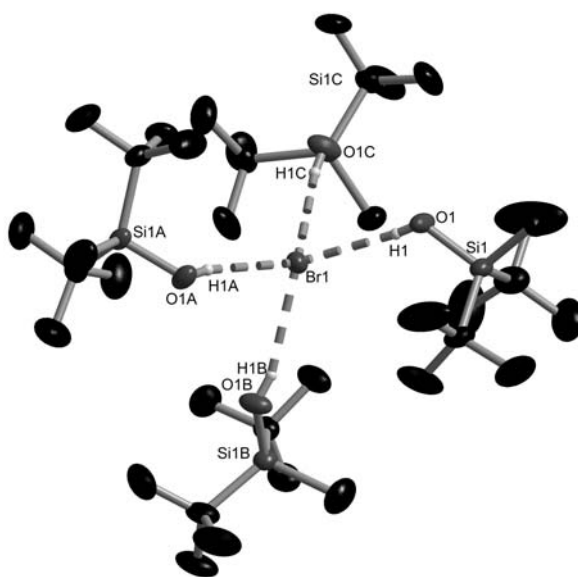
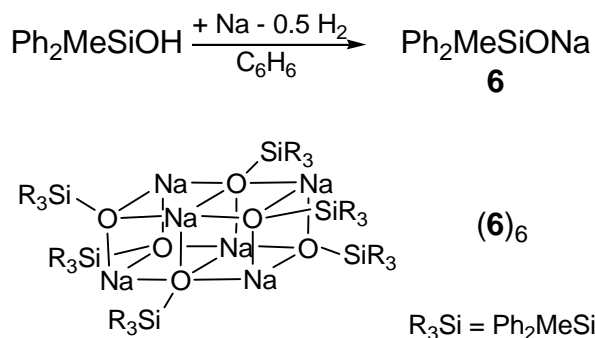


Figure 2.1.2. Solid state structure of the hydrogen-bonded anion of **5**·1/4HBr. Hydrogen atoms not involved in hydrogen bonding have been omitted for clarity.

Sodium siloxides  $\text{R}_3\text{SiONa}$  can be prepared by a number of methods.  $\text{Ph}_2\text{MeSiONa}$ , for example, was first reported as the product of the cleavage of  $\text{Ph}_2\text{MeSi-O-SiMePh}_2$  with NaOH in alcohol.<sup>[73]</sup> Another route, as mentioned above, employs the  $\text{N}_2\text{O}$  oxidation of sodium silanides in THF solution, and is most effective for bulky silyl residues, whose anions are readily synthesized.<sup>[70]</sup> Arguably the most common route to sodium siloxides, however, is the reduction of silanols with elemental sodium.<sup>[68, 74]</sup>

When  $\text{Ph}_2\text{MeSiOH}$  is reduced with sodium metal in benzene,  $\text{Ph}_2\text{MeSiONa}$  (**6**) is produced cleanly and in high yield (4.3.2, Scheme 2.1.5). Recrystallization from benzene yields large colorless crystals, which reveal a hexameric structure (Figure 2.1.3, selected bond lengths and angles Table 2.1.1). A schematic representation of the core of this structure can be found in Figure 2.1.5, upper left. The asymmetric unit contains one complete hexamer and two half hexamers. These oligomers adopt a double heterocubane box-type structure formed by six

sodium atoms and six oxygen atoms, which sit at the vertices and at positions roughly bisecting the long edges of the box. The four corner sodium atoms are each coordinated by three oxygen atoms; the corner oxygen atoms are coordinated by three sodium atoms in addition to the silyl residue. The remaining two sodium atoms are located one each in the middle of opposite long edges of the box and are coordinated to four oxygen atoms. Similarly, the remaining two oxygen atoms are located one each in the middle of the other two long edges and are coordinated to four sodium atoms and one silicon atom.

Scheme 2.1.5. Synthesis of **6****Table 2.1.1.** Selected average bond lengths [ $\text{\AA}$ ] and angles [ $^\circ$ ] for **(6)**<sub>6</sub>

	hexamer 1	hexamer 2	hexamer 3
Na-O	2.342(5)	2.339(5)	2.431(5)
O-Si	1.603(5)	1.612(4)	1.627(5)
Si-C <sub>Ph</sub>	1.897(9)	1.901(7)	1.910(7)
Si-CH <sub>3</sub>	1.878(9)	1.882(7)	1.883(9)
O-Na-O	93.6(2) <sup>[a]</sup>	93.6(2) <sup>[a]</sup>	93.4(2) <sup>[a]</sup>
	171.0(2) <sup>[b]</sup>	173.4(2) <sup>[b]</sup>	172.4(2) <sup>[b]</sup>
Na-O-Na	86.1(2) <sup>[a]</sup>	86.0(2) <sup>[a]</sup>	86.2(2) <sup>[a]</sup>
	164.4(2) <sup>[b]</sup>	163.4(2) <sup>[b]</sup>	166.2(2) <sup>[b]</sup>

[a] vertices (ideal = 90°); [b] edges (ideal = 180°)

The hexamers in **(6)**<sub>6</sub> do not form regular rectangular prisms. The angles around corner sodium atoms tend to be somewhat larger than 90°, while the angles around corner oxygen atoms are generally somewhat smaller than 90°. The edge O-Na-O angles are, on average, 172° and bent toward the center of the box, while the Na-O-Na edge angles are a bit smaller, at an average of 165° and bent away from the center of the box.

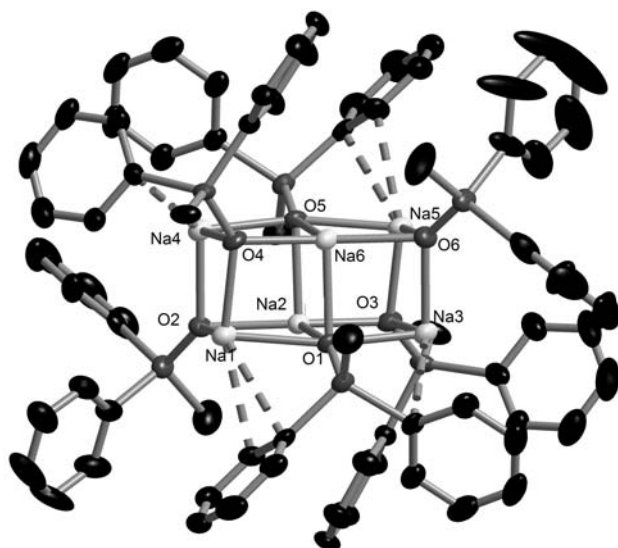


Figure 2.1.3. Solid state structure of  $(\mathbf{6})_6$ . Hydrogen atoms have been omitted for clarity.

The corner sodium atoms, which are only coordinated by three oxygen atoms, are unsupported by any external donor, such as solvent. They do, however, form relatively short contacts to the *ipso* and to one of the *ortho* carbon atoms of one or more neighboring phenylsilyl residues. Of the eight coordinatively unsaturated sodium atoms in the asymmetric unit, only one has a single short contact to an *ipso* carbon atom. Four more sodium atoms have distances under 3.0 Å to both the *ipso* and one *ortho* carbon atom of a single phenyl ring. The remaining three sodium atoms all display a single Na-C distance under 3.0 Å to an *ipso* carbon atom as well as somewhat longer distances (3.0-3.2 Å) to an *ortho* carbon on the same ring and to the *ipso* carbon on a second ring. One of these sodium atoms also displays a short (3.061(6) Å) distance to an *ortho* carbon atom of the second ring. These Na-C distances are comparable to those found in  $(\text{Ph}_3\text{SiSNa})_6(\text{toluene})_2$ , which also displays a double heterocubane structure in which two molecules of toluene stabilize two of the corner sodium atoms, whereas the other two are supported only by contacts to the phenyl substituents of the silyl thiolate.<sup>[75]</sup>

The double heterocubane structure found for  $(\mathbf{6})_6$  is not unprecedented for an alkali metal chalcogenolate, but such structures are rare, particularly for silyl chalcogenolates, and nearly all of the reported examples are supported by additional donor molecules (THF, toluene, diethylether, etc.).<sup>[75-78]</sup> Sodium siloxides, especially those with significant steric bulk, are much more prone to crystallize as tetrameric heterocubanes. These heterocubanes are often free of additional donors, and siloxides  $t\text{Bu}_3\text{SiONa}$ ,  $t\text{Bu}_2\text{PhSiONa}$ <sup>[70]</sup> and  $t\text{Bu}_2\text{MeSiONa}$ <sup>[72]</sup> all adopt this structure. Tetrameric heterocubane structures of siloxides with smaller organic residues have also been reported, although these tend to incorporate donor molecules. For

example,  $\text{Me}_3\text{SiONa}$  displays a heterocubane structure in the solid state in which each sodium atom is supported by one molecule of  $(\text{Me}_2\text{N})_3\text{P}=\text{O}$  solvate.<sup>[79]</sup> A similar tetrameric structure of  $\text{Ph}_3\text{SiONa}$  hydrated by three water molecules has been reported,<sup>[80]</sup> as well as the potassium salt of the same siloxide supported by DME.<sup>[81]</sup> The benzene-supported heterocubane structure of  $\text{PhMe}_2\text{SiOK}$  has also been described.<sup>[82]</sup>

When crystalline  $(\mathbf{6})_6$  is dissolved in THF, the hexameric structure is broken down. Upon concentration of the solution and cooling, the more common tetrameric structure is formed (**4.3.3.1**), in this case supported by four molecules of THF. The tetramer  $(\mathbf{6})_4(\text{THF})_4$  crystallizes in the orthorhombic space group *Aba2* with one half tetramer in the asymmetric unit, which is related to its second half via a two-fold rotational axis. In this heterocubane structure, each sodium atom is bonded to one molecule of THF (Figure 2.1.4, selected bond lengths and angles Table 2.1.2, schematic representation Figure 2.1.5, upper right). As is found for  $(\mathbf{6})_6$ , the angles around corner sodium atoms are somewhat larger than  $90^\circ$ , while those around corner oxygen atoms are somewhat smaller than  $90^\circ$ . Na-O bond lengths vary between  $2.273(3) \text{ \AA}$  and  $2.352(2) \text{ \AA}$  and are in the same range as in  $(\mathbf{6})_6$ . As is to be expected for the four-coordinate sodium atoms, no short Na-C contacts are found in this structure.

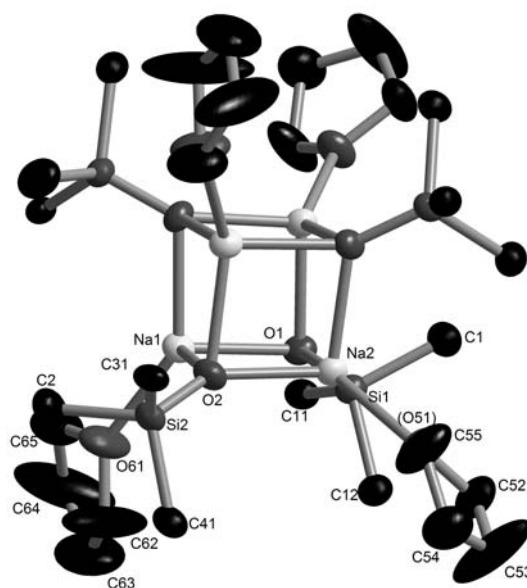


Figure 2.1.4. Solid state structure of  $(\mathbf{6})_4(\text{THF})_4$ . Hydrogen atoms and phenyl ring carbon atoms and not bonded to silicon have been omitted for clarity.

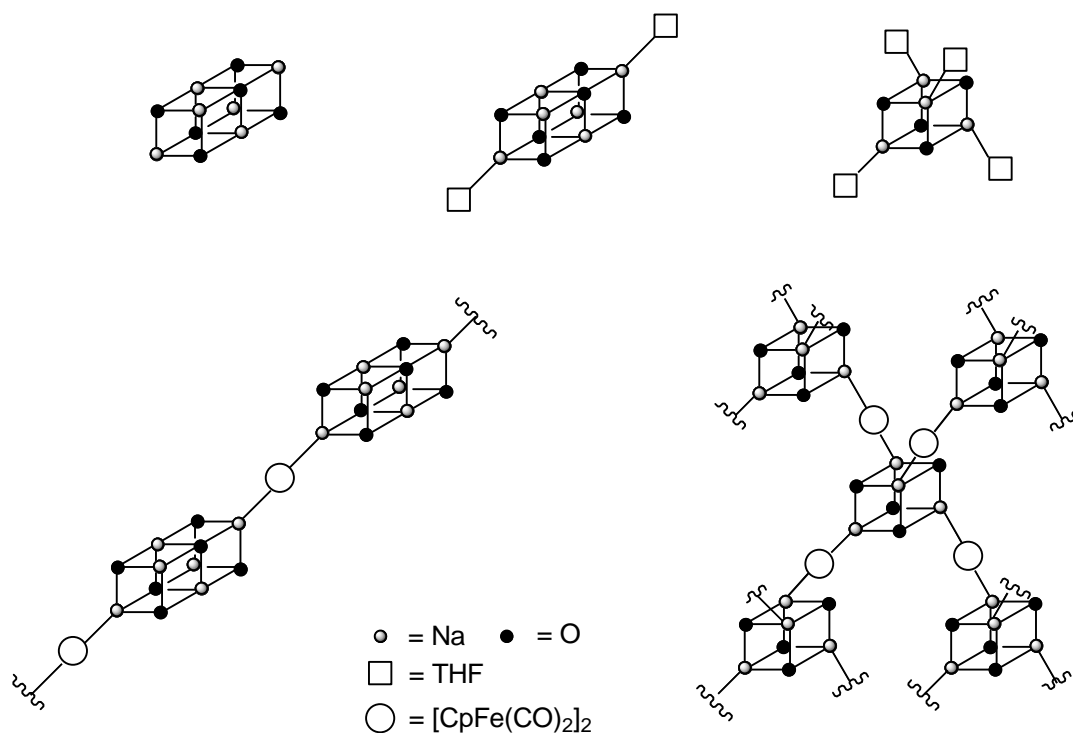


Figure 2.1.5. Schematic representation oligomers and adducts of **6**

This tetrameric structure  $(\mathbf{6})_4(\text{THF})_4$ , however, is only formed when an excess of THF is present. If THF is removed in vacuo from a solution of **6** and the residue recrystallized from toluene, the hexameric, double heterocubane structure  $(\mathbf{6})_6(\text{THF})_2$  is recovered, in which the  $(\mathbf{6})_6$  hexamer is supported by two molecules of THF, which coordinate to sodium atoms at opposite corners of the double heterocubane box (Figure 2.1.6, 4.3.3.2). A schematic representation of this structure is found in Figure 2.1.5, upper center; selected bond lengths and angles can be found in Table 2.1.2. This oligomer crystallizes in the triclinic space group  $P-1$ , and its general structural parameters are similar to those of the donor-free hexamer  $(\mathbf{6})_6$ . The Na-O(siloxide) bonds of the unsupported sodium atom (there is only one in the asymmetric unit; it is related to its equivalent via a crystallographic inversion center) are somewhat shorter than for the THF-bound sodium atom (2.249(2) and 2.272(2) Å vs. 2.288(2) and 2.323(2) Å). Analogous to the sodium atoms in  $(\mathbf{6})_6$ , the unsupported sodium atom displays a short contact (2.731(3) Å) to the *ipso* carbon atom of a neighboring phenylsilyl residue and a somewhat longer distance (2.922(9) Å) to one of the *ortho* carbon atoms on the same phenyl ring.



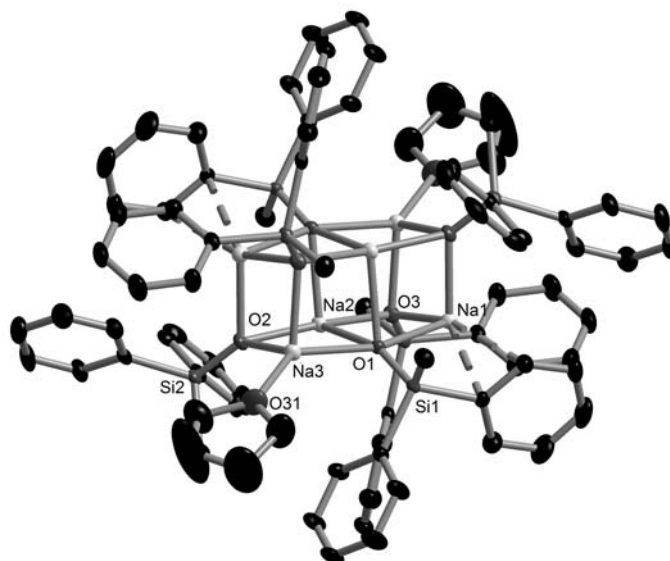


Figure 2.1.6. Solid state structure of  $(\mathbf{6})_6(\text{THF})_2$ . Hydrogen atoms have been omitted for clarity.

Apparently, an excess of donor is needed to break down the  $(\mathbf{6})_6$  double heterocubane. Weak donors, however, are not able to destroy this structure. When colorless  $(\mathbf{6})_6$  is dissolved in toluene and treated with an excess of dark brown  $[\text{CpFe}(\text{CO})_2]_2$ , which has been shown to form adducts via the oxygen atoms of the bridging carbonyl ligands,<sup>[83, 84]</sup> a red solid is formed, which quickly turns brown when exposed to atmospheric conditions (4.3.3.3). Recrystallization from toluene yields X-ray quality crystals. The solid-state structure contains polymeric chains of  $(\mathbf{6})_6[\text{CpFe}(\text{CO})_2]_2$  in which individual double heterocubane units are bridged by iron carbonyl dimers, with each bridging carbonyl ligand forming an adduct with a sodium atom of a different hexameric moiety (Figure 2.1.7, selected bond lengths and angles Table 2.1.2; schematic depiction Figure 2.1.5, lower left). This is, in essence, the same situation as in  $(\mathbf{6})_6(\text{THF})_2$ , where the monofunctional donor THF has been exchanged for the bifunctional donor  $[\text{CpFe}(\text{CO})_2]_2$ .

The Na-OC interaction in  $(\mathbf{6})_6[\text{CpFe}(\text{CO})_2]_2$ , however, is unstable in solution. The UV-vis spectrum of the adduct in toluene solution is identical to that of  $[\text{CpFe}(\text{CO})_2]_2$  alone, and the NMR spectra ( $^1\text{H}$ ,  $^{13}\text{C}$  and  $^{29}\text{Si}$ ) of  $(\mathbf{6})_6[\text{CpFe}(\text{CO})_2]_2$  are identical to a superposition of the individual spectra of  $[\text{CpFe}(\text{CO})_2]_2$  and  $\mathbf{6}$ .

In contrast, the solid-state IR spectrum (KBr pellet) of  $(\mathbf{6})_6[\text{CpFe}(\text{CO})_2]_2$  is significantly different than that of free  $[\text{CpFe}(\text{CO})_2]_2$ . It displays a band in the bridging CO region that is at much lower frequency than for the free dimer (1727 vs. 1755  $\text{cm}^{-1}$ ) and one in the terminal CO region that is of much higher wave number than for the free dimer (2002 vs. 1954  $\text{cm}^{-1}$ ). This is consistent with adduct formation, which reduces the electron density in the bridging

CO ligands, allowing them to accept more electron density from the iron atoms through  $\pi$ -backbonding. Thus, the CO bond is weakened, causing a shift of the stretching band to lower frequency. Strengthening the backbonding to the bridging carbonyls simultaneously weakens the backbonding to the terminal carbonyls, leading to a shift to higher wave numbers.

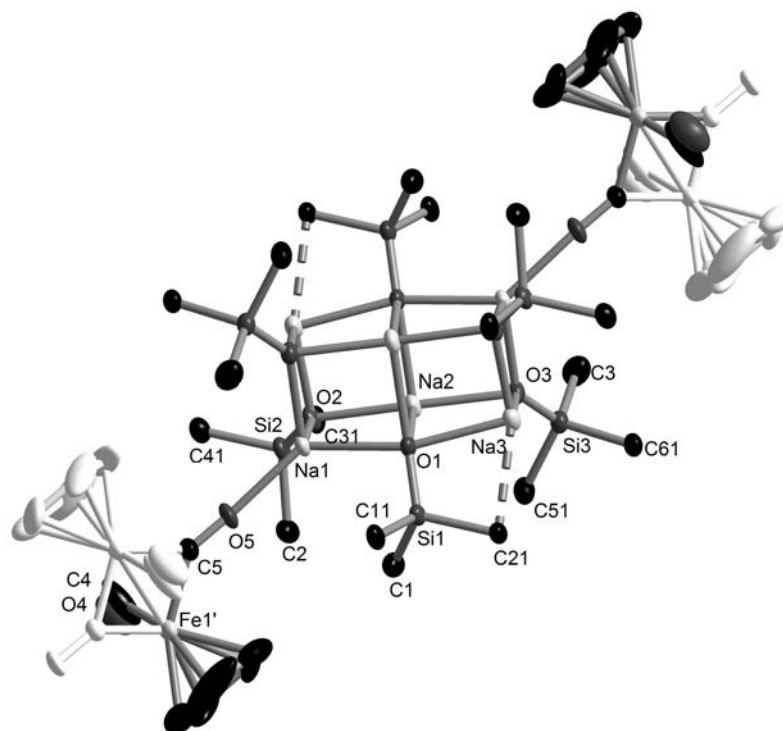


Figure 2.1.7. Solid state structure of  $(\mathbf{6})_6[\text{CpFe}(\text{CO})_2]_2$ . Hydrogen atoms and phenyl ring carbon atoms not bonded to silicon have been removed for clarity.

The structural parameters of  $(\mathbf{6})_6[\text{CpFe}(\text{CO})_2]_2$ , which crystallizes in the triclinic space group  $P-1$ , are comparable to those of the other two hexamers. As in  $(\mathbf{6})_6(\text{THF})_2$ , the Na-O(siloxide) bonds of the donor-supported sodium atom are somewhat longer than those of its unsupported counterpart (2.263(3) and 2.286(3) vs. 2.251(3) and 2.279(3) Å). The unsupported sodium atom in  $(\mathbf{6})_6[\text{CpFe}(\text{CO})_2]_2$  forms a short contact (2.712(10) Å) to the *ipso* carbon atom of a neighboring phenylsilyl residue. In this case, the distances to the *ortho* carbon atoms on the same ring are considerably longer (3.069(12) and 3.202(6) Å). The sodium-carbonyl Na-O-C angle (168.0(3)°) is similar to that found for the compound  $[\text{CpFe}(\text{CO})_2]_2\text{Na}(\text{THF})_4$  (170.5°) which displays the same type of Na-OC interaction.<sup>[83]</sup>

The iron atoms and cyclopentadienyl ligands of the  $[\text{CpFe}(\text{CO})_2]_2$  donor molecules are disordered over two positions, which have an occupancy ratio of roughly 1:4. This disorder was not refined for the carbonyl ligands, resulting in large anisotropic displacement parameters for the terminal carbonyls, which appear to bind to the iron atoms non-linearly

(O4-C4-Fe1 = 155.4(7)°, O4-C4-Fe1'#2 = 135.7(7)°). This unusual geometry is almost certainly an artifact of the disorder.

**Table 2.1.2.** Selected average bond lengths [Å] and angles [°] for adducts of **6**

	( <b>6</b> ) <sub>4</sub> (THF) <sub>4</sub>	( <b>6</b> ) <sub>6</sub> (THF) <sub>2</sub>	( <b>6</b> ) <sub>6</sub> [CpFe(CO) <sub>2</sub> ] <sub>2</sub>	( <b>6</b> ) <sub>4</sub> · {[CpFe(CO) <sub>2</sub> ] <sub>2</sub> } <sub>2</sub>
Na-O(siloxide)	2.310(3)	2.366(2)	2.368(3)	2.348(6)
O-Si	1.594(2)	1.608(2)	1.612(2)	1.606(5)
Si-C <sub>Ph</sub>	1.898(3)	1.901(2)	1.905(4)	1.898(7)
Si-CH <sub>3</sub>	1.885(4)	1.881(2)	1.897(4)	1.863(8)
O(siloxide)-Na-	94.0(1) <sup>[a]</sup>	94.0(1) <sup>[a]</sup>	94.4(1) <sup>[a]</sup>	91.8(2) <sup>[a]</sup>
O(siloxide)		173.0(1) <sup>[b]</sup>	162.2(1) <sup>[b]</sup>	
Na-O(siloxide)-	85.8(1) <sup>[a]</sup>	79.9(1) <sup>[a]</sup>	85.9(1) <sup>[a]</sup>	88.1(2) <sup>[a]</sup>
Na		163.3(1) <sup>[b]</sup>	174.2(1) <sup>[b]</sup>	

[a] vertices (ideal = 90°); [b] edges (ideal = 180°)

The 2:1 adduct of **6** and [CpFe(CO)<sub>2</sub>]<sub>2</sub>, (**6**)<sub>4</sub>{[CpFe(CO)<sub>2</sub>]<sub>2</sub>}<sub>2</sub>, can be isolated from the reaction of CpFe(CO)<sub>2</sub>I with **6** (4.6.6, cf. 2.2.1). This compound exhibits a tetrameric, heterocubane siloxide moiety. Each sodium atom is bonded to the oxygen atom of a bridging carbonyl ligand of the iron complex dimer. Each bridging carbonyl ligand, in turn, is coordinated to a sodium atom, forming a three dimensional network (Figure 2.1.8, selected bond lengths and angles in Table 2.1.2; schematic representation Figure 2.1.5, lower right). As is the case for (**6**)<sub>6</sub>[CpFe(CO)<sub>2</sub>]<sub>2</sub>, this adduct is not stable in solution, and its NMR and UV-vis spectra are the same as those of the starting materials separately. Here, too, differences in the solid-state IR spectrum compared to [CpFe(CO)<sub>2</sub>]<sub>2</sub> can be observed, which correspond to an increase of backbonding to the bridging carbonyls and a decrease of backbonding to the terminal carbonyls.

The structural parameters of this adduct, which crystallizes in the tetragonal space group *I4<sub>1</sub>/acd*, are similar to those of the other compounds described here. There are no Na-C distances smaller than 3.5 Å, and the disorder found for the 6:1 adduct is not observed. The Na-O-C angle (170.1(5)°) is similar to that in the hexameric adduct (**6**)<sub>6</sub>[CpFe(CO)<sub>2</sub>]<sub>2</sub> and to those found for [CpFe(CO)<sub>2</sub>]<sub>2</sub>Na(THF)<sub>4</sub>.<sup>[83]</sup>

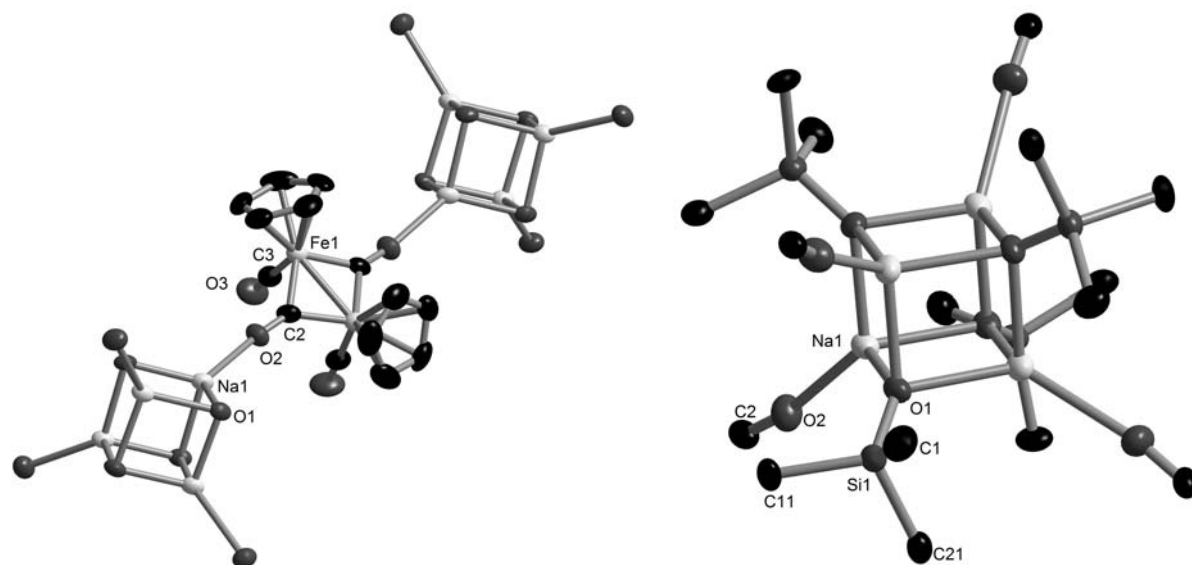


Figure 2.1.8. Molecular structure of  $(\mathbf{6})_4\{[\text{CpFe}(\text{CO})_2]_2\}_2$ . Left: connectivity surrounding  $[\text{CpFe}(\text{CO})_2]_2$  (for clarity, only Na and O atoms of the heterocubane units are shown, and hydrogen atoms have been omitted). Right: connectivity surrounding a  $(\text{Ph}_2\text{MeSiONa})_4$  unit (for clarity, only the bridging carbonyl of bound  $[\text{CpFe}(\text{CO})_2]_2$  are shown, and hydrogen atoms and phenyl ring carbon atoms not bonded to silicon have been removed).

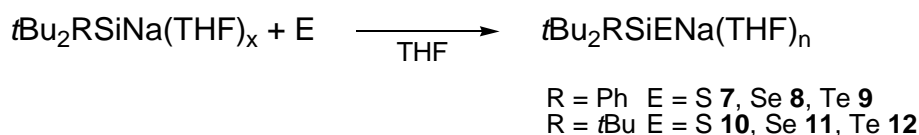
### 2.1.2.2 Higher silyl chalcogenolates $t\text{Bu}_2\text{RSiENa}$ ( $\text{R} = t\text{Bu}, \text{Ph}$ ; $\text{E} = \text{S}, \text{Se}, \text{Te}$ )

Due to the lower electronegativity of the higher chalcogens (S, Se, Te), it is not practical to prepare silyl thiolates, selenolates, and tellurolates by the same routes as applied for siloxides. Although silyl chalcogenolates have received significant attention in the literature in recent years, no single method for their preparation has been favored. When the final synthetic goal is a transition metal complex, the corresponding chalcogenols can be deprotonated *in situ* by metal complexes with basic ancillary ligands.<sup>[85, 86]</sup> Alternatively, disilyl chalcogenides  $\text{R}_3\text{SiE-SiMe}_3$  have been employed in substitution reactions with metal halides, leading to the thermodynamically favorable release of  $\text{Me}_3\text{SiX}$  and coordination of an  $\text{R}_3\text{SiE}$ -ligand to the metal center.<sup>[3, 4]</sup> For alkali metal chalcogenolates, different approaches are used. For example, lithium silylthiolates of the type  $\text{Me}_2\text{RSiSLi}$  ( $\text{R} = \text{Me}, t\text{Bu}$ ) were prepared by cleavage of cyclotrisilathiane  $(\text{Me}_2\text{SiS})_3$  with methyllithium or *tert*-butyllithium.<sup>[14]</sup> Potassium hypersilylchalcogenolates  $(\text{Me}_3\text{Si})_3\text{SiEK}$  ( $\text{E} = \text{S}, \text{Se}, \text{Te}$ ) have been prepared by treating  $(\text{Me}_3\text{Si})_4\text{Si}$  with  $\text{KO}t\text{Bu}$  and elemental chalcogen (S, Se, Te).<sup>[87, 88]</sup>

None of these methods, however, is suitable for the preparation of  $t\text{Bu}_3\text{SiENa}$  and  $t\text{Bu}_2\text{PhSiENa}$ . The bulky organic substituents of these target molecules make the synthesis of corresponding cyclotrisilathianes, for instance, impractical. Of the chalcogenols relevant to the

targeted ligands, only  $t\text{Bu}_3\text{SiSH}$  is known.<sup>[21]</sup> For these reasons, a different synthetic route was applied. This method, previously described by Arnold for a number of related compounds,<sup>[38, 89]</sup> involves the insertion of elemental chalcogen into the silicon-alkali metal bond of precursor alkali silanides.

When elemental chalcogens (S, Se and Te) are treated with a slight excess of sodium silanide  $t\text{Bu}_3\text{SiNa}$  or  $t\text{Bu}_2\text{PhSiNa}$  in THF, the silyl chalcogenolates  $t\text{Bu}_2\text{RSiENa}$  (R = Ph,  $t\text{Bu}$ ; E = S, Se, Te; **7 – 12**) are formed cleanly (Scheme 2.1.6).<sup>[90]</sup> The reaction with sulfur to form **7** and **10** is vigorous, making it advisable to add the silanide dropwise to a cooled suspension of sulfur in THF (4.3.4). Only minor heat evolution is observed for selenium and tellurium, and the reactions with these elements can be safely carried out at room temperature (4.3.5). The reactions with sulfur are faster than with selenium and tellurium, but in all cases conversion is complete after stirring overnight. Concentration of the orange reaction solutions leads to the deposition of colorless crystals of chalcogenolates **7 – 12**.



Scheme 2.1.6. Synthesis of sodium silyl chalcogenolates

This synthesis should be applicable to all compounds for which the alkali metal silanides are available, and it would have been desirable to extend it to derivatives of  $t\text{Bu}_2\text{MeSiNa}$  (**2**). However, this project was not pursued due to the complications associated with the synthesis of this smaller silanide, as described in section 2.1.1.2.

When considering the  $^1\text{H}$ ,  $^{13}\text{C}$ , and  $^{29}\text{Si}$  NMR spectra of the chalcogenolates **7 – 12**, certain general trends can be observed. Upon the replacement of an alkyl group (in **10 – 12**) with an aryl substituent (in **7 – 9**), the signals of the  $^{29}\text{Si}$ ,  $^{13}\text{C}$  (CCH<sub>3</sub> and CCH<sub>3</sub>), and  $^1\text{H}$  (CCH<sub>3</sub>) nuclei are shifted downfield in the  $t\text{Bu}_3\text{Si}$ - compounds as compared to the corresponding compounds with  $t\text{Bu}_2\text{PhSi}$ - substituents. In addition, the signals of the silicon atoms and the quaternary carbon atoms of the *tert*-butyl groups are shifted downfield as the chalcogen is changed from sulfur to selenium to tellurium in the series **7 – 9** and **10 – 12**. This effect is always more pronounced for the  $^{29}\text{Si}$  signals than for the  $^{13}\text{C}$  signals of the quaternary carbon atoms, and the relative difference in chemical shift is generally larger between sulfur and selenium than between selenium and tellurium. The aromatic and alkyl proton signals and the signals of the primary  $^{13}\text{C}$  atoms also tend to be shifted downfield in compounds containing

the heavier chalcogens, but the change in chemical shift is smaller, making such trends more difficult to discern.

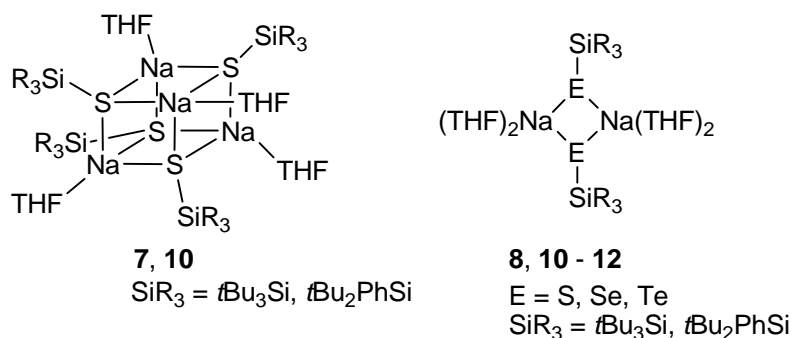


Figure 2.1.9. Schematic representation of the solid-state structures of sodium silyl chalcogenolates

X-ray quality crystals of five of the six sodium silyl chalcogenolates **7** – **12** can be obtained from the THF reaction solutions. For **9**, it was not possible to isolate X-ray quality crystals, despite numerous attempts. Schematic representations of the solid state structures can be found in Figure 2.1.9.

Only one of these compounds (**7**, **4.3.4.1**) crystallizes out of THF solution as a heterocubane (monoclinic,  $P2_1/c$ ; Figure 2.1.10, selected bond lengths and angles Table 2.1.3). Unlike *t*Bu<sub>3</sub>SiONa and *t*Bu<sub>2</sub>PhSiONa, which were crystallized from heptane and are unsupported by external donor, each sodium atom in the tetrameric structure is bound to one molecule of THF.

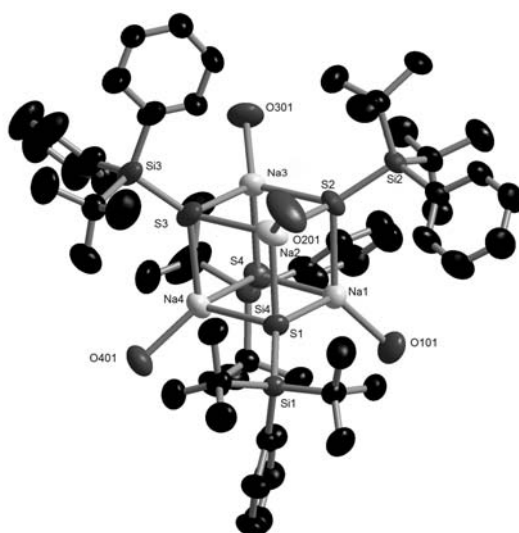


Figure 2.1.10. Solid state structure of **7**(THF). For clarity, only the oxygen atoms of the THF donor molecules are shown.

The heterocubane structure of thiolate **7** is also much closer to a regular cube than that of the homologous siloxide, with Na-S-Na angles which average  $87.71(6)^\circ$  and average S-Na-S angles of  $92.21(6)^\circ$ . The Na-S distances vary between  $2.727(2)$  and  $2.798(2)$  Å and S-Si bond lengths are between  $2.0815(13)$  and  $2.0903(14)$  Å. The Si-C distances vary only little and are in the expected range.

The other sodium silyl thiolate (**10**, 4.3.4.2) crystallizes out of THF as a dimer (monoclinic,  $P2_1/c$ ), with each equivalent of thiolate solvated by two equivalents of THF. A planar four-membered  $S_2Na_2$  ring builds the core of this structure (Figure 2.1.11, selected bond lengths and angles Table 2.1.3). This motif has also been observed in the solid state structures of  $(Me_3Si)_3SiTeLi(THF)_2$ ,<sup>[38]</sup>  $(Me_3Si)_3CMe_2SiOLi(THF)$ ,<sup>[91]</sup> and  $Ph_3SiOLi(DME)$ .<sup>[81]</sup> Only half of the dimer is found in the asymmetric unit; it is related to its second half via a twofold rotational axis. The Na-S-Na angles ( $85.22(8)^\circ$ ) are smaller and the S-Na-S angles ( $94.78(8)^\circ$ ) are larger than in tetrameric **7**(THF), but the Na-S distances,  $2.738(3)$  and  $2.747(3)$  Å are in the same range for both compounds. The coordination spheres around the sodium atoms in **10**(THF)<sub>2</sub> are distorted. The small S-Na-S and O(THF)-Na-O(THF) angles (the latter is  $88.7(2)^\circ$ ) are compensated for by larger S-Na-O(THF) angles, which range between  $101.52(14)^\circ$  and  $137.20(19)^\circ$ . All other structural parameters are in the same range as for **7**(THF).

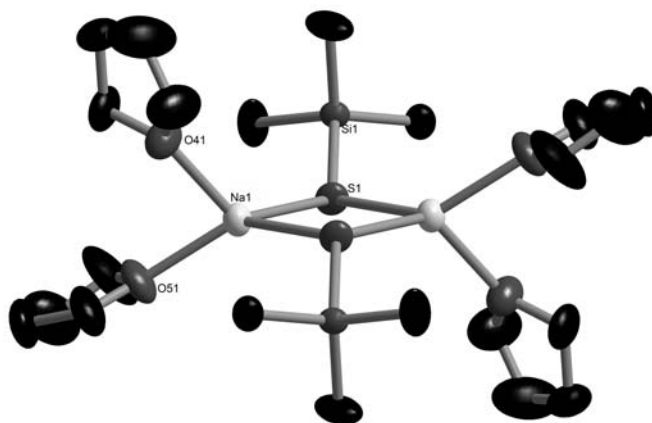


Figure 2.1.11. Solid state structure of **10**(THF)<sub>2</sub>. For clarity, only the quaternary carbon atoms of the *t*Bu<sub>3</sub>Si groups are shown.

If, however, **10** is not recrystallized from THF, but from a non-coordinating solvent, crystals displaying a tetrameric, monosolvated structure **10**(THF) can also be isolated for this species (selected bond lengths and angles Table 2.1.3). As for silyl thiolate **7**(THF), a heterocubane core is adopted in which each sodium atom is supported by one additional THF donor molecule. Tetrameric [**10**(THF)]<sub>4</sub> crystallizes in the monoclinic space group  $P2_1$ . Perhaps due

to the increased steric bulk, it has a somewhat less regular cubane core than **7**(THF), with average Na-S-Na angles of  $83.8(1)^\circ$  and average S-Na-S angles of  $95.8(1)^\circ$ . The Na-S distances are also longer than in **7**(THF) and **10**(THF)<sub>2</sub>, at an average of  $2.816(3)$  Å, which again is probably due to the steric overloading in this compound. This effect can also be observed in the Si-S bond lengths, which average  $2.108(2)$  Å.

**Table 2.1.3.** Selected bond lengths and angles for sodium silyl thiolates

	[ <b>7</b> (THF)] <sub>4</sub>	[ <b>10</b> (THF)] <sub>4</sub>	[ <b>10</b> (THF) <sub>2</sub> ] <sub>2</sub>
Si-S	2.085(2) (av)	2.108(2) (av)	2.090(2) (av)
S-Na	2.766(3) (av)	2.816(3) (av)	2.745(3) (av)
Na-O	2.295(4) (av)	2.324 (av)	2.332(5) (av)
Si-C <sub>tBu</sub>	1.919(5) (av)	1.942(6) (av)	1.955(9) (av)
Si-C <sub>Ph</sub>	1.894(5) (av)		
Na-S-Na	87.71(6) (av)	83.8(1) (av)	85.4(1) (av)
S-Na-S	92.21(6) (av)	95.8(1) (av)	94.6(1) (av)

**Table 2.1.4.** Selected bond lengths [Å] and angles [°] for sodium silyl selenolates **8** and **11** and tellurolate **12**

	[ <b>8</b> (THF) <sub>2</sub> ] <sub>2</sub>	[ <b>11</b> (THF) <sub>2</sub> ] <sub>2</sub>	[ <b>12</b> (THF) <sub>2</sub> ] <sub>2</sub>
Si-E	2.228(4)	2.2364(6)	2.4654(7)
E-Na	2.881(6) (av)	2.8677(9) (av)	3.062(2) (av)
Na-O	2.29(2) (av)	2.309(2) (av)	2.287(3) (av)
Si-C <sub>tBu</sub>	1.93(2) (av)	1.952(2) (av)	1.948(3) (av)
Si-C <sub>Ph</sub>	1.87(2) (av)		
Na-E-Na	82.7(2)	83.01(2)	80.80(3)
E-Na-E	97.3(2)	96.99(2)	99.20(3)

The selenolates **8** (4.3.5.1) and **11** (4.3.5.3) and the tellurolate **12** (4.3.5.4) all crystallize as dimers in the monoclinic space group  $P2_1/n$  with two equivalents of THF per chalcogenolate moiety (selected bond lengths and angles Table 2.1.4). As in thiolate **10**(THF)<sub>2</sub>, the cores of these structures are formed by planar E<sub>2</sub>Na<sub>2</sub> four-membered rings. The Na-E-Na angles are consistently smaller than  $90^\circ$ , and their size decreases from S to Se to Te. Conversely, the E-

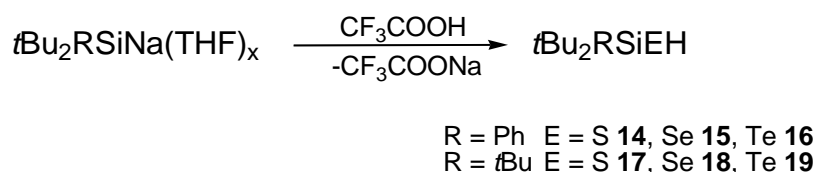


Na-E angles are all larger than  $90^\circ$ , and their size increases with increasing chalcogen atomic number. As is to be expected upon moving steadily to larger chalcogens, the Si-E and E-Na bond lengths increase when moving from S to Se to Te.

Silyl chalcogenolates **7** – **12** can also be easily derivatized. Nucleophilic attack of the supersilyl thiolate **10**(THF)<sub>2</sub> on Me<sub>3</sub>SiCl at 0 °C in THF produces *t*Bu<sub>3</sub>SiSSiMe<sub>3</sub> (**13**) quickly and in high yield (**4.3.6**). The colorless oil can be isolated by removing the solvent and extracting the colorless residue with pentane. Similar R<sub>3</sub>Si-E-SiMe<sub>3</sub> species have been employed by Corrigan et al. in the formation of silyl chalcogenolate transition metal complexes R<sub>3</sub>Si-E-M.<sup>[3, 4]</sup> The thermodynamically favorable release of Me<sub>3</sub>SiX (X = halide or pseudohalide) is the driving force for this reaction.

The formation of silyl chalcogenols has also been reported in the literature. Wiberg, who was primarily responsible for the popularization of the supersilyl moiety in synthetic chemistry, has described the preparation of *t*Bu<sub>3</sub>SiSH by treating *t*Bu<sub>3</sub>SiOTf with NaSH.<sup>[92]</sup> At elevated temperatures, nucleophilic attack yields the thiol. Using (Me<sub>3</sub>Si)<sub>3</sub>SiTeLi(THF)<sub>2</sub> as the starting material, Arnold in 1992 reported the synthesis of thermally stable (Me<sub>3</sub>Si)<sub>3</sub>SiTeH via protonolysis with trifluoromethanesulfonic acid.<sup>[38, 93]</sup> The tellurol proton displays a significant upfield shift in the <sup>1</sup>H NMR spectrum and resonates at  $-8.82$  ppm (C<sub>6</sub>D<sub>6</sub>). In the <sup>125</sup>Te NMR spectrum, the tellurium nucleus has a chemical shift of  $-955$  ppm with  $^1J_{\text{TeH}} = 74$  Hz (C<sub>6</sub>D<sub>6</sub>).

Protonolysis of silyl chalcogenolates **7** – **12** with an excess of trifluoroacetic acid in C<sub>6</sub>D<sub>6</sub> yields the chalcogenols *t*Bu<sub>2</sub>RSiEH (R = Ph, *t*Bu; E = S, Se, Te; **14** – **19**). This reaction occurs quantitatively as determined by <sup>1</sup>H NMR spectroscopy, with the signals of the starting material protons disappearing completely (Scheme 2.1.7, **4.3.7**).



Scheme 2.1.7. Synthesis of silyl chalcogenols **14** – **19**

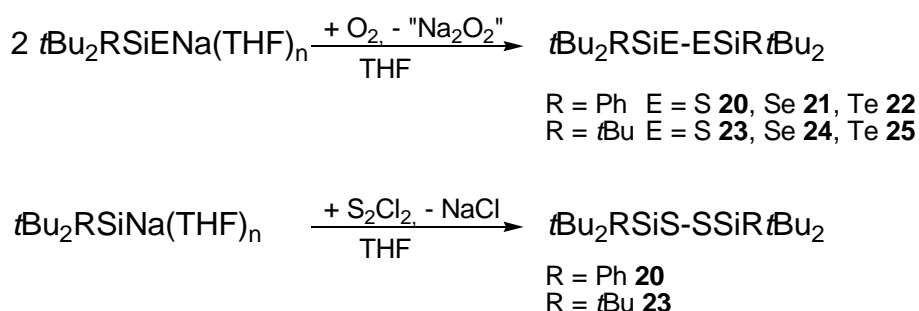
The protonation reaction can also be carried out on a preparative scale. Treating **10**(THF)<sub>2</sub> with acetic acid in dichloromethane followed by aqueous workup yields **17** as a waxy colorless solid in good yield and high purity (**4.3.7.4**). It should be noted here that although the supersilyl group reduces the volatility of its derivatives significantly, the thiol does slowly sublime when exposed to reduced pressure of  $10^{-3}$  mbar.

The products are easily identified by the characteristic upfield shift of the chalcogenol protons in the  $^1\text{H}$  NMR spectra. The tellurol signals at  $-7.48$  (**16** in  $\text{C}_6\text{D}_6$ ) and  $-7.98$  (**19** in  $\text{C}_6\text{D}_6$ ) ppm are close to the resonance reported for  $(\text{Me}_3\text{Si})_3\text{SiTeH}$  ( $-8.82$  ppm in  $\text{C}_6\text{D}_6$ ); the selenol (**15** and **18**) and thiol (**14** and **17**) signals in  $\text{C}_6\text{D}_6$  are found near  $-2.5$  and  $-0.5$  ppm, respectively. The  $^{125}\text{Te}$  NMR resonance for **16** is found at somewhat lower field than for  $(\text{Me}_3\text{Si})_3\text{SiTeH}$  ( $\text{C}_6\text{D}_6$ :  $-863$  vs.  $-955$  ppm), and the coupling constant is also significantly smaller ( $^1J_{\text{TeH}} = 25$  Hz vs.  $74$  Hz).

The same NMR trends as for the silyl chalcogenolates **7** – **12** can be observed for the chalcogenols **14** – **19**. Resonances ( $^1\text{H}$  CCH $_3$ ,  $^{29}\text{Si}$ ,  $^{13}\text{C}$  CCH $_3$ ) are shifted downfield for phenyl species **14** – **16** as compared to *tert*-butyl compounds **17** – **19**, and a continuous downfield shift is observed for chalcogenols with the same silyl residue when moving from sulfur to selenium to tellurium.

### 2.1.3 Disilyl dichalcogenides

Silyl chalcogenolates **7** – **12** are not only sensitive to protonolysis, they are also prone to oxidation. When their THF solutions are exposed to air, the chalcogenolates are converted to the dichalcogenides **20** – **25** (4.4.1, Scheme 2.1.8 top). This reaction is fastest for the tellurium species **22** and **25**, which oxidize within a few hours. The selenium and sulfur species are oxidized overnight. The disulfides (**20** and **23**; 4.4.1.1 and 4.4.1.4) and diselenides (**21** and **24**; 4.4.1.2 and 4.4.1.5) as well as ditelluride **25** (4.4.1.6) are quite stable, although the formation of *t*Bu $_2$ RSiOH can be observed during the reaction if it is run under atmospheric conditions. The tellurium compound **22** (4.4.1.3), on the other hand, is quite air-sensitive, even in the solid state, and for that reason should be prepared using dry air.



Scheme 2.1.8. Synthesis of disilyl dichalcogenides

Disulfides **20** and **23** can be prepared by a second route, which is independent of the oxidation of thiolate. When a solution of sodium silanide *t*Bu $_2$ PhSiNa or *t*Bu $_3$ SiNa in THF is treated with sulfur monochloride ( $\text{S}_2\text{Cl}_2$ ), disulfides **20** and **23**, respectively, are formed rapidly and

in good yield (Scheme 2.1.8, bottom). Isolation can be achieved by removing volatiles, extracting with pentane and filtering off byproduct salts. Concentration of the pentane solutions and cooling leads to the deposition of colorless crystalline blocks of product.

Tellurium monochloride is not commercially available, making this route to the ditellurides unviable. Selenium monochloride can be obtained from commercial sources, but it displays a high sensitivity towards THF, so that the oxidation route is the preferred synthetic method for the preparation of diselenides.

Oxidation is accompanied by a color change to brick red for diselenides **21** and **24**. In the electronic absorption spectrum of **21**, a strong band can be observed at  $\lambda_{\text{max}} = 424$  nm, which is shifted to 418 nm for **24**. The ditellurides **22** and **25** are dark blue or purple, and absorption maxima for **25** are found at 576 and 292 nm. The electronic origin of these effects was not investigated. The disulfides **20** and **23**, like the chalcogenolates **7** – **12**, are colorless.

The oxidation reaction by which the dichalcogenides are generated can be chemically reversed. For example, treating ditelluride **25** with elemental potassium in THF leads to complete conversion to the potassium tellurolate  $t\text{Bu}_3\text{SiTeK}$  (**26**, 4.4.2). Over 24 h at room temperature, the dark blue color of the ditelluride is lost, and in the NMR spectra, signals associated with the **25** disappear completely.

The chemical reversibility of this redox reaction prompted an electrochemical investigation of the dichalcogenides. In THF solution with  $[\text{NBu}_4][\text{PF}_6]$  as the supporting electrolyte, neither an oxidation nor a reduction wave can be observed for **25**. When diselenide **24** is subjected to cyclic voltammetric investigations under the same conditions, an irreversible reduction peak is observed at  $-1.37$  V (vs.  $\text{FcH}/\text{FcH}^+$ ). This is comparable to the reduction of  $\text{PhSe-SePh}$  in acetonitrile, which occurs at  $-0.85$  V vs. SCE<sup>[94]</sup> ( $-1.23$  V vs.  $\text{FcH}/\text{FcH}^+$ ).<sup>[95]</sup> The reduction of  $\text{PhSe-SePh}$ , however, is a reversible one-electron process. The electrochemical irreversibility of the reduction of **24** indicates that the  $\text{SiSe-SeSi}$  moiety is less stable than the  $\text{C}_{\text{Ph}}\text{Se-SeC}_{\text{Ph}}$  unit. This observation can be rationalized by considering the positive inductive effects of the  $t\text{Bu}_3\text{Si}$  substituents, which can be expected to increase the overall electron density in the  $\text{SiSe-SeSi}$  unit, as compared to the negative inductive effects of the phenyl substituents, which should decrease the overall charge density of the  $\text{C}_{\text{Ph}}\text{Se-SeC}_{\text{Ph}}$  moiety.

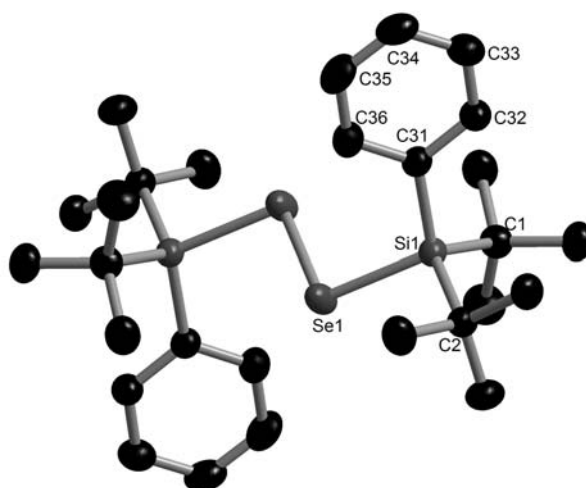
The fact that diselenide **24** can be electrochemically reduced under conditions where no reduction is observed for ditelluride **25** indicates that the reduction potential of **25** is significantly more negative than that of **24**, making tellurium derivative **25** harder to reduce but the corresponding tellurolate **12** easier to oxidize. Indeed, the tell-tale purple color of ditelluride **25** can be seen even in samples of **12** stored under inert atmosphere.

In the literature, an oxidation approach similar to that described here was taken for the conversion of  $(\text{Me}_3\text{Si})_3\text{SiTeLi}(\text{THF})_2$  to  $(\text{Me}_3\text{Si})_3\text{SiTe}-\text{TeSi}(\text{SiMe}_3)_3$ , which can be achieved using either anhydrous  $\text{CuCl}$  or dry  $\text{O}_2$ . The dihypersilyl ditelluride is dark green, and its  $^{125}\text{Te}$  NMR signal in  $\text{C}_6\text{D}_6$  is found at  $-678$  ppm.<sup>[38]</sup> This is in good agreement with the  $^{125}\text{Te}$  NMR resonance for **25** at  $-624$  ppm ( $\text{C}_6\text{D}_6$ ).

**Table 2.1.5.** Selected bond lengths [ $\text{\AA}$ ] and angles [ $^\circ$ ] for disulfides  $t\text{Bu}_2\text{RSiS}-\text{SSiR}t\text{Bu}_2$  (R = Ph **20**,  $t\text{Bu}$  **23**)

	<b>20</b>	<b>23</b>		<b>20</b>	<b>23</b>
S-S	2.0932(9)	2.106(1)	Si- $\text{C}_{t\text{Bu}}$	1.912(2) (av)	1.940 (av)
Si-S	2.1675(6)	2.1781(8)	Si- $\text{C}_{\text{Ph}}$	1.884(2) (av)	
Si-S-S	102.08(3)	105.14(4)	Si-S-S-Si	180	180

Slow evaporation of hydrocarbon solutions of the dichalcogenides yields X-ray quality crystals of all six species. Selected bond lengths and angles for disulfides **20** and **23** are found in Table 2.1.5, for diselenides **21** and **24** in Table 2.1.6 and for ditellurides **22** and **25** in Table 2.1.7.



Figures 2.1.12. Solid state structure of **21**. Hydrogen atoms have been omitted for clarity.

The compounds **20** (monoclinic,  $P2_1/n$ ), **21** (monoclinic,  $P2_1/c$ ), **22** (monoclinic,  $P2_1/c$ ), **23** (monoclinic,  $P2_1/n$ ), and **25** (orthorhombic,  $Pbca$ ) all crystallize with one half molecule in the asymmetric unit, which is related to its second half via a crystallographic inversion center in the middle of the E-E bond. Diselenide **24** (trigonal,  $R-3$ ) crystallizes with two half molecules in the asymmetric unit, which again are related to their second halves via a crystallographic

inversion center. In one of these molecules, the Se-Se unit is disordered over two positions, with a relative population of ca. 75:25. The molecular structures of the dichalcogenides are all quite similar, and only the diselenides **21** and **24** are depicted in Figures 2.1.12 and 2.1.13, respectively.

In all of the dichalcogenides **20** – **25**, the Si-E-E-Si chains are exactly *s-trans*. The corresponding torsional angles of  $180^\circ$  are mandated by the crystallographic inversion centers. These compounds display Si-E-E angles smaller than  $109^\circ$ . The S-S bonds in **20** and **23** are somewhat longer than typical bond lengths for aryl and alkyl substituted disulfides RS-SR (mean S-S distance for aryl disulfides: 2.050 Å; mean for alkyl disulfides: 2.024 Å).<sup>[96]</sup> The Se-Se and Te-Te bonds in the disilyl diselenides **21** and **24** and ditellurides **22** and **25**, however, have bond lengths similar to those found in the corresponding alkyl and aryl substituted dichalcogenides (mean Se-Se bond length for aryl diselenides: 2.347 Å; for alkyl diselenides: 2.310; mean Te-Te bond length for alkyl ditellurides: 2.724 Å).<sup>[96]</sup>

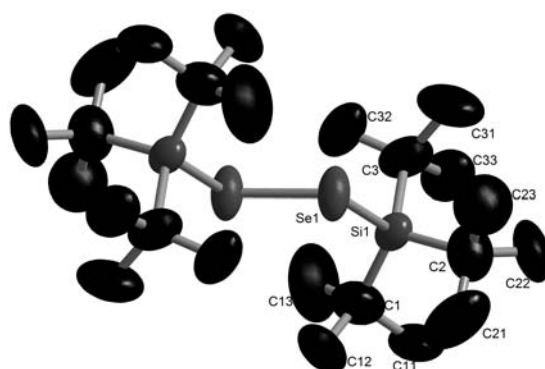


Figure 2.1.13. Solid state structure of **24**. The non-disordered molecule is depicted, and hydrogen atoms have been omitted for clarity.

**Table 2.1.6.** Selected bond lengths [ $\text{\AA}$ ] and angles [ $^\circ$ ] for diselenides  $t\text{Bu}_2\text{RSiSe-SeSiR}t\text{Bu}_2$  (R = Ph **21**,  $t\text{Bu}$  **24**)

	<b>21</b>	<b>24</b>	
		a <sup>[a]</sup>	b
Se-Se	2.3666(5)	2.368(4)	2.39(1)
Si-Se	2.3106(6)	2.361(4)	2.42(1)
Si-Se-Se	100.24(2)	102.3(2)	99.1(3)
Si-C <sub><i>t</i>Bu</sub>	1.919(2) (av)	1.93(2) (av)	1.91(2)
Si-C <sub>Ph</sub>	1.884(2)		
Si-Se-Se-Si	180	180	180

[a] Bond lengths and angles from the more populated Se<sub>2</sub> unit.

**Table 2.1.7.** Selected bond lengths [ $\text{\AA}$ ] and angles [ $^\circ$ ] for ditellurides  $t\text{Bu}_2\text{RSiTe-TeSiR}t\text{Bu}_2$  (R = Ph **22**,  $t\text{Bu}$  **25**)

	<b>22</b>	<b>25</b>		<b>22</b>	<b>25</b>
Te-Te	2.7243(4)	2.7398(7)	Si-C <sub><i>t</i>Bu</sub>	1.923(3) (av)	1.933(6) (av)
Si-Te	2.5180(8)	2.552(2)	Si-C <sub>Ph</sub>	1.884(3)	
Si-Te-Te	98.22(2)	103.03(3)	Si-Te-Te-Si	180	180

### 2.1.4 Oligochalcogen compounds

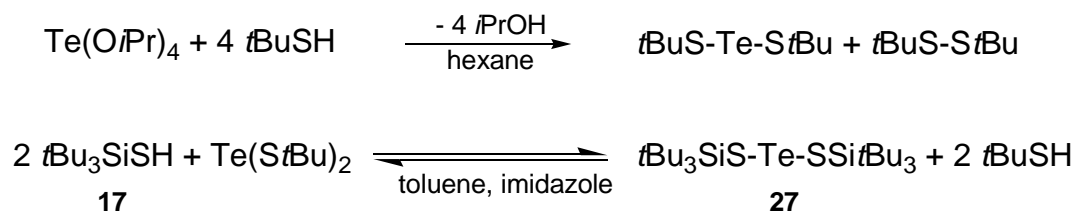
The oxidative addition of dichalcogenides to transition metal centers is a well established method for the synthesis of complexes with chalcogenolate ligands. The application of this chemistry to disilyl dichalcogenides is one main motivation for the compounds described in section 2.1.3. It would, however, be desirable to be able to expand this approach to introduce not only chalcogenolates, but also chalcogenides  $E^{2-}$  or dichalcogenides  $E_2^{2-}$ . Towards this end, the synthesis of silyl-capped oligochalcogen chains of the types RE-E'-ER and RE-E'E'-ER was pursued, where E and E' are either the same or different chalcogens.

One approach to tellurium(II) dithiolates RS-Te-SR that has been described in the literature is the ligand substitution reaction of thiols with  $Te(OiPr)_4$  followed by reductive elimination to give *i*PrOH, RS-Te-SR and RS-SR.<sup>[97]</sup> When RS-Te-SR is treated with a thiol bearing a different organic residue R', an equilibrium is established between RS-Te-SR, R'S-Te-SR and R'S-Te-SR' (and the corresponding thiols). If thiol RSH, a product of the forward reaction, is more volatile than R'SH, it can be removed from the reaction mixture via distillation, forcing the exchange reaction to completion.<sup>[98]</sup>

It is conceivable that reaction of *t*Bu<sub>3</sub>SiSH (**17**) with  $Te(OiPr)_4$  would result in the desired product, (*t*Bu<sub>3</sub>SiS)<sub>2</sub>Te (**27**). It can, however, be expected that the separation of the essentially nonvolatile, aliphatic byproduct *t*Bu<sub>3</sub>SiS-SS*t*Bu<sub>3</sub> (**20**) from the non-polar tellurium(II) dithiolate **27** would be difficult. Furthermore, this reaction uses thiol inefficiently, since it has a maximum theoretical yield of 50 %.

The equilibrium exchange reaction, on the other hand, seems quite promising. The low volatility of **17** should allow for the distillative removal of lower molecular weight alkylthiol, and the maximum theoretical yield based on silylthiol is 100 %. Indeed, when (*t*BuS)<sub>2</sub>Te, synthesized from *t*BuSH and  $Te(OiPr)_4$ ,<sup>[97]</sup> is treated with **17** in toluene, the desired product **27** can be isolated (Scheme 2.1.9). Due to the small amounts of *t*BuSH evolved during the reaction, the partial pressure of this compound is not high enough to allow for it to be distilled separately. Instead, traces of alkylthiol are co-distilled with the reaction medium. For this reason, it is necessary to start from a dilute reaction mixture and slowly distill off the solvent. The highest yield for this reaction was attained using 0.25 mmol (*t*BuS)<sub>2</sub>Te and 0.52 mmol **17** in 20 ml of toluene with distillation at atmospheric pressure over a period of 3 h. The elevated temperature necessary for distillation is also critical in order for the equilibrium state to be reached (and maintained) in a reasonable amount of time. Attempts to run the same reaction at room temperature under reduced pressure (ca. 200 Torr) were unsuccessful. Indeed, it has been reported that the equilibration of a solution of (*i*PrS)<sub>2</sub>Te and *t*BuSH in CHCl<sub>3</sub> took two

weeks at room temperature. In addition to elevated temperature, the equilibrium state is reached much faster in the presence of acid or base.<sup>[99]</sup> The best results for the reaction of  $(t\text{BuS})_2\text{Te}$  and **17** were obtained using equimolar amounts of thiol and imidazole (**4.5.1**).



Scheme 2.1.9. Synthesis of tellurium(II) dithiolate **27**

Nevertheless, it was not possible to shift the equilibrium entirely to the products side, and the maximum yield of **27** was ca. 50 % as determined by <sup>1</sup>H NMR spectroscopy. The desired product, however, is by far the least volatile component in the reaction mixture. Imidazole, toluene, and *t*BuSH, as well as unreacted thiol **17** and  $(t\text{BuS})_2\text{Te}$  can all be removed by evacuation of the reaction vessel overnight at 10<sup>-3</sup> mbar, leaving pure **27** as a brown powdery residue. The <sup>125</sup>Te NMR resonance for **27** is observed at 1222 ppm in C<sub>6</sub>D<sub>6</sub>, which agrees well with the <sup>125</sup>Te NMR chemical shifts of tellurium(II) dialkylthiolates (RS)<sub>2</sub>Te in the same solvent, which range from 1419 ppm (R = Me) to 907 ppm (R = *t*Bu).<sup>[100]</sup> The <sup>29</sup>Si NMR chemical shift (25.3 ppm in C<sub>6</sub>D<sub>6</sub>) is comparable to those of disulfide **23** (24.6 ppm) and thiolate **10**(THF)<sub>2</sub> (25.6 ppm) in C<sub>6</sub>D<sub>6</sub>.

Tellurium(II) dithiolates are reasonably stable towards air and water, but alkyl derivatives are reported to be photo- and thermolabile, decomposing to elemental tellurium and dialkyl disulfide upon prolonged exposure to bright light or high temperatures.<sup>[97, 98]</sup> The bulky *tert*-butylsilyl groups in **27** appear to kinetically stabilize this species. Under inert conditions at room temperature with normal lighting, no decomposition can be detected. If a sample of **27** in C<sub>6</sub>D<sub>6</sub> is placed directly in front of a fluorescent light bulb, elemental tellurium is slowly deposited, and after two weeks, ca. 60 % conversion to disulfide **23** has occurred.

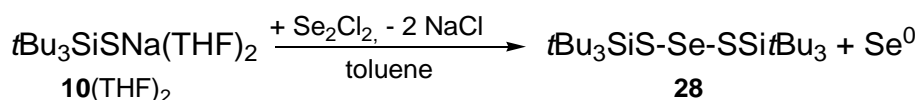
Encouraged by the successful synthesis of tellurium(II) dithiolate **27**, a preparative route to comparable selenium-based species was sought. For selenium(II) dithiolates, however, no similar exchange equilibrium method has been established. Indeed, there is evidence that in some reactions of RSH with R'S-SeR' and R'S-Se-SR', attack takes place at sulfur rather than selenium.<sup>[101]</sup> As a consequence, the exchange reaction of thiol **17** with (RS)<sub>2</sub>Se was deemed unpromising.

On the other hand, there is evidence that reaction of thiols with SeO<sub>2</sub>, in analogy to the reaction of Te(O*i*Pr)<sub>4</sub> with RSH to obtain (RS)<sub>2</sub>Te and RS-SR, produces selenium(II)



dithiolates along with byproduct disulfide.<sup>[102]</sup> These reactions are described as taking place in a mixture of water and acetonitrile,<sup>[103]</sup> and this protocol was applied to the reaction of **17** with SeO<sub>2</sub>. Unfortunately, the poor solubility of thiol **17** in the polar solvent mixture precluded any detectable reaction. When the same reaction is performed in ethanol, the reaction remains slow (less than 50 % conversion in 5 d). Furthermore, the major product (ca. 50 %) is not the desired selenium(II) dithiolate (*t*Bu<sub>3</sub>SiS)<sub>2</sub>Se, but silanol *t*Bu<sub>3</sub>SiOH, apparently resulting from cleavage of the Si-S bond. When the solvent is removed from the reaction mixture and the residue extracted with C<sub>6</sub>D<sub>6</sub>, slow concentration leads to the deposition of orange needles, which were identified as a mixture of elemental sulfur and selenium via single crystal X-ray diffraction. In order to rule out hydrolysis as the cause of Si-S bond scission, the reaction was carried out in dry THF under an atmosphere of dry nitrogen. Again, the major product could be identified as *t*Bu<sub>3</sub>SiOH.

In light of the unpromising results obtained with SeO<sub>2</sub> and *t*Bu<sub>3</sub>SiSH, a different approach was sought for the synthesis of silyl-capped chains of sulfur and selenium. Since the silyl thiolate **10**(THF)<sub>2</sub> is readily accessible, a double nucleophilic substitution reaction with Se<sub>2</sub>Cl<sub>2</sub> was attempted (4.5.2). For this reaction, toluene was chosen as the solvent due to the instability of Se<sub>2</sub>Cl<sub>2</sub> in THF. The reaction proceeds quickly, and after one hour stirring, a red solid can be separated from the yellow solution via filtration. Evaporating the filtrate to dryness yields an orange residue, the NMR spectra of which indicate that it is a mixture of two species in a 3:1 ratio. Elemental analysis of the residue suggests that its main component is not the expected 2,3-diselenotetrasulfane *t*Bu<sub>3</sub>Si-S-Se<sub>2</sub>-S-Si*t*Bu<sub>3</sub>. Instead, it consists mainly of selenium(II) dithiolate (*t*Bu<sub>3</sub>SiS)<sub>2</sub>Se (**28**), which is formed by elimination of elemental selenium from intermediate diselenotetrasulfane (Scheme 2.1.10).



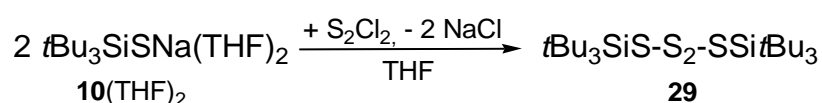
Scheme 2.1.10. Synthesis of selenium(II) dithiolate **28**

The selenium(II) dithiolate **28** itself, however, is also not stable indefinitely. Upon standing in solution under inert atmosphere, elemental selenium is deposited with concomitant formation of disulfide. It therefore was not possible to isolate an analytically pure sample of **28**.

While mixed chains of selenium and sulfur longer than three atoms are extremely rare in the literature, there are numerous reports of organyl and silyl-capped sulfur chains. Despite the instability of the product, the apparent success of the nucleophilic substitution reaction of

thiolate **10**(THF)<sub>2</sub> with Se<sub>2</sub>Cl<sub>2</sub> suggested that the analogous reaction with S<sub>2</sub>Cl<sub>2</sub> might yield isolable products.

When S<sub>2</sub>Cl<sub>2</sub> is treated with two equivalents of **10**(THF)<sub>2</sub> in THF, *t*Bu<sub>3</sub>SiS-S<sub>2</sub>-SSi*t*Bu<sub>3</sub> (**29**) is formed quantitatively (4.5.3, Scheme 2.1.11). Changing the solvent to pentane, filtering, and slowly concentrating the filtrate leads to the deposition of colorless crystals of **29**. The extremely soluble tetrasulfane **29** is stable to air and moisture both in the solid state and in solution, and it demonstrates no tendency to rearrange or to deposit elemental sulfur in favor of trisulfane or disulfide. Heating at 100 °C in C<sub>6</sub>D<sub>6</sub> solution in a sealed NMR tube for 8 – 10 weeks leads to unselective decomposition.



Scheme 2.1.11. Synthesis of tetrasulfane **29**

There are three disilyl tetrasulfanes that have been described in the literature, and all of them have been prepared by treating S<sub>2</sub>Cl<sub>2</sub> with silyl thiolate.<sup>[104-107]</sup> The tri-*tert*-butoxy derivative (*t*BuO)<sub>3</sub>SiS-S<sub>2</sub>-SSi(*Ot*Bu)<sub>3</sub> has also been prepared by treating S<sub>2</sub>Cl<sub>2</sub> with thiol in the presence of pyridine. NMR data have only been reported for Ph<sub>3</sub>SiS-S<sub>2</sub>-SSiPh<sub>3</sub>, the silicon atoms of which resonate at 6.9 ppm in the <sup>29</sup>Si NMR spectrum.<sup>[107]</sup> The <sup>29</sup>Si NMR signal for **29**, on the other hand, is found at 26.7 ppm (C<sub>6</sub>D<sub>6</sub>), indicating that the organic substituents at silicon have a much greater influence on the <sup>29</sup>Si chemical shift than the identity of the chalcogen chain.

Tetrasulfane **29** crystallizes in the monoclinic space group *P*2<sub>1</sub>/*c* with one complete molecule in the asymmetric unit (Figure 2.1.14, selected bond lengths and angles Table 2.1.8). The central S-S bond is somewhat shorter than the terminal S-S bonds, which are, in turn, shorter than the S-S bond in disulfide **23**. In contrast, the Si-S and Si-C bonds are a bit longer in **29** compared to **23**.

There is only one other crystallographically characterized disilyl tetrasulfane reported in the literature, Ph<sub>3</sub>SiS-S<sub>2</sub>-SSiPh<sub>3</sub>.<sup>[107]</sup> Both the internal and the terminal S-S bonds in **29** are longer than the corresponding bonds in the triphenylsilyl species (terminal: 2.058(6) and 2.066(6) Å, internal: 2.025(6) Å). Bond elongation can also be observed for the Si-S bonds (Ph<sub>3</sub>SiS-S<sub>2</sub>-SSiPh<sub>3</sub>: 2.170(7) and 2.180(6) Å), which is to be expected due to the increased steric bulk of the *tert*-butyl groups compared to the phenyl substituents.

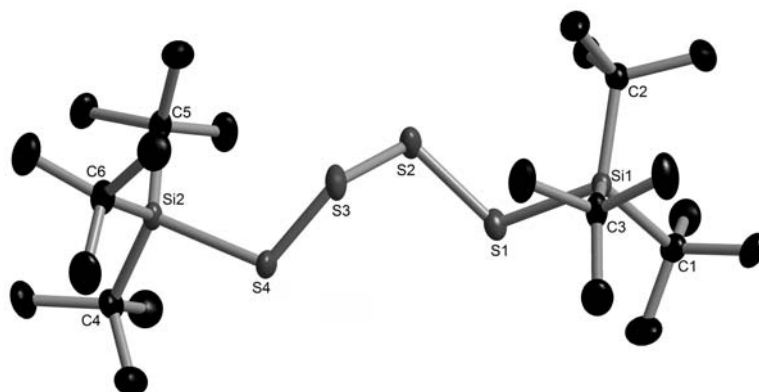


Figure 2.1.14. Solid state structure of **29**. For clarity, hydrogen atoms are not shown.

**Table 2.1.8.** Selected bond lengths [ $\text{\AA}$ ], angles [ $^\circ$ ] and torsion angles [ $^\circ$ ] for **29**

S1-S2	2.0808(10)	Si1-S1-S2	109.10(4)
S2-S3	2.0487(10)	S1-S2-S3	108.39(4)
S3-S4	2.0742(10)	S2-S3-S4	108.60(4)
Si1-S1	2.2094(9)	S3-S4-Si2	110.25(4)
Si2-S4	2.2095(9)	Si1-S1-S2-S3	-105.48(4)
Si-C (av)	1.952	S1-S2-S3-S4	-76.32(5)
		S2-S3-S4-Si1	-103.42(4)

## 2.2 Transition metal complexes of silanides and silyl chalcogenolates

With this battery of potential ligand precursors in hand, the coordination properties of silyl chalcogenolates were investigated. In order to better compare the isoelectronic species phosphines, phosphanyl borohydrides and silanides, silyl complexes were also targeted.

### 2.2.1 Complexes of the type $[\text{CpFe}(\text{CO})_2\text{L}]$

The  $[\text{CpFe}(\text{CO})_2]^+$  fragment enjoys significant popularity among coordination chemists. It is especially well suited to comparisons of related ligands, such as silyl, phosphanyl borohydride and phosphine compounds. It has one free coordination site (often occupied by halides or donor solvent molecules in its isolable derivatives), which allows for the controlled synthesis of complexes with monodentate ligands. In addition, both neutral (i.e. with silyl and phosphanyl borohydride ligands) and charged complexes (i.e. with phosphine ligands) can be prepared. This makes a detailed structural comparison of species with different charges possible. The IR stretching frequencies of the carbonyl ligands are indicative of the degree of backbonding, allowing investigators to glean information about the electronic properties of the complexes.<sup>[108]</sup> Furthermore, the Cp and CO resonances in the  $^{13}\text{C}$  NMR spectra offer additional information about the electron density at the metal center.<sup>[109-111]</sup>

#### 2.2.1.1 $\text{CpFe}(\text{CO})_2\text{SiPh}_2\text{Me}$ : comparison to $\text{CpFe}(\text{CO})_2\text{PPh}_2\text{BH}_3$ and $[\text{CpFe}(\text{CO})_2\text{PPh}_2\text{Me}]\text{I}$

As has already been mentioned, one goal of the investigations presented here is to compare isoelectronic compounds of the type  $\text{R}_3\text{Si}^-$ ,  $\text{R}_2(\text{BR}'_3)\text{P}^-$  and  $\text{R}_3\text{P}$ . Due to difficulties in the preparation of  $\text{R}_2(\text{BR}'_3)\text{P}^-$  with  $\text{R}' = \text{alkyl}$ , only species of the type  $\text{R}_2\text{BH}_3\text{P}^-$  are accessible.<sup>[13]</sup> Of these,  $\text{Ph}_2\text{BH}_3\text{P}^-$  and  $t\text{Bu}_2\text{BH}_3\text{P}^-$  are the best characterized systems.<sup>[11, 12]</sup> Difficulties with the preparation of less sterically bulky silanides  $t\text{Bu}_2\text{MeSi}^-$  and  $\text{Ph}_2\text{MeSi}^-$ , as described in section 2.1.1.2, preclude a direct comparison of silanides and phosphanyl borohydrides in the form of their alkali metal salts. Furthermore, the ionic nature of the silanides and phosphanyl borohydrides makes a meaningful structural comparison to the neutral phosphines impossible. In light of these difficulties, coordination complexes using the  $[\text{CpFe}(\text{CO})_2]^+$  fragment (in future referred to as  $\text{Fp}^+$ ) were investigated.

In the literature there are no structurally characterized monomeric  $\text{FpSiR}_3$  complexes in which the silyl ligand bears only alkyl and/or aryl substituents. Nevertheless, there are a number of structurally characterized silyl complexes where the silicon atom is bound to electron

withdrawing functional groups.<sup>[112-115]</sup> Complexes of  $\text{Fp}^+$  bearing silyl ligands with solely aromatic and/or aliphatic residues have, however, been spectroscopically characterized and are typically obtained by treating  $\text{NaFp}$  with triorganylsilyl chloride.<sup>[116-119]</sup>

On the other hand, terminal, unbridged phosphine complexes of  $\text{Fp}^+$  are well known. Two general routes to these compounds have been described. The first involves treating  $\text{Fp}^+$  complexes containing labile ligands such as THF or  $\text{I}^-$  with phosphines.<sup>[120-123]</sup> In the second,  $\text{Fp}_2$  is oxidized in the presence of phosphine ligand, typically with ferrocenium or cobaltocenium ions.<sup>[124-126]</sup> Using a different approach,  $[\text{FpPPh}_2\text{Me}]\text{I}$  can be prepared by reaction of the corresponding diphenylphosphido complex with iodomethane. The phosphine complex has been characterized both structurally and spectroscopically.<sup>[127]</sup>

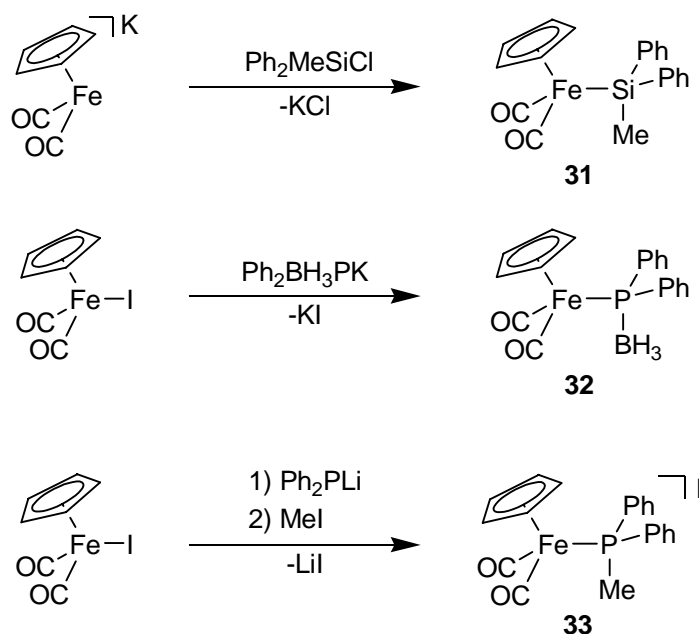
The only  $\text{Fp}^+$  complexes of phosphanyl borohydrides with known solid-state structures are  $\text{FpPPh}_2\text{BH}_3$  and  $\text{FpP}t\text{Bu}_2\text{BH}_3$ , which were prepared by treating  $\text{FpI}$  with  $\text{Ph}_2\text{BH}_3\text{PK}$  and  $t\text{Bu}_2\text{BH}_3\text{PK}$ , respectively.<sup>[127]</sup> However, the related complex  $\text{Fp}(\text{DPB})$  ( $\text{DPB}$  = diphenylphosphidoboratabenzene) was reported by Fu et al. in a 1996 paper.<sup>[128]</sup> The pentamethylcyclopentadienyliron dicarbonyl complex  $(\text{C}_5\text{Me}_5)\text{Fe}(\text{CO})_2(\text{PPh}_2\text{BH}_3)$  is accessible by treating the corresponding diphenylphosphido complex with  $\text{BH}_3\cdot\text{THF}$  and has also been characterized by X-ray crystallography.<sup>[45]</sup>

In pursuit of complexes of the type  $\text{FpSiR}_3$  ( $\text{R}$  = alkyl or aryl),  $\text{FpI}$  was first treated with sodium silanides  $t\text{Bu}_2\text{MeSiNa}(\text{THF})_x$  ( $2(\text{THF})_x$ , **4.6.3**) and  $t\text{Bu}_3\text{SiNa}(\text{THF})_x$  (**4.6.4**). Both reactions proceed unselectively. The only spectroscopically identifiable silicon-containing products are  $t\text{Bu}_2\text{MeSiI}$  (**30**) and  $t\text{Bu}_3\text{SiI}$ ,<sup>[60, 129]</sup> respectively, indicating that attack takes place not at the iron center, but at the iodo ligand. The identity of **30** was confirmed by comparison with an authentic sample prepared by treating  $t\text{Bu}_2\text{MeSiH}$  with  $\text{I}_2$  (**4.6.5**). In both cases, the only identifiable iron-containing species is  $\text{Fp}_2$ .

When umpolung is employed and  $\text{KFp}$  is treated with the sterically hindered bromosilane  $t\text{Bu}_3\text{SiBr}$ , no reaction can be detected even after two months at room temperature. When the smaller bromosilane  $t\text{Bu}_2\text{MeSiBr}$  (**1**) is used and the temperature raised to  $50^\circ\text{C}$ , after one month only half of the bromosilane has been consumed. Despite its slow rate, the reaction is unselective, with at least five different silicon-containing products being formed, none of which are readily identified.

Since the complexes  $[\text{FpPPh}_2\text{Me}]\text{I}$  (**33**) and  $\text{FpPPh}_2\text{BH}_3$  (**32**) have both been structurally and spectroscopically characterized,<sup>[127]</sup> the synthesis of the isosteric silyl analog  $\text{FpSiPh}_2\text{Me}$  (**31**)<sup>[119]</sup> was attempted. When  $\text{KFp}$  is treated with  $\text{Ph}_2\text{MeSiCl}$  in THF, the desired complex is formed in nearly quantitative yield (Scheme 2.2.1), and the crude product is recovered as a

brown oil. Filtration over silica gel using hexane/ $\text{CH}_2\text{Cl}_2$  2:1 as the eluent separates a yellow band (product) from a brown and a red band, which remain essentially stationary. Recrystallization from hexane at  $-25\text{ }^\circ\text{C}$  yields the complex as pale yellow needles (**4.6.1**).



Scheme 2.2.1. Synthesis of isoelectronic complexes **31** – **33**

The silyl complex **31** crystallizes in the orthorhombic space group  $P2_12_12_1$  and has an Fe-Si bond of 2.3353(5) Å (Figure 2.2.1, selected bond lengths in Table 2.2.1). Of the structurally characterized Fp-silyl complexes in the literature, only those with donor silicon atoms bound to silyl residues lacking electron withdrawing substituents have longer Fe-Si bonds (FpSiMe<sub>2</sub>SiPh<sub>3</sub>: 2.346(1) Å<sup>[130]</sup>, FpSiPh(SiMe<sub>3</sub>)<sub>2</sub>: 2.366(1) and 2.355(1) Å in two crystallographically independent molecules<sup>[131]</sup>).

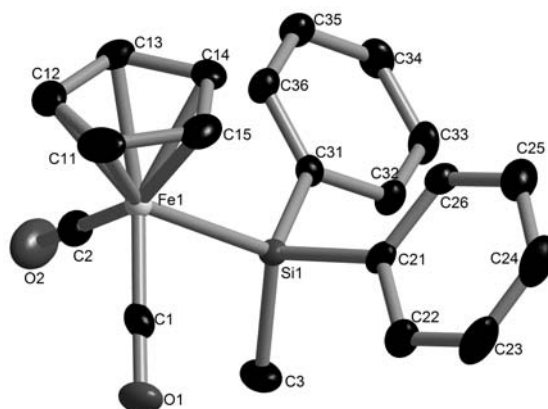


Figure 2.2.1. Solid state structure of **31**. For clarity, hydrogen atoms are not shown.

The Fe-CO distances in **31** are comparable to those found in other FpSiR<sub>3</sub> complexes<sup>[96]</sup> but shorter than in **32** and **33**. The C-O bond lengths found in **31** (avg. 1.160(3) Å) are roughly 0.015 Å longer than in **32** and **33**. This result indicates that the  $\pi$ -backbonding from the iron center to the CO ligands is strongest in the silyl complex, suggesting that Ph<sub>2</sub>MeSi<sup>-</sup> is the strongest donor of the isoelectronic series Ph<sub>2</sub>MeSi<sup>-</sup>, Ph<sub>2</sub>BH<sub>3</sub>P<sup>-</sup> and Ph<sub>2</sub>MeP.

**Table 2.2.1.** Selected bond lengths [Å] for **31** – **33**

	Fe-P/Si	Fe-CO (avg)	C-O (avg)
<b>31</b>	2.3353(5)	1.755(2)	1.160(3)
<b>32</b>	2.2705(6)	1.772(2)	1.141(2)
<b>33</b>	2.236(2)	1.779(9)	1.146(10)

This interpretation of relative donor strength is supported by the <sup>13</sup>C NMR chemical shifts of the carbonyl carbon atoms (a summary of spectroscopic data can be found in Table 2.2.2). It has been shown in the literature that an increase in the donor strength of an ancillary ligand in a carbonyl complex leads to a chemical shift of the carbonyl carbon atom signal to lower field.<sup>[109, 110]</sup> The carbonyl carbon atom of **31** resonates at 215.8 ppm. The <sup>13</sup>C NMR spectrum of phosphanyl borohydride complex **32** displays the corresponding signal at 213.5 ppm and the phosphine complex **33** at 210.4 ppm. This trend indicates that the donor strength of the isoelectronic, isosteric ligands Ph<sub>2</sub>MeSi<sup>-</sup>, Ph<sub>2</sub>BH<sub>3</sub>P<sup>-</sup> and Ph<sub>2</sub>MeP decreases in that order.

**Table 2.2.2.** Selected spectroscopic parameters for **31** – **33**

	$\delta$ <sup>13</sup> C(CO) <sup>[a]</sup>	$\delta$ <sup>13</sup> C(Cp) <sup>[a]</sup>	$\tilde{\nu}$ (CO) [cm <sup>-1</sup> ] <sup>[b]</sup>
<b>31</b>	215.8	84.3	1994, 1938
<b>32</b>	213.5	86.8	2030, 1982
<b>33</b>	210.4	89.1	2055, 2011

[a] **31** and **32** C<sub>6</sub>D<sub>6</sub>, **33** CDCl<sub>3</sub> [b] CH<sub>3</sub>CN

It has also been observed that <sup>13</sup>C NMR chemical shifts of cyclopentadienyl ligands in metal carbonyl complexes can be correlated to the electron density at the metal center. In this case, higher electron density corresponds to a shift to higher field.<sup>[109, 111]</sup> As is expected based on the carbonyl carbon atom resonances, the phosphine complex **33** bears the Cp ring with the most deshielded carbon nuclei (89.1 ppm). The carbon atoms in the cyclopentadienyl ring of **32** resonate at 86.8 ppm, while the corresponding signal for silyl complex **31** can be seen at

84.3 ppm. Again, this evidence supports the conclusion that  $\text{Ph}_2\text{MeSi}^-$  is the strongest donor in this comparison.

Carbonyl IR stretching frequencies are, of course, also an important measure of donor strength in carbonyl complexes<sup>[108]</sup> (see Table 2.2.2 for IR stretching frequencies). In accordance with the interpretation of the  $^{13}\text{C}$  NMR spectra, the phosphine complex **33** is found to have the highest CO stretching frequencies (2055 and 2011  $\text{cm}^{-1}$ ,  $\text{CH}_3\text{CN}$ ). These values compare favorably with those found in the literature for similar complexes (e.g.  $[\text{FpPPh}_3]\text{PF}_6$  ( $\text{CH}_2\text{Cl}_2$ ) 2055, 2010  $\text{cm}^{-1}$ <sup>[132]</sup>). Introduction of the  $\text{BH}_3$  moiety and consequently of a negative charge in complex **32** leads to a marked downward shift of these bands to 2030 and 1982  $\text{cm}^{-1}$  ( $\text{CH}_3\text{CN}$ ). The silyl complex **31** displays the lowest CO stretching frequencies at 1994 and 1938  $\text{cm}^{-1}$  ( $\text{CH}_3\text{CN}$ ). These bands are at somewhat lower frequencies than those found for comparable complexes in the literature, although this may be a solvent effect ( $\text{FpSiMe}_2\text{Ph}$  (cyclohexane) 1998, 1947  $\text{cm}^{-1}$ ;<sup>[133]</sup>  $\text{FpSiPh}_2\text{OMe}$  (THF) 1998, 1947  $\text{cm}^{-1}$ ;<sup>[114]</sup>  $\text{FpSiMe}_2\text{SiMe}_3$  (cyclohexane) 1996, 1952  $\text{cm}^{-1}$ <sup>[134]</sup>). For the same complex,  $\text{FpSiPh}_2\text{Me}$ , in cyclohexane, CO-stretches at 2002 and 1951  $\text{cm}^{-1}$  have been reported.<sup>[119]</sup> The relatively low-energy bands found for **31** are consistent with the NMR data, which indicate that the silyl ligand is the strongest donor of the three.

When comparing the complexes **31** – **33**, it is also interesting to consider the effect of exchanging the Cp ligand for  $\text{Cp}^*$  ( $\text{Cp}^* = \text{Me}_5\text{C}_5^-$ ) while leaving the other ligands unchanged. While the  $\text{Cp}^*$  silyl complex has not been described in the literature, both the phosphine and phosphanyl borohydride adducts were reported by Malisch et al.<sup>[45]</sup> For the phosphine complex  $[\text{Cp}^*\text{Fe}(\text{CO})_2\text{PPh}_2\text{Me}]\text{I}$  in  $\text{CH}_2\text{Cl}_2$ , the CO stretching frequencies are observed at 2029 and 1987  $\text{cm}^{-1}$ , demonstrating that the effect of exchanging Cp for  $\text{Cp}^*$  is comparable to exchanging the phosphine ligand for the corresponding phosphanyl borohydride. Bands attributable to the CO ligands in  $\text{Cp}^*\text{Fe}(\text{CO})_2\text{PPh}_2\text{BH}_3$ , on the other hand, are found at 2007 and 1959  $\text{cm}^{-1}$  ( $\text{CH}_2\text{Cl}_2$ ). These frequencies lie above those seen for silyl complex **31**, indicating that moving from the phosphanyl borohydride to the silyl ligand has a more dramatic effect on the electronic structure of the compound than replacing Cp with  $\text{Cp}^*$ . Taken together, these results suggest that, viewed electronically, the difference between the phosphine and phosphanyl borohydride ligands is smaller than between the phosphanyl borohydride and silyl ligands.



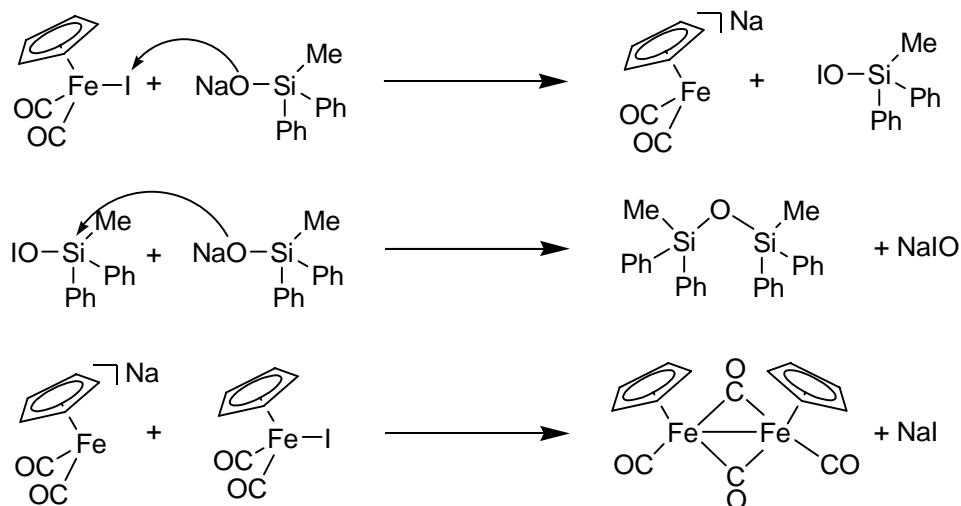
### 2.2.1.2 Reactions of $[\text{CpFe}(\text{CO})_2]^+$ with silyl chalcogenolates

After the successful and instructive comparison of silyl complex **31** with isoelectronic, isosteric phosphanyl borohydride and phosphine compounds, a similar study with silyl chalcogenolates was undertaken.

For reasons of comparability,  $\text{Ph}_2\text{MeSiONa}$  (**6**) was selected for initial investigation. However, when a THF solution of  $\text{FpI}$  is treated with **6**, the only Cp-containing product is  $\text{Fp}_2$  (**4.6.6**). In the  $^{29}\text{Si}$  NMR spectrum,  $(\text{Ph}_2\text{MeSi})_2\text{O}$  can be identified as the major silicon-containing product (its  $^1\text{H}$ ,  $^{13}\text{C}$  and  $^{29}\text{Si}$  NMR shifts correspond to an authentic sample prepared from  $\text{Ph}_2\text{MeSiCl}$  and  $\text{Ph}_2\text{MeSiONa}$ ). This result is particularly interesting since the same reaction using  $\text{Ph}_2\text{BH}_3\text{POK}$  also yields  $\text{Fp}_2$ . For reaction of the phosphanyl borohydride oxide,  $^1\text{H}$  NMR spectroscopy indicates the presences of  $\text{FpH}$ , which is known to decompose to  $\text{Fp}_2$  and  $\text{H}_2$ ,<sup>[135-137]</sup> suggesting that hydride transfer from the  $\text{BH}_3$  moiety to the iron center has occurred.

This reaction pathway, however, seems unlikely for **6**, since hydride transfer from a methyl group is unusual. Although no mechanistic studies were undertaken, it is plausible that the nucleophilic siloxide reacts at the iodide ligand rather than attacking the iron atom, as observed for the silanides  $t\text{Bu}_3\text{SiNa}$  and  $t\text{Bu}_2\text{MeSiNa}$  (**2**) in their reactions with  $\text{FpI}$  (cf. 2.2.1.1). This would leave a  $\text{Fp}^-$  fragment and intermediate “ $\text{IOSiPh}_2\text{Me}$ .” The intermediate silicon-containing species could subsequently be attacked by one equivalent of unreacted siloxide to give disiloxane  $(\text{Ph}_2\text{MeSi})_2\text{O}$  and  $\text{NaIO}$ . The complex iron anion would react with one equivalent of  $\text{FpI}$  to give  $\text{Fp}_2$  and  $\text{I}^-$  (Scheme 2.2.2). This suggested mechanism is also supported by the reaction of **6** with  $\text{I}_2$ , which produces disiloxane  $(\text{Ph}_2\text{MeSi})_2\text{O}$  as the major product; this can be thought of as analogous to the reaction of  $\text{I}_2$  with  $\text{OH}^-$ , which results in  $\text{IO}_3^-$ ,  $\text{I}^-$  and  $\text{H}_2\text{O}$ .<sup>[19]</sup>

However, the formation of  $\text{Fp}_2$  and  $(\text{Ph}_2\text{MeSi})_2\text{O}$  from **6** and  $\text{FpI}$  is slow, with ca. 50 % starting material left after 2 weeks stirring at room temperature. This slow reaction rate allows for the isolation of an adduct of **6** and  $\text{Fp}_2$  in which the siloxide sodium atoms are supported by donor-acceptor interactions with the oxygen atoms of the bridging carbonyl ligands in  $\text{Fp}_2$ . The red solid precipitates from benzene solution and can be recrystallized from toluene. UV-vis and NMR investigations indicate that the donor-acceptor bond is not stable in solution. The structural details of this adduct have been discussed together with related adducts of **6** in section 2.1.2.1.

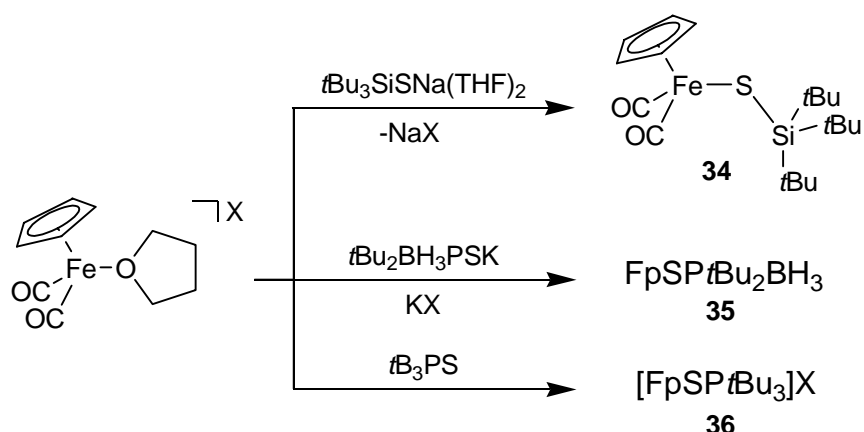


Scheme 2.2.2. Proposed mechanism for the reaction of Ph<sub>2</sub>MeSiONa (**6**) with FpI

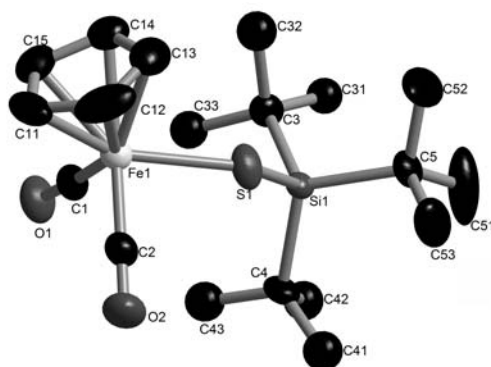
Due to the unsatisfactory results using FpI, a different Fp<sup>+</sup> starting material was sought in the hope that this would give more defined complexes in the reaction with silyl chalcogenolates. However, when **6** is reacted with FpBr, the same main products as in the reaction with FpI can be identified. Since the siloxide appears to attack at the halide ligand of FpI and FpBr, the complex cation [Fp(THF)]<sup>+</sup> was chosen, in which the halide is replaced with the neutral donor THF. Unfortunately, the reaction of **6** with [Fp(THF)]PF<sub>6</sub> is no more successful than that with FpI. Significant amounts of Fp<sub>2</sub> are formed, despite that fact that the siloxide can no longer attack at iodine (**4.6.7**). In this reaction, however, ferrocene is formed in addition to Fp<sub>2</sub>. The mechanism for this reaction is necessarily different from that suggested for the reaction of FpI with **6**, but its details are unclear.

Still searching for a method to prepare chalcogenolate complexes of Fp<sup>+</sup>, the reaction of silyl thiolate **10**(THF)<sub>2</sub> with [Fp(THF)]<sup>+</sup> was investigated. This compound reacts readily with [Fp(THF)]BF<sub>4</sub> in THF at room temperature to give the desired complex FpSSi*t*Bu<sub>3</sub> (**34**, **4.6.2**, Scheme 2.2.3). Recrystallization from a concentrated pentane solution yields X-ray quality crystals (Figure 2.2.2). The phosphine sulfide and phosphanyl borohydride sulfide complexes necessary for comparison, FpSP*t*Bu<sub>2</sub>BH<sub>3</sub> (**35**) and [FpSP*t*Bu<sub>3</sub>]PF<sub>6</sub> (**36**) have been reported and structurally and spectroscopically characterized.<sup>[127]</sup>

All three complexes adopt the expected structure with monodentate, end-on coordination of the sulfur donor ligands. In **36**, separated ion pairs are found. The molecular structure of **34** can be found in Figure 2.2.2; selected bond lengths and angles for all three compounds are in Table 2.2.3.

Scheme 2.2.3. Synthesis of isoelectronic complexes **34** – **36**

The effect of the increased steric bulk of **34** and **36** compared to **35** is most noticeable in the Fe-S-E bond, which is nearly  $130^\circ$  in **34** ( $129.01(7)^\circ$ ) and **36** ( $127.88(2)^\circ$ ), compared to  $115.86(4)^\circ$  in **35**. The Fe-S bond is also affected by the steric strain. For **34** and **36**, the longest reported Fe-S bonds in Fp complexes with terminal sulfur ligands are found ( $2.345(2)$  Å and  $2.3469(4)$  Å, respectively).<sup>[96]</sup> Less sterically hindered **35**, on the other hand, has a shorter Fe-S bond ( $2.3125(8)$  Å). This complex also displays a OC-Fe-CO angle of  $98.0(2)^\circ$ , nearly  $5^\circ$  larger than those found for the two complexes with three *t*Bu residues, **34** and **36**. For comparison, the Fe-S bond in FpSSiPh<sub>3</sub> is  $2.3195(11)$  Å, and the OC-Fe-CO angle is  $92.8(2)^\circ$ .<sup>[138]</sup>

Figure 2.2.2. Solid state structure of **34**. For clarity, hydrogen atoms have been omitted.

The iron-carbonyl bond lengths and the C-O distances in the carbonyl ligands, however, seem to follow trends that are independent of steric hindrance. Of the complexes **34** – **36**, the phosphine sulfide derivative complex **36** displays the longest Fe-CO and the shortest C-O distances (an average of  $1.799(2)$  and  $1.139(3)$  Å, respectively). The equally sterically hindered silyl thiolate complex **34**, on the other hand, has the shortest Fe-CO and the longest

C-O distances (an average of 1.776(5) and 1.151(6) Å, respectively). The phosphanyl borohydride sulfide complex **35** displays intermediate average bond lengths of 1.784(3) Å (Fe-CO) and 1.144(4) Å (C-O). These results suggest that the donor strength trends observed for the non-chalcogen complexes also hold true for the sulfur derivatives. The silyl thiolate  $t\text{Bu}_3\text{SiS}^-$  appears to be the strongest donor, causing increased Fe-CO backbonding, leading to lengthened C-O bonds and shortened Fe-CO bonds, followed by  $t\text{Bu}_2\text{BH}_3\text{PS}^-$  and finally  $t\text{Bu}_3\text{PS}$ .

**Table 2.2.3.** Selected bond lengths [Å] and angles [°] for **34** – **36**

	Fe-S	S-P/Si	C-O (avg)	Fe-CO (avg)	OC-Fe-CO	Fe-S-P/Si
<b>34</b>	2.345(2)	2.147(2)	1.151(6)	1.776(5)	93.1(2)	129.01(7)
<b>35</b>	2.3125(8)	2.087(1)	1.144(4)	1.784(3)	98.0(2)	115.86(4)
<b>36</b>	2.3469(4)	2.0473(5)	1.139(3)	1.799(2)	93.35(9)	127.88(2)

This general trend is also supported by the chemical shifts of the CO carbon atoms in the  $^{13}\text{C}$  NMR spectra (selected spectroscopic data Table 2.2.4). As explained above, a less shielded CO carbon atom correlates to a stronger donor ligand being attached to the same metal center.<sup>[109-111]</sup> The silyl thiolate complex **34** has the furthest downfield CO resonance (215.1 ppm), indicating that the silyl thiolate is the strongest donor of the three ligands. The CO resonances of **35** (213.1 ppm) and **36** (211.5 ppm) support this trend. Literature values for silyl thiolate and phosphine sulfide complexes of the types  $\text{FpSSiR}_3$  and  $[\text{FpSPR}_3]^+$  also suggest that silyl thiolates are stronger donors (e. g.  $\text{FpSSiPh}_3$ : 213.5 ppm;  $\text{FpSSi}i\text{Pr}_3$ : 214.7 ppm;<sup>[138]</sup>  $[\text{FpSPMe}_3]\text{PF}_6$ : 212.4 ppm;  $[\text{FpSPPPh}_3]\text{PF}_6$ : 211.3 ppm<sup>[139]</sup>). In contrast to the non-chalcogen compounds **31** – **33** (2.2.1.1), the differences in the chemical shifts of the Cp carbon atoms in the iron-sulfur complexes **34** – **36** are too small for any meaningful trend to be discerned.

When considering the IR data, **34** is found to have considerably lower carbonyl stretching frequencies than its isoelectronic, phosphorus-containing analogs. Silyl thiolate complex **34** has CO vibrations at 2030 and 1982  $\text{cm}^{-1}$ , compared to 2040 and 1994  $\text{cm}^{-1}$  for **35** and 2054 and 2010  $\text{cm}^{-1}$  for **36**. These results correspond well with those found in the literature. The lowest CO stretching frequencies reported for a phosphine sulfide complex of this type are for  $[\text{FpSPMe}_3]\text{BF}_4$  (2048 and 2000  $\text{cm}^{-1}$ )<sup>[140]</sup> and are well above the highest  $\tilde{\nu}(\text{CO})$  for a Fp-silyl thiolate complex ( $\text{FpSSiPh}_3$ : 2035 and 1988  $\text{cm}^{-1}$ ).<sup>[138]</sup> The CO stretching frequencies in the IR thus clearly demonstrate that the silyl thiolate is the strongest donor of the three, while the

phosphine sulfide is the weakest. In sum, the IR and NMR data indicate that the same trend observed for the non-chalcogen complexes **31** – **33** can be observed for the sulfur complexes **34** – **36**. However, the differences found for the iron-sulfur complexes are less than half as large as for the non-chalcogen derivatives.

**Table 2.2.4.** Selected spectroscopic parameters for **34** – **36**

	$\tilde{\nu}$ (CO) [cm <sup>-1</sup> ]	$\delta^{31}\text{P}/^{29}\text{Si}$	$\delta^{13}\text{C}$ (CO)	$\delta^{13}\text{C}$ (CMe <sub>3</sub> )	$\delta^{13}\text{C}$ (Cp)
<b>34</b>	2030, 1982	29.2 <sup>[a]</sup>	215.1	25.3	86.9
<b>35</b>	2040, 1994	86.8	213.1	36.8	86.5
<b>36</b>	2054, 2010 <sup>[140]</sup>	93.8	211.5	44.1	87.4

IR spectra measured in CH<sub>2</sub>Cl<sub>2</sub>; NMR spectra measured in CD<sub>2</sub>Cl<sub>2</sub> unless otherwise noted.  
[a] C<sub>6</sub>D<sub>6</sub>

## 2.2.2 Other transition metal complexes

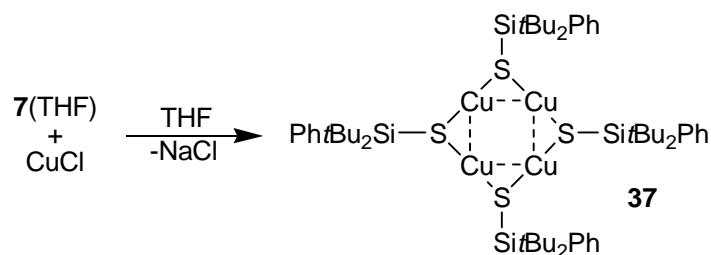
Apart from comparison with isoelectronic phosphorus-based species, it is also interesting to investigate the complexation behavior of silyl chalcogenolates in their own right. Such compounds have been employed to explore diverse and intriguing fields of chemistry. For example, Wolczanski has used the siloxide *t*Bu<sub>3</sub>SiO<sup>-</sup> to stabilize the olefin-to-alkylidene rearrangement of olefins in complexes of the type (*t*Bu<sub>3</sub>SiO)<sub>3</sub>ML (M = Nb, Ta; L = CH<sub>2</sub>=CHR),<sup>[9]</sup> and palladium(II) siloxide complexes have been implicated as critical intermediates in the cross-coupling of aryl iodides and siloxide-bound alkenes.<sup>[32]</sup> Furthermore, Corrigan has reported the synthesis of a number of L<sub>n</sub>MESiMe<sub>3</sub> complexes, which can be used as precursors to ternary MM'E clusters, which are of interest in semiconductor and nanomaterials technology.<sup>[2-4]</sup>

### 2.2.2.1 Synthesis via salt metathesis

One common method for the preparation of transition metal complexes is salt metathesis of alkali metal ligand salts and transition metal halides. This route has proven successful for silyl chalcogenolates as well,<sup>[90]</sup> producing compounds which display interesting properties. For example, the salt metathesis products of Fe(II), Co(II) and Ni(II) halides aggregate to macromolecular wheel or ellipse-shaped structures [MX(SSi*t*Bu<sub>3</sub>)]<sub>n</sub> (M = Fe, Co, Ni; X = Cl, Br, I; n = 12, 14) when exposed to elevated temperature under vacuum.<sup>[10, 141]</sup>

Salt metathesis was therefore applied to the sterically hindered silyl chalcogenolates that are the subject of the present investigation. When CuCl is treated with one equivalent of **7**(THF)

in THF, the tetrameric copper complex  $[\text{Cu}(\text{SSi}t\text{Bu}_2\text{Ph})]_4$  (**37**) is formed in moderate yield (4.7.1, Scheme 2.2.4). Recrystallization from toluene yields colorless needles of product.



Scheme 2.2.4 Synthesis of  $[\text{Cu}(\text{SSi}t\text{Bu}_2\text{Ph})]_4$  (**37**)

The tetramer crystallizes in the tetragonal space group  $I-4$  (Figure 2.2.3, selected bond lengths and angles in Table 2.2.5). The four copper atoms form a planar square with thiolate ligands bridging pairs of adjacent copper atoms. The  $\text{Cu}_4\text{S}_4$  core of the complex is bent, with two opposite thiolate sulfur atoms above the  $\text{Cu}_4$  plane and the other two below. The S-Cu-S angles, at  $178.38(4)^\circ$ , deviate slightly from linearity, while the Cu-S bond lengths are typical for bridging thiolates. The  $\text{Cu}\cdots\text{Cu}$  distances ( $2.861(1) \text{ \AA}$ ) are only  $0.3 \text{ \AA}$  longer than the Cu-Cu distance in copper metal.

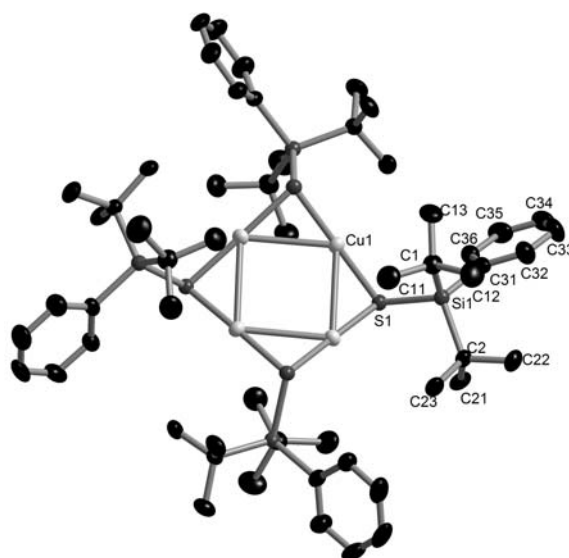


Figure 2.2.3. Solid state structure of **37**. For clarity, hydrogen atoms have been omitted.

Similar structural motifs, including short  $\text{M}\cdots\text{M}$  distances, have been observed for other chalcogenolate complexes of coinage metals.<sup>[14, 37, 39, 142]</sup> The gold trisyl chalcogenolates  $[\text{AuTeC}(\text{SiMe}_3)_3]_4$  and  $[\text{AuSC}(\text{SiMe}_3)_3]_4$  both display a tetrameric structure, although the  $\text{Au}\cdots\text{Au}$  distances are roughly  $0.7 \text{ \AA}$  longer than in gold metal for the tellurium derivative and  $0.4 \text{ \AA}$  longer for the sulfur compound. The tellurolate complex displays a bent core geometry

similar to that found for **37**, whereas the Au<sub>4</sub>S<sub>4</sub> core of the gold thiolate complex is nearly planar. Recently, the silver siloxide tetramer [Ag(OSi*t*Pr<sub>3</sub>)<sub>4</sub>]<sub>4</sub>, which contains a planar eight-membered Ag<sub>4</sub>O<sub>4</sub> ring, was also reported.<sup>[142]</sup>

**Table 2.2.5.** Selected bond lengths [Å] and angles [°] for **37**.

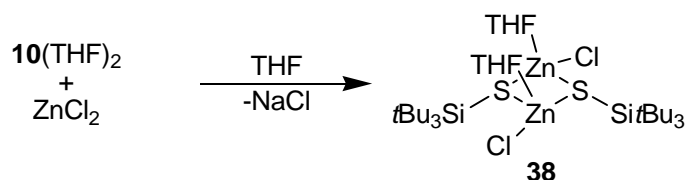
Cu(1)-S(1)	2.1582(10)	S(1)-Si(1)	2.1727(14)
Cu(1)-S(1)#1	2.1611(10)	Si(1)-C(1)	1.930(5)
Cu(1)-Cu(1)#2	2.8612(7)	Si(1)-C(2)	1.918(4)
Cu(1)-Cu(1)#1	2.8613(7)	Si(1)-C(31)	1.895(4)
S(1)-Cu(1)-S(1)#1	178.38(4)	Cu(1)-S(1)-Si(1)	108.85(5)
Cu(1)-S(1)-Cu(1)#2	82.97(4)	Cu(1)#2-S(1)-Si(1)	104.77(5)
Cu(1)#2-Cu(1)-Cu(1)#1	89.984(1)		

Symmetry transformations used to generate equivalent atoms:

#1 -y+1/2,x+1/2,-z+3/2 #2 y-1/2,-x+1/2,-z+3/2

The copper silyl thiolate complexes [Cu(SSiPh<sub>3</sub>)<sub>4</sub>]<sup>[14]</sup> and [Cu(SSiMe<sub>2</sub>*t*Bu)<sub>4</sub>]<sup>[37]</sup> both display the central Cu<sub>4</sub>S<sub>4</sub> eight-membered ring, although in these complexes, there are two shorter Cu⋯Cu interactions ([Cu(SSiPh<sub>3</sub>)<sub>4</sub>]<sub>4</sub>: 2.852(1) Å, [Cu(SSiMe<sub>2</sub>*t*Bu)<sub>4</sub>]<sub>4</sub>: 2.8128(6) and 2.7413(7) Å) and two longer ones ([Cu(SSiPh<sub>3</sub>)<sub>4</sub>]<sub>4</sub>: 3.027(1) Å, [Cu(SSiMe<sub>2</sub>*t*Bu)<sub>4</sub>]<sub>4</sub>: 2.9680(9) and 2.9541(9) Å), rather than four contacts of the same length, as seen in **37**. The complex with the sterically more hindered ligands [Cu(SSiMe<sub>2</sub>*t*Bu)<sub>4</sub>] displays a bent Cu<sub>4</sub>S<sub>4</sub> core, whereas in [Cu(SSiPh<sub>3</sub>)<sub>4</sub>]<sub>4</sub>, the core is essentially planar.

A compound with a more unusual coordination situation is obtained when ZnCl<sub>2</sub> is treated with one equivalent of **10**(THF)<sub>2</sub>. Filtration of the reaction mixture and recrystallization from toluene yields colorless blocks of [ZnCl(SSi*t*Bu<sub>3</sub>)(THF)]<sub>2</sub> (**38**, 4.7.2, Scheme 2.2.5).



Scheme 2.2.5 Synthesis of [ZnCl(SSi*t*Bu<sub>3</sub>)(THF)]<sub>2</sub> (**38**)

**Table 2.2.6.** Selected bond lengths [Å] for **38**

Zn(1)-S(1)	2.3478(17)	Zn(3)-S(3)	2.3324(18)
Zn(1)-S(2)	2.3359(14)	Zn(3)-S(3)#1	2.338(2)
Zn(2)-S(1)	2.3283(14)	Zn(4)-S(4)	2.327(2)
Zn(2)-S(2)	2.3393(17)	Zn(4)-S(4)#1	2.350(2)
Zn(1)-Cl(1)	2.1874(15)	Zn(3)-Cl(3)	2.184(2)
Zn(2)-Cl(2)	2.1759(17)	Zn(4)-Cl(4)	2.187(2)
Zn(1)-O(101)	2.055(4)	Zn(3)-O(301)	2.058(5)
Zn(2)-O(201)	2.087(4)	Zn(4)-O(401)	2.057(5)

Symmetry transformations used to generate equivalent atoms:  
 #1 -x+2,y,-z+3/2

The zinc silyl thiolate **38** (monoclinic  $C2/c$ ) crystallizes with one complete and two half molecules in the asymmetric unit (the full molecule is shown in Figure 2.2.4, selected bond lengths can be found in Table 2.2.6 and selected angles in Table 2.2.7). The two half molecules are both related to their second halves via a two-fold rotational axis. The structure displays a dimer with a central  $Zn_2S_2$  ring in which the zinc atoms are bridged by the two thiolate ligands. Terminal *cis*-chloro and *cis*-THF ligands complete the coordination spheres. The zinc centers are coordinated in a distorted tetrahedral fashion; the Cl-Zn-S angles ( $127.47(7)^\circ - 130.04(7)^\circ$ ) are widened considerably, while the S-Zn-S angles ( $88.18(6)^\circ - 88.54(8)^\circ$ ) are quite small.

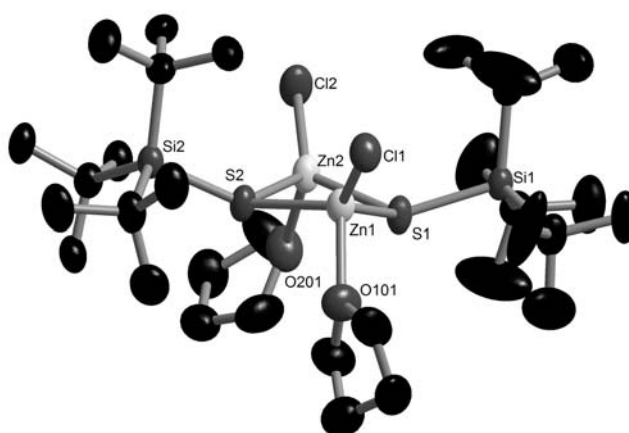


Figure 2.2.4. Solid state structure of  $[ZnCl(SSi(tBu)_3)(THF)]_2$  (**38**). For clarity, hydrogen atoms have been omitted.

The Zn-ligand distances vary only slightly between the four zinc atoms in the asymmetric unit, and all bond lengths are in the expected ranges. Such dimeric zinc thiolate structures are



fairly common, but nearly all of the reported examples are either homoleptic<sup>[143-147]</sup> or supported by chelating ligands.<sup>[143, 146, 148-151]</sup> For zinc chloride complexes, such structures are more unusual. Only two other examples have been structurally characterized, and both contain dichloro zinc moieties.<sup>[152, 153]</sup>

**Table 2.2.7.** Selected bond angles [°] for **38**

O(101)-Zn(1)-Cl(1)	101.99(12)	O(301)-Zn(3)-Cl(3)	101.65(18)
O(101)-Zn(1)-S(2)	101.15(13)	O(301)-Zn(3)-S(3)	102.45(16)
Cl(1)-Zn(1)-S(2)	129.07(7)	Cl(3)-Zn(3)-S(3)	129.62(9)
O(101)-Zn(1)-S(1)	100.88(15)	O(301)-Zn(3)-S(3)#1	102.96(18)
Cl(1)-Zn(1)-S(1)	130.04(7)	Cl(3)-Zn(3)-S(3)#1	127.56(10)
S(2)-Zn(1)-S(1)	88.31(6)	S(3)-Zn(3)-S(3)#1	88.41(7)
Zn(2)-S(1)-Zn(1)	88.15(6)	Zn(3)-S(3)-Zn(3)#1	88.76(7)
O(201)-Zn(2)-Cl(2)	101.74(15)	O(401)-Zn(4)-Cl(4)	102.35(18)
O(201)-Zn(2)-S(1)	102.67(15)	O(401)-Zn(4)-S(4)	102.49(17)
Cl(2)-Zn(2)-S(1)	129.33(7)	Cl(4)-Zn(4)-S(4)	128.35(9)
O(201)-Zn(2)-S(2)	102.82(15)	O(401)-Zn(4)-S(4)#1	101.2(2)
Cl(2)-Zn(2)-S(2)	127.47(7)	Cl(4)-Zn(4)-S(4)#1	129.19(9)
S(1)-Zn(2)-S(2)	88.69(6)	S(4)-Zn(4)-S(4)#1	88.54(8)
Zn(1)-S(2)-Zn(2)	88.18(6)	Zn(4)-S(4)-Zn(4)#1	87.68(7)

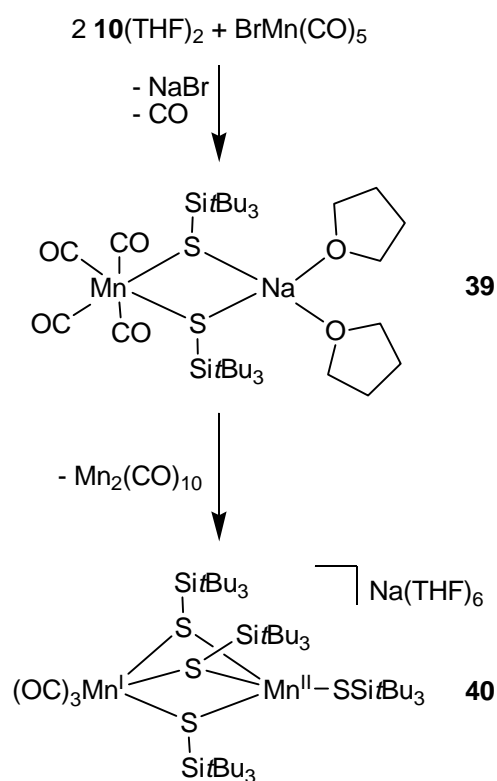
Symmetry transformations used to generate equivalent atoms: #1 -x+2,y,-z+3/2

These two multinuclear complexes, **37** and **38**, demonstrate the utility of salt metathesis reactions employing the silyl chalcogenolates presented here and could find long-term application as starting materials for larger aggregates. For example, it has been shown that transition-metal thiolate complexes are capable of reducing elemental sulfur and selenium, leading to cluster formation.<sup>[154, 155]</sup> In this case, such a reaction might be used to form multinuclear compounds containing not only thiolate ligands, but also coordinated sulfide or selenide.

Another approach to complexes with mixed chalcogen coordination is to start from materials which after salt metathesis leave the possibility of further manipulation. For example, in BrMn(CO)<sub>5</sub> the bromo ligand could be exchanged for a chalcogenolate, leaving unreacted CO ligands. These could then be expelled during a subsequent oxidative addition reaction, for

example with a dichalcogenide  $R_3SiE-ESiR_3$ . To this end, the reactivity of  $BrMn(CO)_5$  with  $10(THF)_2$  was explored.

When  $BrMn(CO)_5$  in THF is treated with two equivalents of  $10(THF)_2$ , immediate gas evolution is observed, and the reaction mixture quickly becomes heterogeneous. After 3 h, the thiolate has been completely consumed (as determined by NMR spectroscopy). Changing the solvent to pentane, filtering, and slowly concentrating the filtrate leads to deposition of X-ray quality crystals of  $(CO)_4Mn(\mu-SSi^tBu_3)_2Na(THF)_2$  (**39**, 4.7.3, Scheme 2.2.6). This complex crystallizes in the monoclinic space group  $P2_1/c$  with two crystallographically independent molecules in the asymmetric unit. These two molecules, however, display very similar structural parameters, and only one is shown in Figure 2.2.5 (selected bond lengths and angles in Table 2.2.8).



Scheme 2.2.6. Reaction of  $BrMn(CO)_5$  with two equivalents of  $10(THF)_2$

The core of **39** is formed by a four-membered  $MnS_2Na$  ring in which two bridging thiolate ligands bind to both the manganese and the sodium atom. Although a number of structurally characterized dimanganese complexes with  $(CO)_4Mn$  moieties and bridging thiolate ligands are known in the literature,<sup>[156-167]</sup> heterodinuclear complexes are less common,<sup>[168, 169]</sup> and none with alkali metals have been reported.<sup>[96]</sup>

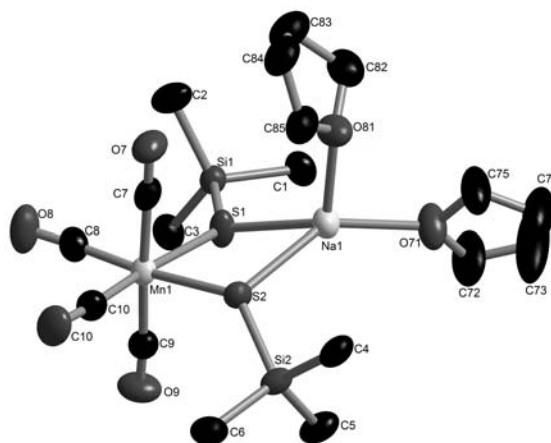


Figure 2.2.5. Solid state structure of **39**. For clarity, hydrogen atoms have been omitted, and only the quaternary carbon atoms of *t*Bu<sub>3</sub>Si groups are shown.

In contrast to the Na<sub>2</sub>E<sub>2</sub> four-membered rings formed by the sodium chalcogenolates *t*Bu<sub>3</sub>SiE<sub>2</sub>Na(THF)<sub>2</sub> (**10** – **12**), the M-S-M angles in **39** are significantly larger than 90°, while the S-M-S angles are smaller than 90°. Furthermore, the core four-membered rings of the sodium chalcogenolates **10** – **12** are planar, but the M<sub>2</sub>S<sub>2</sub> unit in **39** is bent. The two planes defined by sodium, manganese and one sulfur atom meet at an angle of 21.3° (29.1° for the second molecule), while the S<sub>2</sub>Mn plane meets the S<sub>2</sub>Na plane at an angle of 17.8° (24.8° for the second molecule).

**Table 2.2.8.** Selected bond lengths [Å] and angles [°] for **39**

Mn(1)-C(7)	1.868(6)	1.849(6) <sup>[a]</sup>	Mn(1)-C(9)	1.874(6)	1.855(6)
Mn(1)-C(8)	1.785(6)	1.787(6)	Mn(1)-C(10)	1.802(6)	1.769(5)
Mn(1)-S(1)	2.480(1)	2.454(2)	Mn(1)-S(2)	2.475(2)	2.488(2)
Na(1)-S(1)	2.744(3)	2.764(2)	Na(1)-S(2)	2.757(2)	2.755(2)
S(1)-Si(1)	2.144(2)	2.139(2)	S(2)-Si(2)	2.151(2)	2.141(2)
S(1)-Mn(1)-S(2)	83.67(5)	84.15(5)	S(1)-Na(1)-S(2)	73.86(6)	73.75(6)
Mn(1)-S(1)-Na(1)	99.69(6)	98.15(6)	Mn(1)-S(2)-Na(1)	99.47(6)	97.57(6)

[a] second number from the second molecule in the asymmetric unit, labelled “A” (e. g. Mn(1A)-C(7A) 1.849(6) Å)

The Mn atom is coordinated in a distorted octahedral fashion. Those C-Mn-C and C-Mn-S angles which are closest to 90° range between 82.2(2)° (C7-Mn1-S2) and 97.9(2)° (C8-Mn1-S1) for the first molecule and 80.2(2)° (C7A-Mn1A-S2A) and 99.1(2)° (C9A-Mn1A-S2A) for the second molecule, while those that are close to linearity are between 172.2(2)° (C8-Mn1-

S2) and  $175.0(2)^\circ$  (C7-Mn1-C9;  $169.2(2)^\circ$  and  $175.7(2)^\circ$  for the second molecule). The sodium atom has a distorted coordination sphere, with L-Na-L angles ranging from  $73.86(6)^\circ$  (S1-Na1-S2;  $73.75(6)^\circ$  for the second molecule) to  $138.1(2)^\circ$  (O71-Na1-S2;  $134.51$  for the second molecule). Furthermore, the Mn-S bond lengths are the longest found for a structurally characterized  $(\text{CO})_4\text{Mn-SR}$  compound.<sup>[96]</sup>

The  $^{29}\text{Si}$  NMR signal for **39** ( $\text{C}_6\text{D}_6$ : 29.5 ppm) is shifted downfield compared to **10**(THF)<sub>2</sub> (25.6 ppm). The IR stretching frequencies ( $\text{CH}_2\text{Cl}_2$  solution) are shifted to lower frequencies by  $30\text{-}40\text{ cm}^{-1}$  compared to reported complexes of the type  $(\text{CO})_4\text{Mn}(\mu\text{-SR})_2\text{Mn}(\text{CO})_4$ .<sup>[157, 158, 164]</sup> This result can be rationalized by assuming that the Na-SR interaction in **39** is primarily electrostatic in nature. This would mean that the thiolate ligands will act as stronger donors towards a single Mn center in the case of **39** rather than towards two Mn centers as in  $(\text{CO})_4\text{Mn}(\mu\text{-SR})_2\text{Mn}(\text{CO})_4$ , leading to stronger Mn-CO backbonding and consequently lower CO stretching frequencies in the Mn/Na complex **39** than in  $(\text{CO})_4\text{Mn}(\mu\text{-SR})_2\text{Mn}(\text{CO})_4$ .

When a solution of **39** is left to stand for a period of several weeks, crystals with different unit cell parameters than crystals of **39** can be isolated. These contain the Mn(I)Mn(II) complex  $\text{Na}(\text{THF})_6[(\text{CO})_3\text{Mn}(\mu\text{-SSi}t\text{Bu}_3)_3\text{Mn}(\text{SSi}t\text{Bu}_3)]$  (**40**, Figure 2.2.6, selected bond lengths and angles in Table 2.2.9) and trisulfane  $t\text{Bu}_3\text{SiS-S-Si}t\text{Bu}_3$  (Scheme 2.2.6).

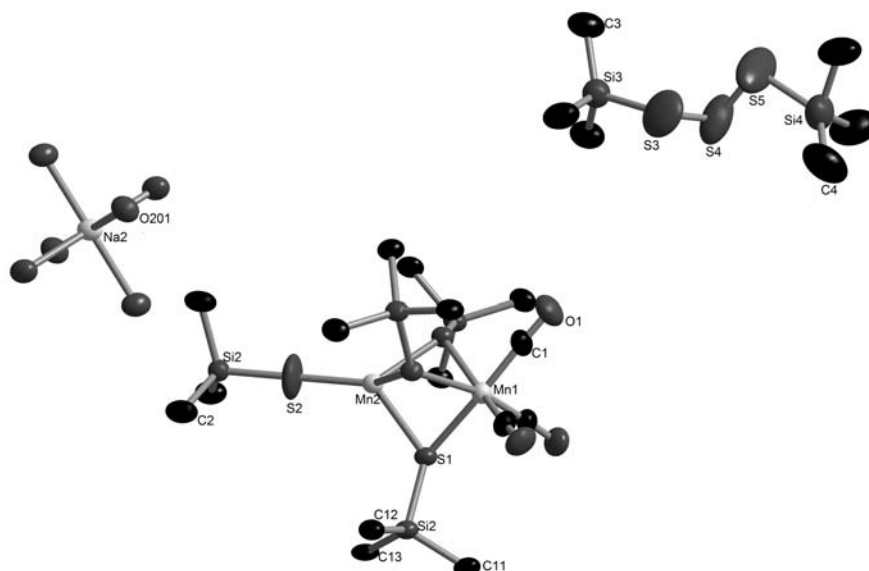


Figure 2.2.6. Solid state structure of **40** and co-crystallized  $t\text{Bu}_3\text{SiS-S-Si}t\text{Bu}_3$ . For clarity, only manganese and silicon bound carbon atoms are shown.

While the exact origin of these oxidation products is unclear, the molecular structure of **40** is quite interesting. The complex anion is situated on a three-fold rotational axis in the crystal, with the result that one-third of the molecule is contained in the asymmetric unit. The core of

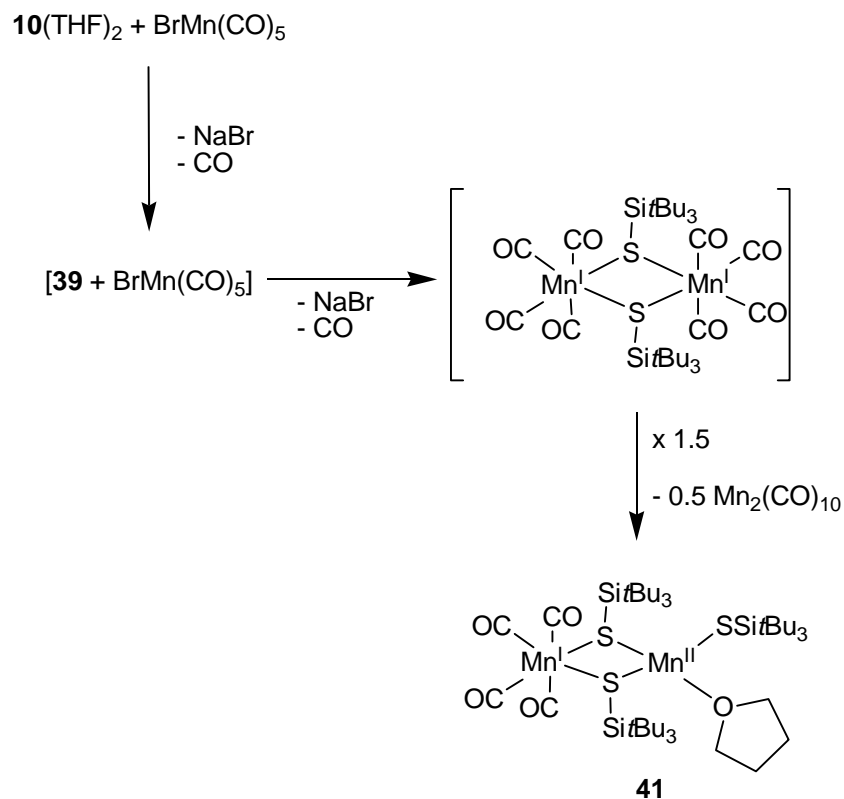
the structure consists of two manganese atoms bridged by three thiolate ligands. The Mn-S distances for the bridging thiolates are in the same range as those observed for **39**. The Mn-S bond to the terminal thiolate, however, is quite short (2.269(5) Å). Moreover, the Mn-S-Si angle is strictly linear, since the Mn-S and S-Si bonds lie on the three-fold rotational axis. The thermal ellipsoid of S3 (from the terminally bound thiolate) is fairly small, indicating that this linearity is not simply an artifact of crystallographic symmetry. This is significant, because there is a very limited number of transition metal complexes of silyl or alkyl chalcogenolates with linear coordination.<sup>[16]</sup> As discussed in the Introduction, it has been postulated in the literature that chalcogenolate ligands can act as six-electron donors (analogous to Cp) by donating 2  $\sigma$  and 4  $\pi$  electrons.<sup>[7]</sup> The prerequisite for this type of donation, however, is linear coordination, which is rarely observed. In the case of **40**, the significant steric hindrance of the supersilyl groups enforces such linear coordination, thus allowing for six-electron donation.

**Table 2.2.9.** Selected bond lengths [Å] and angles [°] for **40**

Mn(1)-C(1)	1.769(9)	Mn(2)-S(2)	2.269(5)
Mn(1)-S(1)	2.496(2)	S(1)-Si(1)	2.152(3)
Mn(1)-Mn(2)	3.063(3)	S(2)-Si(2)	2.064(6)
S(1)-Mn(2)	2.471(2)		
C(1)#1-Mn(1)-C(1)	91.0(4)	S(1)#1-Mn(2)-S(1)#2	86.50(8)
C(1)#1-Mn(1)-S(1)	84.4(3)	S(2)-Mn(2)-S(1)	127.71(6)
C(1)#2-Mn(1)-S(1)	100.2(3)	Si(2)-S(2)-Mn(2)	180.000(1)
C(1)-Mn(1)-S(1)	167.9(3)	Si(1)-S(1)-Mn(2)	126.16(10)
S(1)-Mn(1)-S(1)#1	85.43(8)	Si(1)-S(1)-Mn(1)	134.32(10)
Mn(2)-S(1)-Mn(1)	76.14(7)		

When  $\text{BrMn}(\text{CO})_5$  is treated with only one equivalent of  $\mathbf{10}(\text{THF})_2$  (**4.7.4**), the reaction initially proceeds as described above using two equivalents of thiolate. After 2 h, NMR spectra ( $^1\text{H}$ ,  $^{13}\text{C}$  and  $^{29}\text{Si}$ ) show that  $\mathbf{10}(\text{THF})_2$  has been completely consumed, and the dominant signals can be assigned to the 1:2 product **39** (Scheme 2.2.7). This compound reacts with the remaining equivalent of  $\text{BrMn}(\text{CO})_5$ , and after 4 h, the NMR spectra indicate that a single new main product has formed in good yield. Its  $^{29}\text{Si}$  NMR signal in  $\text{C}_6\text{D}_6$  is shifted slightly downfield from **39** (31.4 vs. 29.5 ppm). The same product can be identified in the

NMR spectra when a purified sample of **39** is treated with one equivalent of  $\text{BrMn}(\text{CO})_5$  (4.7.5).



Scheme 2.2.7. Reaction of  $\text{BrMn}(\text{CO})_5$  with one equivalent of **10**(THF)<sub>2</sub>

Unfortunately, this 1:1 substitution product could not be isolated. When the solvent is changed from THF to pentane, the mixture filtered and the filtrate concentrated, no crystalline product is recovered. When the concentrated filtrate is left to stand for two weeks at  $-20\text{ }^\circ\text{C}$ , orange crystals can be isolated. The solid-state structure, however, does not reveal the expected 1:1 thiolate complex with Mn(I), but rather the dinuclear Mn(I)Mn(II) complex  $(\text{CO})_4\text{Mn}(\mu\text{-SSi}t\text{Bu}_3)_2\text{Mn}(\text{SSi}t\text{Bu}_3)(\text{THF})$  (**41**). After several weeks at  $4\text{ }^\circ\text{C}$ , pale yellow crystals of  $\text{Mn}_2(\text{CO})_{10}$  separate from the mother liquor. Apparently, the intermediate observed in the NMR spectra disproportionates to Mn(0) carbonyl and **41** (Scheme 2.2.7).

Complex **41** crystallizes in the monoclinic space group  $C2/c$  with one complete molecule in the asymmetric unit (Figure 2.2.7, selected bond lengths and angles in Table 2.2.10). The core of the complex is formed by a  $\text{Mn}_2\text{S}_2$  four-membered ring. As in **39**, the S-M-S angles are considerably smaller than  $90^\circ$ , while the M-S-M angles are considerably larger. Mn1 is coordinated by four terminal carbonyl ligands and two bridging thiolates in a distorted octahedral fashion, while Mn2 is bound to two bridging thiolates and one terminal thiolate ligand. Its distorted coordination sphere is completed by one molecule of THF. The L-Mn-L

angles around Mn2 range from 82.04(7)° (S1-Mn2-S2) to 141.94(9)° (S2-Mn2-S3), and the Mn-S distances to the bridging thiolates are even longer than in **39**.

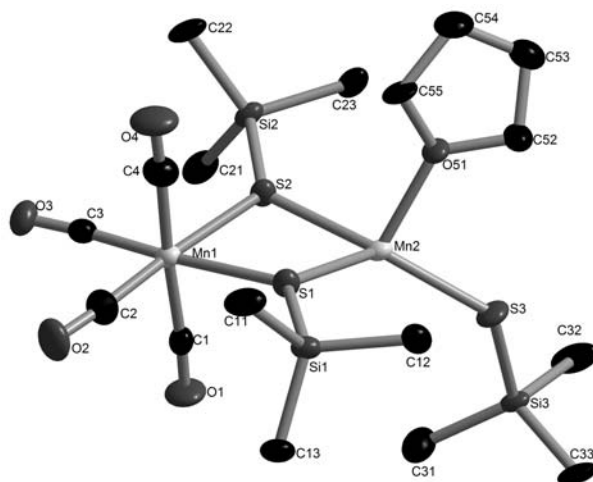


Figure 2.2.7. Solid state structure of **41**. For clarity, hydrogen atoms and methyl groups have been omitted.

The Mn2-S3-Si3 angle of the terminally bound thiolate ligand is 130.9(2)°. This considerable bend eliminates the possibility of six-electron donation from the thiolate to the manganese center. The Mn2-S3 bond is 2.349(2) Å, nearly 0.1 Å longer than the terminal Mn-S bond for the linearly bound thiolate in **40**, again supporting the conclusion that a bent coordination angle leads to less electron donation from the thiolate ligand.

**Table 2.2.10.** Selected bond lengths [Å] and angles [°] for **41**

Mn(1)-C(1)	1.832(9)	S(1)-Mn(1)-S(2)	81.41(7)
Mn(1)-C(2)	1.788(10)	S(1)-Mn(2)-S(2)	82.04(7)
Mn(1)-C(3)	1.844(9)	Mn(1)-S(1)-Mn(2)	96.20(8)
Mn(1)-C(4)	1.822(9)	Mn(1)-S(2)-Mn(2)	96.73(8)
Mn(1)-S(1)	2.543(2)	O(51)-Mn(2)-S(3)	94.2(2)
Mn(1)-S(2)	2.484(2)	O(51)-Mn(2)-S(1)	104.6(2)
Mn(2)-S(1)	2.478(2)	S(1)-Mn(2)-S(3)	127.45(9)
Mn(2)-S(2)	2.517(2)	O(51)-Mn(2)-S(2)	101.1(2)
Mn(2)-S(3)	2.349(2)	S(2)-Mn(2)-S(3)	141.94(9)
Mn(2)-O(51)	2.145(6)	Si(3)-S(3)-Mn(2)	130.9(2)

In the carbonyl stretching region of the IR spectrum, **41** shows bands of similar intensity to those in the spectrum of **39**. However, for dimanganese complex **41**, the CO stretches are

shifted to higher frequency by 10-20  $\text{cm}^{-1}$  compared to **39**. This is consistent with a more covalent bond between the bridging thiolates and Mn2 in **41** than from the bridging thiolates to Na in **39**. On the other hand, the carbonyl bands observed for **41** are still some 20  $\text{cm}^{-1}$  lower than those reported for complexes of the type  $(\text{CO})_4\text{Mn}(\mu\text{-SR})_2\text{Mn}(\text{CO})_4$ .<sup>[157, 158, 164]</sup> This can be rationalized by considering the higher  $\pi$ -accepting character of four carbonyl ligands coordinated to the second Mn atom in  $(\text{CO})_4\text{Mn}(\mu\text{-SR})_2\text{Mn}(\text{CO})_4$  as compared to one silyl thiolate and one THF in **41**.

The dinuclear manganese complex **41** is paramagnetic, since charge balance dictates that it contain one Mn(I) ( $d^6$ ) and one Mn(II) ( $d^5$ ) center. In order to quantify this effect, the Evans method was applied,<sup>[170, 171]</sup> and  $\mu_{\text{eff}}$  was determined to be 4.901  $\mu_{\text{B}}$ , corresponding to four unpaired electrons. This outcome confirms the strong paramagnetism of the dinuclear Mn(I)Mn(II) complex, but it is inconsistent with the expected result of  $\mu_{\text{eff}} = 5.9 \mu_{\text{B}}$  for a high-spin Mn(II) center (five unpaired electrons). Indeed, the experimental result of  $N = 4$  indicates an even number of d-electrons, which clearly cannot be reconciled with charge balance in the system, which requires there to be an odd number of d-electrons. Since the Evans method is sensitive to the concentration of analyte in the solution, it is possible that despite careful washing, the sample of **41** was contaminated with co-crystallized  $\text{Mn}_2(\text{CO})_{10}$ , a diamagnetic species which would decrease the overall paramagnetism of the sample, leading to a smaller experimental value for  $\mu_{\text{eff}}$ .

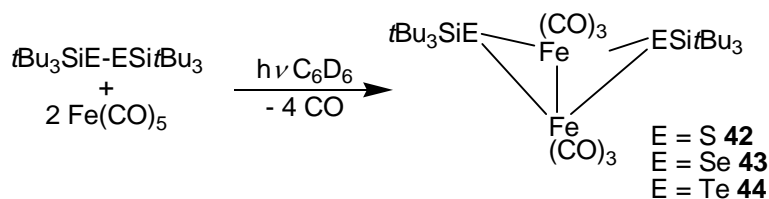
### 2.2.2.2 Synthesis via oxidative addition

Having explored salt metathesis as a means of synthesizing transition metal complexes of silyl chalcogenolates, oxidative addition of disilyl dichalcogenides to suitable transition metal centers was investigated as an alternative route. In the literature, this method has been successfully applied to the synthesis of transition metal chalcogenolate complexes<sup>[17, 18, 30, 31]</sup> Oxidative addition of diorganyl dichalcogenides has been exploited in the catalytic addition of RSe-SeR to alkynes,<sup>[17]</sup> and theoretical calculations of the oxidative addition of RE-ER (R = H, Me; E = S, Se, Te) to Pd(0) and Pt(0) complexes have been carried out.<sup>[18]</sup>

The iron carbonyl  $\text{Fe}(\text{CO})_5$  was chosen for oxidative addition studies since it is easily activated photochemically, and since its iron center is in a low oxidation state. When a 2:1  $\text{C}_6\text{D}_6$  solution of  $\text{Fe}(\text{CO})_5$  and ditelluride **25** ( $t\text{Bu}_3\text{SiTe-TeSi}t\text{Bu}_3$ ) is irradiated with a commonplace fluorescent lamp, the deep blue color of **25** turns to deep red over the course of 8 h. The NMR spectra indicate that **25** has been completely consumed and that a single new product has formed. Slow evaporation of the solvent leads to the deposition of deep red



needles of  $[(\text{CO})_3\text{Fe}(\text{TeSi}t\text{Bu}_3)]_2$  (**44**, 4.7.8, Scheme 2.2.8). If the same procedure is followed using diselenide **24** ( $t\text{Bu}_3\text{SiSe-SeSi}t\text{Bu}_3$ ) and  $\text{Fe}(\text{CO})_5$ , the end result is the homologous complex **43** with bridging selenolates ligands, but the reaction takes two weeks rather than 8 h to go to completion (4.7.7). The reaction of the disulfide **23** ( $t\text{Bu}_3\text{SiS-SSi}t\text{Bu}_3$ ) with  $\text{Fe}(\text{CO})_5$  to obtain **42** is not complete even after six months (4.7.6). Irradiation with a more powerful lamp does speed up the rate of reaction, but the reaction is not as specific, and significant amounts of byproduct are obtained.



Scheme 2.2.8 Oxidative addition of disilyl dichalcogenides to  $\text{Fe}(\text{CO})_5$

Obviously, the reactivity of the dichalcogenides differs significantly. Based on this evidence, the rate-determining step in these reactions is probably not the conversion of  $\text{Fe}(\text{CO})_5$  to  $\text{Fe}(\text{CO})_4$  and free CO, but appears to involve the activation of the chalcogen-chalcogen bond.

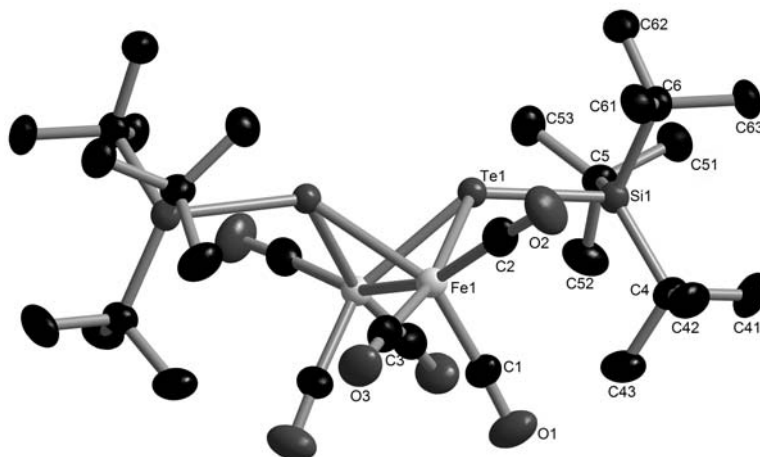


Figure 2.2.8. Solid state structure of **44**. For clarity, hydrogen atoms have been omitted.

This conclusion is consistent with theoretical studies of the addition of RE-ER (E = S, Se, Te) to Pd(0) and Pt(0) species.<sup>[18]</sup> It was demonstrated that the energetic barrier to oxidative addition is smallest for ditellurides and largest for disulfides, all else being equal. This can be attributed to the weaker Te-Te bond compared to the S-S bond. Conversely, formation of  $\text{M}(\text{SR})_2$  was found to be more exothermic than formation of  $\text{M}(\text{TeR})_2$ . For both activation barrier and exothermicity, the selenium species were found to lie between corresponding sulfur and tellurium compounds.

The dinuclear complexes **42** – **44** all adopt a butterfly-type structure in which each of the iron atoms is coordinated by three carbonyl ligands and two bridging chalcogenolates. The distorted octahedral coordination spheres are completed by an iron-iron bond. Since all three complexes adopt very similar structures, only the solid state structure of tellurolate **44** is shown in Figure 2.2.8. Selected bond lengths and angles for all three compounds are given in Table 2.2.11.

**Table 2.2.11.** Selected bond lengths [Å] and angles [°] for **42** – **44**

	<b>42</b>	<b>43</b>	<b>44</b>
Fe-Fe	2.5432(8)	2.5786(7)	2.645(2)
Fe-E	2.303(2), 2.318(2) 2.317(2), 2.322(2)	2.4026(6), 2.4175(7) 2.4301(6), 2.4340(7)	2.584(2), 2.619(2)
Fe-C (avg)	1.783(6)	1.792(5)	1.784(9)
E-Si	2.231(2), 2.210(2)	2.382(2), 2.372(2)	2.622(2)
Fe-E-Fe	66.79(4), 66.50(4)	64.68(2), 64.03(2)	61.11(4)
E-Fe-E	82.55(4), 82.74(5)	83.63(2), 83.86(2)	77.04(3)
C-Fe-E	156.6(2), 83.2(2) 106.9(2), 98.0(2) 156.2(2), 103.1(2) 96.8(2), 157.3(2) 102.5(2), 157.0(2) 83.8(2), 107.5(2)	97.8(2), 156.8(2) 101.6(2), 157.6(2) 82.2(2), 105.6(2) 96.0(2), 100.3(2) 157.8(2), 158.4(2) 105.1(2), 83.7(2)	144.9(3), 112.9(3) 90.8(3), 93.0(2) 167.9(3), 99.1(2)
C-Fe-Fe	104.0(2), 99.8(2) 152.9(2), 103.9(2) 100.5(2), 153.1(2)	103.9(2), 99.4(2) 152.5(2), 103.8(2) 151.5(2), 99.8(2)	151.5(2), 114.7(3) 87.7(3)

The “butterfly” structural motif observed in **42** – **44** is also found in other iron carbonyl chalcogenolates,<sup>[172-179]</sup> although no other similar complex with a silyl chalcogenolate has yet been reported. The iron-iron distances reported in the literature for tellurolate complexes of the type  $[(\text{CO})_3\text{Fe}(\text{TeR})]_2$  (2.605 – 2.657 Å) are in the same range as for **44** (2.645(2) Å). The Fe-Te distances, however, are somewhat shorter (average 2.54 Å vs. 2.607(2) Å). This disparity can be attributed to the differences between the silyl substituents in **44** and the alkyl

substituents in the literature complexes. These general trends also hold true for selenolate and thiolate derivatives, with similar Fe-Fe distances in the silyl and alkyl species, but with longer Fe-E bonds for the silyl chalcogenolates **42** and **43**. The exception is the thiolate complex bearing the bulky 2,4,6-tri-*iso*-propylthiophenolate ligand, which displays a short Fe-Fe distance (2.466(2) Å) and Fe-S bonds (2.311(2) - 2.321(2) Å) of roughly the same length as in  $[(\text{CO})_3\text{Fe}(\text{SSi}t\text{Bu}_3)]_2$ .<sup>[178]</sup>

When considering the carbonyl IR stretching frequencies of the complexes **42** – **44**, it is immediately apparent that the bands observed for the tellurolate complex are shifted to lower wavenumbers compared to the selenolate and thiolate species, which display similar spectra (Table 2.2.12). Apparently, the tellurolate is the strongest donor in this series. The carbonyl stretching frequencies reported in the literature for complexes of the type  $[(\text{CO})_3\text{Fe}(\text{ER})]_2$  also seem to follow this trend, but no homologous series has been published, so comparisons are hard to draw.<sup>[172, 173, 175-179]</sup>

**Table 2.2.12.** Carbonyl IR stretching frequencies [ $\text{cm}^{-1}$ ] for **42** – **44**

<b>42</b>	2068	2035	1999	1989
<b>43</b>	2066	2028	1982	
<b>44</b>	2048	2016	1977	

As these results clearly demonstrate, oxidative addition is a viable route to transition metal complexes of silyl chalcogenolates, including those which maintain potentially reactive coordination sites, such as CO. Recalling our long-term goal of synthesizing multinuclear clusters with different chalcogen-based ligands, the next step in this approach is to test the reactivity of oligochalcogen chains (as discussed in section 2.1.4) with suitable metal centers. Preliminary results show that when  $\text{Fe}(\text{CO})_5$  is treated with  $t\text{Bu}_3\text{SiS-S}_2\text{-SSi}t\text{Bu}_3$  (**29**) or  $(t\text{Bu}_3\text{SiS})_2\text{Te}$  (**27**), reaction occurs. Unfortunately, these reactions do not proceed selectively, and dark solid precipitates. The exploration and optimization of these and similar reactions should be the subject of future research.

### 3 Conclusion

In the literature, silyl chalcogenolates have been used to stabilize a wide variety of compounds.<sup>[7, 21, 32]</sup> In the course of the research presented here, this intriguing chemistry was explored further.

The sodium siloxide  $\text{Ph}_2\text{MeSiONa}$  (**6**), prepared from  $\text{Ph}_2\text{MeSiOH}$  and sodium in benzene, displays an interesting variety of structural motifs depending on crystallization conditions. Free of donor solvent, hexameric (**6**)<sub>6</sub> crystallizes in a double heterocubane structure. When the amount of donor solvent is limited, or a weak donor is used, an adduct between the hexamer and two molecules of donor is formed. Using an excess of strong donor leads to the formation of a tetrameric heterocubane supported by four molecules of donor.<sup>[180]</sup> A schematic depiction of these adducts is shown in Figure 3.1.

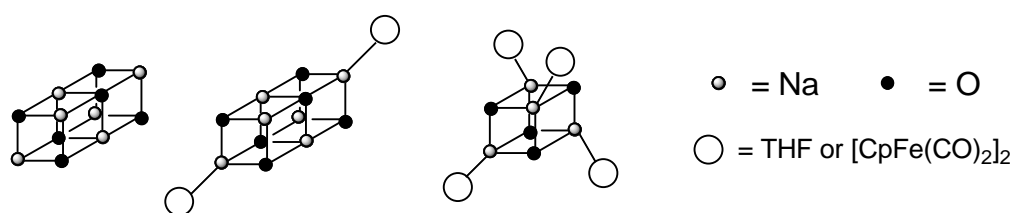


Fig 3.1. Schematic depiction of  $\text{Ph}_2\text{MeSiONa}$  adducts

In the past, silyl chalcogenolate research has focused mainly on siloxides, and the chemistry of higher homologues ( $\text{R}_3\text{SiS}^-$ ,  $\text{R}_3\text{SiSe}^-$ ,  $\text{R}_3\text{SiTe}^-$ ) has remained poorly explored. In order to investigate the properties of such compounds, the bulky silyl chalcogenolates  $t\text{Bu}_3\text{SiENa}$  and  $t\text{Bu}_2\text{PhSiENa}$  ( $\text{E} = \text{S}, \text{Se}, \text{Te}$ ; **7** – **12**) were synthesized (Figure 3.2).

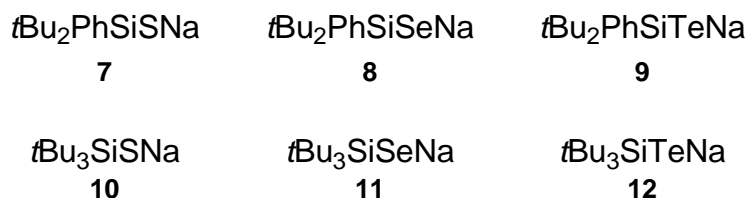


Figure 3.2. Sodium silyl chalcogenolates studied

The steric bulk of the silyl residues employed here allows facile access to alkali metal silanides  $t\text{Bu}_2\text{PhSiNa}$  and  $t\text{Bu}_3\text{SiNa}$ , which nucleophilically degrade elemental chalcogens to produce silyl chalcogenolates. X-ray crystal structure analyses of chalcogenolates **7** – **12**

reveal either dimers with central  $\text{Na}_2\text{E}_2$  four-membered rings or tetramers with  $\text{Na}_4\text{E}_4$  heterocubane cores.<sup>[90]</sup>

Compounds **7** – **12** can be easily derivatized. Protonolysis leads to chalcogenols  $t\text{Bu}_2\text{RSiEH}$  ( $\text{R} = \text{Ph}, t\text{Bu}$ ;  $\text{E} = \text{S}, \text{Se}, \text{Te}$ ; **14** – **19**), which display characteristic downfield shifts of the chalcogenol hydrogen atoms in their  $^1\text{H}$  NMR spectra. When the chalcogenolates **7** – **12** are exposed to atmospheric conditions, oxidation takes place faster than protonation, and the corresponding disilyl dichalcogenides  $t\text{Bu}_2\text{RSiE-ESiR}t\text{Bu}_2$  ( $\text{R} = \text{Ph}, t\text{Bu}$ ;  $\text{E} = \text{S}, \text{Se}, \text{Te}$ ; **20** – **25**) are formed. Disulfides  $t\text{Bu}_2\text{PhSiS-SSiPh}t\text{Bu}_2$  (**20**) and  $t\text{Bu}_3\text{SiS-SSi}t\text{Bu}_3$  (**23**) can also be prepared by reaction of the appropriate sodium silanide  $t\text{Bu}_2\text{RSiNa}$  ( $\text{R} = \text{Ph}, t\text{Bu}$ ) with  $\text{S}_2\text{Cl}_2$ . Dichalcogenides **20** – **25** all display the same core molecular structure in the solid state, with Si-E-E-Si torsion angles of exactly  $180^\circ$ .<sup>[90]</sup> Nucleophilic substitution can also be employed in the synthesis of  $t\text{Bu}_3\text{SiSSiMe}_3$  from  $t\text{Bu}_3\text{SiSNa}$  (**10**) and  $\text{ClSiMe}_3$ .

Oxidative addition of dichalcogenides to low oxidation state metal centers is a well established pathway to transition metal chalcogenolates.<sup>[17, 18, 30, 31]</sup> In an expansion of this principle, it would be interesting to use oxidative addition to simultaneously introduce not only chalcogenolates  $\text{RE}^-$ , but also chalcogenides  $\text{E}^{2-}$  or dichalcogenides  $\text{E}_2^{2-}$ . In order to explore the viability of this new concept, oligochalcogen chains are required, which could give rise to coordinated chalcogens in different bonding situations. For example, a molecule of the type  $\text{RS-S-SR}$  could be used to simultaneously introduce two thiolate ligands  $\text{RS}^-$  and one metal-bound sulfide  $\text{S}^{2-}$ .

To this end, three oligochalcogen species were synthesized. The tetrasulfane  $t\text{Bu}_3\text{SiS-S}_2\text{-SSi}t\text{Bu}_3$  (**29**) can be prepared from  $t\text{Bu}_3\text{SiSNa}$  (**10**) and  $\text{S}_2\text{Cl}_2$  in a double nucleophilic substitution reaction. It is stable to atmospheric conditions as a solid and in solution, and it shows no tendency to eliminate sulfur to form trisulfane or disulfide. Its solid state structure is shown in Figure 3.3.

The analogous reaction using  $\text{Se}_2\text{Cl}_2$  appears to result in initial formation of the 1,4-disilyl-2,3-diselenotetrasulfane  $t\text{Bu}_3\text{SiS-Se}_2\text{-SSi}t\text{Bu}_3$ , but one equivalent of elemental selenium is quickly eliminated to give the selenium(II) dithiolate  $(t\text{Bu}_3\text{SiS})_2\text{Se}$  (**28**). This species is metastable, and slow extrusion of the second selenium atom results in formation of disulfide  $t\text{Bu}_3\text{SiS-SSi}t\text{Bu}_3$  (**23**). The stable tellurium(II) dithiolate  $(t\text{Bu}_3\text{SiS})_2\text{Te}$  (**27**) was successfully prepared in an exchange reaction of  $t\text{Bu}_3\text{SiSH}$  (**17**) with  $(t\text{BuS})_2\text{Te}$ . Slow removal of low-boiling  $t\text{BuSH}$  together with the solvent via distillation at normal pressure shifts the equilibrium to the products side, and tellurium(II) dithiolate (**27**) can be recovered in good yield.

Before investigating the coordination chemistry and reactivity of these main-group ligand precursors, an excursion was made into the comparison of isoelectronic ligands. Silanides  $R_3Si^-$  can be seen as the anionic analogs of phosphines  $R_3P$ , where the phosphorus atom has been replaced by silicon, thus introducing a negative charge. Phosphanyl borohydrides  $R_2BH_3P^-$ , in which a substituent methyl group from a phosphine has been replaced with a  $BH_3$  moiety, are a ligand class with intermediate properties in which the central atom (phosphorus) is retained, but a negative charge has been introduced.<sup>[11]</sup> The same analogy can be drawn for the chalcogen derivatives (i. e. phosphine oxides, phosphanyl borohydride oxides, and siloxides; cf. Figure 3.4).<sup>[12]</sup>

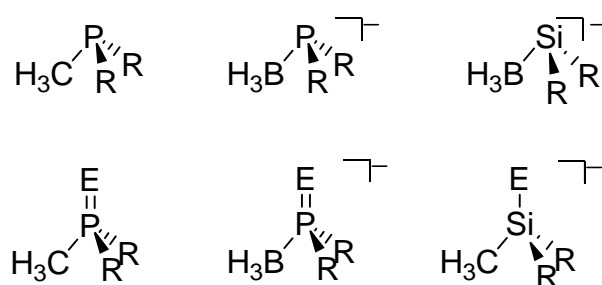


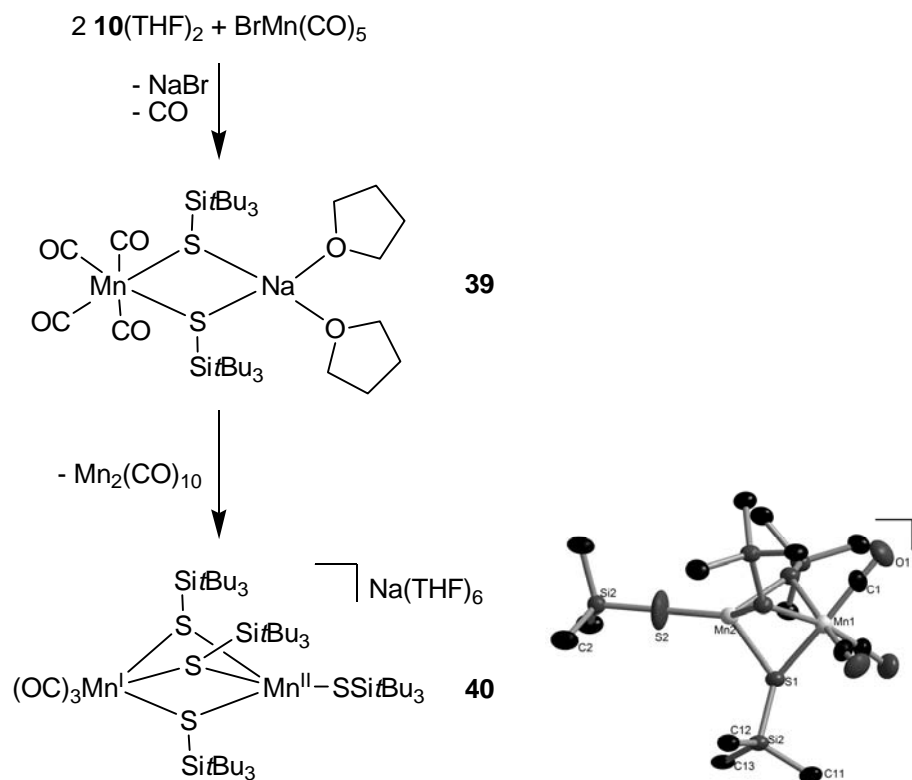
Figure 3.4. Isoelectronic ligands phosphines, phosphanyl borohydrides and silanides (top) with their chalcogen derivatives (bottom)

In order to compare isoelectronic, isosteric transition metal complexes,  $CpFe(CO)_2SiPh_2Me$  (**31**) was prepared and characterized spectroscopically and by X-ray structure analysis. In comparison to the isoelectronic compounds  $CpFe(CO)_2PPh_2BH_3$  and  $[CpFe(CO)_2PPh_2Me]^+$ , silyl complex **31** was found to have the highest electron density at the iron center and the strongest  $\pi$ -backbonding to the carbonyl ligands, indicating that the silyl ligand is a stronger donor than the phosphanyl borohydride or phosphine.

Similarly, thiolate complex  $CpFe(CO)_2SSi^iBu_3$  (**34**) was synthesized and compared to  $CpFe(CO)_2SP^iBu_2BH_3$  and  $[CpFe(CO)_2SP^iBu_3]^+$ . On the basis of structural and spectroscopic data, thiolate  $^iBu_3SiS^-$  was determined to be a stronger donor than  $^iBu_3PS$  or  $BH_3^iBu_2PS^-$ , although the difference in donor strength is of about half the magnitude as for the non-chalcogen compounds.<sup>[127]</sup>

Beyond the comparison of isoelectronic ligands, silyl chalcogenolates **7 – 12** proved suitable for the synthesis of transition metal complexes. Salt metathesis with metal halides yields coordination complexes. In this manner, the tetrameric copper(I) thiolate  $[Cu(SSi^iBu_2Ph)]_4$  (**37**) can be prepared from  $^iBu_2PhSiNa(THF)$  (**7(THF)**) and  $CuCl$ . In the solid-state,  $[Cu(SSi^iBu_2Ph)]_4$  (**37**) displays short  $Cu\cdots Cu$  distances.

Furthermore, a dimeric zinc(II) thiolate can be isolated from the reaction of  $t\text{Bu}_3\text{SiNa}(\text{THF})_2$  ( $\mathbf{10}(\text{THF})_2$ ) and  $\text{ZnCl}_2$ . The unusual solid-state structure of  $[\text{ZnCl}(\text{SSi}t\text{Bu}_3)(\text{THF})]_2$  ( $\mathbf{38}$ ) contains a central  $\text{Zn}_2\text{S}_2$  four-membered ring in which the four-coordinate zinc atoms are bound to two bridging thiolates as well as to *cis*-chloro and THF ligands. <sup>[90]</sup>

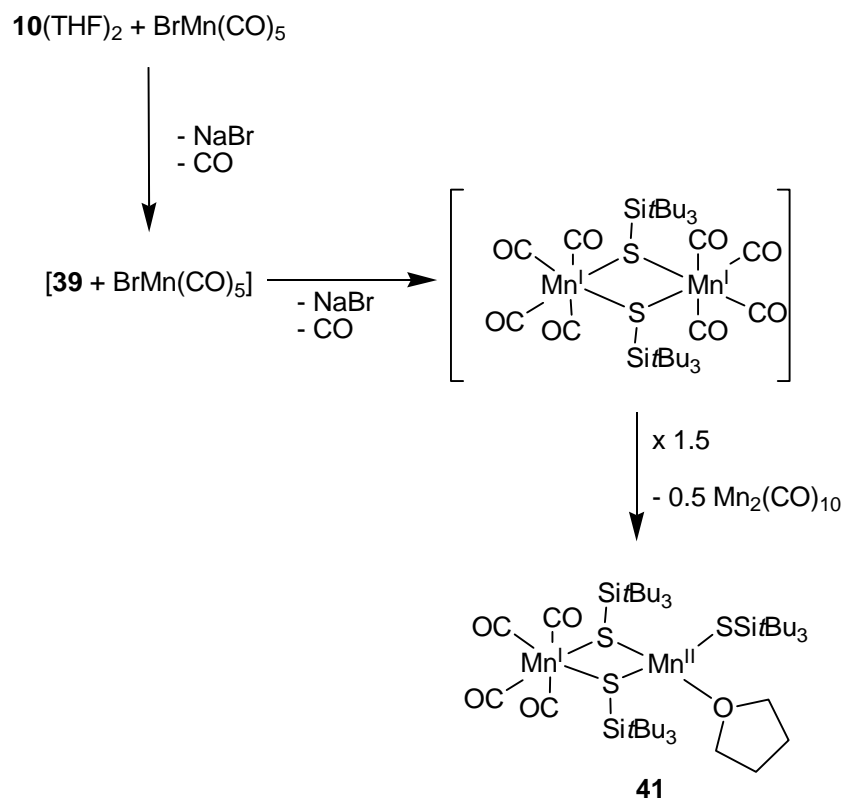


Scheme 3.1. Reaction of  $\text{BrMn}(\text{CO})_5$  with two equivalents  $t\text{Bu}_3\text{SiNa}(\text{THF})_2$  ( $\mathbf{10}(\text{THF})_2$ ; left) and solid state structure of the complex  $\text{Mn}(\text{I})\text{Mn}(\text{II})$  anion  $\mathbf{40}$  (right). For clarity, only the quaternary carbon atoms of the  $t\text{Bu}_3\text{Si}$  substituents are shown.

The application of salt metathesis to systems which retain reactive ligands such as CO opens new possibilities for the synthesis of chalcogenolate complexes. When  $\text{BrMn}(\text{CO})_5$  is treated with one or two equivalents of  $t\text{Bu}_3\text{SiNa}(\text{THF})_2$  ( $\mathbf{10}(\text{THF})_2$ ), the 1:2 substitution product  $(\text{CO})_4\text{Mn}(\mu\text{-SSi}t\text{Bu}_3)_2\text{Na}(\text{THF})_2$  ( $\mathbf{39}$ ) is formed quickly (Schemes 3.1 and 3.2).

When an additional equivalent of  $\text{BrMn}(\text{CO})_5$  is present (as in the 1:1 reaction) or subsequently added to the reaction mixture, the 1:1 exchange product can be observed in the NMR spectra. This unstable species disproportionates, and crystals of the dinuclear  $\text{Mn}(\text{I})\text{Mn}(\text{II})$  complex  $(\text{CO})_4\text{Mn}(\mu\text{-SSi}t\text{Bu}_3)_2\text{Mn}(\text{SSi}t\text{Bu}_3)(\text{THF})$  ( $\mathbf{41}$ ) can be isolated along with  $\text{Mn}_2(\text{CO})_{10}$  (Scheme 3.2). The 1:2 product  $(\text{CO})_4\text{Mn}(\mu\text{-SSi}t\text{Bu}_3)_2\text{Na}(\text{THF})_2$  ( $\mathbf{39}$ ) also disproportionates after standing for several weeks, and crystals containing the anionic dinuclear  $\text{Mn}(\text{I})\text{Mn}(\text{II})$  species  $[(\text{CO})_3\text{Mn}(\mu\text{-SSi}t\text{Bu}_3)_3\text{Mn}(\text{SSi}t\text{Bu}_3)]^-$  ( $\mathbf{40}$ ) are deposited (Scheme 3.1). The complex anion contains a terminal thiolate ligand with a linear  $\text{Mn-S-Si}$

angle. The prerequisite for six-electron donation ( $2 \sigma$  and  $4 \pi e^-$ ) is thus fulfilled, clearing the way for comparisons to the analogous six-electron donor  $\text{Cp}^-$ .



Scheme 3.2. Reaction of  $\text{BrMn}(\text{CO})_5$  with one equivalent  $t\text{Bu}_3\text{SiNa}(\text{THF})_2$  ( $\mathbf{10}(\text{THF})_2$ )

Oxidative addition of dichalcogenides to low oxidation state metal centers is also a feasible method for the synthesis of transition metal complexes of silyl chalcogenolates.<sup>[90]</sup> When  $\text{Fe}(\text{CO})_5$  is treated with one of the dichalcogenides  $t\text{Bu}_3\text{SiS-Si}t\text{Bu}_3$  ( $\mathbf{23}$ ),  $t\text{Bu}_3\text{SiSe-SeSi}t\text{Bu}_3$  ( $\mathbf{24}$ ), or  $t\text{Bu}_3\text{SiTe-TeSi}t\text{Bu}_3$  ( $\mathbf{25}$ ), the corresponding dinuclear complex  $[(\text{CO})_3\text{Fe}(\text{ESi}t\text{Bu}_3)]_2$  ( $\text{E} = \text{S}, \text{Se}, \text{Te}; \mathbf{42} - \mathbf{44}$ ) is formed. All three complexes adopt a butterfly-type structure in the solid state in which the distorted octahedral coordination sphere around the iron atoms is formed by three CO ligands, two bridging chalcogenolates and completed by an iron-iron bond. The molecular structure of the tellurolate complex  $\mathbf{44}$  is shown in Figure 3.5.

The reaction of  $\text{Fe}(\text{CO})_5$  with  $t\text{Bu}_3\text{SiE-ESi}t\text{Bu}_3$  ( $\mathbf{23} - \mathbf{25}$ ) is activated photochemically with mild irradiation from a fluorescent lamp. Under these conditions, the tellurolate complex  $\mathbf{44}$  forms quantitatively within 8 h. Reaction of diselenide  $t\text{Bu}_3\text{SiSe-SeSi}t\text{Bu}_3$  ( $\mathbf{24}$ ) with  $\text{Fe}(\text{CO})_5$  to form selenolate complex  $\mathbf{43}$  is complete after 14 d, whereas the thiolate complex  $[(\text{CO})_3\text{Fe}(\text{SSi}t\text{Bu}_3)]_2$  ( $\mathbf{42}$ ) forms slowly over the course of six months. Obviously, the reactivity of dichalcogenides  $\mathbf{23} - \mathbf{25}$  differs significantly. The rate-determining step in these reactions is probably not the conversion of  $\text{Fe}(\text{CO})_5$  to  $\text{Fe}(\text{CO})_4$  and free CO, but appears to



involve the activation of the chalcogen-chalcogen bond. The IR spectra of the three homologous complexes **42** – **44** indicate that the telluroate is the strongest donor.

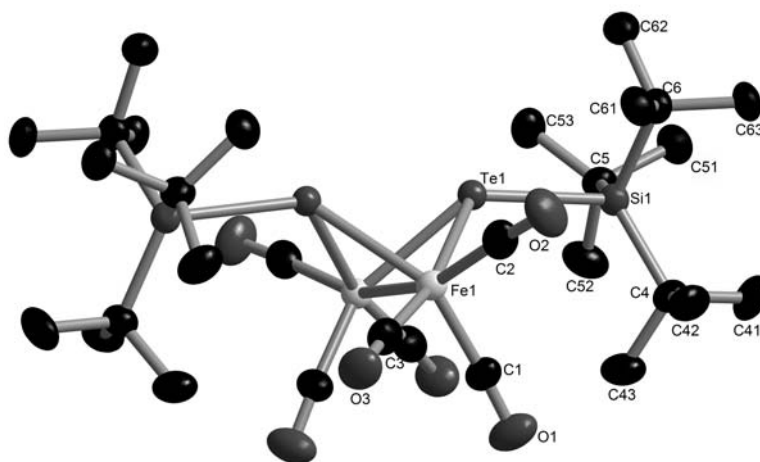


Figure 3.5. Molecular structure of the iron telluroate  $[(CO)_3Fe(TeSi^tBu_3)]_2$  (**44**). For clarity, hydrogen atoms have been omitted.

In the course of the work presented here, the chemistry of a group of sodium silyl chalcogenolates was investigated. Transition metal complexes were prepared via salt metathesis and, in part, display novel coordination modes. Oxidative addition reactions open new possibilities for the synthesis of transition metal complexes of silyl chalcogenolates. Through the development of new silyl-capped oligochalcogen species, the groundwork was laid for the preparation of multinuclear compounds containing both chalcogenolate and chalcogenide ligands.

## 4 Experimental

### 4.1 General considerations

All experiments were carried out under dry argon or nitrogen using standard Schlenk and glove box techniques, unless otherwise noted. Alkane solvents were dried over sodium/lead alloy and freshly distilled prior to use. Ethereal and aromatic solvents were distilled from sodium/benzophenone. Chlorinated solvents were dried over molecular sieves. Unless otherwise noted, starting materials were purchased from commercial sources and used without further purification. NMR spectra were recorded on a Bruker AM 250, a Bruker DPX 250, a Bruker Avance 300, and a Bruker Avance 400 spectrometer. Tetramethylsilane was used as an external standard for  $^1\text{H}$ ,  $^{13}\text{C}$  and  $^{29}\text{Si}$  spectra. The  $^{29}\text{Si}$  spectra were recorded using the INEPT pulse sequence with empirically optimized parameters for polarization transfer from the *tert*-butyl (*t*Bu<sub>3</sub>Si-, *t*Bu<sub>2</sub>PhSi- and *t*Bu<sub>2</sub>MeSi-) or methyl (Ph<sub>2</sub>MeSi-) substituents. Using Te(OH)<sub>6</sub> in D<sub>2</sub>O at 712 ppm as an external standard,  $^{125}\text{Te}$  spectra were referenced to Me<sub>2</sub>Te at 0 ppm.  $^{77}\text{Se}$  spectra were referenced to Me<sub>2</sub>Se at 0 ppm. IR spectra were recorded on a Perkin-Elmer 1650 FTIR spectrophotometer or on a Jasco FTIR-420 spectrophotometer. Elemental analyses were performed at the microanalytical laboratories of the Universität Frankfurt. Cyclic voltammetry was performed on a Princeton Applied Research potentiostat in THF solution with [NBu<sub>4</sub>][PF<sub>6</sub>] as the electrolyte. A platinum electrode was used with ferrocene as an internal standard. Mass spectrometry (ESI) was performed with a Fisons VG Platform II instrument. UV-vis absorption spectroscopy was carried out in cyclohexane using a Varian Cary 50 Scan spectrophotometer and a Perkin Elmer 555 spectrophotometer.

### 4.2 Syntheses associated with 2.1.1 Sodium silanides

Di-*tert*-butylmethylsilane (*t*Bu<sub>2</sub>MeSiH)<sup>[60]</sup> and 4,4'-bis(trimethylsilyl)biphenyl (**4**)<sup>[181]</sup> were prepared according to the literature procedures.

#### 4.2.1 *t*Bu<sub>2</sub>MeSiBr (**1**)

A solution of Br<sub>2</sub> (4.85 ml, 15.13 g, 94.7 mmol) in pentane (15 ml) is added to a solution of *t*Bu<sub>2</sub>MeSiH (14.49 g, 92.0 mmol) in pentane (60 ml) at 0 °C. After complete addition, the mixture is warmed to room temperature and volatiles are removed at 40 torr. The resulting oily residue is distilled (80-90 °C at 10-15 torr) and the pure product recovered as a colorless,

crystalline, low-melting solid.  $^1\text{H}$  NMR ( $\text{C}_6\text{D}_6$ , 250.1 MHz) = 0.987 (s, 18H,  $\text{CCH}_3$ ), 0.301 (s, 3H,  $\text{SiCH}_3$ ) ppm.  $^{13}\text{C}$  NMR ( $\text{C}_6\text{D}_6$ , 62.90 MHz) = 27.7 ( $\text{CCH}_3$ ), 21.7 ( $\text{CCH}_3$ ), n. o. ( $\text{SiCH}_3$ ) ppm.  $^{29}\text{Si}$  NMR ( $\text{C}_6\text{D}_6$ , 49.7 MHz) = 39.6 ppm.

#### 4.2.2 *t*Bu<sub>2</sub>MeSiNa(THF)<sub>x</sub>(2(THF)<sub>x</sub>)

Sodium (ca. 2 g, 87 mmol) and biphenyl (1.29 g, 8.3 mmol) are stirred overnight in THF (20 ml), giving a dark green solution surrounding blocks of unreacted sodium. To this mixture is added dropwise a solution of **1** (4.2.1, 3.38 g, 14.2 mmol) in THF (15 ml) over 2.5 hours. After 16 h stirring, all volatiles are removed in vacuo and the dark brown residue is extracted with pentane (25 ml), the extract filtered, and the filter cake washed with pentane (10 ml). Volatiles are removed from the dark brown filtrate in vacuo overnight, and the resulting brown residue is dissolved in THF (30 ml) to give a 0.305 M solution of the product in THF (9.15 mmol, 64 %).  $^1\text{H}$  NMR ( $\text{C}_6\text{D}_6$ , 250.1 MHz) = 3.450 (m, 4H, THF  $\text{OCH}_2$ ) 1.346 (s, 18H,  $\text{CCH}_3$ ), 0.330 (s, 3H,  $\text{SiCH}_3$ ), n.o. (THF  $\text{CCH}_2$ ) ppm.  $^{13}\text{C}$  NMR ( $\text{C}_6\text{D}_6$ , 62.90 MHz) = 68.0 (THF  $\text{OCH}_2$ ), 32.2 ( $\text{CCH}_3$ ), 25.4 (THF  $\text{CCH}_2$ ) 21.3 ( $\text{CCH}_3$ ), 0.3 ( $\text{SiCH}_3$ ) ppm.  $^{29}\text{Si}$  NMR ( $\text{C}_6\text{D}_6$ , 49.7 MHz) = 14.4 ppm.

#### 4.2.3 Bis(THF)(18-crown-6)sodium 4,4'-bis(di-*tert*-butylmethylsilyl)biphenylide (**3**)

To a solution of **2**(THF)<sub>x</sub> in THF (4.4.2, 0.305 M, 3.00 ml, 0.92 mmol) is added 18-crown-6 (241 mg, 0.91 mmol). Concentration of the solution to ca. 0.75 ml leads to the deposition of dark green, nearly opaque, extremely air-sensitive needles (42 mg, 0.05 mmol, 5 %), which were characterized by X-ray crystallography.

#### 4.2.4 4,4'-Bis(di-*tert*-butylmethylsilyl)biphenyl

Exposure of dark green crystals of **3** (4.2.3) to air causes an immediate loss of color and oxidation to the neutral species.  $^1\text{H}$  NMR ( $\text{C}_6\text{D}_6$ , 250.1 MHz) = 7.71-7.63 (m, 8H, Ar), 3.517 (s, 24H, 18-c-6), 1.060 (s, 18H,  $\text{CCH}_3$ ), 0.296 (s, 3H,  $\text{SiCH}_3$ ) ppm.  $^{13}\text{C}$  NMR ( $\text{C}_6\text{D}_6$ , 62.9 MHz) = 141.6 (1,1'-Ar), 136.1 (3,3',5,5'-Ar), 135.9 (4,4'-Ar), 126.4 (2,2',6,6'-Ar), 71.1 (18-c-6), 29.1 ( $\text{CCH}_3$ ), 19.5 ( $\text{CCH}_3$ ), -8.6 ( $\text{SiCH}_3$ ) ppm.  $^{29}\text{Si}$  NMR ( $\text{C}_6\text{D}_6$ , 49.7 MHz) = 4.7 ppm.

#### 4.2.5 Crystallization of 4,4'-Bis(trimethylsilyl)biphenyl (**4**)

A sample of **4** was extracted with acetonitrile. The supernatant solution was removed and left to stand. Colorless crystals formed quickly and were subjected to X-ray crystallographic analysis.

### 4.3 Syntheses associated with 2.1.2. Sodium silyl chalcogenolates

Sodium silanides  $t\text{Bu}_3\text{SiNa}(\text{THF})_x$ <sup>[47]</sup> and  $t\text{Bu}_2\text{PhSiNa}(\text{THF})_x$ <sup>[57]</sup> and silanol  $\text{Ph}_2\text{MeSiOH}$ <sup>[71]</sup> were prepared according to the published procedures.

#### 4.3.1 $t\text{Bu}_2\text{MeSiOH}$ (5)

A solution of **1** (4.2.1, 537 mg, 2.26 mmol) in  $\text{CH}_2\text{Cl}_2$  (30 ml) is combined with a solution of KOH (307 mg, 5.47 mmol) in water (30 ml) and stirred vigorously under ambient conditions. 18-crown-6 (53 mg, 0.20 mmol) is added as a phase-transfer catalyst. After 7 d stirring, the reaction is complete. The reaction mixture is neutralized with 40 ml saturated  $\text{NH}_4\text{Cl}_{(\text{aq})}$  solution and the phases separated. The aqueous phase is extracted with hexane (3 x 15 ml). The combined organic phases are washed with brine, dried over  $\text{MgSO}_4$  and filtered, and volatiles are removed under reduced pressure. Slow evaporation of residual solvent leads to the deposition of colorless needles of  $t\text{Bu}_2\text{MeSiOH}\cdot 1/4\text{HBr}\cdot 1/4\text{H}_2\text{O}$  (200 mg, 51 %).  $^1\text{H}$  NMR ( $\text{C}_6\text{D}_6$ , 250.1 MHz) = 0.970 (s, 18H,  $\text{CCH}_3$ ), -0.33 (s, 3H,  $\text{SiCH}_3$ ) ppm.  $^{13}\text{C}$  NMR ( $\text{C}_6\text{D}_6$ , 62.90 MHz) = 27.7 ( $\text{CCH}_3$ ), 21.3 ( $\text{CCH}_3$ ), -6.5 ( $\text{SiCH}_3$ ) ppm.  $^{29}\text{Si}$  NMR ( $\text{C}_6\text{D}_6$ , 49.7 MHz) = 18.8 ppm.

#### 4.3.2 $\text{Ph}_2\text{MeSiONa}$ (6)

Diphenylmethylsilanol (1.992 g, 9.29 mmol) is dissolved in 20 ml benzene. An excess of sodium metal (ca. 0.32 g, 14 mmol) is added. After 20 h stirring, the clear, colorless solution is removed from excess sodium. Slow concentration of the reaction solution yields large colorless blocks of product (2.110 g, 8.93 mmol, 96 %).  $^1\text{H}$  NMR (toluene- $\text{D}_8$ , 250.1 MHz) = 7.420 (m, 4H, m-Ph), 7.114 (m, 6H, o/p-Ph), 0.391 (s, 3H, Me) ppm.  $^{13}\text{C}$  NMR (toluene- $\text{D}_8$ , 62.9 MHz) = 143.7 (i-Ph), 137.1 (o-Ph), 133.1 (p-Ph), 128.6 (m-Ph), 1.0 (Me) ppm.  $^{29}\text{Si}$  NMR (toluene- $\text{D}_8$ , 49.7 MHz) = -19.1 ppm.  $^1\text{H}$  NMR (THF- $\text{D}_8$ , 250.1 MHz) = 7.571 (m, 4H, m-Ph), 7.157 (m, 6H, o/p-Ph), 0.496 (s, 3H,  $\text{CH}_3$ ) ppm.  $^{13}\text{C}$  NMR (THF- $\text{D}_8$ , 62.9 MHz) = 147.0 (i-Ph), 134.6 (o-Ph), 128.3 (p-Ph), 128.0 (m-Ph), 3.4 ( $\text{CH}_3$ ) ppm.  $^{29}\text{Si}$  NMR (THF- $\text{D}_8$ , 49.7 MHz) = -23.6 ppm.  $^{13}\text{C}$  NMR ( $\text{C}_6\text{D}_6$ , 62.9 MHz) = 143.7 (i-Ph), 133.5 (o-Ph), 129.1 (p-Ph), 128.6 (m-Ph), 1.3 ( $\text{CH}_3$ ) ppm.  $^{29}\text{Si}$  NMR ( $\text{C}_6\text{D}_6$ , 49.7 MHz) = -18.0 ppm. MS (ES<sup>-</sup>):  $m/z$  = 213 (100 %,  $\text{Ph}_2\text{MeSiO}^-$ ). Elem. anal. calcd (%) for  $\text{C}_{13}\text{H}_{13}\text{NaOSi}$  (236.1): C 66.07, H 5.54; found: C 64.42, H 5.76.

### 4.3.3 Adducts of $\text{Ph}_2\text{MeSiONa}$ (**6**)

#### 4.3.3.1 $(\text{Ph}_2\text{MeSiONa})_4(\text{THF})_4$ (**6**) $_4(\text{THF})_4$

A solution of (**6**)<sub>6</sub> (**4.3.2**) in THF is concentrated slowly, leading to the deposition of colorless needles of product.

#### 4.3.3.2 $(\text{Ph}_2\text{MeSiONa})_6(\text{THF})_2$ (**6**) $_6(\text{THF})_2$

Solid (**6**)<sub>6</sub> (**4.3.2**) is dissolved in 1 ml THF and stirred for two hours, at which time all volatile components are removed under reduced pressure. The colorless residue is dissolved in toluene and cooled, leading to the deposition of colorless crystals of product.

#### 4.3.3.3 $(\text{Ph}_2\text{MeSiONa})_6[\text{CpFe}(\text{CO})_2]_2$ (**6**) $_6[\text{CpFe}(\text{CO})_2]_2$

Solid (**6**)<sub>6</sub> (**4.3.2**, 122 mg, 0.09 mmol) is dissolved in 5 ml toluene, to which  $[\text{CpFe}(\text{CO})_2]_2$  (183 mg, 0.52 mmol) is added. After stirring overnight, a red solid has deposited. The mother liquor is removed and the solid washed with benzene (2 x 1 ml). Yield: 150 mg (0.085 mmol, 98 %). Recrystallization from toluene yields X-ray quality crystals. IR (KBr)  $\tilde{\nu}$  = 2002 (m), 1959 (s), 1935 (s), 1769 (s), 1756 (s), 1727 (m)  $\text{cm}^{-1}$  (CO).

### 4.3.4 Synthesis of sodium silyl thiolates

To a suspension of one equivalent elemental sulfur in 10 ml THF at 0 °C is added dropwise 1.02 equivalents sodium silanide solution in THF. After stirring overnight, concentration of the solution leads to the deposition of colorless crystals.

#### 4.3.4.1 $t\text{Bu}_2\text{PhSiNa}(\text{THF})$ (**7**) $(\text{THF})$

109 mg (3.40 mmol) sulfur, 10 ml  $t\text{Bu}_2\text{PhSiNa}$  (0.35 M, 3.5 mmol). X-ray quality crystals can be obtained by recrystallization from THF.  $^1\text{H}$  NMR ( $\text{C}_6\text{D}_6$ , 250.1 MHz) = 8.376 (m, 2H, m-Ph), 7.414 (m, 2H, o-Ph), 7.262 (m, 1H, p-Ph), 3.513 (m, 4H, THF  $\text{OCH}_2$ ), 1.403 (s, 18H,  $\text{CCH}_3$ ), 1.335 (m, 4H, THF  $\text{CCH}_2$ ) ppm.  $^{13}\text{C}$  NMR ( $\text{C}_6\text{D}_6$ , 62.9 MHz) = 141.9 (i-Ph), 136.8 (o-Ph), 127.9 (m-Ph), 127.0 (p-Ph), 68.0 (THF  $\text{OCH}_2$ ), 30.4 ( $\text{CCH}_3$ ), 25.5 (THF  $\text{CCH}_2$ ), 19.1 ( $\text{CCH}_3$ ) ppm.  $^{29}\text{Si}$  NMR ( $\text{C}_6\text{D}_6$ , 49.7 MHz) = 19.4 ppm.

#### 4.3.4.2 $t\text{Bu}_3\text{SiNa}(\text{THF})_2$ (**10**) $(\text{THF})_2$

263 mg (8.20 mmol) sulfur, 15.0 ml  $t\text{Bu}_3\text{SiNa}$  in THF (0.56 M, 8.40 mmol). X-ray quality crystals can be obtained by recrystallization from THF.  $^1\text{H}$  NMR ( $\text{C}_6\text{D}_6$ , 300 MHz) = 3.574 (m, 8H, THF  $\text{OCH}_2$ ), 1.531 (m, 8H, THF  $\text{CCH}_2$ ), 1.350 (s, 27H,  $\text{CCH}_3$ ) ppm.  $^{13}\text{C}$  NMR

(C<sub>6</sub>D<sub>6</sub>, 75.4 MHz) = 68.3 (THF OCH<sub>2</sub>), 31.7 (CCH<sub>3</sub>), 25.5 (THF CCH<sub>2</sub>), 24.4 (CCH<sub>3</sub>) ppm.  
<sup>29</sup>Si NMR (C<sub>6</sub>D<sub>6</sub>, 59.6 MHz) = 25.6 ppm.

#### 4.3.5 Synthesis of sodium silyl selenolates and tellurolates

A solution of one equivalent of silanide in THF is added in one portion to 1.02 equivalents solid chalcogen and stirred overnight. Concentration of the orange solution yields the product as colorless crystals.

##### 4.3.5.1 *t*Bu<sub>2</sub>PhSiSeNa(THF)<sub>2</sub> (**8**(THF)<sub>2</sub>)

268 mg (3.39 mmol) selenium, 10.0 ml *t*Bu<sub>2</sub>PhSiNa (0.35 M, 3.50 mmol). X-ray quality crystals can be obtained by recrystallization from THF. <sup>1</sup>H NMR (C<sub>6</sub>D<sub>6</sub>, 250.1 MHz) = 8.393 (m, 2H, m-Ph), 7.340 (m, 2H, o-Ph), 7.193 (m, 1H, p-Ph), 3.455 (m, 8H, THF OCH<sub>2</sub>), 1.379 (s, 18H, CCH<sub>3</sub>), 1.294 (m, 8H, THF CCH<sub>2</sub>) ppm. <sup>13</sup>C NMR (C<sub>6</sub>D<sub>6</sub>, 62.9 MHz) = 141.0 (i-Ph), 137.3 (o-Ph), 128.3 (m-Ph), 127.0 (p-Ph), 68.0 (THF OCH<sub>2</sub>), 30.5 (CCH<sub>3</sub>), 25.5 (THF CCH<sub>2</sub>), 22.4 (CCH<sub>3</sub>) ppm. <sup>29</sup>Si NMR (C<sub>6</sub>D<sub>6</sub>, 49.7 MHz) = 25.9 ppm.

##### 4.3.5.2 *t*Bu<sub>2</sub>PhSiTeNa(THF)<sub>2</sub> (**9**(THF)<sub>2</sub>)

434 mg (3.40 mmol) tellurium, 10 ml *t*Bu<sub>2</sub>PhSiNa (0.35 M, 3.5 mmol). <sup>1</sup>H NMR (C<sub>6</sub>D<sub>6</sub>, 250.1 MHz) = 8.470 (m, 2H, m-Ph), 7.324 (m, 2H, o-Ph), 7.177 (m, 1H, p-Ph), 3.524 (m, 8H, THF OCH<sub>2</sub>), 1.442 (s, 18H, CCH<sub>3</sub>), 1.344 (m, 8H, THF CCH<sub>2</sub>) ppm. <sup>13</sup>C NMR (C<sub>6</sub>D<sub>6</sub>, 100.6 MHz) = 139.9 (i-Ph), 138.2 (o-Ph), 128.1 (m-Ph), 127.1 (p-Ph), 68.1 (THF OCH<sub>2</sub>), 30.8 (CCH<sub>3</sub>), 25.5 (THF CCH<sub>2</sub>), 22.0 (CCH<sub>3</sub>) ppm. <sup>29</sup>Si NMR (C<sub>6</sub>D<sub>6</sub>, 79.5 MHz) = 29.4 ppm. <sup>125</sup>Te NMR (C<sub>6</sub>D<sub>6</sub>, 126.0 MHz) = -1458 ppm.

##### 4.3.5.3 *t*Bu<sub>3</sub>SiSeNa(THF)<sub>2</sub> (**11**(THF)<sub>2</sub>)

647 mg (8.19 mmol) selenium, 15.0 ml *t*Bu<sub>3</sub>SiNa in THF (0.56 M, 8.40 mmol). X-ray quality crystals can be obtained by recrystallization from THF. <sup>1</sup>H NMR (C<sub>6</sub>D<sub>6</sub>, 300 MHz) = 3.676 (m, 8H, THF OCH<sub>2</sub>), 1.449 (m, 8 H, THF CCH<sub>2</sub>), 1.410 (s, 27 H, CCH<sub>3</sub>) ppm. <sup>13</sup>C NMR (C<sub>6</sub>D<sub>6</sub>, 75.4 MHz) = 68.3 (THF OCH<sub>2</sub>), 31.8 (CCH<sub>3</sub>), 25.5 (THF CCH<sub>2</sub>), 24.4 (CCH<sub>3</sub>) ppm. <sup>29</sup>Si NMR (C<sub>6</sub>D<sub>6</sub>, 59.6 MHz) = 32.8 ppm (<sup>1</sup>J<sub>SiSe</sub> = 50 Hz).

##### 4.3.5.4 *t*Bu<sub>3</sub>SiTeNa(THF)<sub>2</sub> (**12**(THF)<sub>2</sub>)

1046 mg (8.20 mmol) tellurium, 15.0 ml *t*Bu<sub>3</sub>SiNa in THF (0.56 M, 8.40 mmol). X-ray quality crystals can be obtained by recrystallization from THF. <sup>1</sup>H NMR (C<sub>6</sub>D<sub>6</sub>, 300.0 MHz) = 3.709 (m, 8H, THF OCH<sub>2</sub>), 1.457 (s, 27H, CCH<sub>3</sub>), n. o. (THF CCH<sub>2</sub>) ppm. <sup>13</sup>C NMR (C<sub>6</sub>D<sub>6</sub>,

75.4 MHz) = 68.2 (THF OCH<sub>2</sub>), 32.2 (CCH<sub>3</sub>), 25.6 (THF CCH<sub>2</sub>), 24.0 (CCH<sub>3</sub>) ppm. <sup>29</sup>Si NMR (C<sub>6</sub>D<sub>6</sub>, 59.6 MHz, C<sub>6</sub>D<sub>6</sub>) = 38.0 (<sup>1</sup>J<sub>SiTe</sub> = 47.3 Hz) ppm.

#### 4.3.6 *t*Bu<sub>3</sub>SiSSiMe<sub>3</sub> (13)

Sodium tri-*tert*-butylsilyl thiolate **10**(THF)<sub>2</sub> (**4.3.4.2**, 410 mg, 1.60 mmol) is dissolved in 7 ml THF and cooled to 0 °C. Chlorotrimethylsilane (0.20 ml, 1.60 mmol) in 3 ml THF is added dropwise, yielding a milky, colorless mixture. After 1 h stirring, the volatiles are removed in vacuo. The colorless residue is extracted with pentane (10 ml) and filtered over diatomaceous earth on a glass frit. The filter cake is washed with pentane (2 x 3 ml). Removing volatiles from the filtrate yields the product as a colorless oil. <sup>1</sup>H NMR (C<sub>6</sub>D<sub>6</sub>, 250.1 MHz) = 1.226 (s, 27H, CCH<sub>3</sub>), 0.400 (s, 3H, SiCH<sub>3</sub>) ppm. <sup>13</sup>C NMR (C<sub>6</sub>D<sub>6</sub>, 62.9 MHz) = 31.0 (CCH<sub>3</sub>), 24.7 (CCH<sub>3</sub>), 5.5 (SiCH<sub>3</sub>) ppm. <sup>29</sup>Si NMR (C<sub>6</sub>D<sub>6</sub>, 49.7 MHz) = 30.7 (*t*Bu<sub>3</sub>Si), 14.8 (Me<sub>3</sub>Si) ppm. MS (ES<sup>-</sup>): *m/z* = 231 (100 %, *t*Bu<sub>3</sub>SiS<sup>-</sup>). Elem. anal. calcd (%) for C<sub>15</sub>H<sub>36</sub>SSi<sub>2</sub> (304): C 59.13, H 11.91 found: C 59.24, H 11.91.

#### 4.3.7 Synthesis of silyl chalcogenols *t*Bu<sub>2</sub>RSiEH (R = Ph, *t*Bu; E = S, Se, Te)

The sodium silyl chalcogenolates **7** – **12** (**4.3.4** and **4.3.5**) are treated with an excess of trifluoroacetic acid in C<sub>6</sub>D<sub>6</sub> (0.6 ml). Conversion is quantitative as determined by NMR spectroscopy.

##### 4.3.7.1 *t*Bu<sub>2</sub>PhSiSH (14)

14 mg *t*Bu<sub>2</sub>PhSiSNa(THF) (**7**(THF), **4.3.4.1**, 0.04 mmol), 10 μl CF<sub>3</sub>COOH (15 mg, 0.13 mmol). <sup>1</sup>H NMR (C<sub>6</sub>D<sub>6</sub>, 250.1 MHz) = 7.807 (m, 2H, *m*-Ph), 7.167 (m, 3H, *o/p*-Ph), 1.059 (s, 18H, CCH<sub>3</sub>), -0.221 (s, 1 H, SH) ppm. <sup>13</sup>C NMR (C<sub>6</sub>D<sub>6</sub>, 100.6 MHz) = 135.7 (*o*-Ph), 134.6 (*i*-Ph), 129.6 (*m*-Ph), 127.8 (*p*-Ph), 28.8 (CCH<sub>3</sub>), 21.6 (CCH<sub>3</sub>) ppm. <sup>29</sup>Si NMR (C<sub>6</sub>D<sub>6</sub>, 79.5 MHz) = 21.7 ppm.

##### 4.3.7.2 *t*Bu<sub>2</sub>PhSiSeH (15)

19 mg *t*Bu<sub>2</sub>PhSiSeNa(THF)<sub>2</sub> (**8**(THF)<sub>2</sub>, **4.3.5.1**, 0.04 mmol), 10 μl CF<sub>3</sub>COOH (15 mg, 0.13 mmol). <sup>1</sup>H NMR (C<sub>6</sub>D<sub>6</sub>, 250.1 MHz) = 7.834 (m, 2H, *m*-Ph), 7.145 (m, 3H, *o/p*-Ph), 1.095 (s, 18H, CCH<sub>3</sub>), -2.294 (s, 1H, SeH) ppm. <sup>13</sup>C NMR (C<sub>6</sub>D<sub>6</sub>, 100.6 MHz) = 136.2 (*o*-Ph), 134.3 (*i*-Ph), 129.6 (*m*-Ph), 127.8 (*p*-Ph), 29.1 (CCH<sub>3</sub>), 21.9 (CCH<sub>3</sub>) ppm. <sup>29</sup>Si NMR (C<sub>6</sub>D<sub>6</sub>, 79.5 MHz) = 28.3 (<sup>1</sup>J<sub>SeSi</sub> = 106 Hz) ppm. <sup>77</sup>Se NMR (C<sub>6</sub>D<sub>6</sub>, 76.3 MHz) = -413.8 (<sup>1</sup>J<sub>SeH</sub> = 53.4 Hz) ppm.

**4.3.7.3 *t*Bu<sub>2</sub>PhSiTeH (16)**

21 mg *t*Bu<sub>2</sub>PhSiTeNa(THF)<sub>2</sub> (**9**(THF)<sub>2</sub>, **4.3.5.2**, 0.04 mmol), 10 μl CF<sub>3</sub>COOH (15 mg, 0.13 mmol). <sup>1</sup>H NMR (C<sub>6</sub>D<sub>6</sub>, 250.1 MHz) = 7.869 (m, 2H, m-Ph), 7.120 (m, 3H, o/p-Ph), 1.100 (s, 18H, CCH<sub>3</sub>), -7.504 (s, 1H, TeH) ppm. <sup>13</sup>C NMR (C<sub>6</sub>D<sub>6</sub>, 100.6 MHz) = 136.9 (o-Ph), 129.62 (m-Ph), 127.8 (p-Ph), 29.5 (CCH<sub>3</sub>), 22.2 (CCH<sub>3</sub>), n. o. (i-Ph) ppm. <sup>29</sup>Si NMR (C<sub>6</sub>D<sub>6</sub>, 79.5 MHz) = 34.4 (<sup>1</sup>J<sub>TeSi</sub> = 277 Hz) ppm. <sup>125</sup>Te NMR (C<sub>6</sub>D<sub>6</sub>, 126.1 MHz) = -863 (<sup>1</sup>J<sub>TeH</sub> = 25 Hz) ppm.

**4.3.7.4 *t*Bu<sub>3</sub>SiSH (17)**

Preparative synthesis: Sodium tri-*tert*-butylsilylthiolate (**10**(THF)<sub>2</sub>, **4.3.4.2** 1.160 g, 2.91 mmol) is dissolved in CH<sub>2</sub>Cl<sub>2</sub> (25 ml). Acetic acid (0.25 ml, 4.37 mmol) in CH<sub>2</sub>Cl<sub>2</sub> (10 ml) is added dropwise. After one hour stirring, the cloudy solution is washed with water (4 x 20 ml). The organic phase is dried over MgSO<sub>4</sub>, filtered and the solvent removed. The product is recovered as a colorless, waxy solid (640 mg, 2.75 mmol, 95 %).

<sup>1</sup>H NMR (C<sub>6</sub>D<sub>6</sub>, 250.1 MHz) = 1.097 (s, 27H, CCH<sub>3</sub>), -0.566 (s, 1H, SH) ppm. <sup>13</sup>C (C<sub>6</sub>D<sub>6</sub>, 62.9 MHz) = 30.3 (CCH<sub>3</sub>), 23.7 (CCH<sub>3</sub>) ppm. <sup>29</sup>Si (C<sub>6</sub>D<sub>6</sub>, 49.7 MHz) = 27.8 ppm. Elem. anal. calcd (%) for C<sub>12</sub>H<sub>28</sub>SSi (232.4): C 61.99, H 12.14; found: C 62.15, H 12.27.

**4.3.7.5 *t*Bu<sub>3</sub>SiSeH (18)**

18 mg *t*Bu<sub>3</sub>SiSeNa(THF)<sub>2</sub> (**11**(THF)<sub>2</sub>, **4.3.5.3**, 0.04 mmol), 10 μl CF<sub>3</sub>COOH (15 mg, 0.13 mmol). <sup>1</sup>H NMR (C<sub>6</sub>D<sub>6</sub>, 250.1 MHz) = 1.122 (s, 27H, CCH<sub>3</sub>), -2.677 (s, 1H, SeH) ppm. <sup>13</sup>C (C<sub>6</sub>D<sub>6</sub>, 62.9 MHz) = 30.5 (CCH<sub>3</sub>), 24.0 (CCH<sub>3</sub>) ppm. <sup>29</sup>Si (C<sub>6</sub>D<sub>6</sub>, 49.7 MHz) = 35.0 (<sup>1</sup>J<sub>SeSi</sub> = 106 Hz) ppm. <sup>77</sup>Se (C<sub>6</sub>D<sub>6</sub>, 76.3 MHz) = -413.9 (<sup>1</sup>J<sub>SeH</sub> = 52.6 Hz) ppm.

**4.3.7.6 *t*Bu<sub>3</sub>SiTeH (19)**

20 mg *t*Bu<sub>3</sub>SiTeNa(THF)<sub>2</sub> (**12**(THF)<sub>2</sub>, **4.3.5.4**, 0.04 mmol), 10 μl CF<sub>3</sub>COOH (15 mg, 0.13 mmol). <sup>1</sup>H NMR (C<sub>6</sub>D<sub>6</sub>, 250.1 MHz) = 1.143 (s, 27H, CCH<sub>3</sub>), -7.983 (s, 1H, TeH) ppm. <sup>13</sup>C (C<sub>6</sub>D<sub>6</sub>, 62.9 MHz) = 31.0 (CCH<sub>3</sub>), 24.1 (CCH<sub>3</sub>) ppm. <sup>29</sup>Si (C<sub>6</sub>D<sub>6</sub>, 49.7 MHz) = 42.4 (<sup>1</sup>J<sub>TeSi</sub> = 271 Hz) ppm.



## 4.4 Syntheses associated with 2.1.3 *Disilyl dichalcogenides*

### 4.4.1 Synthesis of disilyldichalcogenides $t\text{Bu}_2\text{RSiE-ESiR}t\text{Bu}_2$ (R = Ph, *t*Bu; E = S, Se, Te)

Oxidation of THF solutions (ca. 0.05 M) of the sodium silyl chalcogenolates **7 – 12** (4.3.4 and 4.3.5) with dry air yields the corresponding disilyldichalcogenides in 50 % yield, as determined by NMR spectroscopy. These compounds can be freed of byproduct salts by removal of the THF solvent, extraction with pentane, and filtration.

#### Alternate method for preparation of disulfides $t\text{Bu}_2\text{PhSiS-SSiPh}t\text{Bu}_2$ (**20**) and $t\text{Bu}_3\text{SiS-SSi}t\text{Bu}_3$ (**23**)

To a stirring solution of one equivalent sodium silanide in THF is added 0.5 equivalents  $\text{S}_2\text{Cl}_2$ . After one hour, the solvent is removed and the residue extracted with pentane. Filtration and concentration of the filtrate yields the products as pale yellow solids.

##### 4.4.1.1 $t\text{Bu}_2\text{PhSiS-SSiPh}t\text{Bu}_2$ (**20**)

6.37 ml  $t\text{Bu}_2\text{PhSiNa}$  solution in THF (0.16 M, 1.02 mmol), 0.04 ml  $\text{S}_2\text{Cl}_2$  (67 mg, 0.50 mmol). Recrystallization from pentane at 4 °C yields the product as pale yellow blocks.  $^1\text{H}$  NMR ( $\text{C}_6\text{D}_6$ , 300.0 MHz) = 7.724 (m, 4H, m-Ph), 7.049-6.921 (m, 6H, o/p-Ph), 1.208 (s, 36H,  $\text{CCH}_3$ ) ppm.  $^{13}\text{C}$  NMR ( $\text{C}_6\text{D}_6$ , 75.4 MHz) = 136.7 (o-Ph), 129.3 (m-Ph), 127.1 (p-Ph), 29.8 ( $\text{CCH}_3$ ), 23.7 ( $\text{CCH}_3$ ) n. o. (i-Ph) ppm.  $^{29}\text{Si}$  NMR ( $\text{C}_6\text{D}_6$ , 59.6 MHz) = 23.2 ppm. MS (ES<sup>-</sup>):  $m/z$  = 251 (100 %,  $t\text{Bu}_2\text{PhSiS}^-$ ). Elem. anal. calcd (%) for  $\text{C}_{28}\text{H}_{46}\text{S}_2\text{Si}_2$  (503.0): C 66.86, H 9.22; found: C 64.66, H 9.42.

##### 4.4.1.2 $t\text{Bu}_2\text{PhSiSe-SeSiPh}t\text{Bu}_2$ (**21**)

Red blocks of product can be obtained by recrystallization from pentane.  $^1\text{H}$  NMR ( $\text{C}_6\text{D}_6$ , 250.1 MHz) = 8.431 (m, 4H, m-Ph), 7.386 (m, 4H, o-Ph), 7.225 (m, 2H, p-Ph), 1.418 (s, 36H,  $\text{CCH}_3$ ) ppm.  $^{13}\text{C}$  NMR ( $\text{C}_6\text{D}_6$ , 62.9 MHz) = 140.9 (i-Ph), 137.3 (o-Ph), 128.3 (m-Ph), 127.1 (p-Ph), 30.5 ( $\text{CCH}_3$ ), 22.7 ( $\text{CCH}_3$ ) ppm.  $^{29}\text{Si}$  NMR (49.7 MHz,  $\text{C}_6\text{D}_6$ ) = 25.4 ppm. MS (ES<sup>-</sup>):  $m/z$  = 299 (100 %,  $t\text{Bu}_2\text{PhSiSe}^-$ , correct isotope pattern), 163 (52 %,  $t\text{BuPhSi}^-$ ). Elem. anal. calcd (%) for  $\text{C}_{28}\text{H}_{46}\text{Se}_2\text{Si}_2$  (596.8): C 56.35, H: 7.77; found: C 55.99, H 7.86. UV-vis:  $\lambda_{\text{max}}$  = 424 nm.

#### 4.4.1.3 *t*Bu<sub>2</sub>PhSiTe-TeSiPh*t*Bu<sub>2</sub> (22)

Recrystallization from pentane yields the product as dark blue blocks. <sup>1</sup>H NMR (C<sub>6</sub>D<sub>6</sub>, 250.1 MHz) = 8.071 (m, 4H, m-Ph), 7.176 (m, 6H, o/p-Ph), 1.273 (s, 36H, CCH<sub>3</sub>) ppm. <sup>13</sup>C NMR (C<sub>6</sub>D<sub>6</sub>, 62.9 MHz) = 137.7 (o-Ph), 133.7 (i-Ph), 129.7 (m-Ph), 128.0 (p-Ph), 30.6 (CCH<sub>3</sub>), 24.0 (CCH<sub>3</sub>) ppm. <sup>29</sup>Si NMR (C<sub>6</sub>D<sub>6</sub>, 49.7 MHz) = 25.9 ppm. MS (ES<sup>-</sup>): *m/z* = 349 (20 %, *t*Bu<sub>2</sub>PhSiTe<sup>2-</sup>, correct isotope pattern), 269 (33 %, Ph*t*BuSiTe<sup>-</sup>), 235 (100 %, Ph*t*Bu<sub>2</sub>SiO<sup>-</sup>), 163 (17 %, *t*BuPhSi<sup>-</sup>). Elem. anal. calcd (%) for C<sub>28</sub>H<sub>46</sub>Te<sub>2</sub>Si<sub>2</sub> (694.0): C 48.46, H 6.68; found: C 47.82, H 7.14.

#### 4.4.1.4 *t*Bu<sub>3</sub>SiS-SS*t*Bu<sub>3</sub> (23)

15.0 ml *t*Bu<sub>3</sub>SiNa solution in THF (0.38 M, 5.70 mmol), 0.23 ml S<sub>2</sub>Cl<sub>2</sub> (395 mg, 2.85 mmol). The disulfide can be obtained as colorless needles by slow evaporation of a cooled pentane solution. <sup>1</sup>H NMR (C<sub>6</sub>D<sub>6</sub>, 400.1 MHz) = 1.313 (s, 54H, CCH<sub>3</sub>) ppm. <sup>13</sup>C NMR (C<sub>6</sub>D<sub>6</sub>, 100 MHz) = 30.8 (CCH<sub>3</sub>), 26.0 (CCH<sub>3</sub>) ppm. <sup>29</sup>Si NMR (C<sub>6</sub>D<sub>6</sub>, 79.5 MHz) = 24.6 ppm. MS (ES<sup>-</sup>): *m/z* = 351 (14 %, *t*Bu<sub>4</sub>Si<sub>2</sub>S<sub>2</sub><sup>-</sup>), 263 (21 %, *t*Bu<sub>3</sub>SiS<sub>2</sub><sup>-</sup>), 231 (100 %, *t*Bu<sub>3</sub>SiS<sup>-</sup>). Elem. anal. calcd (%) for C<sub>24</sub>H<sub>54</sub>S<sub>2</sub>Si<sub>2</sub> (463.0): C 62.26, H 11.76; found: C 61.99, H 11.66.

#### 4.4.1.5 *t*Bu<sub>3</sub>SiSe-SeSi*t*Bu<sub>3</sub> (24)

The diselenide can be obtained as brick red blocks by recrystallization from pentane. <sup>1</sup>H NMR (C<sub>6</sub>D<sub>6</sub>, 400 MHz) = 1.314 (s, 54H, CCH<sub>3</sub>) ppm. <sup>13</sup>C NMR (C<sub>6</sub>D<sub>6</sub>, 100.6 MHz) = 31.1 (CCH<sub>3</sub>), 26.4 (CCH<sub>3</sub>) ppm. <sup>29</sup>Si NMR (C<sub>6</sub>D<sub>6</sub>, 79.5 MHz) = 30.2 ppm. MS (ES<sup>-</sup>): *m/z* = 279 (100 %, *t*Bu<sub>3</sub>SiSe<sup>-</sup>, correct isotope pattern), 215 (80 %, Si<sub>2</sub>Se<sub>2</sub><sup>-</sup>). Elem. anal. calcd (%) for C<sub>24</sub>H<sub>54</sub>Se<sub>2</sub>Si<sub>2</sub> (556.8): C 51.77, H 9.78; found: C 51.90, H 9.87. UV-vis: λ<sub>max</sub> = 418 nm.

#### 4.4.1.6 *t*Bu<sub>3</sub>SiTe-TeSi*t*Bu<sub>3</sub> (25)

Recrystallization from pentane results in the deposition of large, ink blue plates of ditelluride. <sup>1</sup>H NMR (C<sub>6</sub>D<sub>6</sub>, 250.1 MHz) = 1.308 (s, 54H, CCH<sub>3</sub>) ppm. <sup>13</sup>C NMR (C<sub>6</sub>D<sub>6</sub>, 62.9 MHz) = 31.5 (CCH<sub>3</sub>), 26.3 (CCH<sub>3</sub>) ppm. <sup>29</sup>Si NMR (C<sub>6</sub>D<sub>6</sub>, 49.7 MHz) = 34.1 ppm. <sup>125</sup>Te NMR (C<sub>6</sub>D<sub>6</sub>, 126.2 MHz) = -627 ppm. Elem. anal. calcd (%) for C<sub>24</sub>H<sub>54</sub>Te<sub>2</sub>Si<sub>2</sub> (654.1): C 44.07, H 8.32; found: C 42.57, H 8.43. UV-vis: λ<sub>max</sub> = 576 nm, 292 nm.

#### 4.4.2 Synthesis of potassium silyl tellurolate *t*Bu<sub>3</sub>SiTeK (26)

Ditelluride **25** (4.4.1.6, 20 mg, 0.03 mmol) and potassium metal (ca. 20 mg, 0.5 mmol) are combined in THF (0.6 ml). After 24 h at room temperature, the color has changed from blue to colorless and in the NMR spectra, only signals associated with *t*Bu<sub>3</sub>SiTeK are observed. <sup>1</sup>H

NMR (250.1 MHz, THF-D<sub>8</sub>) = 1.165 (s, 27H, CCH<sub>3</sub>) ppm. <sup>13</sup>C NMR (100 MHz, THF-D<sub>8</sub>) = 33.2 (CCH<sub>3</sub>), 24.4 (CCH<sub>3</sub>) ppm. <sup>29</sup>Si NMR (79.5 MHz, THF-D<sub>8</sub>) = 31.8 ppm.

## 4.5 Syntheses associated with 2.1.4 Oligochalcogen compounds

Ligand exchange of Te(O*i*Pr)<sub>4</sub> with *t*BuSH and subsequent reductive elimination according to the method of Fleischer et al. yields (*t*BuS)<sub>2</sub>Te.<sup>[97]</sup>

### 4.5.1 (tBu<sub>3</sub>SiS)<sub>2</sub>Te (27)

Solid **17** (4.3.7.4, 121 mg, 0.52 mmol), (*t*BuS)<sub>2</sub>Te (78 mg, 0.25 mmol) and imidazole (35 mg, 0.52 mmol) are combined in toluene (20 ml). The solvent is slowly distilled off under atmospheric pressure over a period of three hours. When distillation has ceased, volatiles are removed in vacuo over 20 h, leaving a brown, powdery residue (55 mg, 0.09 mmol, 38 %). <sup>1</sup>H NMR (C<sub>6</sub>D<sub>6</sub>, 250.1 MHz) = 1.265 (s, 27H, CCH<sub>3</sub>) ppm. <sup>13</sup>C NMR (C<sub>6</sub>D<sub>6</sub>, 62.9 MHz) = 31.1 (CCH<sub>3</sub>), 25.7 (CCH<sub>3</sub>) ppm. <sup>29</sup>Si NMR (C<sub>6</sub>D<sub>6</sub>, 79.5 MHz) = 25.3 ppm. <sup>125</sup>Te NMR (C<sub>6</sub>D<sub>6</sub>, 94.7 MHz) = 1222 ppm. Elem. anal. calcd (%) for C<sub>24</sub>H<sub>54</sub>S<sub>2</sub>Si<sub>2</sub>Te (686.1): C 48.81, H 9.22; found: C 48.19, H 9.12.

### 4.5.2 (tBu<sub>3</sub>SiS)<sub>2</sub>Se (28)

A solution of Se<sub>2</sub>Cl<sub>2</sub> (13.3 μl, 37 mg, 0.16 mmol) in toluene is added dropwise to a solution of **10**(THF)<sub>2</sub> (4.3.4.2, 129 mg, 0.32 mmol) in 6 ml toluene. After one hour, NaCl and Se<sup>0</sup> are removed via filtration over diatomaceous earth on a frit and the filter cake is washed with toluene (3 ml). Removal of the solvent from the filtrate yields the product as a yellow-orange solid. <sup>1</sup>H NMR (C<sub>6</sub>D<sub>6</sub>, 400.1 MHz) = 1.258 (s, 27 H, CCH<sub>3</sub>) ppm. <sup>13</sup>C NMR (C<sub>6</sub>D<sub>6</sub>, 100.6 MHz) = 31.0 (CCH<sub>3</sub>), 25.6 (CCH<sub>3</sub>) ppm. <sup>29</sup>Si NMR (C<sub>6</sub>D<sub>6</sub>, 79.5 MHz) = 25.4 ppm. <sup>77</sup>Se NMR (C<sub>6</sub>D<sub>6</sub>, 57.2 MHz) = 584 ppm. Elem. anal. calcd for C<sub>24</sub>H<sub>54</sub>S<sub>2</sub>Si<sub>2</sub>Se (588.8): C 53.19, H 10.04; found: C 51.46, H 9.65.

### 4.5.3 *t*Bu<sub>3</sub>SiS-S<sub>2</sub>-SSi*t*Bu<sub>3</sub> (29)

Sulfur monochloride (69.8 μl, 0.87 mmol) is added to **10**(THF)<sub>2</sub> (4.3.4.2, 442 mg, 1.11 mmol) in 10 ml THF. The yellow mixture is stirred for 90 min, at which time the volatiles are removed in vacuo. The yellow residue is extracted with pentane (5 ml) and filtered over diatomaceous earth on a frit. The filter cake is washed with pentane (4 x 2 ml) and the filtrate concentrated to 2 ml, during which time colorless crystals (235 mg, 0.44 mmol, 80 %) are deposited. <sup>1</sup>H NMR (C<sub>6</sub>D<sub>6</sub>, 400.1 MHz) = 1.208 (s, 27 H, CCH<sub>3</sub>) ppm. <sup>13</sup>C NMR (C<sub>6</sub>D<sub>6</sub>,

100.6 MHz) = 30.8 (CCH<sub>3</sub>), 25.5 (CCH<sub>3</sub>) ppm. <sup>29</sup>Si NMR (C<sub>6</sub>D<sub>6</sub>, 79.5 MHz) = 26.7 ppm. MS (ES+) = 527 (100 %, M<sup>+</sup>), 295 (62 %, *t*Bu<sub>3</sub>SiS<sub>3</sub><sup>+</sup>), 545 (60 %, M + NH<sub>4</sub><sup>+</sup>). Elemental anal. calcd (%) for C<sub>24</sub>H<sub>54</sub>S<sub>4</sub>Si<sub>2</sub> (526): C 54.69, H 10.33; found: C 54.45, H 10.40.

#### 4.6 Syntheses associated with 2.2.1 Complexes of the type [CpFe(CO)<sub>2</sub>L]

Iron complex anion K[CpFe(CO)<sub>2</sub>]<sup>[182]</sup> and THF adduct salts [CpFe(CO)<sub>2</sub>(THF)]BF<sub>4</sub><sup>[183]</sup> and [CpFe(CO)<sub>2</sub>(THF)]PF<sub>6</sub><sup>[184]</sup> were prepared according to literature procedures.

##### 4.6.1 CpFe(CO)<sub>2</sub>SiPh<sub>2</sub>Me (31)

The iron complex anion K[CpFe(CO)<sub>2</sub>] (307 mg, 1.42 mmol) is suspended in THF (10 ml). A solution of Ph<sub>2</sub>MeSiCl (0.33 ml, 367 mg, 1.57 mmol) in THF (8 ml) is added dropwise. After stirring overnight, volatiles are removed in vacuo. The brown residue is extracted with pentane (4 x 10 ml) and filtered. Removal of the solvent yields the crude product as a brown oil (392 mg, 1.04 mmol, 74 %). The crude product is purified via silica gel filtration under inert atmosphere using 2:1 hexane:CH<sub>2</sub>Cl<sub>2</sub> as the eluent, which yields the product as a yellow solid after removal of volatiles in vacuo. X-ray quality crystals can be obtained from hexane solution at -20 °C. <sup>1</sup>H NMR (C<sub>6</sub>D<sub>6</sub>, 300 MHz) = 7.692 (m, 4H, m-Ph), 7.214 (m, 6H, o/p-Ph), 0.953 (s, 3H, CH<sub>3</sub>) ppm. <sup>13</sup>C NMR (C<sub>6</sub>D<sub>6</sub>, 75.4 MHz) = 215.8 (CO), 144.6 (i-Ph), 134.6 (o-Ph), 128.4 (p-Ph), 128.0 (m-Ph), 84.3 (Cp), 5.5 (CH<sub>3</sub>) ppm. <sup>29</sup>Si NMR (C<sub>6</sub>D<sub>6</sub>, 59.6 MHz) = 35.1 ppm. IR (CH<sub>3</sub>CN):  $\tilde{\nu}$  = 1994 (m), 1938 (m) cm<sup>-1</sup> (CO). Elem. anal. calcd. (%) for C<sub>20</sub>H<sub>18</sub>FeO<sub>2</sub>Si (374.04): C 64.18, H 4.85; found: C 64.14, H 4.88.

##### 4.6.2 CpFe(CO)<sub>2</sub>SSi*t*Bu<sub>3</sub> (34)

To a solution of [CpFe(CO)<sub>2</sub>(THF)]BF<sub>4</sub> (131 mg, 0.39 mmol) in CH<sub>2</sub>Cl<sub>2</sub> (12 ml) is added solid **10**(THF)<sub>2</sub> (4.3.4.2, 155 mg, 0.39 mmol) in one portion. After four hours stirring, volatiles are removed from the reaction mixture and the brown residue is extracted with pentane (5 ml) and filtered over celite on a frit. The filter cake is washed with pentane (2 x 5 ml). Slow concentration of the filtrate yields a dark brown, microcrystalline solid (156 mg, 0.38 mmol, 98 %). Recrystallization from pentane yields X-ray quality crystals. <sup>1</sup>H NMR (C<sub>6</sub>D<sub>6</sub>, 400.1 MHz) = 4.108 (s, 5H, Cp), 1.391 (s, 27H, CCH<sub>3</sub>) ppm. <sup>13</sup>C NMR (C<sub>6</sub>D<sub>6</sub>, 100.6 MHz) = 215.1 (CO), 86.2 (Cp), 31.6 (CCH<sub>3</sub>), 25.5 (CCH<sub>3</sub>) ppm. <sup>29</sup>Si NMR (C<sub>6</sub>D<sub>6</sub>, 59.6 MHz) = 29.2 ppm. <sup>1</sup>H NMR (CD<sub>2</sub>Cl<sub>2</sub>, 300.0 MHz) = 5.025 (s, 5H, Cp), 1.140 (s, 27H, CCH<sub>3</sub>) ppm. <sup>13</sup>C NMR (CD<sub>2</sub>Cl<sub>2</sub>, 75.4 MHz) = 214.8 (CO), 86.6 (Cp), 31.0 (CCH<sub>3</sub>), 25.0 (CCH<sub>3</sub>) ppm. IR

(hexane):  $\tilde{\nu} = 2035$  (s), 1988 (s)  $\text{cm}^{-1}$  (CO). IR ( $\text{CH}_2\text{Cl}_2$ ):  $\tilde{\nu} = 2030$  (s), 1982 (s)  $\text{cm}^{-1}$  (CO).  
Elem. anal. calcd. (%) for  $\text{C}_{19}\text{H}_{32}\text{FeO}_2\text{SSi}$  (408.5): C 55.87, H 7.90; found: C 54.59, H 7.85.

#### 4.6.3 Reaction of $\text{CpFe}(\text{CO})_2\text{I}$ with **2**

A Schlenk flask is charged with  $\text{CpFe}(\text{CO})_2\text{I}$  (278 mg, 0.92 mmol) in THF (5 ml) and cooled to  $-78$  °C. A solution of **2** (4.2.2, 162 mg, 0.92 mmol) in THF (3 ml) is added dropwise. After warming to room temperature overnight, an NMR sample is taken. The results of the NMR analysis are summarized in Table 4.6.1 and Table 4.6.2.

**Table 4.6.1.**  $^1\text{H}$  NMR (THF- $\text{D}_8$ , Cp region)

$t\text{Bu}_2\text{MeSiNa} + \text{CpFe}(\text{CO})_2\text{I}^{[a]}$

$\delta$	integral	assignment
5.028	0.078	
4.823	1.497	$[\text{CpFe}(\text{CO})_2]_2$
4.564	0.071	
4.068	0.070	

[a] Signals in the  $\text{CCH}_3$  and  $\text{SiCH}_3$  regions are not resolved, precluding integration and assignment

**Table 4.6.2.**  $^{29}\text{Si}$  NMR  $t\text{Bu}_2\text{MeSiNa} + \text{CpFe}(\text{CO})_2\text{I}$

$\delta$	intensity	assignment	$\delta$	intensity	assignment
41.1	w	$t\text{Bu}_2\text{MeSiI}$	7.1	w	$(t\text{Bu}_2\text{MeSi})_2$
24.4	w		5.2	s	
19.5	m		5.0	s	
12.5	w		4.2	s	
10.5	m	$t\text{Bu}_2\text{MeSiH}$			

#### 4.6.4 Reaction of $\text{CpFe}(\text{CO})_2\text{I}$ with $t\text{Bu}_3\text{SiNa}$

A Schlenk flask is charged with  $\text{CpFe}(\text{CO})_2\text{I}$  (92 mg, 0.30 mmol) in THF (5 ml) and cooled to  $-78$  °C. A 0.30 M solution of  $t\text{Bu}_3\text{SiNa}$  in THF (1.0 ml, 0.30 mmol) is added dropwise. After warming to room temperature overnight, the solvent is removed and the brown residue extracted with pentane. The extract is filtered and an NMR sample taken from the filtrate. The results of the NMR analysis are summarized in Table 4.6.3 and Table 4.6.4.

**Table 4.6.3.**  $^1\text{H}$  NMR ( $\text{C}_6\text{D}_6$ , Cp region)  $t\text{Bu}_3\text{SiNa} + \text{CpFe}(\text{CO})_2\text{I}^{[\text{a}]}$ 

$\delta$	multiplicity	integral	assignment
5.000	pseudo tr	1.2	
4.250	s	2.0	$[\text{CpFe}(\text{CO})_2]_2$
4.214	s	2.0	
4.078	pseudo tr	1.3	

[a] Signals in the  $\text{CCH}_3$  region are not resolved, precluding integration and assignment

**Table 4.6.4.**  $^{29}\text{Si}$  NMR ( $\text{C}_6\text{D}_6$ )  $t\text{Bu}_3\text{SiNa} + \text{CpFe}(\text{CO})_2\text{I}$ 

$\delta$	intensity	assignment
48.1	m	$t\text{Bu}_2\text{MeSiI}$
17.8	m	$t\text{Bu}_2\text{MeSiH}$
3.9	s	

#### 4.6.5 $t\text{Bu}_2\text{MeSiI}$ (30)

To an ice cooled solution of  $t\text{Bu}_2\text{MeSiH}$  (429 mg, 2.71 mmol) in  $\text{CH}_2\text{Cl}_2$  (8 ml) is added dropwise a solution of  $\text{I}_2$  (722 mg, 2.84 mmol) in  $\text{CH}_2\text{Cl}_2$  (8 ml). The solution is warmed to room temperature and stirred overnight. Volatiles are removed at 70 torr to give a red, oily solid.  $^1\text{H}$  NMR ( $\text{C}_6\text{D}_6$ , 250.1 MHz) = 0.991 (s, 18H,  $\text{CCH}_3$ ), 0.476 (s, 3H,  $\text{SiCH}_3$ ) ppm.  $^{13}\text{C}$  NMR ( $\text{C}_6\text{D}_6$ , 62.9 MHz) = 28.1 ( $\text{CCH}_3$ ), 21.5 ( $\text{CCH}_3$ ), -2.3 ( $\text{SiCH}_3$ ) ppm.  $^{29}\text{Si}$  NMR ( $\text{C}_6\text{D}_6$ , 49.7 MHz) = 40.7 ppm.

#### 4.6.6 Reaction of $\text{CpFe}(\text{CO})_2\text{I}$ with 6

A Schlenk flask is charged with  $\text{CpFe}(\text{CO})_2\text{I}$  (217 mg, 0.71 mmol) in 5 ml THF and cooled to  $-78^\circ\text{C}$ . To this solution is added dropwise a solution of **6** (**4.3.2**, 168 mg, 0.71 mmol) in THF (5 ml). The mixture is allowed to warm to room temperature overnight. Volatile reaction components are removed in vacuo, and the brown residue is extracted with toluene and filtered. Red crystals of  $(\mathbf{6})_4\{[\text{CpFe}(\text{CO})_2]_2\}_2$  can be isolated by removing toluene from the filtrate, washing the residue with benzene, and recrystallizing from toluene. Note: the adduct is considerably more soluble in toluene than in benzene. IR (adduct, KBr):  $\tilde{\nu} = 2005$  (m), 1957 (s), 1932 (m), 1976 (m), 1735 (s), 1982 (s)  $\text{cm}^{-1}$  (CO).

#### 4.6.7 Reaction of [CpFe(CO)<sub>2</sub>(THF)]PF<sub>6</sub> with 6

Solid **6** (**4.3.2**, 0.063 g, 0.27 mmol) was added to [CpFe(CO)<sub>2</sub>(THF)]PF<sub>6</sub> (0.105 g, 0.27 mmol) in CH<sub>2</sub>Cl<sub>2</sub> (10 ml) and stirred overnight. The dark red reaction mixture was filtered over diatomaceous earth on a frit and volatiles removed from the filtrate in vacuo. Analysis of the brown residue via NMR spectroscopy (C<sub>6</sub>D<sub>6</sub>) showed several unidentified silicon-containing products. The main products containing a Cp moiety were ferrocene (ca. 30 % of the total <sup>1</sup>H Cp region integral) and Fp<sub>2</sub> (ca. 55 % of the total <sup>1</sup>H Cp region integral). The identities of the main Cp-containing species as ferrocene and Fp<sub>2</sub> were confirmed by <sup>13</sup>C NMR spectroscopy.

### 4.7 Syntheses associated with 2.2.2 Other transition metal complexes

#### 4.7.1 [Cu(SSi<sup>t</sup>Bu<sub>2</sub>Ph)]<sub>4</sub> (**37**)

A solution of **7**(THF) (**4.3.4.1**, 111 mg 0.32 mmol) in 1 ml THF is added dropwise to solid CuCl (40 mg, 0.32 mmol). The red-brown solution is stirred overnight. After removal of the solvent under reduced pressure, the residue is extracted with toluene and filtered. Slow evaporation of the solvent yields the product as crystalline colorless needles (37 mg, 0.029 mmol, 37 %) <sup>1</sup>H NMR (C<sub>6</sub>D<sub>6</sub>, 250.1 MHz) = 8.138 (m, 2H, m-Ph), 7.229 (m, 3H, o/p-Ph), 1.337 (s, 18H, CCH<sub>3</sub>) ppm. <sup>13</sup>C NMR (C<sub>6</sub>D<sub>6</sub>, 100.6 MHz) = 136.7 (i-Ph), 129.3 (o-Ph), 128.5 (m-Ph), 125.6 (p-Ph), 30.2 (CCH<sub>3</sub>), 23.0 (CCH<sub>3</sub>) ppm. <sup>29</sup>Si NMR (C<sub>6</sub>D<sub>6</sub>, 79.5 MHz) = 23.1 ppm.

#### 4.7.2 [ZnCl(SSi<sup>t</sup>Bu<sub>3</sub>)(THF)]<sub>2</sub> (**38**)

A solution of **10**(THF)<sub>2</sub> (**4.3.4.2**, 398 mg, 1.00 mmol) in 2.5 ml THF is added dropwise to solid ZnCl<sub>2</sub> (74 mg, 0.54 mmol). The orange solution is stirred overnight. After removal of the solvent under reduced pressure, the residue is extracted with toluene and filtered. Slow evaporation of the solvent yields the product as colorless crystalline blocks (130 mg, 0.16 mmol, 64 %) <sup>1</sup>H NMR (C<sub>6</sub>D<sub>6</sub>, 250.1 MHz) = 3.735 (m, 8H, THF OCH<sub>2</sub>), 1.373 (s, 54H, CCH<sub>3</sub>), 1.298 (m, 8H, THF CCH<sub>2</sub>) ppm. <sup>13</sup>C NMR (C<sub>6</sub>D<sub>6</sub>, 62.9 MHz) = 69.4 (THF OCH<sub>2</sub>), 30.9 (CCH<sub>3</sub>), 25.3 (THF CCH<sub>2</sub>), 24.9 (CCH<sub>3</sub>) ppm. <sup>29</sup>Si NMR (C<sub>6</sub>D<sub>6</sub>, 49.7 MHz) = 34.0 ppm.

#### 4.7.3 (CO)<sub>4</sub>Mn(μ-SSi<sup>t</sup>Bu<sub>3</sub>)<sub>2</sub>Na(THF)<sub>2</sub> (**39**)

To a solution of BrMn(CO)<sub>5</sub> (128 mg, 0.46 mmol) in 15 ml THF is added **10**(THF)<sub>2</sub> (**4.3.4.2**, 378 mg, 0.95 mmol) in one portion. The orange solution quickly becomes cloudy. After three hours, volatiles are removed in vacuo and the brown residue is extracted with pentane (10 ml).

The extract is filtered over diatomaceous earth on a frit. The filter cake is washed with pentane (2 x 5 ml). Slow concentration of the filtrate leads to the deposition of the product as a microcrystalline solid. X-ray quality crystals can be obtained by recrystallization from pentane at  $-20\text{ }^{\circ}\text{C}$ . Yield: 167 mg (0.21 mmol, 45 %). If a solution of **39** is left to stand for several weeks, crystals of the composition  $\text{Na}(\text{THF})_6[(\text{CO})_4\text{Mn}(\mu\text{-SSi}t\text{Bu}_3)_3\text{Mn}(\text{SSi}t\text{Bu}_3)]$  (**40**) +  $t\text{Bu}_3\text{Si-S}_3\text{-Si}t\text{Bu}_3$  can be isolated. Due to the low yield of this species, no further characterization could be undertaken.

Analytical data for **39**:  $^1\text{H}$  NMR ( $\text{C}_6\text{D}_6$ , 250.1 MHz) = 3.453 (br s,  $\nu_{1/2} = 30\text{ Hz}$ , 8H, THF OCH<sub>2</sub>), 1.375 (s, 54H, CCH<sub>3</sub>), n.o. (THF CCH<sub>2</sub>) ppm.  $^{13}\text{C}$  NMR ( $\text{C}_6\text{D}_6$ , 62.9 MHz) = 31.7 (CCH<sub>3</sub>), 25.3 (CCH<sub>3</sub>), n. o. (CO, THF) ppm.  $^{29}\text{Si}$  NMR ( $\text{C}_6\text{D}_6$ , 79.5 MHz) = 29.5 ppm. IR ( $\text{CH}_2\text{Cl}_2$ ):  $\tilde{\nu} = 2035$  (m), 2001 (s), 1972 (m), 1925 (m)  $\text{cm}^{-1}$  (CO). Elem. anal. calcd (%) for  $\text{C}_{32}\text{H}_{62}\text{MnNaO}_5\text{S}_2\text{Si}_2$  (797.2): C 53.01, H 8.62 found: C 52.77, H 8.88.

#### 4.7.4 $(\text{CO})_4\text{Mn}(\mu\text{-SSi}t\text{Bu}_3)_2\text{Mn}(\text{SSi}t\text{Bu}_3)(\text{THF})$ (**41**)

To a solution of  $\text{BrMn}(\text{CO})_5$  (143 mg, 0.53 mmol) in 15 ml THF is added **10**(THF)<sub>2</sub> (**4.3.4.2**, 205 mg, 0.51 mmol) in one portion. The orange solution quickly becomes cloudy. After four hours, no unreacted thiolate can be observed in the NMR spectra of the reaction mixture, and signals consistent with a substitution product have grown in ( $\text{C}_6\text{D}_6$ ,  $^1\text{H}$  NMR 1.317 ppm,  $^{13}\text{C}$  NMR 31.5, 26.0 ppm,  $^{29}\text{Si}$  NMR 31.4 ppm). Volatiles are removed in vacuo and the brown residue is extracted with pentane (10 ml). The extract is filtered over diatomaceous earth on a frit. The filter cake is washed with pentane (2 x 5 ml). After standing at  $-20\text{ }^{\circ}\text{C}$  for several weeks, X-ray quality crystals of **41** can be obtained from a pentane solution. Yield: 50 mg (0.05 mmol, 29 %). Concentration of the mother liquor and standing for several weeks leads to the deposition of crystals of  $\text{Mn}_2(\text{CO})_{10}$ .

Analytical data for **41**:  $^1\text{H}$  NMR ( $\text{C}_6\text{D}_6$ , 250.1 MHz) = 1.396 (s, CCH<sub>3</sub>). IR (hexane):  $\tilde{\nu} = 2044$  (m), 2015 (s), 1992 (m), 1949 (m)  $\text{cm}^{-1}$  (CO). Elem. anal. calcd (%) for  $\text{C}_{44}\text{H}_{89}\text{Mn}_2\text{O}_5\text{S}_3\text{Si}_3$  (988.5): C 53.46, H 9.08 found: C 51.13, H 8.80.

#### 4.7.5 Reaction of **39** with $\text{BrMn}(\text{CO})_5$

Solid  $\text{BrMn}(\text{CO})_5$  (10 mg, 0.04 mmol) and **39** (**4.7.3**, 28 mg, 0.04 mmol) are combined in an NMR tube and dissolved in 0.6 ml THF-D<sub>8</sub>. Immediate gas evolution from the orange solution is observed. The tube is flame-sealed. After NMR investigation, the solution is removed from the tube, the volatiles removed, and the orange residue dissolved in  $\text{C}_6\text{D}_6$ .



$^1\text{H}$  NMR (THF- $\text{D}_8$ , 300.0 MHz) = 1.211 (CCH<sub>3</sub>, product), 1.174 ppm (CCH<sub>3</sub>, *t*Bu<sub>3</sub>SiSH).  $^{29}\text{Si}$  NMR (THF- $\text{D}_8$ , 59.6 MHz) = 30.9 (product), 27.2 ppm (*t*Bu<sub>3</sub>SiSH).  $^1\text{H}$  NMR (C<sub>6</sub>D<sub>6</sub>, 300.0 MHz) = 1.315 (CCH<sub>3</sub>, product), 1.192 (CCH<sub>3</sub>, by-product), 1.097 ppm (CCH<sub>3</sub>, *t*Bu<sub>3</sub>SiSH).  $^{29}\text{Si}$  NMR (C<sub>6</sub>D<sub>6</sub>, 59.6 MHz) = 40.1 (by-product), 301.3 (product), 27.2 ppm (*t*Bu<sub>3</sub>SiSH).

#### 4.7.6 [Fe(SSi*t*Bu<sub>3</sub>)(CO)<sub>3</sub>]<sub>2</sub> (42)

Disulfide **23** (4.4.1.4, 11.6 mg, 0.025 mmol) and Fe(CO)<sub>5</sub> (6.6  $\mu\text{l}$ , 9.8 mg, 0.05 mmol) are combined in C<sub>6</sub>D<sub>6</sub> in an NMR tube, which is then flame-sealed. The colorless solution is irradiated with a fluorescent light bulb for 8 months. After 5 months and again after 6 months, the NMR tube is cracked and the solution transferred to a new NMR tube and again flame-sealed. Over the course of the reaction, an accompanying color change to deep red is observed. Conversion is ca. 75 % as determined by NMR spectroscopy. Slow evaporation of the solvent yields the product as blood red needles.  $^1\text{H}$  NMR (C<sub>6</sub>D<sub>6</sub>, 250.1 MHz) = 1.193 (s, 54 H, CCH<sub>3</sub>) ppm.  $^{13}\text{C}$  NMR (C<sub>6</sub>D<sub>6</sub>, 75.4 MHz) = 209.4 (CO), 31.3 (CCH<sub>3</sub>), 25.6 (CCH<sub>3</sub>) ppm.  $^{29}\text{Si}$  NMR (C<sub>6</sub>D<sub>6</sub>, 59.6 MHz) = 39.7 ppm. IR (hexane):  $\tilde{\nu}$  = 2068 (m), 2035 (s), 1999 (m), 1989 (s)  $\text{cm}^{-1}$  (CO). Elem. anal. calcd. for C<sub>30</sub>H<sub>54</sub>Fe<sub>2</sub>O<sub>6</sub>S<sub>2</sub>Si<sub>2</sub> (742.7): C 48.51, H 7.33 found: C 49.03, H 7.80.

#### 4.7.7 [Fe(SeSi*t*Bu<sub>3</sub>)(CO)<sub>3</sub>]<sub>2</sub> (43)

Diselenide **24** (4.4.1.5, 20 mg, 0.036 mmol) and Fe(CO)<sub>5</sub> (14 mg, 0.072 mmol) are combined in C<sub>6</sub>D<sub>6</sub> in an NMR tube, which is then flame-sealed. The orange solution is irradiated with a fluorescent light bulb for 14 d. An accompanying color change to deep red is observed. Conversion is quantitative as determined by NMR spectroscopy. Slow evaporation of the solvent yields the product as blood red needles.  $^1\text{H}$  NMR (C<sub>6</sub>D<sub>6</sub>, 400.1 MHz) = 1.201 (s, 54H, CCH<sub>3</sub>) ppm.  $^{13}\text{C}$  NMR (C<sub>6</sub>D<sub>6</sub>, 62.9 MHz) = 31.3 (CCH<sub>3</sub>), 26.1 (CCH<sub>3</sub>), n. o. (CO) ppm.  $^{29}\text{Si}$  NMR (C<sub>6</sub>D<sub>6</sub>, 79.5 MHz) = 45.5 ppm.  $^{77}\text{Se}$  NMR (C<sub>6</sub>D<sub>6</sub>, 57.2 MHz) = -165 ppm. IR (hexane):  $\tilde{\nu}$  = 2066 (m), 2028 (s), 1982 (s)  $\text{cm}^{-1}$  (CO). Elem. anal. calcd. (%) for C<sub>30</sub>H<sub>54</sub>Fe<sub>2</sub>O<sub>6</sub>Se<sub>2</sub>Si<sub>2</sub> (836.5): C 43.07, H 6.51 found: C 43.79, H 6.84.

#### 4.7.8 [Fe(TeSi*t*Bu<sub>3</sub>)(CO)<sub>3</sub>]<sub>2</sub> (44)

Ditelluride **25** (4.4.1.6, 17 mg, 0.025 mmol) and Fe(CO)<sub>5</sub> (10 mg, 0.05 mmol) are combined in C<sub>6</sub>D<sub>6</sub> in an NMR tube, which is then flame-sealed. The blue solution is irradiated with a fluorescent light bulb for 8 h. An accompanying color change to red is observed. Conversion is quantitative as determined by NMR spectroscopy. Slow evaporation of the solvent yields the product as blood red plates.  $^1\text{H}$  NMR (C<sub>6</sub>D<sub>6</sub>, 250.1 MHz) = 1.195 (s, 54H, CCH<sub>3</sub>) ppm.

$^{13}\text{C}$  NMR ( $\text{C}_6\text{D}_6$ , 62.9 MHz) = 213.4 (CO), 31.5 ( $\text{CCH}_3$ ), 26.5 ( $\text{CCH}_3$ ), ppm.  $^{29}\text{Si}$  NMR ( $\text{C}_6\text{D}_6$ , 49.7 MHz) = 45.1 ppm.  $^{125}\text{Te}$  NMR ( $\text{C}_6\text{D}_6$ , 126.2 MHz) = -1280 ppm. IR (KBr pellet):  $\tilde{\nu}$  = 2044 (vs), 2007 (vs), 1979 (s), 1963 (s), 1954 (s)  $\text{cm}^{-1}$  (CO). IR (hexane):  $\tilde{\nu}$  = 2048 (s), 2016 (vs), 1977 (vs)  $\text{cm}^{-1}$ . Elem. anal. calcd (%) for  $\text{C}_{30}\text{H}_{54}\text{Fe}_2\text{O}_6\text{Te}_2\text{Si}_2$  (933.8): C 38.59, H 5.83; found: C 39.62, H 6.41.

## 4.8 X-ray structure determination

Data collection: Stoe-IPDS-II diffractometer, graphite monochromated Mo  $\text{K}_\alpha$  radiation;  $T$  = 173 K. Empirical absorption correction using MULABS,<sup>[185]</sup> structure solution by direct methods,<sup>[186]</sup> structure refinement by full-matrix least-squares on  $F^2$  with SHELXL-97.<sup>[187]</sup> Hydrogen atoms not involved in hydrogen bonding were placed on ideal positions and refined with fixed isotropic displacement parameters using a riding model.

## 5 Literature

- [1] J. J. R. Fraústo da Silva and R. J. P. Williams, *The Biological Chemistry of the Elements*, Clarendon Press, Oxford, **1991**, p. 561.
- [2] M. W. DeGroot and J. F. Corrigan, *Z. Anorg. Allg. Chem.* **2006**, 632, 19-29.
- [3] D. T. T. Tran and J. F. Corrigan, *Organometallics* **2000**, 19, 5202-5208.
- [4] M. W. DeGroot and J. F. Corrigan, *Organometallics* **2005**, 24, 3378-3385.
- [5] C. P. Gerlach, V. Christou and J. Arnold, *Inorg. Chem.* **1996**, 35, 2758-2766.
- [6] P. J. Bonasia and J. Arnold, *Inorg. Chem.* **1992**, 31, 2508-2514.
- [7] P. T. Wolczanski, *Polyhedron* **1995**, 14, 3335-3362.
- [8] J. L. Bennett and P. T. Wolczanski, *J. Am. Chem. Soc.* **1994**, 116, 2179-2180.
- [9] K. F. Hirsekorn, A. S. Veige, M. P. Marshak, Y. Koldobskaya, P. T. Wolczanski, T. R. Cundari and E. B. Lobkovsky, *J. Am. Chem. Soc.* **2005**, 127, 4809-4830.
- [10] O. L. Sydora, T. P. Henry, P. T. Wolczanski, E. B. Lobkovsky, E. Rumberger and D. N. Hendrickson, *Inorg. Chem.* **2006**, 45, 609-626.
- [11] F. Dornhaus, M. Bolte, H.-W. Lerner and M. Wagner, *Eur. J. Inorg. Chem.* **2006**, 1777-1785.
- [12] F. Dornhaus, M. Bolte, H.-W. Lerner and M. Wagner, *Eur. J. Inorg. Chem.* **2006**, in press.
- [13] F. Dornhaus *PhD Thesis* Johann Wolfgang Goethe-Universität, Frankfurt, Germany, **2007**.
- [14] T. Komuro, T. Matsuo, H. Kawaguchi and K. Tatsumi, *Dalton Trans.* **2004**, 1618-1625.
- [15] C. A. Tolman, *Chem. Rev.* **1977**, 77, 313-348.
- [16] I. Medina, H. Jacobsen, J. T. Mague and M. J. Fink, *Inorg. Chem.* **2006**, 45, 8844-8846.
- [17] V. P. Ananikov, I. P. Beletskaya, G. G. Aleksandrov and I. L. Eremenko, *Organometallics* **2003**, 22, 1414-1421.
- [18] J. M. Gonzales, D. G. Musaev and K. Morokuma, *Organometallics* **2005**, 24, 4908-4914.
- [19] Holleman and Wiberg, *Lehrbuch der Anorganischen Chemie*, Walter de Gruyter, Berlin, **1995**, p. 2033.
- [20] N. Wiberg (Eds.: A. R. Bassindale and P. P. Gaspar), Royal Society of Chemistry, Cambridge, **1991**, p. S263.
- [21] N. Wiberg, *Coord. Chem. Rev.* **1997**, 163, 217-252.
- [22] S. Henkel, K. W. Klinkhammer and W. Schwarz, *Angew. Chem.* **1994**, 106, 721-723.

- [23] N. Wiberg, K. Amelunxen, H. Nöth, M. Schmidt and H. Schwenk, *Angew. Chem.* **1996**, *108*, 110-112.
- [24] N. Wiberg, T. Blank, H.-W. Lerner, D. Fenske and G. Linti, *Angew. Chem.* **2001**, *113*, 1275-1278.
- [25] N. Wiberg, H.-W. Lerner, S.-K. Vasisht, S. Wagner, K. Karaghiosoff, H. Nöth and W. Ponikvar, *Eur. J. Inorg. Chem.* **1999**, 1211-1218.
- [26] A. Sekiguchi, T. Fukawa, M. Nakamoto, V. Y. Lee and M. Ichinohe, *J. Am. Chem. Soc.* **2002**, *124*, 9865-9869.
- [27] A. Sekiguchi, R. Kinjo and M. Ichinohe, *Science* **2004**, *305*, 1755-1757.
- [28] P. Jiang and P. P. Gaspar, *J. Am. Chem. Soc.* **2001**, *123*, 8622-8623.
- [29] D. Voet and J. G. Voet, *Biochemistry*, John Wiley and Sons, Inc., New York, **1995**, p. 1361.
- [30] V. G. Albano, M. Monari, I. Orabona, A. Panunzi and F. Ruffo, *J. Am. Chem. Soc.* **2001**, *123*, 4352-4353.
- [31] W. F. Liaw, M. H. Chiang, C. J. Liu, P. J. Harn and L. K. Liu, *Inorg. Chem.* **1993**, *32*, 1536-1538.
- [32] S. E. Denmark and J. D. Baird, *Chem. Eur. J.* **2006**, *12*, 4954-4963.
- [33] B. Marciniak, P. Krzyzanowski, E. Walczuk-Gusciora and W. Duczmal, *J. Mol. Catal. A: Chem.* **1999**, *144*, 263-271.
- [34] B. Marciniak and H. Maciejewski, *Coord. Chem. Rev.* **2001**, *223*, 301-335.
- [35] D. Fenske, J. Ohmer, J. Hachgenei and K. Merzweiler, *Angew. Chem.* **1988**, *100*, 1300-1320.
- [36] D. Fenske and J. F. Corrigan in *Metal Clusters in Chemistry, Vol. 3* (Eds.: P. Braunstein, L. A. Oro and P. R. Raithby), Wiley-VCH, Weinheim, **1999**, p. 1302.
- [37] T. Komuro, H. Kawaguchi and K. Tatsumi, *Inorg. Chem.* **2002**, *41*, 5083-5090.
- [38] P. J. Bonasia, D. E. Gindelberger, B. O. Dabbousi and J. Arnold, *J. Am. Chem. Soc.* **1992**, *114*, 5209.
- [39] P. J. Bonasia, D. E. Gindelberger and J. Arnold, *Inorg. Chem.* **1993**, *32*, 5126-5131.
- [40] T. S. Lobana in *Coordination chemistry of phosphine chalcogenides and their analytical and catalytic applications, Vol. 2* (Ed. F. R. Hartley), John Wiley & Sons, Chichester, **1992**, pp. 409-566.
- [41] T. D. Tilley in *The Chemistry of Organic Silicon Compounds, Vol. 1* (Eds.: S. Patai and Z. Rappoport), J. Wiley and Sons, New York, **1989**, pp. 1415-1477.
- [42] C. A. Jaska, A. J. Lough and I. Manners, *Inorg. Chem.* **2004**, *43*, 1090-1099.

- [43] H. Dorn, C. A. Jaska, R. A. Singh, A. J. Lough and I. Manners, *Chem. Commun.* **2000**, 1041-1042.
- [44] A.-C. Gaumont, M. B. Hursthouse, S. J. Coles and J. M. Brown, *Chem. Commun.* **1999**, 63-64.
- [45] W. Angerer, W. S. Sheldrick and W. Malisch, *Chem. Ber.* **1985**, *118*, 1261-1266.
- [46] G. Müller and J. Brand, *Organometallics* **2003**, *22*, 1463-1467.
- [47] N. Wiberg, K. Amelunxen, H.-W. Lerner, H. Schuster, H. Nöth, I. Krossing, M. Schmidt-Amelunxen and T. Seifert, *J. Organomet. Chem.* **1997**, *542*, 1-18.
- [48] C. Kayser, R. Fischer, J. Baumgartner and C. Marschner, *Organometallics* **2002**, *21*, 1023-1030.
- [49] D. M. Jenkins, W. Teng, U. Englich, D. Stone and K. Ruhlandt-Senge, *Organometallics* **2001**, *20*, 4600-4606.
- [50] N. Wiberg, T. Blank, H.-W. Lerner, D. Fenske and G. Linti, *Angew. Chem. Int. Ed.* **2001**, *40*, 1232-1235.
- [51] S. Henkel, K. W. Klinkhammer and W. Schwarz, *Angew. Chem. Int. Ed.* **1994**, *33*, 681-683.
- [52] M. P. Doyle and C. T. West, *J. Am. Chem. Soc.* **1975**, *97*, 3777-3782.
- [53] E. M. Dexheimer and L. Spialter, *Tetrahedron Lett.* **1975**, *16*, 1771-1772.
- [54] M. Weidenbruch and W. Peter, *Angew. Chem. Int. Ed.* **1975**, *14*, 642-643.
- [55] E. M. Dexheimer, L. Spialter and J. Smithson, *J. Organomet. Chem.* **1975**, *102*, 21-27.
- [56] N. Wiberg and K. Schurz, *J. Organomet. Chem.* **1988**, *341*, 145-163.
- [57] H.-W. Lerner, S. Scholz and M. Bolte, *Z. Anorg. Allg. Chem.* **2001**, *627*, 1638-1642.
- [58] H.-W. Lerner, S. Scholz, M. Bolte and M. Wagner, *Z. Anorg. Allg. Chem.* **2004**, *630*, 443-451.
- [59] F. W. G. Fearon and H. Gilman, *J. Organomet. Chem.* **1967**, *9*, 403-411.
- [60] T. J. Barton and C. R. Tully, *J. Org. Chem.* **1978**, *43*, 3649-3653.
- [61] J. H. Noordik, J. Schreurs, R. O. Gould, J. J. Mooji and E. de Boer, *J. Phys. Chem.* **1978**, *82*, 1105-1110.
- [62] J. J. Mooji, A. A. K. Klaassen, E. de Boer, H. M. L. Degens, T. E. M. van den Hark and J. H. Noordik, *J. Am. Chem. Soc.* **1976**, *98*, 680-685.
- [63] J. P. Dunne, M. Bockmeyer and M. Tacke, *Eur. J. Inorg. Chem.* **2003**, 458-466.
- [64] H. Yoshida, Y. Yamaro, J. Ohshita and A. Kunai, *Tetrahedron Lett.* **2003**, *44*, 1541-1544.
- [65] H. Yoshida, Y. Yamaro, J. Ohshita and A. Kunai, *Chem. Commun.* **2003**, 1510-1511.

- [66] D. M. L. Goodgame, P. D. Lickiss, S. Menzer, S. J. Rooke and D. J. Williams, *J. Organomet. Chem.* **2000**, 593-594, 161-166.
- [67] V. Chandrasekhar, R. Boomishankar and S. Nagendran, *Chem. Rev.* **2004**, 104, 5847-5910.
- [68] A. R. Chadeayne, P. T. Wolczanski and E. B. Lobkovsky, *Inorg. Chem.* **2004**, 43, 3421-3432.
- [69] S. M. Sieburth and L. Fensterbank, *J. Org. Chem.* **1993**, 58, 6314-6318.
- [70] H.-W. Lerner, S. Scholz and M. Bolte, *Organometallics* **2002**, 21, 3827-3830.
- [71] K. Hirabayashi, J.-i. Ando, J. Kawashima, Y. Nishihara, A. Mori and T. Hiyama, *Bull. Chem. Soc. Jpn.* **2000**, 73, 1409-1417.
- [72] S. Schütte, C. Freire-Erdbrügger, U. Klingebiel and G. M. Sheldrick, *Phosphorus, Sulfur and Silicon* **1993**, 78, 75-81.
- [73] J. F. Hyde, O. K. Johansson, W. H. Daudt, R. F. Fleming, H. B. Laudenslager and M. P. Roche, *J. Am. Chem. Soc.* **1953**, 75, 5615-5618.
- [74] W. S. Tatlock and E. G. Rochow, *J. Org. Chem.* **1952**, 17, 1555-1563.
- [75] S. Chadwick, U. Englisch and K. Ruhlandt-Senge, *Organometallics* **1997**, 16, 5792-5803.
- [76] U. Englisch, S. Chadwick and K. Ruhlandt-Senge, *Inorg. Chem.* **1998**, 37, 283.
- [77] M. Kunert, E. Kinjus, M. Nauck and J. Sieler, *Chem. Ber.* **1997**, 130, 1461.
- [78] K. Ruhlandt-Senge and U. Englisch, *Chem. Commun.* **1996**, 147.
- [79] O. V. Kononov, V. D. Lobkov, V. A. Igonin, S. V. Lindeman, V. E. Shklover and Y. T. Struchov, *Metalloorg. Khim. (Russ.)* **1991**, 4, 784.
- [80] A. Mommertz, K. Dehnicke and J. Magull, *Z. Naturforsch., B: Chem. Sci.* **1996**, 51, 1583.
- [81] M. J. McGeary, K. Folting, W. E. Streib, J. C. Huffman and K. G. Caulton, *Polyhedron* **1991**, 10, 2699.
- [82] G. R. Fuentes, P. S. Coan, W. E. Streib and K. G. Caulton, *Polyhedron* **1991**, 10, 2371.
- [83] N. Hu, G. Nie, Z. Jin and W. Chen, *J. Organomet. Chem.* **1989**, 377, 137-143.
- [84] J. S. Kristoff and D. F. Shriver, *Inorg. Chem.* **1974**, 13, 499-506.
- [85] T. Komuro, H. Kawaguchi and K. Tatsumi, *Inorg. Chem.* **2002**, 41, 5083.
- [86] D. E. Gindelberger and J. Arnold, *Inorg. Chem.* **1993**, 32, 5813.
- [87] H. Lange, U. Herzog, H. Borrmann and B. Walfort, *J. Organomet. Chem.* **2004**, 689, 4897-4908.
- [88] H. Lange and U. Herzog, *J. Organomet. Chem.* **2002**, 660, 36-42.
- [89] P. J. Bonasia, V. Christou and J. Arnold, *J. Am. Chem. Soc.* **1993**, 115, 6777-6781.

- [90] T. I. Kückmann, M. Hermsen, M. Bolte, M. Wagner and H.-W. Lerner, *Inorg. Chem.* **2005**, *44*, 3449-3458.
- [91] P. B. Hitchcock, N. H. Buttrus and A. C. Sullivan, *J. Organomet. Chem.* **1986**, *303*, 321.
- [92] N. Wiberg and H. Schuster, *Chem. Ber.* **1991**, *124*, 93.
- [93] B. O. Dabbousi, P. J. Bonasia and J. Arnold, *J. Am. Chem. Soc.* **1991**, *113*, 3186-3188.
- [94] A. Sobkowiak and D. T. Sawyer, *Inorg. Chem.* **1990**, *29*, 1248.
- [95] N. G. Connelly and W. E. Geiger, *Chem. Rev.* **1996**, *96*, 877-910.
- [96] Cambridge Structural Database version 5.27, updated August 2006
- [97] H. Fleischer, S. Stauf and D. Schollmeyer, *Inorg. Chem.* **1999**, *38*, 3725-3729.
- [98] H. Fleischer, S. Hennig and D. Schollmeyer, *Z. Anorg. Allg. Chem.* **2003**, *629*, 1969-1974.
- [99] H. Fleischer, Phosphorus, Sulfur Silicon Relat. Elem. **2005**, *180*, 815-825.
- [100] H. Fleischer, N. W. Mitzel and D. Schollmeyer, *Eur. J. Inorg. Chem.* **2003**, 815-821.
- [101] J. L. Kice and H. Slebocka-Tilk, *J. Am. Chem. Soc.* **1982**, *104*, 7123-7130.
- [102] J. L. Kice, T. W. S. Lee and S.-t. Pan, *J. Am. Chem. Soc.* **1980**, *102*, 4448-4455.
- [103] J. L. Kice, D. M. Wilson and J. M. Espinola, *J. Org. Chem.* **1991**, *56*, 3520-3524.
- [104] F. Fehér and H. Goller, *Z. Naturforsch., B: Chem. Sci.* **1967**, *22*, 1224-1225.
- [105] J. Hahn and K. Altenbach, *Z. Naturforsch., B: Chem. Sci.* **1986**, *41*, 675-679.
- [106] W. Wojnowski, M. Wojnowska and B. Becker, *Z. Anorg. Allg. Chem.* **1988**, *561*, 167-173.
- [107] R. Minkwitz, A. Kornath and H. Preut, *Z. Anorg. Allg. Chem.* **1994**, *620*, 981-986.
- [108] F. A. Cotton and C. S. Kraihanzel, *J. Am. Chem. Soc.* **1962**, *84*, 4432-4438.
- [109] N. Kuhn and H. Schumann, *J. Organomet. Chem.* **1984**, *276*, 55-66.
- [110] P. S. Braterman, D. W. Milne, E. W. Randall and E. Rosenberg, *J. Chem. Soc. Dalton Trans* **1973**, 1027-1031.
- [111] B. E. Mann and B. F. Taylor, *<sup>13</sup>C NMR Data for Organometallic Compounds*, Academic Press, London, **1981**, p. 326.
- [112] W. Malisch, H. Jehle, S. Möller, G. Thum, J. Reising, A. Gbureck, V. Nagel, C. Fickert, W. Kiefer and M. Nieger, *Eur. J. Inorg. Chem.* **1999**, 1597-1605.
- [113] W. Malisch, H. Jehle, D. Schumacher, M. Binnewies and N. Söger, *J. Organomet. Chem.* **2003**, *667*, 35-41.
- [114] J. S. McIndoe and B. K. Nicholson, *J. Organomet. Chem.* **2002**, *648*, 237-245.
- [115] U. Schubert, G. Kraft and E. Walther, *Z. Anorg. Allg. Chem.* **1984**, *519*, 96-106.
- [116] T. S. Piper, D. Lemal and G. Wilkinson, *Naturwissenschaften* **1956**, *43*, 129.

- [117] W. Malisch and M. Kuhn, *Chem. Ber.* **1974**, *107*, 979-995.
- [118] R. J. P. Corriu and W. E. Douglas, *J. Organomet. Chem.* **1973**, *51*, C3-C4.
- [119] G. Cerveau, E. Colomer, R. Corriu and W. E. Douglas, *J. Organomet. Chem.* **1977**, *135*, 373-386.
- [120] P. M. Treichel and D. A. Komar, *J. Organomet. Chem.* **1981**, *206*, 77-88.
- [121] H. Schumann and L. Eguren, *J. Organomet. Chem.* **1991**, *403*, 183-193.
- [122] E. E. Isaacs and W. A. G. Graham, *J. Organomet. Chem.* **1976**, *120*, 407-421.
- [123] M. L. Brown, J. L. Cramer, J. A. Ferguson, T. J. Meyer and N. Winterton, *J. Am. Chem. Soc.* **1972**, *94*, 8707-8710.
- [124] A. S. Goldman and D. R. Tyler, *Inorg. Chem.* **1987**, *26*, 253-258.
- [125] E. Louattani, A. Lledós and J. Suades, *Organometallics* **1995**, *14*, 1053-1060.
- [126] H. Schumann, *J. Organomet. Chem.* **1987**, *320*, 145-162.
- [127] T. I. Kückmann, F. Dornhaus, M. Bolte, H.-W. Lerner and M. Wagner, *Chem. Eur. J.* **2007**, *submitted for publication*.
- [128] D. A. Hoic, W. M. Davis and G. C. Fu, *J. Am. Chem. Soc.* **1996**, *118*, 8176-8177.
- [129] M. Weidenbruch and W. Peter, *Angewandte Chemie* **1975**, *87*, 670.
- [130] L. Párkányi, K. H. Pannell and C. Hernandez, *J. Organomet. Chem.* **1983**, *252*, 127-132.
- [131] R. West and E. K. Pham, *J. Organomet. Chem.* **1991**, *402*, 215-220.
- [132] P. M. Treichel, R. L. Shubkin, K. W. Barnett and D. Reichard, *Inorg. Chem.* **1966**, *5*, 1177-1181.
- [133] R. J. P. Corriu and W. E. Douglas, *J. Organomet. Chem.* **1973**, *51*, C3-C4.
- [134] R. B. King, K. H. Pannell, C. R. Bennet and M. Ishaq, *J. Organomet. Chem.* **1969**, *19*, 327-337.
- [135] S. B. Fergusson, L. J. Sanderson, T. A. Shackleton and M. C. Baird, *Inorg. Chim. Acta* **1984**, *83*, L45-L47.
- [136] M. L. H. Green, C. N. Street and G. Wilkinson, *Z. Naturforsch., B: Chem. Sci.* **1959**, *14*, 738.
- [137] T. H. Whitesides and J. Shelly, *J. Organomet. Chem.* **1975**, *92*, 215-226.
- [138] I. Kovács, F. Bélanger-Gariépy and A. Shaver, *Inorg. Chem.* **2003**, *42*, 2988-2991.
- [139] M. Morán, I. Cuadrado, C. Pascual, J. R. Masaguer and J. Losada, *Inorg. Chim. Acta* **1987**, *132*, 257-262.
- [140] N. Kuhn and H. Schumann, *J. Organomet. Chem.* **1986**, *304*, 181-193.



- [141] O. L. Sydora, P. T. Wolczanski and E. B. Lobkovsky, *Angew. Chem.* **2003**, *115*, 2789-2791.
- [142] A. Reisinger, D. Himmel and I. Krossing, *Angew. Chem.* **2006**, *118*, 7153-7156.
- [143] N. Sreehari, B. Varghese and P. T. Manoharan, *Inorg. Chem.* **1990**, *29*, 4011.
- [144] A. D. Watson, C. P. Rao, J. R. Dorfmann and H. R. Holm, *Inorg. Chem.* **1985**, *24*, 2820.
- [145] I. L. Abrahams, C. D. Garner and W. Clegg, *J. Chem. Soc. Dalton Trans* **1987**, 1577.
- [146] C. Zhang, R. Chadha, K. H. Reddy and G. N. Schrauzer, *Inorg. Chem.* **1991**, *30*, 3865.
- [147] H. Grutzmacher, M. Steiner, H. Pritzkow, L. Zsolani, G. Huttner and A. Sebald, *Chem. Ber.* **1992**, *125*, 2199.
- [148] B. Kersting, *Angew. Chem. Int. Ed.* **2001**, *40*, 3987.
- [149] M. Mikuriya, X. Jian, S. Ikemi, T. Kawahashi and H. Tsutsumi, *Bull. Chem. Soc. Jpn.* **1998**, *71*, 2161.
- [150] T. Tuntulani, J. H. Reibenspies, P. J. Farmer and M. Y. Darensbourg, *Inorg. Chem.* **1992**, *31*, 3497.
- [151] B. Becker, A. Dolega, A. Konitz and W. Wojnowski, *Polyhedron* **2001**, *20*, 949.
- [152] K. S. Anjali and J. J. Vittal, *Main Group Met. Chem.* **2001**, *24*, 129.
- [153] M. C. Brioso, J. L. Brioso, W. Gaete, J. Ros and C. Suner, *J. Chem. Soc. Dalton Trans* **1981**, 852.
- [154] I. Dance and K. Fisher in *Metal chalcogenide cluster chemistry, Vol. 41* (Ed. K. D. Karlin), John Wiley and Sons, New York, **1994**, pp. 637-803.
- [155] S. A. Al-Ahmand, J. W. Kampf, R. W. Dunham and D. Coucouvanis, *Inorg. Chem.* **1991**, *30*, 1163-1164.
- [156] A. Winter, G. Huttner, M. Gottlieb and I. Jibril, *J. Organomet. Chem.* **1985**, *286*, 317-327.
- [157] P. M. Treichel and P. C. Nakagaki, *Organometallics* **1986**, *5*, 711-716.
- [158] J. Chem, V. G. Young and R. J. Angelici, *Organometallics* **1996**, *15*, 325-331.
- [159] E. Lindner, K. Auch, K. Hiller and R. Fawzi, *Z. Naturforsch., B: Chem. Sci.* **1967**, *42*, 454.
- [160] J. Grobe, J. Vetter, B. Krebs and M. Pascaly, *Z. Anorg. Allg. Chem.* **626**, 430-443.
- [161] W. J. Mace, L. Main, B. K. Nicholson and M. Hagyard, *J. Organomet. Chem.* **2002**, *664*, 288-293.
- [162] X. Zhang, C. A. Dullaghan, G. B. Carpenter, D. A. Swaigart and Q. Meng, *Chem. Commun.* **1998**, 93.

- [163] S. Onaka and Y. Kalukawa, *J. Coord. Chem.* **1996**, 135.
- [164] D. S. Choi, S. H. Hong, S. S. Lee and Y. K. Chung, *J. Organomet. Chem.* **1999**, 579, 385-390.
- [165] C. A. Dullaghan, G. B. Carpenter, D. A. Sweigart, D. S. Choi, S. S. Lee and Y. K. Chung, *Organometallics* **1997**, 16, 5688-5695.
- [166] X. Zhang, C. A. Dullaghan, E. J. Watson, G. B. Carpenter and D. A. Sweigart, *Organometallics* **1998**, 17, 2067-2075.
- [167] M. Herberhold, W. Milius and J. Liu, *Z. Naturforsch., B: Chem. Sci.* **2004**, 59, 673-680.
- [168] W.-F. Liaw, C.-M. Lee, L. Homg, G.-H. Lee and S.-M. Peng, *Organometallics* **1999**, 18, 782.
- [169] S. Komiya, S.-y. Muroi, M. Furuya and M. Hirano, *J. Am. Chem. Soc.* **2000**, 122, 170-171.
- [170] D. F. Evans, *J. Chem. Soc.* **1959**, 2003-2005.
- [171] E. M. Schubert, *J. Chem. Educ.* **1992**, 69, 62.
- [172] M. M. Shieh, P.-F. Chen, Y.-C. Tsai, M.-H. Shieh, S.-M. Peng and L. G.-H., *Inorg. Chem.* **1995**, 34, 2251.
- [173] R. E. Bachman and K. H. Witmire, *Organometallics* **1993**, 12, 1988.
- [174] P. Mathur, V. D. Reddy, K. Das and U. C. Sinha, *J. Organomet. Chem.* **1991**, 409, 255-261.
- [175] P. Mathur, R. Trivedi, M. Hossain, S. S. Tavale and V. G. Puranik, *J. Organomet. Chem.* **1995**, 491, 291-294.
- [176] S. Jäger, P. G. Jones, J. Laube and C. Thöne, *Z. Anorg. Allg. Chem.* **1999**, 625, 352-358.
- [177] S. Jeannin, Y. Jeannin, F. Robert and C. Rosenberger, *J. Organomet. Chem.* **1993**, 448, 151-155.
- [178] E. Delgado, E. Hernández, N. Mansilla, F. Zamora and L. A. Martínez-Cruz, *Inorg. Chim. Acta* **1999**, 284, 14-19.
- [179] M. T. Ashby, *Inorg. Chem.* **1995**, 34, 5429-5436.
- [180] T. I. Kückmann, M. Bolte, H.-W. Lerner and M. Wagner, *Z. Anorg. Allg. Chem.* **2006**, in press.
- [181] M. Haberecht *Ph.D.Thesis*, University of Frankfurt, Frankfurt, Germany, **2005**.
- [182] T. Ohishi, Y. Shiotani and M. Yamashita, *J. Org. Chem.* **1994**, 59, 250.
- [183] D. L. Reger and C. Coleman, *J. Organomet. Chem.* **1977**, 131, 153-162.
- [184] D. Catheline and D. Astruc, *Organometallics* **1984**, 3, 1094-1100.
- [185] R. H. Blessing, *Acta Crystallogr. Sect. A* **1995**, 51, 33-38.

[186] G. M. Sheldrick, *Acta Crystallogr. Sect. A* **1990**, *46*, 467.

[187] G. M. Sheldrick, *SHELXL 97*, University of Göttingen, Göttingen, Germany, **1997**.

## **6 Appendix**

### **6.1 Crystallographic data**

Crystal data and structure refinement for **3**bis(THF)(18-crown-6)sodium 4,4'-bis(di-*tert*-butylmethylsilyl)biphenylide (**4.2.3**)

Empirical formula	C <sub>58</sub> H <sub>106</sub> NaO <sub>10</sub> Si <sub>2</sub>	
Formula weight	1042.60	
Temperature	173(2) K	
Wavelength	0.71073 Å	
Crystal system	Monoclinic	
Space group	<i>P</i> 2 <sub>1</sub> / <i>c</i>	
Unit cell dimensions	a = 13.1292(8) Å	α = 90°
	b = 18.3379(8) Å	β = 113.233(4)°
	c = 14.4381(8) Å	γ = 90°
Volume	3194.3(3) Å <sup>3</sup>	
Z	2	
Density (calculated)	1.084 Mg/m <sup>3</sup>	
Absorption coefficient	0.112 mm <sup>-1</sup>	
F(000)	1146	
Crystal size	0.40 x 0.23 x 0.22 mm <sup>3</sup>	
Theta range for data collection	3.56 to 25.48°.	
Index ranges	-15 ≤ h ≤ 15, -22 ≤ k ≤ 22, -17 ≤ l ≤ 17	
Reflections collected	40036	
Independent reflections	5846 [R(int) = 0.0665]	
Completeness to theta = 25.00°	99.1 %	
Absorption correction	Semi-empirical from equivalents	
Max. and min. transmission	0.9757 and 0.9564	
Refinement method	Full-matrix least-squares on F <sup>2</sup>	
Data / restraints / parameters	5846 / 12 / 318	
Goodness-of-fit on F <sup>2</sup>	1.086	
Final R indices [I > 2σ(I)]	R1 = 0.0999, wR2 = 0.2692	
R indices (all data)	R1 = 0.1169, wR2 = 0.2834	
Largest diff. peak and hole	0.716 and -0.528 e.Å <sup>-3</sup>	

## Crystal structure and data refinement for 4,4'-bis(trimethylsilyl)biphenyl (4.3.5)

Empirical formula	C <sub>18</sub> H <sub>26</sub> Si <sub>2</sub>	
Formula weight	298.57	
Temperature	173(2) K	
Wavelength	0.71073 Å	
Crystal system	Monoclinic	
Space group	C2/c	
Unit cell dimensions	a = 86.216(16) Å	α = 90°.
	b = 7.4953(9) Å	β = 91.585(17)°.
	c = 25.327(6) Å	γ = 90°.
Volume	16360(5) Å <sup>3</sup>	
Z	36	
Density (calculated)	1.091 Mg/m <sup>3</sup>	
Absorption coefficient	0.186 mm <sup>-1</sup>	
F(000)	5832	
Crystal size	0.42 x 0.27 x 0.11 mm <sup>3</sup>	
Theta range for data collection	1.42 to 24.60°.	
Index ranges	-97 ≤ h ≤ 100, -8 ≤ k ≤ 8, -29 ≤ l ≤ 25	
Reflections collected	35858	
Independent reflections	13339 [R(int) = 0.2724]	
Completeness to theta = 24.60°	97.0 %	
Absorption correction	Semi-empirical from equivalents	
Max. and min. transmission	0.9799 and 0.9261	
Refinement method	Full-matrix least-squares on F <sup>2</sup>	
Data / restraints / parameters	13339 / 1377 / 811	
Goodness-of-fit on F <sup>2</sup>	0.656	
Final R indices [I > 2σ(I)]	R1 = 0.0729, wR2 = 0.1305	
R indices (all data)	R1 = 0.3916, wR2 = 0.2039	
Largest diff. peak and hole	0.228 and -0.285 e.Å <sup>-3</sup>	

Crystal data and structure refinement for  $5 \cdot 1/4\text{HBr} \cdot 1/4\text{H}_2\text{O}$   
 $t\text{Bu}_2\text{MeSiOH} \cdot 1/4\text{HBr} \cdot 1/4\text{H}_2\text{O}$  (**4.3.1**)

Empirical formula	$\text{C}_9\text{H}_{23.25}\text{Br}_{0.25}\text{O}_{1.50}\text{Si}$	
Formula weight	203.59	
Temperature	173(2) K	
Wavelength	0.71073 Å	
Crystal system	Monoclinic	
Space group	$P2_1/n$	
Unit cell dimensions	$a = 16.4814(8)$ Å	$\alpha = 90^\circ$
	$b = 16.1107(5)$ Å	$\beta = 98.510(4)^\circ$
	$c = 20.0624(10)$ Å	$\gamma = 90^\circ$
Volume	$5268.5(4)$ Å <sup>3</sup>	
Z	16	
Density (calculated)	1.027 Mg/m <sup>3</sup>	
Absorption coefficient	0.904 mm <sup>-1</sup>	
F(000)	1792	
Crystal size	0.30 x 0.13 x 0.12 mm <sup>3</sup>	
Theta range for data collection	3.46 to 25.69°.	
Index ranges	$-20 \leq h \leq 20$ , $-18 \leq k \leq 19$ , $-24 \leq l \leq 24$	
Reflections collected	69100	
Independent reflections	9889 [R(int) = 0.0654]	
Completeness to theta = 25.00°	99.7 %	
Absorption correction	Semi-empirical from equivalents	
Max. and min. transmission	0.8993 and 0.7732	
Refinement method	Full-matrix least-squares on F <sup>2</sup>	
Data / restraints / parameters	9889 / 0 / 440	
Goodness-of-fit on F <sup>2</sup>	1.065	
Final R indices [I > 2sigma(I)]	R1 = 0.0485, wR2 = 0.1053	
R indices (all data)	R1 = 0.0631, wR2 = 0.1112	
Largest diff. peak and hole	1.370 and -0.425 e.Å <sup>-3</sup>	

Crystal data and structure refinement for (6)<sub>6</sub> (Ph<sub>2</sub>MeSiONa)<sub>6</sub> (4.3.2)

Empirical formula	C <sub>78</sub> H <sub>78</sub> Na <sub>6</sub> O <sub>6</sub> Si <sub>6</sub>	
Formula weight	1417.88	
Temperature	173(2) K	
Wavelength	0.71073 Å	
Crystal system	Triclinic	
Space group	<i>P</i> -1	
Unit cell dimensions	a = 14.7578(7) Å	α = 74.415(4)°
	b = 23.2395(11) Å	β = 87.130(4)°
	c = 24.0857(12) Å	γ = 73.998(4)°
Volume	7645.9(6) Å <sup>3</sup>	
Z	4	
Density (calculated)	1.232 Mg/m <sup>3</sup>	
Absorption coefficient	0.193 mm <sup>-1</sup>	
F(000)	2976	
Crystal size	0.26 x 0.24 x 0.18 mm <sup>3</sup>	
Theta range for data collection	3.35 to 25.69°.	
Index ranges	-17 ≤ h ≤ 17, -28 ≤ k ≤ 28, -29 ≤ l ≤ 29	
Reflections collected	110599	
Independent reflections	28559 [R(int) = 0.0902]	
Completeness to theta = 25.00°	99.5 %	
Absorption correction	Semi-empirical from equivalents	
Max. and min. transmission	0.9660 and 0.9514	
Refinement method	Full-matrix least-squares on F <sup>2</sup>	
Data / restraints / parameters	28559 / 0 / 1729	
Goodness-of-fit on F <sup>2</sup>	1.039	
Final R indices [I > 2σ(I)]	R1 = 0.0978, wR2 = 0.2405	
R indices (all data)	R1 = 0.1642, wR2 = 0.2789	
Largest diff. peak and hole	6.135 and -1.108 e.Å <sup>-3</sup>	



Crystal data and structure refinement for (6)<sub>4</sub>(THF)<sub>4</sub>(Ph<sub>2</sub>MeSiONa)<sub>4</sub>(THF)<sub>4</sub> (4.3.3.1)

Empirical formula	C <sub>68</sub> H <sub>84</sub> Na <sub>4</sub> O <sub>8</sub> Si <sub>4</sub>	
Formula weight	1233.67	
Temperature	173(2) K	
Wavelength	0.71073 Å	
Crystal system	Orthorhombic	
Space group	<i>Aba2</i>	
Unit cell dimensions	a = 17.8310(12) Å	α = 90°
	b = 19.2935(17) Å	β = 90°
	c = 20.2998(15) Å	γ = 90°
Volume	6983.6(9) Å <sup>3</sup>	
Z	4	
Density (calculated)	1.173 Mg/m <sup>3</sup>	
Absorption coefficient	0.160 mm <sup>-1</sup>	
F(000)	2624	
Crystal size	0.49 x 0.37 x 0.35 mm <sup>3</sup>	
Theta range for data collection	3.04 to 25.16°.	
Index ranges	-21 ≤ h ≤ 20, -19 ≤ k ≤ 22, -24 ≤ l ≤ 20	
Reflections collected	10640	
Independent reflections	5381 [R(int) = 0.0354]	
Completeness to theta = 25.00°	99.7 %	
Absorption correction	Semi-empirical from equivalents	
Max. and min. transmission	0.9460 and 0.9256	
Refinement method	Full-matrix least-squares on F <sup>2</sup>	
Data / restraints / parameters	5381 / 1 / 379	
Goodness-of-fit on F <sup>2</sup>	1.028	
Final R indices [I > 2σ(I)]	R1 = 0.0458, wR2 = 0.1151	
R indices (all data)	R1 = 0.0513, wR2 = 0.1186	
Absolute structure parameter	0.05(13)	
Largest diff. peak and hole	0.373 and -0.366 e.Å <sup>-3</sup>	

Crystal data and structure refinement for **(6)<sub>6</sub>(THF)<sub>2</sub>(Ph<sub>2</sub>MeSiONa)<sub>6</sub>(THF)<sub>2</sub> (4.3.3.2)**

Empirical formula	C <sub>100</sub> H <sub>110</sub> Na <sub>6</sub> O <sub>8</sub> Si <sub>6</sub>	
Formula weight	1746.36	
Temperature	173(2) K	
Wavelength	0.71073 Å	
Crystal system	Triclinic	
Space group	<i>P</i> -1	
Unit cell dimensions	a = 13.0974(10) Å	α = 86.573(6)°
	b = 13.1518(9) Å	β = 78.550(6)°
	c = 14.7573(12) Å	γ = 77.605(6)°
Volume	2433.0(3) Å <sup>3</sup>	
Z	1	
Density (calculated)	1.192 Mg/m <sup>3</sup>	
Absorption coefficient	0.166 mm <sup>-1</sup>	
F(000)	924	
Crystal size	0.47 x 0.44 x 0.40 mm <sup>3</sup>	
Theta range for data collection	3.69 to 25.80°.	
Index ranges	-16 ≤ h ≤ 16, -15 ≤ k ≤ 16, -18 ≤ l ≤ 16	
Reflections collected	18579	
Independent reflections	9237 [R(int) = 0.0269]	
Completeness to theta = 25.00°	99.1 %	
Absorption correction	Semi-empirical from equivalents	
Max. and min. transmission	0.9366 and 0.9261	
Refinement method	Full-matrix least-squares on F <sup>2</sup>	
Data / restraints / parameters	9237 / 42 / 541	
Goodness-of-fit on F <sup>2</sup>	1.019	
Final R indices [I > 2σ(I)]	R1 = 0.0479, wR2 = 0.1187	
R indices (all data)	R1 = 0.0553, wR2 = 0.1232	
Largest diff. peak and hole	0.906 and -0.745 e.Å <sup>-3</sup>	

Crystal data and structure refinement for **(6)<sub>6</sub>[CpFe(CO)<sub>2</sub>]<sub>2</sub>**  
**(Ph<sub>2</sub>MeSiONa)<sub>6</sub>[CpFe(CO)<sub>2</sub>]<sub>2</sub> (4.3.3.3)**

Empirical formula	C <sub>92</sub> H <sub>88</sub> Fe <sub>2</sub> Na <sub>6</sub> O <sub>10</sub> Si <sub>6</sub>	
Formula weight	1771.80	
Temperature	173(2) K	
Wavelength	0.71073 Å	
Crystal system	Triclinic	
Space group	<i>P</i> -1	
Unit cell dimensions	a = 13.7166(11) Å	α = 66.601(6)°
	b = 13.7667(11) Å	β = 63.288(6)°
	c = 14.4555(12) Å	γ = 78.556(7)°
Volume	2237.2(3) Å <sup>3</sup>	
Z	1	
Density (calculated)	1.315 Mg/m <sup>3</sup>	
Absorption coefficient	0.491 mm <sup>-1</sup>	
F(000)	922	
Crystal size	0.23 x 0.16 x 0.12 mm <sup>3</sup>	
Theta range for data collection	3.59 to 25.87°.	
Index ranges	-16 ≤ h ≤ 16, -16 ≤ k ≤ 16, -17 ≤ l ≤ 17	
Reflections collected	38468	
Independent reflections	8585 [R(int) = 0.1276]	
Completeness to theta = 25.00°	99.7 %	
Absorption correction	Semi-empirical from equivalents	
Max. and min. transmission	0.9435 and 0.8955	
Refinement method	Full-matrix least-squares on F <sup>2</sup>	
Data / restraints / parameters	8585 / 0 / 561	
Goodness-of-fit on F <sup>2</sup>	1.032	
Final R indices [I > 2σ(I)]	R1 = 0.0693, wR2 = 0.1663	
R indices (all data)	R1 = 0.0922, wR2 = 0.1805	
Extinction coefficient	0.013(2)	
Largest diff. peak and hole	0.715 and -0.616 e.Å <sup>-3</sup>	

Crystal data and structure refinement for 7(THF) *t*Bu<sub>2</sub>PhSiSNa(THF) (4.3.4.1)

Empirical formula	C <sub>72</sub> H <sub>124</sub> Na <sub>4</sub> O <sub>4</sub> S <sub>4</sub> Si <sub>4</sub>	
Formula weight	1386.27	
Temperature	173(2) K	
Wavelength	0.71073 Å	
Crystal system	Monoclinic	
Space group	<i>P</i> 2 <sub>1</sub> / <i>c</i>	
Unit cell dimensions	<i>a</i> = 21.3211(14) Å	$\alpha = 90^\circ$
	<i>b</i> = 14.6608(9) Å	$\beta = 90.022(5)^\circ$
	<i>c</i> = 29.3513(18) Å	$\gamma = 90^\circ$
Volume	9174.8(10) Å <sup>3</sup>	
<i>Z</i>	4	
Density (calculated)	1.004 Mg/m <sup>3</sup>	
Absorption coefficient	0.212 mm <sup>-1</sup>	
F(000)	3008	
Crystal size	0.52 x 0.46 x 0.33 mm <sup>3</sup>	
Theta range for data collection	2.18 to 25.40°.	
Index ranges	-25 ≤ <i>h</i> ≤ 25, -17 ≤ <i>k</i> ≤ 17, -35 ≤ <i>l</i> ≤ 35	
Reflections collected	49292	
Independent reflections	16315 [R(int) = 0.1028]	
Completeness to theta = 25.00°	97.6 %	
Absorption correction	Semi-empirical from equivalents	
Max. and min. transmission	0.9333 and 0.8977	
Refinement method	Full-matrix least-squares on F <sup>2</sup>	
Data / restraints / parameters	16315 / 0 / 867	
Goodness-of-fit on F <sup>2</sup>	0.953	
Final R indices [I > 2σ(I)]	R1 = 0.0828, wR2 = 0.2030	
R indices (all data)	R1 = 0.1164, wR2 = 0.2209	
Largest diff. peak and hole	0.683 and -0.521 e.Å <sup>-3</sup>	

Crystal data and structure refinement for **10**(THF)<sub>2</sub> *t*Bu<sub>3</sub>SiSNa(THF)<sub>2</sub> (**4.3.4.2**)

Empirical formula	C <sub>40</sub> H <sub>86</sub> Na <sub>2</sub> O <sub>4</sub> S <sub>2</sub> Si <sub>2</sub>	
Formula weight	797.37	
Temperature	173(2) K	
Wavelength	0.71073 Å	
Crystal system	Monoclinic	
Space group	<i>P</i> 2 <sub>1</sub> / <i>c</i>	
Unit cell dimensions	<i>a</i> = 18.9536(18) Å	$\alpha = 90^\circ$
	<i>b</i> = 15.6396(10) Å	$\beta = 118.517(7)^\circ$
	<i>c</i> = 18.9675(19) Å	$\gamma = 90^\circ$
Volume	4940.3(8) Å <sup>3</sup>	
<i>Z</i>	4	
Density (calculated)	1.072 Mg/m <sup>3</sup>	
Absorption coefficient	0.207 mm <sup>-1</sup>	
<i>F</i> (000)	1760	
Crystal size	0.52 x 0.48 x 0.47 mm <sup>3</sup>	
Theta range for data collection	3.47 to 25.73°.	
Index ranges	-23 ≤ <i>h</i> ≤ 21, -17 ≤ <i>k</i> ≤ 18, -22 ≤ <i>l</i> ≤ 23	
Reflections collected	33368	
Independent reflections	9409 [R(int) = 0.1505]	
Completeness to theta = 25.00°	99.6 %	
Absorption correction	Semi-empirical from equivalents	
Max. and min. transmission	0.9089 and 0.8999	
Refinement method	Full-matrix least-squares on <i>F</i> <sup>2</sup>	
Data / restraints / parameters	9409 / 6 / 452	
Goodness-of-fit on <i>F</i> <sup>2</sup>	1.026	
Final <i>R</i> indices [ <i>I</i> > 2σ( <i>I</i> )]	<i>R</i> 1 = 0.0772, <i>wR</i> 2 = 0.2117	
<i>R</i> indices (all data)	<i>R</i> 1 = 0.1242, <i>wR</i> 2 = 0.2512	
Largest diff. peak and hole	0.786 and -0.542 e.Å <sup>-3</sup>	

Crystal data and structure refinement for **10**(THF) *t*Bu<sub>3</sub>SiSNa(THF) (4.3.4.2)

Empirical formula	C <sub>64</sub> H <sub>140</sub> Na <sub>4</sub> O <sub>4</sub> S <sub>4</sub> Si <sub>4</sub>	
Formula weight	1306.32	
Temperature	173(2) K	
Wavelength	0.71073 Å	
Crystal system	Monoclinic	
Space group	P2 <sub>1</sub>	
Unit cell dimensions	a = 13.3756(6) Å	α = 90°
	b = 15.3886(4) Å	β = 90.623(3)°
	c = 19.9654(8) Å	γ = 90°
Volume	4109.3(3) Å <sup>3</sup>	
Z	2	
Density (calculated)	1.056 Mg/m <sup>3</sup>	
Absorption coefficient	0.233 mm <sup>-1</sup>	
F(000)	1440	
Crystal size	0.24 x 0.22 x 0.21 mm <sup>3</sup>	
Theta range for data collection	2.25 to 25.49°.	
Index ranges	-16 ≤ h ≤ 16, -18 ≤ k ≤ 18, -24 ≤ l ≤ 24	
Reflections collected	81742	
Independent reflections	15095 [R(int) = 0.0727]	
Completeness to theta = 25.00°	99.9 %	
Absorption correction	Semi-empirical from equivalents	
Max. and min. transmission	0.9527 and 0.9462	
Refinement method	Full-matrix least-squares on F <sup>2</sup>	
Data / restraints / parameters	15095 / 1 / 718	
Goodness-of-fit on F <sup>2</sup>	1.051	
Final R indices [I > 2σ(I)]	R1 = 0.0640, wR2 = 0.1636	
R indices (all data)	R1 = 0.0727, wR2 = 0.1755	
Absolute structure parameter	-0.03(12)	
Largest diff. peak and hole	0.468 and -0.401 e.Å <sup>-3</sup>	

Crystal data and structure refinement for **8**(THF)<sub>2</sub> *t*Bu<sub>2</sub>PhSiSeNa(THF)<sub>2</sub> (**4.3.5.1**)

Empirical formula	C <sub>44</sub> H <sub>78</sub> Na <sub>2</sub> O <sub>4</sub> Se <sub>2</sub> Si <sub>2</sub>	
Formula weight	931.14	
Temperature	173(2) K	
Wavelength	0.71073 Å	
Crystal system	Monoclinic	
Space group	<i>P</i> 2 <sub>1</sub> / <i>n</i>	
Unit cell dimensions	<i>a</i> = 10.1564(17) Å	$\alpha = 90^\circ$
	<i>b</i> = 14.708(2) Å	$\beta = 98.172(12)^\circ$
	<i>c</i> = 17.355(2) Å	$\gamma = 90^\circ$
Volume	2566.2(6) Å <sup>3</sup>	
<i>Z</i>	2	
Density (calculated)	1.205 Mg/m <sup>3</sup>	
Absorption coefficient	1.540 m <sup>-1</sup>	
<i>F</i> (000)	984	
Crystal size	0.42 x 0.38 x 0.35 mm <sup>3</sup>	
Theta range for data collection	2.20 to 25.02°.	
Index ranges	-12 ≤ <i>h</i> ≤ 12, -17 ≤ <i>k</i> ≤ 17, -20 ≤ <i>l</i> ≤ 20	
Reflections collected	24241	
Independent reflections	4531 [R(int) = 0.1540]	
Completeness to theta = 25.00°	100.0 %	
Absorption correction	Semi-empirical from equivalents	
Max. and min. transmission	0.6148 and 0.5640	
Refinement method	Full-matrix least-squares on <i>F</i> <sup>2</sup>	
Data / restraints / parameters	4531 / 0 / 244	
Goodness-of-fit on <i>F</i> <sup>2</sup>	1.196	
Final <i>R</i> indices [ <i>I</i> > 2σ( <i>I</i> )]	<i>R</i> 1 = 0.1691, <i>wR</i> 2 = 0.3697	
<i>R</i> indices (all data)	<i>R</i> 1 = 0.1812, <i>wR</i> 2 = 0.3771	
Largest diff. peak and hole	3.330 and -1.908 e.Å <sup>-3</sup>	

Crystal data and structure refinement for **11**(THF)<sub>2</sub> *t*Bu<sub>3</sub>SiSeNa(THF)<sub>2</sub> (**4.3.5.3**)

Empirical formula	C <sub>40</sub> H <sub>86</sub> Na <sub>2</sub> O <sub>4</sub> Se <sub>2</sub> Si <sub>2</sub>	
Formula weight	891.17	
Temperature	173(2) K	
Wavelength	0.71073 Å	
Crystal system	Monoclinic	
Space group	<i>P</i> 2 <sub>1</sub> / <i>n</i>	
Unit cell dimensions	<i>a</i> = 8.9662(8) Å	$\alpha = 90^\circ$
	<i>b</i> = 15.6100(9) Å	$\beta = 90.224(7)^\circ$
	<i>c</i> = 17.4525(15) Å	$\gamma = 90^\circ$
Volume	2442.7(3) Å <sup>3</sup>	
<i>Z</i>	2	
Density (calculated)	1.212 Mg/m <sup>3</sup>	
Absorption coefficient	1.614 mm <sup>-1</sup>	
<i>F</i> (000)	952	
Crystal size	0.34 x 0.28 x 0.22 mm <sup>3</sup>	
Theta range for data collection	3.66 to 25.76°.	
Index ranges	-10 ≤ <i>h</i> ≤ 10, -19 ≤ <i>k</i> ≤ 18, -21 ≤ <i>l</i> ≤ 21	
Reflections collected	25568	
Independent reflections	4610 [R(int) = 0.0600]	
Completeness to theta = 25.00°	99.7 %	
Absorption correction	Semi-empirical from equivalents	
Max. and min. transmission	0.7178 and 0.6098	
Refinement method	Full-matrix least-squares on <i>F</i> <sup>2</sup>	
Data / restraints / parameters	4610 / 0 / 226	
Goodness-of-fit on <i>F</i> <sup>2</sup>	0.942	
Final <i>R</i> indices [ <i>I</i> > 2σ( <i>I</i> )]	<i>R</i> 1 = 0.0289, <i>wR</i> 2 = 0.0574	
<i>R</i> indices (all data)	<i>R</i> 1 = 0.0453, <i>wR</i> 2 = 0.0610	
Largest diff. peak and hole	0.442 and -0.271 e.Å <sup>-3</sup>	



Crystal data and structure refinement for **12**(THF)<sub>2</sub> *t*Bu<sub>3</sub>SiTeNa(THF)<sub>2</sub> (**4.3.5.4**)

Empirical formula	C <sub>40</sub> H <sub>86</sub> Na <sub>2</sub> O <sub>4</sub> Si <sub>2</sub> Te <sub>2</sub>	
Formula weight	988.45	
Temperature	173(2) K	
Wavelength	0.71073 Å	
Crystal system	Monoclinic	
Space group	<i>P</i> 2 <sub>1</sub> / <i>n</i>	
Unit cell dimensions	<i>a</i> = 9.0926(6) Å	$\alpha = 90^\circ$
	<i>b</i> = 16.5792(13) Å	$\beta = 90.693(5)^\circ$
	<i>c</i> = 17.0318(11) Å	$\gamma = 90^\circ$
Volume	2567.3(3) Å <sup>3</sup>	
<i>Z</i>	2	
Density (calculated)	1.279 Mg/m <sup>3</sup>	
Absorption coefficient	1.232 mm <sup>-1</sup>	
F(000)	1024	
Crystal size	0.36 x 0.26 x 0.20 mm <sup>3</sup>	
Theta range for data collection	3.79 to 26.02°.	
Index ranges	-11 ≤ <i>h</i> ≤ 11, -20 ≤ <i>k</i> ≤ 20, -20 ≤ <i>l</i> ≤ 20	
Reflections collected	28074	
Independent reflections	5006 [R(int) = 0.0413]	
Completeness to theta = 25.00°	99.6 %	
Absorption correction	Semi-empirical from equivalents	
Max. and min. transmission	0.7907 and 0.6654	
Refinement method	Full-matrix least-squares on F <sup>2</sup>	
Data / restraints / parameters	5006 / 0 / 226	
Goodness-of-fit on F <sup>2</sup>	0.907	
Final R indices [I > 2σ(I)]	R1 = 0.0263, wR2 = 0.0606	
R indices (all data)	R1 = 0.0405, wR2 = 0.0634	
Largest diff. peak and hole	0.729 and -0.594 e.Å <sup>-3</sup>	

Crystal data and structure refinement for **20** *t*Bu<sub>2</sub>PhSiS-SSiPh*t*Bu<sub>2</sub> (4.4.1.1)

Empirical formula	C <sub>28</sub> H <sub>46</sub> S <sub>2</sub> Si <sub>2</sub>	
Formula weight	502.95	
Temperature	173(2) K	
Wavelength	0.71073 Å	
Crystal system	Monoclinic	
Space group	<i>P</i> 2 <sub>1</sub> / <i>n</i>	
Unit cell dimensions	<i>a</i> = 8.7385(9) Å	$\alpha = 90^\circ$
	<i>b</i> = 14.8594(18) Å	$\beta = 108.113(8)^\circ$
	<i>c</i> = 11.8876(12) Å	$\gamma = 90^\circ$
Volume	1467.1(3) Å <sup>3</sup>	
<i>Z</i>	2	
Density (calculated)	1.139 Mg/m <sup>3</sup>	
Absorption coefficient	0.277 mm <sup>-1</sup>	
F(000)	548	
Crystal size	0.19 x 0.15 x 0.09 mm <sup>3</sup>	
Theta range for data collection	3.47 to 26.08°.	
Index ranges	-10 ≤ <i>h</i> ≤ 10, -18 ≤ <i>k</i> ≤ 18, -14 ≤ <i>l</i> ≤ 14	
Reflections collected	13328	
Independent reflections	2879 [R(int) = 0.0681]	
Completeness to theta = 25.00°	99.7 %	
Absorption correction	Semi-empirical from equivalents	
Max. and min. transmission	0.9755 and 0.9492	
Refinement method	Full-matrix least-squares on F <sup>2</sup>	
Data / restraints / parameters	2879 / 0 / 145	
Goodness-of-fit on F <sup>2</sup>	0.894	
Final R indices [I > 2σ(I)]	R1 = 0.0327, wR2 = 0.0719	
R indices (all data)	R1 = 0.0511, wR2 = 0.0758	
Largest diff. peak and hole	0.411 and -0.171 e.Å <sup>-3</sup>	

Crystal data and structure refinement for **21** *t*Bu<sub>2</sub>PhSiSe-SeSiPh*t*Bu<sub>2</sub> (**4.4.1.2**)

Empirical formula	C <sub>28</sub> H <sub>46</sub> Se <sub>2</sub> Si <sub>2</sub>	
Formula weight	596.75	
Temperature	173(2) K	
Wavelength	0.71073 Å	
Crystal system	Monoclinic	
Space group	<i>P</i> 2 <sub>1</sub> / <i>c</i>	
Unit cell dimensions	<i>a</i> = 8.2842(7) Å	$\alpha = 90^\circ$
	<i>b</i> = 14.9971(11) Å	$\beta = 105.242(7)^\circ$
	<i>c</i> = 12.4940(11) Å	$\gamma = 90^\circ$
Volume	1497.6(2) Å <sup>3</sup>	
<i>Z</i>	2	
Density (calculated)	1.323 Mg/m <sup>3</sup>	
Absorption coefficient	2.563 mm <sup>-1</sup>	
F(000)	620	
Crystal size	0.32 x 0.24 x 0.16 mm <sup>3</sup>	
Theta range for data collection	3.64 to 26.55°.	
Index ranges	-10 ≤ <i>h</i> ≤ 10, -18 ≤ <i>k</i> ≤ 18, -15 ≤ <i>l</i> ≤ 15	
Reflections collected	22434	
Independent reflections	3083 [R(int) = 0.0704]	
Completeness to theta = 26.55°	98.6 %	
Absorption correction	Semi-empirical from equivalents	
Max. and min. transmission	0.6846 and 0.4943	
Refinement method	Full-matrix least-squares on F <sup>2</sup>	
Data / restraints / parameters	3083 / 0 / 145	
Goodness-of-fit on F <sup>2</sup>	1.047	
Final R indices [I > 2σ(I)]	R1 = 0.0301, wR2 = 0.0678	
R indices (all data)	R1 = 0.0402, wR2 = 0.0708	
Largest diff. peak and hole	0.465 and -0.526 e.Å <sup>-3</sup>	

Crystal data and structure refinement for **22** *t*Bu<sub>2</sub>PhSiTe-TeSiPh*t*Bu<sub>2</sub> (4.4.1.3)

Empirical formula	C <sub>28</sub> H <sub>46</sub> Si <sub>2</sub> Te <sub>2</sub>	
Formula weight	694.03	
Temperature	173(2) K	
Wavelength	0.71073 Å	
Crystal system	Monoclinic	
Space group	<i>P</i> 2 <sub>1</sub> / <i>c</i>	
Unit cell dimensions	<i>a</i> = 8.2602(7) Å	$\alpha = 90^\circ$
	<i>b</i> = 15.4176(9) Å	$\beta = 106.888(7)^\circ$
	<i>c</i> = 12.8106(10) Å	$\gamma = 90^\circ$
Volume	1561.1(2) Å <sup>3</sup>	
<i>Z</i>	2	
Density (calculated)	1.476 Mg/m <sup>3</sup>	
Absorption coefficient	1.959 mm <sup>-1</sup>	
<i>F</i> (000)	692	
Crystal size	0.39 x 0.32 x 0.26 mm <sup>3</sup>	
Theta range for data collection	3.69 to 29.78°.	
Index ranges	-11 ≤ <i>h</i> ≤ 11, -21 ≤ <i>k</i> ≤ 21, -17 ≤ <i>l</i> ≤ 17	
Reflections collected	23713	
Independent reflections	4415 [R(int) = 0.0307]	
Completeness to theta = 29.78°	98.8 %	
Absorption correction	Semi-empirical from equivalents	
Max. and min. transmission	0.6299 and 0.5154	
Refinement method	Full-matrix least-squares on <i>F</i> <sup>2</sup>	
Data / restraints / parameters	4415 / 0 / 145	
Goodness-of-fit on <i>F</i> <sup>2</sup>	1.054	
Final R indices [ <i>I</i> > 2σ( <i>I</i> )]	R1 = 0.0387, wR2 = 0.1030	
R indices (all data)	R1 = 0.0457, wR2 = 0.1062	
Largest diff. peak and hole	3.008 and -1.655 e.Å <sup>-3</sup>	

Crystal data and structure refinement for **23** *t*Bu<sub>3</sub>SiS-SSi*t*Bu<sub>3</sub> (**4.4.1.4**)

Empirical formula	C <sub>24</sub> H <sub>54</sub> S <sub>2</sub> Si <sub>2</sub>	
Formula weight	462.97	
Temperature	173(2) K	
Wavelength	0.71073 Å	
Crystal system	Monoclinic	
Space group	<i>P</i> 2 <sub>1</sub> / <i>n</i>	
Unit cell dimensions	<i>a</i> = 8.6760(12) Å	$\alpha = 90^\circ$
	<i>b</i> = 13.9235(16) Å	$\beta = 90.171(10)^\circ$
	<i>c</i> = 12.3224(15) Å	$\gamma = 90^\circ$
Volume	1488.5(3) Å <sup>3</sup>	
<i>Z</i>	2	
Density (calculated)	1.033 Mg/m <sup>3</sup>	
Absorption coefficient	0.268 mm <sup>-1</sup>	
<i>F</i> (000)	516	
Crystal size	0.37 x 0.13 x 0.12 mm <sup>3</sup>	
Theta range for data collection	3.62 to 25.64°.	
Index ranges	-10 ≤ <i>h</i> ≤ 9, -16 ≤ <i>k</i> ≤ 12, -14 ≤ <i>l</i> ≤ 14	
Reflections collected	7069	
Independent reflections	2767 [R(int) = 0.0485]	
Completeness to theta = 25.00°	99.4 %	
Absorption correction	Semi-empirical from equivalents	
Max. and min. transmission	0.9686 and 0.9074	
Refinement method	Full-matrix least-squares on <i>F</i> <sup>2</sup>	
Data / restraints / parameters	2767 / 0 / 128	
Goodness-of-fit on <i>F</i> <sup>2</sup>	1.041	
Final <i>R</i> indices [ <i>I</i> > 2σ( <i>I</i> )]	<i>R</i> 1 = 0.0365, <i>wR</i> 2 = 0.0945	
<i>R</i> indices (all data)	<i>R</i> 1 = 0.0394, <i>wR</i> 2 = 0.0959	
Largest diff. peak and hole	0.327 and -0.372 e.Å <sup>-3</sup>	

Crystal data and structure refinement for **24** *t*Bu<sub>3</sub>SiSe-SeSi*t*Bu<sub>3</sub> (**4.4.1.5**)

Empirical formula	C <sub>24</sub> H <sub>54</sub> Se <sub>2</sub> Si <sub>2</sub>	
Formula weight	556.77	
Temperature	173(2) K	
Wavelength	0.71073 Å	
Crystal system	Trigonal	
Space group	<i>R</i> -3	
Unit cell dimensions	a = 20.188(2) Å	α = 90°
	b = 20.188(2) Å	β = 90°
	c = 25.220(3) Å	γ = 120°
Volume	8901.5(16) Å <sup>3</sup>	
Z	12	
Density (calculated)	1.246 Mg/m <sup>3</sup>	
Absorption coefficient	2.582 mm <sup>-1</sup>	
F(000)	3528	
Crystal size	0.36 x 0.32 x 0.28 mm <sup>3</sup>	
Theta range for data collection	3.98 to 25.27°.	
Index ranges	-23 ≤ h ≤ 24, -24 ≤ k ≤ 23, -30 ≤ l ≤ 22	
Reflections collected	12998	
Independent reflections	3537 [R(int) = 0.1398]	
Completeness to theta = 25.00°	99.3 %	
Absorption correction	Semi-empirical from equivalents	
Max. and min. transmission	0.5318 and 0.4567	
Refinement method	Full-matrix least-squares on F <sup>2</sup>	
Data / restraints / parameters	3537 / 0 / 185	
Goodness-of-fit on F <sup>2</sup>	1.091	
Final R indices [I > 2σ(I)]	R1 = 0.1596, wR2 = 0.3927	
R indices (all data)	R1 = 0.1976, wR2 = 0.4161	
Largest diff. peak and hole	1.587 and -0.747 e.Å <sup>-3</sup>	

Crystal data and structure refinement for **25** *t*Bu<sub>3</sub>SiTe-TeSi*t*Bu<sub>3</sub> (**4.4.1.6**)

Empirical formula	C <sub>24</sub> H <sub>54</sub> Si <sub>2</sub> Te <sub>2</sub>	
Formula weight	654.05	
Temperature	173(2) K	
Wavelength	0.71073 Å	
Crystal system	Orthorhombic	
Space group	<i>Pbca</i>	
Unit cell dimensions	a = 14.6569(16) Å	α = 90°
	b = 13.5911(17) Å	β = 90°
	c = 15.1033(16) Å	γ = 90°
Volume	3008.6(6) Å <sup>3</sup>	
Z	4	
Density (calculated)	1.444 Mg/m <sup>3</sup>	
Absorption coefficient	2.027 mm <sup>-3</sup>	
F(000)	1320	
Crystal size	0.13 x 0.13 x 0.13 mm <sup>3</sup>	
Theta range for data collection	3.87 to 25.13°.	
Index ranges	-17 ≤ h ≤ 16, -16 ≤ k ≤ 16, -17 ≤ l ≤ 17	
Reflections collected	15595	
Independent reflections	2657 [R(int) = 0.0812]	
Completeness to theta = 25.00°	99.5 %	
Absorption correction	Semi-empirical from equivalents	
Max. and min. transmission	0.7785 and 0.7785	
Refinement method	Full-matrix least-squares on F <sup>2</sup>	
Data / restraints / parameters	2657 / 0 / 127	
Goodness-of-fit on F <sup>2</sup>	0.877	
Final R indices [I > 2σ(I)]	R1 = 0.0366, wR2 = 0.0616	
R indices (all data)	R1 = 0.0683, wR2 = 0.0671	
Largest diff. peak and hole	0.399 and -0.466 e.Å <sup>-3</sup>	

Crystal data and structure refinement for **29** *t*Bu<sub>3</sub>SiS-S<sub>2</sub>-SSi*t*Bu<sub>3</sub> (**4.5.3**)

Empirical formula	C <sub>24</sub> H <sub>54</sub> S <sub>4</sub> Si <sub>2</sub>	
Formula weight	527.09	
Temperature	173(2) K	
Wavelength	0.71073 Å	
Crystal system	Monoclinic	
Space group	<i>P</i> 2 <sub>1</sub> / <i>c</i>	
Unit cell dimensions	<i>a</i> = 14.4591(9) Å	$\alpha = 90^\circ$
	<i>b</i> = 14.4382(9) Å	$\beta = 94.506(6)^\circ$
	<i>c</i> = 15.1523(12) Å	$\gamma = 90^\circ$
Volume	3153.5(4) Å <sup>3</sup>	
<i>Z</i>	4	
Density (calculated)	1.110 Mg/m <sup>3</sup>	
Absorption coefficient	0.388 mm <sup>-1</sup>	
F(000)	1160	
Crystal size	0.33 x 0.18 x 0.12 mm <sup>3</sup>	
Theta range for data collection	3.52 to 25.75°	
Index ranges	-17 ≤ <i>h</i> ≤ 17, -17 ≤ <i>k</i> ≤ 17, -18 ≤ <i>l</i> ≤ 18	
Reflections collected	38940	
Independent reflections	5931 [R(int) = 0.0736]	
Completeness to theta = 25.00°	99.7 %	
Absorption correction	Semi-empirical from equivalents	
Max. and min. transmission	0.9549 and 0.8827	
Refinement method	Full-matrix least-squares on F <sup>2</sup>	
Data / restraints / parameters	5931 / 0 / 272	
Goodness-of-fit on F <sup>2</sup>	1.023	
Final R indices [I > 2σ(I)]	R1 = 0.0485, wR2 = 0.1054	
R indices (all data)	R1 = 0.0685, wR2 = 0.1131	
Extinction coefficient	0.0075(10)	
Largest diff. peak and hole	0.517 and -0.328 e.Å <sup>-3</sup>	



Crystal data and structure refinement for **31** CpFe(CO)<sub>2</sub>SiPh<sub>2</sub>Me (**4.6.1**)

Empirical formula	C <sub>20</sub> H <sub>18</sub> FeO <sub>2</sub> Si	
Formula weight	374.28	
Temperature	173(2) K	
Wavelength	0.71073 Å	
Crystal system	Orthorhombic	
Space group	P2 <sub>1</sub> 2 <sub>1</sub> 2 <sub>1</sub>	
Unit cell dimensions	a = 7.2717(6) Å	α = 90°
	b = 15.5320(12) Å	β = 90°
	c = 16.0550(13) Å	γ = 90°
Volume	1813.3(3) Å <sup>3</sup>	
Z	4	
Density (calculated)	1.371 Mg/m <sup>3</sup>	
Absorption coefficient	0.906 mm <sup>-1</sup>	
F(000)	776	
Crystal size	0.32 x 0.26 x 0.11 mm <sup>3</sup>	
Theta range for data collection	3.65 to 25.55°	
Index ranges	-8 ≤ h ≤ 8, -16 ≤ k ≤ 18, -19 ≤ l ≤ 19	
Reflections collected	9046	
Independent reflections	3321 [R(int) = 0.0292]	
Completeness to theta = 25.00°	99.5 %	
Absorption correction	Semi-empirical from equivalents	
Max. and min. transmission	0.9069 and 0.7604	
Refinement method	Full-matrix least-squares on F <sup>2</sup>	
Data / restraints / parameters	3321 / 0 / 218	
Goodness-of-fit on F <sup>2</sup>	1.005	
Final R indices [I > 2σ(I)]	R1 = 0.0223, wR2 = 0.0512	
R indices (all data)	R1 = 0.0259, wR2 = 0.0522	
Absolute structure parameter	0.005(12)	
Extinction coefficient	0.0103(9)	
Largest diff. peak and hole	0.187 and -0.195 e.Å <sup>-3</sup>	

Crystal data and structure refinement for **34** CpFe(CO)<sub>2</sub>SSi*t*Bu<sub>3</sub> (**4.6.2**)

Empirical formula	C <sub>19</sub> H <sub>32</sub> FeO <sub>2</sub> SSi	
Formula weight	408.45	
Temperature	173(2) K	
Wavelength	0.71073 Å	
Crystal system	Triclinic	
Space group	<i>P</i> -1	
Unit cell dimensions	a = 8.6706(12) Å	α = 86.248(12)°
	b = 8.7067(13) Å	β = 88.782(12)°
	c = 16.215(2) Å	γ = 62.460(11)°
Volume	1083.0(3) Å <sup>3</sup>	
Z	2	
Density (calculated)	1.252 Mg/m <sup>3</sup>	
Absorption coefficient	0.856 mm <sup>-1</sup>	
F(000)	436	
Crystal size	0.18 x 0.15 x 0.08 mm <sup>3</sup>	
Theta range for data collection	3.63 to 25.64°.	
Index ranges	-10 ≤ h ≤ 10, -10 ≤ k ≤ 10, -19 ≤ l ≤ 17	
Reflections collected	10454	
Independent reflections	3997 [R(int) = 0.0996]	
Completeness to theta = 25.00°	98.4 %	
Absorption correction	Semi-empirical from equivalents	
Max. and min. transmission	0.9347 and 0.8612	
Refinement method	Full-matrix least-squares on F <sup>2</sup>	
Data / restraints / parameters	3997 / 60 / 213	
Goodness-of-fit on F <sup>2</sup>	0.952	
Final R indices [I > 2σ(I)]	R1 = 0.0699, wR2 = 0.1704	
R indices (all data)	R1 = 0.0986, wR2 = 0.1888	
Largest diff. peak and hole	0.530 and -0.744 e.Å <sup>-3</sup>	

Crystal data and structure refinement for  $(\mathbf{6})_4\{[\text{CpFe}(\text{CO})_2]_2\}_2$   
 $(\text{Ph}_2\text{MeSiONa})_4\{[\text{CpFe}(\text{CO})_2]_2\}_2$  (**4.6.6**)

Empirical formula	$\text{C}_{92}\text{H}_{84}\text{Fe}_4\text{Na}_4\text{O}_{12}\text{Si}_4$
Formula weight	1809.31
Temperature	173(2) K
Wavelength	0.71073 Å
Crystal system	Tetragonal
Space group	$I4_1/acd$
Unit cell dimensions	$a = 22.2061(14)$ Å $\alpha = 90^\circ$ . $b = 22.2061(14)$ Å $\beta = 90^\circ$ . $c = 36.082(3)$ Å $\gamma = 90^\circ$ .
Volume	$17792(2)$ Å <sup>3</sup>
Z	8
Density (calculated)	1.351 Mg/m <sup>3</sup>
Absorption coefficient	$0.772$ mm <sup>-1</sup>
F(000)	7488
Crystal size	$0.14 \times 0.12 \times 0.07$ mm <sup>3</sup>
Theta range for data collection	$1.83$ to $25.10^\circ$ .
Index ranges	$-26 \leq h \leq 26$ , $-23 \leq k \leq 26$ , $-42 \leq l \leq 41$
Reflections collected	55319
Independent reflections	3950 [R(int) = 0.1304]
Completeness to theta = $25.00^\circ$	99.9 %
Absorption correction	Semi-empirical from equivalents
Max. and min. transmission	0.9480 and 0.8996
Refinement method	Full-matrix least-squares on F <sup>2</sup>
Data / restraints / parameters	3950 / 14 / 263
Goodness-of-fit on F <sup>2</sup>	1.098
Final R indices [I > 2sigma(I)]	R1 = 0.0936, wR2 = 0.2008
R indices (all data)	R1 = 0.1395, wR2 = 0.2227
Largest diff. peak and hole	0.865 and -0.546 e.Å <sup>-3</sup>

Crystal data and structure refinement for **37** [Cu(SSiPh*t*Bu<sub>2</sub>)]<sub>4</sub> (**4.7.1**)

Empirical formula	C <sub>56</sub> H <sub>92</sub> Cu <sub>4</sub> S <sub>4</sub> Si <sub>4</sub>	
Formula weight	1260.06	
Temperature	173(2) K	
Wavelength	0.71073 Å	
Crystal system	Tetragonal	
Space group	<i>I</i> -4	
Unit cell dimensions	a = 20.106(2) Å	α = 90°
	b = 20.106(2) Å	β = 90°
	c = 7.7980(8) Å	γ = 90°
Volume	3152.4(5) Å <sup>3</sup>	
Z	2	
Density (calculated)	1.328 Mg/m <sup>3</sup>	
Absorption coefficient	1.573 mm <sup>-1</sup>	
F(000)	1328	
Crystal size	0.38 x 0.08 x 0.06 mm <sup>3</sup>	
Theta range for data collection	3.46 to 25.76°.	
Index ranges	-24 ≤ h ≤ 24, -24 ≤ k ≤ 23, -9 ≤ l ≤ 9	
Reflections collected	9708	
Independent reflections	2988 [R(int) = 0.0708]	
Completeness to theta = 25.00°	99.5 %	
Absorption correction	Semi-empirical from equivalents	
Max. and min. transmission	0.9115 and 0.5864	
Refinement method	Full-matrix least-squares on F <sup>2</sup>	
Data / restraints / parameters	2988 / 0 / 154	
Goodness-of-fit on F <sup>2</sup>	0.927	
Final R indices [I > 2σ(I)]	R1 = 0.0359, wR2 = 0.0696	
R indices (all data)	R1 = 0.0481, wR2 = 0.0726	
Absolute structure parameter	-0.010(18)	
Largest diff. peak and hole	0.499 and -0.264 e.Å <sup>-3</sup>	

Crystal data and structure refinement for **38** [ZnCl(SSi*t*Bu<sub>3</sub>)(THF)]<sub>2</sub> (**4.7.2**)

Empirical formula	C <sub>32</sub> H <sub>70</sub> Cl <sub>2</sub> O <sub>2</sub> S <sub>2</sub> Si <sub>2</sub> Zn <sub>2</sub>	
Formula weight	808.82	
Temperature	173(2) K	
Wavelength	0.71073 Å	
Crystal system	Monoclinic	
Space group	C2/c	
Unit cell dimensions	a = 44.727(3) Å	α = 90°
	b = 17.3710(9) Å	β = 101.404(5)°
	c = 21.8803(13) Å	γ = 90°
Volume	16664.3(17) Å <sup>3</sup>	
Z	16	
Density (calculated)	1.290 Mg/m <sup>3</sup>	
Absorption coefficient	1.463 mm <sup>-1</sup>	
F(000)	6912	
Crystal size	0.42 x 0.35 x 0.28 mm <sup>3</sup>	
Theta range for data collection	1.82 to 25.70°.	
Index ranges	-54 ≤ h ≤ 51, -21 ≤ k ≤ 21, -26 ≤ l ≤ 26	
Reflections collected	104097	
Independent reflections	15698 [R(int) = 0.1237]	
Completeness to theta = 25.00°	99.9 %	
Absorption correction	Semi-empirical from equivalents	
Max. and min. transmission	0.6848 and 0.5786	
Refinement method	Full-matrix least-squares on F <sup>2</sup>	
Data / restraints / parameters	15698 / 336 / 757	
Goodness-of-fit on F <sup>2</sup>	0.916	
Final R indices [I > 2σ(I)]	R1 = 0.0631, wR2 = 0.1664	
R indices (all data)	R1 = 0.1202, wR2 = 0.1897	
Largest diff. peak and hole	0.619 and -2.138 e.Å <sup>-3</sup>	

Crystal data and structure refinement for **39** (CO)<sub>4</sub>Mn( $\mu$ -SSi*t*Bu<sub>3</sub>)<sub>2</sub>Na(THF)<sub>2</sub> (**4.7.3**)

Empirical formula	C <sub>36</sub> H <sub>70</sub> MnNaO <sub>6</sub> S <sub>2</sub> Si <sub>2</sub>	
Formula weight	797.15	
Temperature	173(2) K	
Wavelength	0.71073 Å	
Crystal system	Monoclinic	
Space group	<i>P2</i> <sub>1</sub> / <i>c</i>	
Unit cell dimensions	a = 23.1442(11) Å	$\alpha = 90^\circ$
	b = 17.4691(6) Å	$\beta = 104.506(4)^\circ$
	c = 23.2056(12) Å	$\gamma = 90^\circ$
Volume	9083.1(7) Å <sup>3</sup>	
Z	8	
Density (calculated)	1.166 Mg/m <sup>3</sup>	
Absorption coefficient	0.482 mm <sup>-1</sup>	
F(000)	3440	
Crystal size	0.31 x 0.12 x 0.12 mm <sup>3</sup>	
Theta range for data collection	2.72 to 25.64°	
Index ranges	-28 ≤ h ≤ 28, -20 ≤ k ≤ 21, -27 ≤ l ≤ 28	
Reflections collected	78803	
Independent reflections	17283 [R(int) = 0.1118]	
Completeness to theta = 25.00°	99.9 %	
Absorption correction	Semi-empirical from equivalents	
Max. and min. transmission	0.9444 and 0.8649	
Refinement method	Full-matrix least-squares on F <sup>2</sup>	
Data / restraints / parameters	17283 / 0 / 867	
Goodness-of-fit on F <sup>2</sup>	0.957	
Final R indices [I > 2σ(I)]	R1 = 0.0566, wR2 = 0.1214	
R indices (all data)	R1 = 0.0884, wR2 = 0.1345	
Extinction coefficient	0.00149(15)	
Largest diff. peak and hole	0.579 and -0.375 e.Å <sup>-3</sup>	

Crystal data and structure refinement for **40**Na(THF)<sub>6</sub>[(CO)<sub>3</sub>Mn( $\mu$ -SSi*t*Bu<sub>3</sub>)<sub>3</sub>Mn(SSi*t*Bu<sub>3</sub>)]·(*t*Bu<sub>3</sub>Si)<sub>2</sub>S<sub>3</sub> (**4.7.3**)

Empirical formula	C <sub>99</sub> H <sub>210</sub> Mn <sub>2</sub> NaO <sub>9</sub> S <sub>7</sub> Si <sub>6</sub>	
Formula weight	2070.50	
Temperature	173(2) K	
Wavelength	0.71073 Å	
Crystal system	Trigonal	
Space group	<i>R</i> -3	
Unit cell dimensions	<i>a</i> = 14.6380(5) Å	$\alpha$ = 90°
	<i>b</i> = 14.6380(5) Å	$\beta$ = 90°
	<i>c</i> = 101.570(7) Å	$\gamma$ = 120°
Volume	18847.7(16) Å <sup>3</sup>	
<i>Z</i>	6	
Density (calculated)	1.095 Mg/m <sup>3</sup>	
Absorption coefficient	0.423 mm <sup>-1</sup>	
F(000)	6798	
Crystal size	0.27 x 0.25 x 0.14 mm <sup>3</sup>	
Theta range for data collection	2.13 to 25.01°	
Index ranges	-17 ≤ <i>h</i> ≤ 17, -17 ≤ <i>k</i> ≤ 17, -120 ≤ <i>l</i> ≤ 120	
Reflections collected	70191	
Independent reflections	7364 [R(int) = 0.1004]	
Completeness to theta = 25.00°	99.5 %	
Absorption correction	Semi-empirical from equivalents	
Max. and min. transmission	0.9431 and 0.8942	
Refinement method	Full-matrix least-squares on F <sup>2</sup>	
Data / restraints / parameters	7364 / 0 / 392	
Goodness-of-fit on F <sup>2</sup>	1.036	
Final R indices [I > 2σ(I)]	R1 = 0.1075, wR2 = 0.2847	
R indices (all data)	R1 = 0.1766, wR2 = 0.3175	
Largest diff. peak and hole	1.077 and -0.873 e.Å <sup>-3</sup>	

Crystal data and structure refinement for **41** (CO)<sub>4</sub>Mn( $\mu$ -SSitBu<sub>3</sub>)<sub>2</sub>Mn(SSitBu<sub>3</sub>)(THF) (**4.7.4**)

Empirical formula	C <sub>44</sub> H <sub>89</sub> Mn <sub>2</sub> O <sub>5</sub> S <sub>3</sub> Si <sub>3</sub>	
Formula weight	988.48	
Temperature	173(2) K	
Wavelength	0.71073 Å	
Crystal system	Monoclinic	
Space group	C2/c	
Unit cell dimensions	a = 24.9621(12) Å	$\alpha = 90^\circ$
	b = 13.3952(4) Å	$\beta = 109.554(4)^\circ$
	c = 34.7460(18) Å	$\gamma = 90^\circ$
Volume	10948.0(8) Å <sup>3</sup>	
Z	8	
Density (calculated)	1.199 Mg/m <sup>3</sup>	
Absorption coefficient	0.679 mm <sup>-1</sup>	
F(000)	4264	
Crystal size	0.33 x 0.30 x 0.27 mm <sup>3</sup>	
Theta range for data collection	2.31 to 26.25°.	
Index ranges	-30 ≤ h ≤ 30, -16 ≤ k ≤ 16, -42 ≤ l ≤ 42	
Reflections collected	88081	
Independent reflections	10102 [R(int) = 0.1224]	
Completeness to theta = 25.00°	99.7 %	
Absorption correction	Semi-empirical from equivalents	
Max. and min. transmission	0.8379 and 0.8070	
Refinement method	Full-matrix least-squares on F <sup>2</sup>	
Data / restraints / parameters	10102 / 126 / 508	
Goodness-of-fit on F <sup>2</sup>	1.199	
Final R indices [I > 2σ(I)]	R1 = 0.1296, wR2 = 0.2596	
R indices (all data)	R1 = 0.1388, wR2 = 0.2642	
Largest diff. peak and hole	1.139 and -1.065 e.Å <sup>-3</sup>	



Crystal data and structure refinement for **42** [Fe(SSi*t*Bu<sub>3</sub>)(CO)<sub>3</sub>]<sub>2</sub> (**4.7.6**)

Empirical formula	C <sub>30</sub> H <sub>54</sub> Fe <sub>2</sub> O <sub>6</sub> S <sub>2</sub> Si <sub>2</sub>	
Formula weight	742.73	
Temperature	173(2) K	
Wavelength	0.71073 Å	
Crystal system	Monoclinic	
Space group	<i>P2<sub>1</sub>/n</i>	
Unit cell dimensions	<i>a</i> = 8.9399(6) Å	$\alpha = 90^\circ$
	<i>b</i> = 27.2788(14) Å	$\beta = 90.427(5)^\circ$
	<i>c</i> = 15.4510(9) Å	$\gamma = 90^\circ$
Volume	3767.9(4) Å <sup>3</sup>	
<i>Z</i>	4	
Density (calculated)	1.309 Mg/m <sup>3</sup>	
Absorption coefficient	0.981 mm <sup>-1</sup>	
<i>F</i> (000)	1576	
Crystal size	0.23 x 0.09 x 0.04 mm <sup>3</sup>	
Theta range for data collection	2.40 to 26.03°.	
Index ranges	-10 ≤ <i>h</i> ≤ 11, -33 ≤ <i>k</i> ≤ 33, -19 ≤ <i>l</i> ≤ 18	
Reflections collected	64413	
Independent reflections	7337 [R(int) = 0.0896]	
Completeness to theta = 25.00°	100.0 %	
Absorption correction	Semi-empirical from equivalents	
Max. and min. transmission	0.9618 and 0.8059	
Refinement method	Full-matrix least-squares on <i>F</i> <sup>2</sup>	
Data / restraints / parameters	7337 / 0 / 379	
Goodness-of-fit on <i>F</i> <sup>2</sup>	1.101	
Final <i>R</i> indices [ <i>I</i> > 2σ( <i>I</i> )]	<i>R</i> 1 = 0.0591, <i>wR</i> 2 = 0.0960	
<i>R</i> indices (all data)	<i>R</i> 1 = 0.1054, <i>wR</i> 2 = 0.1052	
Largest diff. peak and hole	0.380 and -1.005 e.Å <sup>-3</sup>	

Crystal data and structure refinement for **43** [Fe(SeSi<sub>2</sub>Bu<sub>3</sub>)(CO)<sub>3</sub>]<sub>2</sub> (**4.7.7**)

Empirical formula	C <sub>30</sub> H <sub>54</sub> Fe <sub>2</sub> O <sub>6</sub> Se <sub>2</sub> Si <sub>2</sub>	
Formula weight	836.53	
Temperature	173(2) K	
Wavelength	0.71073 Å	
Crystal system	Monoclinic	
Space group	<i>P2<sub>1</sub>/n</i>	
Unit cell dimensions	a = 8.9357(5) Å	α = 90°
	b = 27.8681(19) Å	β = 91.034(4)°
	c = 15.3592(8) Å	γ = 90°
Volume	3824.1(4) Å <sup>3</sup>	
Z	4	
Density (calculated)	1.453 Mg/m <sup>3</sup>	
Absorption coefficient	2.761 mm <sup>-1</sup>	
F(000)	1720	
Crystal size	0.21 x 0.12 x 0.09 mm <sup>3</sup>	
Theta range for data collection	2.39 to 25.44°	
Index ranges	-10 ≤ h ≤ 10, -33 ≤ k ≤ 33, -18 ≤ l ≤ 17	
Reflections collected	22777	
Independent reflections	7031 [R(int) = 0.0815]	
Completeness to theta = 25.00°	99.9 %	
Absorption correction	Semi-empirical from equivalents	
Max. and min. transmission	0.7892 and 0.5948	
Refinement method	Full-matrix least-squares on F <sup>2</sup>	
Data / restraints / parameters	7031 / 0 / 379	
Goodness-of-fit on F <sup>2</sup>	0.922	
Final R indices [I > 2σ(I)]	R1 = 0.0378, wR2 = 0.0681	
R indices (all data)	R1 = 0.0667, wR2 = 0.0742	
Largest diff. peak and hole	0.417 and -0.685 e.Å <sup>-3</sup>	

Crystal data and structure refinement for **44** [Fe(TeSi $t$ Bu $_3$ )(CO) $_3$ ] $_2$  (**4.7.8**)

Empirical formula	C $_{30}$ H $_{54}$ Fe $_2$ O $_6$ Si $_2$ Te $_2$	
Formula weight	933.81	
Temperature	173(2) K	
Wavelength	0.71073 Å	
Crystal system	Monoclinic	
Space group	C2/c	
Unit cell dimensions	a = 15.975(2) Å	$\alpha = 90^\circ$
	b = 28.272(3) Å	$\beta = 131.151(9)^\circ$
	c = 11.2282(16) Å	$\gamma = 90^\circ$
Volume	3818.5(8) Å $^3$	
Z	4	
Density (calculated)	1.624 Mg/m $^3$	
Absorption coefficient	2.356 mm $^{-1}$	
F(000)	1864	
Crystal size	0.24 x 0.20 x 0.06 mm $^3$	
Theta range for data collection	3.68 to 25.67°	
Index ranges	-19 $\leq$ h $\leq$ 19, -32 $\leq$ k $\leq$ 34, -13 $\leq$ l $\leq$ 13	
Reflections collected	14814	
Independent reflections	3583 [R(int) = 0.0771]	
Completeness to theta = 25.00°	99.6 %	
Absorption correction	Semi-empirical from equivalents	
Max. and min. transmission	0.8715 and 0.6017	
Refinement method	Full-matrix least-squares on F $^2$	
Data / restraints / parameters	3583 / 0 / 190	
Goodness-of-fit on F $^2$	1.053	
Final R indices [I > 2 $\sigma$ (I)]	R1 = 0.0498, wR2 = 0.1287	
R indices (all data)	R1 = 0.0707, wR2 = 0.1346	
Largest diff. peak and hole	1.621 and -1.414 e.Å $^{-3}$	

## 6.2 Abbreviations

18-c-6	crown ether 18-crown-6
Ar	aryl
Bu	butyl
<i>t</i> Bu	tertiary-butyl
Cp	cyclopentadienyl
Cp*	pentamethylcyclopentadienyl
Cys	cysteine
d	day(s)
DME	1,2-dimethoxyethane
DMPE	1,2-bis(dimethylphospha)ethane
DMPM	bis(dimethylphospha)methane
Do	donor
DPPE	1,2-bis(diphenylphospha)ethane
DPB	diphenylboratabenzene
e <sup>-</sup>	electron
Et	ethyl
Et <sub>2</sub> O	diethyl ether
FcH	ferrocene
Fp	cyclopentadienyl iron dicarbonyl [CpFe(CO) <sub>2</sub> ]
h	hour(s)
hypersilyl	tris(trimethylsilyl)silyl
IR	infrared
Me	methyl
$\mu_{\text{eff}}$	effective magnetic moment
$\mu_{\text{B}}$	Bohr magneton
n	normal (unbranched)
NMR	nuclear magnetic resonance
Ph	phenyl
ppm	parts per million
<i>i</i> Pr	<i>iso</i> -propyl
SCE	standard calomel electrode

supersilyl

tri-*tertiary*-butylsilyl

THF

tetrahydrofurane

UV-vis

ultraviolet-visible

### 6.3 Curriculum Vitae

#### Theresa I. Kückmann

Cohausenstr. 3  
D-60439 Frankfurt

Born:	Theresa I. Zahn 21 Nov 1980 in Stevens Point, WI, USA
Marital Status:	Married
Nationality:	US-American
4/2004 - 12/2006	Johann Wolfgang Goethe-Universität Frankfurt Doctoral thesis under Prof. M. Wagner "Silyl Chalcogenolates: Synthesis, Reactivity, and Transition Metal Complexes"
10/2002 - 3/2004 10/2003 - 3/2004	Freie Universität Berlin Masters thesis under Prof. U. Abram "Oxorhenium(V) Complexes of 1,3-Dialkyl-4,5-dimethyl-imidazol-2-ylidenes"
19 March 2004	Master of Science in Chemistry (average = 1.1 = A, 1.0 = very good, 6.0 = unacceptable)
09/1998 - 05/2002 01/2002 - 05/2002	University of Minnesota-Twin Cities, Minneapolis, MN, USA Bachelors thesis under Prof. W. B. Tolman "Synthesis of a Sterically Hindered Nitrogen-Donor Ligand for Development of Mixed-Valence Copper Complexes"
18 May 2002	Bachelor of Science in Chemistry, summa cum laude, Institute of Technology Honors Division (average = 3.97 = A, 4.0 = very good, 0.0 = unacceptable)
10/2000 - 07/2001	Technische Universität Carolo-Wilhelmina zu Braunschweig (foreign exchange year during bachelors studies)
08/1994 - 05/1998 24 May 1998	Stevens Point Area Senior High, Stevens Point, WI, USA High school diploma (average = 4.0 = A, 4.0 = very good, 0.0 = unacceptable)
08/1997 - 07/1998	Elsa-Brändström-Schule, Hannover (foreign exchange year during high school)

## **6.4 Eidesstattliche Erklärung**

Ich erkläre hiermit an Eides Statt, dass ich die vorgelegte Dissertation über „Silyl Chalcogenolates: Synthesis, Reactivity, and Transition Metal Complexes“ selbständig angefertigt und mich anderer Hilfsmittel als der in ihr angegebenen nicht bedient habe, insbesondere, dass aus Schriften Entlehnungen, soweit sie in der Dissertation nicht ausdrücklich als solche mit Angabe der betreffenden Schrift bezeichnet sind, nicht stattgefunden haben.

Desweiteren erkläre ich hiermit, dass ich mich bisher keiner Doktorprüfung unterzogen habe.

Frankfurt am Main, 1. December 2006

Theresa I. Kückmann